SUPERCONDUCTIVITY, HIGH-TEMPERATURE SUPERCONDUCTIVITY

The emergence of resistive state in the Meissner phase of superconductors upon an increase in temperature below the critical point

N. B. Brandt, G. A. Mironova, and V. V. Rzhevskii

*Low Temperature Physics Department, Moscow State University, 119899 Moscow, Russia**
(Submitted September 22, 1997; revised March 19, 1998)
Fiz. Nizk. Temp. **24**, 711–715 (August 1998)

It is shown that the resistive state emerging upon an increase in temperature in the region below the critical point in the Meissner phase of superconductors can be detected by measuring the variation of the frozen magnetic field in a mesoscopic hollow cylindrical sample upon its heating in the superconducting state. Owing to magnetic flux quantization, the decrease in the magnetic field upon heating must be step-wise. © *1998 American Institute of Physics.* [S1063-777X(98)00108-X]

According to Gor'kov,[1] the order parameter Ψ in the Ginzburg–Landau theory is connected with the energy gap Δ in pure superconductors (whose the electron mean free path l in the normal state is much longer than the coherence length ξ) in the BCS theory through the relation

$$\Psi(T)=\left[\frac{8.4mv_F^2N(0)}{2\pi^2k_B^2T_c^2}\right]^{1/2}\Delta(T), \tag{1}$$

which is valid for $T\to T_c$. Here m is the electron mass, v_F the Fermi velocity, $N(0)$ the density of electron states at the Fermi level, k_B Boltzmann's constant, and T_c the superconducting transition temperature. In the Ginzburg–Landau theory, the square of the order parameter modulus determines the number density of superconducting electrons: $|\Psi|^2=n_s/2$. By ''superconducting electrons'' we mean those creating the superconducting current

$$\mathbf{j}_s=n_se\mathbf{v}_s, \tag{2}$$

where e is the electron charge and $\mathbf{v}_s$ the velocity of ordered motion of electrons creating superconducting current. Substituting into (1) the expression

$$N(0)=\frac{8\sqrt{2\pi}\,m^{3/2}\varepsilon_F^{1/2}}{(2\pi\hbar)^3} \tag{3}$$

for the electron density of states in the normal state and considering that the electron number density is given by

$$n_0=2\cdot\frac{4}{3}\frac{\pi p_F^3}{(2\pi\hbar)^3},$$

where $p_F=mv_F$ is the Fermi momentum, we obtain the following expression determining the temperature dependence of the number density of superconducting electrons near T_c:

$$n_s(T)\approx n_0\,\frac{\Delta^2(T)}{k_B^2T_c^2}. \tag{4}$$

In the case of dirty superconductors ($l<\xi$), the dependence similar to (1) has the form

$$\Psi_d(T)=\left[\frac{\pi mv_FN(0)l}{12\hbar k_BT_c}\right]^{1/2}\Delta(T) \tag{5}$$

and accordingly

$$n_s(T)\approx n_0\,\frac{l}{\hbar v_F}\,\frac{\Delta^2(T)}{k_BT_c}. \tag{6}$$

On the other hand, it follows from experimental data that the electron number density n_s at $T\ll T_c$ virtually coincides with the value of n_0 for the London type superconductors (whose the coherence length ξ is much smaller then the magnetic field penetration depth λ_L for the superconductor) and is of the order of $n_0\lambda_p/\xi$ for the Pippard type superconductors (whose penetration depth λ_p is smaller than ξ). Thus, the number density of superconducting electrons decreases upon an increase of temperature from a value of the order of $\sim n_0$ at $T\ll T_c$ to zero at $T=T_c$. The approximate form of this dependence is shown in Fig. 1.

Let us consider a superconductor carrying the current j_s created by an external source at $T\ll T_c$. The current involves electrons having the number density $n_{s_0}\sim n_0$ and moving with the velocity v_{s_0} defined by (2). As the temperature increases, the number density of superconducting electrons becomes lower. The fraction δn_s of electrons participating in the creation of supercurrent loses the velocity v_{s_0} and transfers the kinetic energy (evolved in the form of the Joule heat) to the crystal lattice. Moreover the current in the superconductor is sustained by the emerging electric field accelerating the remaining superconducting electrons. As a result, a resistive state characterized by a nonzero electric resistance must be formed upon heating.

In order to estimate the resistivity ρ emerging in this case, we assume that the entire kinetic energy of electrons per unit volume ($\delta n_s mv_s^2/2$) is liberated during heating in the form of Joule heat:

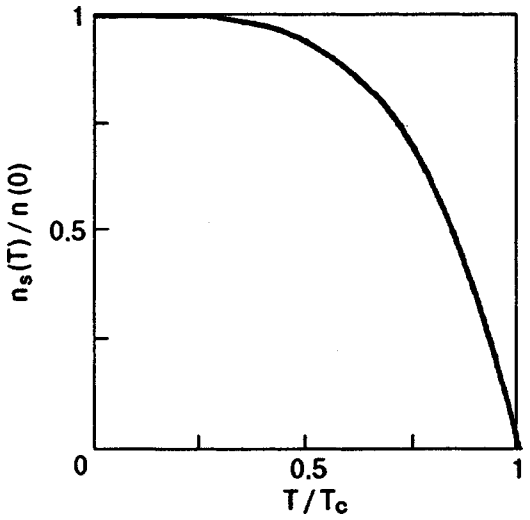

FIG. 1. Dependence of relative variation of superconducting electron concentration on relative temperature.

$$\delta n_s \frac{mv_s^2}{2} \sim (n_s e v_s)^2 \rho t.$$

Assuming that $\delta n_s \sim n_s$, we obtain $\rho \cong m/2n_s e^2 t$.

For the time of heating $t \cong 1$ s, $\rho = 10^{-16}\ \Omega \cdot$m, which is smaller than the copper resistance at room temperature by a factor of 10^8. This value is so small that it can be neglected practically. It is probably for this reason that this effect has not been studied (to our knowledge). However, the emergence of the resistive state in closed mesoscopic superconducting systems upon an increase in temperature can be detected and the effect can be appreciable.

Let us consider a long hollow superconducting cylinder of radius R, whose wall thickness d is larger that the magnetic field penetration depth λ for the superconductor. At $T_1 \ll T_c$, we induce a supercurrent in the cylinder of density much smaller than the critical current density at this temperature (for this purpose, we cool the sample to the temperature T_1 in a constant external magnetic field which is removed after cooling). This current creates a magnetic field of strength H_1 in the cylinder which is also much smaller than the critical field $H_c(T_1)$. We heat the cylinder to the temperature T_2 at which the field H_2 is still smaller than the field $H_c(T_2)$ at this temperature. The decrease in the number density $n_s(T)$ of superconducting electrons upon heating leads to a decrease in the supercurrent density, and hence in the field strength H in the cylinder. The change in the field leads to the emergence of induced emf which accelerates superconducting electrons as well as one-particle elementary excitations whose number density increases upon heating. Since these two processes occur at the expense of the energy of the magnetic field, the value of the field decreases. The possible decrease $\delta H = H(T_1) - H(T_2)$ of the field can be estimated by comparing the variation of the magnetic field energy E_H in the cylinder with the change in the current energy E_J due to the above-mentioned processes. We can write the following expressions per unit length of the cylinder:

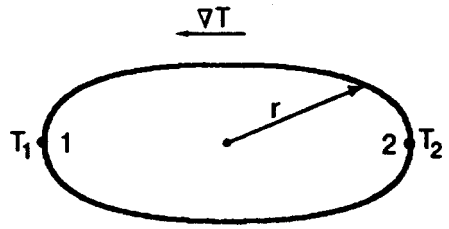

FIG. 2. A ring with a temperature gradient in its plane: the temperatures T_1 and T_2 are maintained at points 1 and 2, $T_1 < T_2$. Both temperatures are lower than the superconducting transition temperature ($T_1, T_2 < T_c$).

$$E_H = \int \frac{H^2(T_1)}{8\pi}\, dS; \quad E_J = \int n_s(T_1)\, \frac{mv_s^2}{2}\, dS; \tag{7}$$

$$A = \frac{E_J}{E_H} = \frac{2\lambda}{R}\left(1 - \exp\left(-\frac{2d}{\lambda}\right)\right). \tag{8}$$

It follows from energy balance and relation (8) that the changes in the field and superconducting electron concentration are connected through the following relation (we assume that the changes in the field and current are smaller than the initial values):

$$\frac{\delta H}{H(T_1)} \sim A\, \frac{\delta n_s}{n_s(T_1) - \delta n_s}. \tag{9}$$

Thus, the decrease in the number density of superconducting electrons upon an increase in temperature from T_1 to T_2 must be accompanied by a decrease in the magnetic field strength in the cavity of the cylinder.

If we now cool the cylinder from T_2 to T_1, the concentration of electrons creating supercurrent corresponding to temperature T_2 must remain unchanged. For this reason, the field $H(T_2)$ must not vary in the next cooling–heating cycles.

The validity of this assumption is confirmed by the following arguments. Let us consider a macroscopic superconducting ring carrying a circulating supercurrent with a temperature gradient in its plane (Fig. 2). The temperature T_1 maintained at point 1 is lower than the temperature T_2 at point 2 ($T_1 < T_2$). Both temperatures are lower than T_c.

We assume that the supercurrent at each point of the ring is created by the equilibrium concentration of superconducting electrons corresponding to the temperature at the given point. During motion of superconducting electrons from point 1 to point 2, energy must be dissipated as a result of a decrease in the electron number density (as well as a result of heating), i.e., the current in the superconducting ring must attenuate as a result of temperature gradient ∇T. The current attenuation time can be estimated by the formula

$$\Delta t = \frac{\Delta i}{i}\, \frac{L}{R}. \tag{10}$$

For a ring of diameter $2r = 5$ cm and cross-sectional radius $a = 10^{-2}$ cm, the self-inductance L is given by ($r \gg a$)

$$L = \mu_0 r[\ln(r/a) + 0.23],$$

where $\mu_0 = 4\pi \times 10^{-7}$ V·s/A. The resistance $R = \rho l/S$ of the ring can be estimated by formula (7) if we replace in it the

time t of heating by the time of motion of superconducting electrons from point 1 to point 2. Assuming that the average velocity of superconducting electrons is $v_s = 10^3$ cm/s, we find that the supercurrent i decreases to half the initial value during the time $t \cong 10^2$ s. The results of experiments on the effect of thermo-emf in a superconducting ring with a temperature gradient[2] show, however, that the supercurrent in the ring does not attenuate significantly over periods of time much longer than $\cong 10^2$ s.

Thus, the assumption that the current at each point of the ring is determined by the equilibrium concentration of superconducting electrons at the corresponding temperature contradicts the experimental data. Apparently, the current in a ring with a temperature gradient is apparently determined by the value of the minimum concentration of superconducting electrons corresponding to the maximum temperature T_2 at each point of the ring. Since this concentration does not change during motion of electrons from point 1 to point 2, there is no energy dissipation in the ring, and the supercurrent circulates without attenuation irrespective of the temperature gradient in the plane of the ring.

In this case, an interesting situation emerges at the temperature T_1: the supercurrent is created only by a fraction of superconducting electrons. Another fraction of these electrons equal to $n_s(T_1) - n_s(T_2)$ does not participate in the supercurrent, and their total momentum remains zero. This is equivalent to the stratification of the superconducting liquid into the current-carrying and ''stationary'' components upon cooling.

The resistive state can be observed when the following two conditions are satisfied. First, the field variation δH must be large enough for measuring. Among other things, this quantity depends on the cylinder radius R and increases with decreasing R in accordance with (9). However, the effect of quantization of the magnetic flux through the cylinder becomes significant with decreasing R. Consequently, the second requirement is that $H(T_1)$ must be larger than the field $H_0(T) \approx \Phi_0/\pi[R+\lambda(T)]^2$, corresponding to the magnetic flux quantum $\Phi_0 = 2.07\times10^{-7}$ G·cm^2. Let us now estimate the magnitude of the effect in real superconductors. Apparently, appropriate substances are Ta ($T_c = 4.48$ K, $H_c(0) = 830$ G, $\lambda(0) = 5.4\times10^{-6}$ cm) and Nb ($T_c = 9.46$ K, $H_c(0) = 1944$ G, $\lambda(0) = 4.7\times10^{-6}$ cm). We assume that the thickness of the cylinder walls is $d > \lambda$. In this case, the exponential term in (8) can be neglected. Suppose that $R = 2\times10^{-4}$ cm; then $H_0 \approx 2$ G. For Ta with $\delta n_s/n_s(T_1) \simeq 1/2$ and $H(T_1) \cong 100$ G, we have $\delta H \approx H(T_1) \times(2\lambda/R)\{\delta n_s/[n_s(T_1) - \delta n_s]\} \approx 5$ G. The frozen field $H(T_1)$ for Nb can be chosen of the order of 200 G. In this case, $\delta H \approx 10$ G for the same geometry ($H_0 \approx 2$ G).

In determining the temperature dependence of the field $H(T_1)$, we must take in to account the following factors. The concentration of superconducting electrons changes with increasing temperature monotonically (see Fig. 1). Irrespective of the magnetic flux quantization effect, this decrease in $n_s(T)$ must correspond to a monotonic increase in the magnetic field penetration depth λ for the superconductor. But since the magnetic flux through the cylinder $\Phi = \Phi_0 n$ (n is an integer) can change only in quanta, and the flux for a given n must remain unchanged, the increase in λ with heating must be accompanied by a decrease in the field strength in the inner cavity of the cylinder. Thus, the field strength $H(T)$ must decrease monotonically during sample heating for each value of n, while a change in n by unity causes a field jump, the magnitude of each next jump being smaller than the previous value. The expected nature of variation of the frozen field as a result of sample heating from T_1 to T_2 (curve *1*) and subsequent cooling–heating cycles (curve *2*) is illustrated in Fig. 3. The shape of the steps depends significantly on the ratio λ/R: the steps are flat for $\lambda/R \ll 1$ and convex for $\lambda/R \sim 1$.

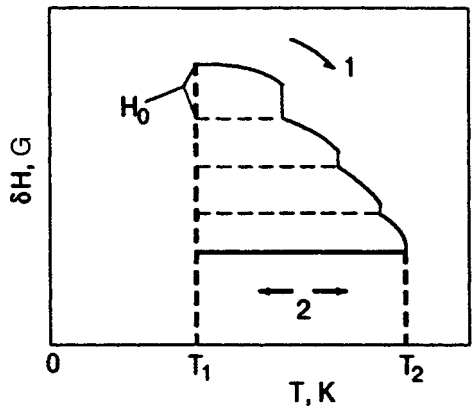

FIG. 3. Expected variation of the frozen magnetic field $\delta H(T)$ in the sample upon heating (curve *1*) and subsequent cooling–heating cycles (curve *2*) in the temperature interval T_1-T_2.

It should be emphasized that such a form of variation of the magnetic field in the cylinder can be observed only in the first cycle of sample heating from T_1 to T_2. Subsequent cooling–heating cycles do not lead to the emergence of a resistive state, and the magnetic field strength in the cylinder remains unchanged (curve *2*). For the above parameters of the samples, the number of steps on curve *1* must be approximately equal to three for Ta and six for Nb. It should be noted that this effect is a nonlinear function of the ratio $\delta n_s/n_s(T_1)$. For example, the above estimates of δH become twice as large for $\delta n_s/n_s(T_1) \sim 2/3$.

Thus, we propose an experiment for observing the new effect, viz., the emergence of a finite resistance in the vortex-free Meissner phase of superconductors in which the temperature increases in the range of temperatures, magnetic fields, and supercurrents much smaller than the critical values. It is shown that this effect in mesoscopic samples becomes so strong that it can be detected by measuring the magnetic field frozen in a hollow superconducting cylinder. The temperature dependence of field variation in the first heating cycle is step-wise. This is interesting as a new method of determining the magnetic flux quantum.

*E-mail: rzhevski@mig.phys.msu.su

[1] L. P. Gor'kov, Zh. Éksp. Teor. Fiz. **37**, 1918 (1959) [Sov. Phys. JETP **10**, 1364 (1959)].
[2] V. L. Ginzburg, Usp. Fiz. Nauk **161**, 1 (1991) [Sov. Phys. Usp. **34**, 101 (1991).

Translated by R. S. Wadhwa

Quantum levels and quasi-local states of *SINIS* structures

G. A. Gogadze and A. M. Kosevich

*B. Verkin Institute for Low Temperature Physics and Engineering, National Academy of Sciences of the Ukraine, 310164 Kharkov, Ukraine**

(Submitted July 15, 1997; revised February 16, 1998)
Fiz. Nizk. Temp. **24**, 716–725 (August 1998)

Quantum states of a superconductor–insulator–normal metal–insulator–superconductor sandwich (the *SINIS* structure) are investigated on the basis of the Bogoliubov–de Gennes equations. The dispersion equation is obtained for the quasiparticle spectrum for energies $E<\Delta$ (Δ is the energy gap in the superconductor) taking into account the Andreev scattering as well as conventional electron reflection at the interfaces of the *SINIS* structure. The spectrum makes it possible to calculate the Josephson current in the system. The transparency coefficient of the system for electrons with a continuous energy spectrum is calculated, and quasi-local states (''resonance levels'' of transparency) are determined for the structure under investigation.
 [S1063-777X(98)00208-4]

1. INTRODUCTION

The wave properties of an electron moving in the field of a spatially varying potential are manifested clearly when the potential varies significantly over distances of the order of the de Broglie wavelength of the electron. In the physics of electron tunneling through potential barriers, this leads to resonant tunneling of quasiparticles. In particular, this phenomenon takes place in the case of two-barrier structure which is interesting from the points of view of physics and applications, and is characterized by an abrupt increase in the transparency of the entire system. Such a problem was considered for the first time in the solid state physics by Iogansen[1] who formulated the conditions under which the transparency of the electron system increases from the product of transparencies of individual barriers to unity.

Clearly, the effect is observed only in the case of highly specular reflection of quasiparticles at film boundaries and for a long electron mean free path (as compared to the film thickness). Under these conditions, quasilocal energy levels formed in the potential well between insulating barriers correspond to metastable bound states of quasiparticles. If the energy of a tunneling electron coincides with a quasi-local level of the system, premises for resonant tunneling through the structure are created.

The idea of resonant tunneling was used in a number of theoretical publications for explaining the anomalously high conductance of tunnel barriers containing ''traps'' [2] and for studying superlattices.[3]

Among experimental works on resonant tunneling in normal (nonsuperconducting) structures, Refs. 4 and 5 are worth mentioning.

The study of structures containing junctions between normal and superconducting metals revealed new effects and initiated a large series of theoretical and experimental publications devoted to this problem. Among these publications, we must mention the article by Andreev[6] who predicted theoretically a basically new mechanism of peculiar reflection of electrons at the interface between normal (N) and superconducting (S) metals, i.e., the so-called Andreev's reflection. In this phenomenon, the electron quasimomentum remains virtually unchanged, and the group velocity reverses its sign.[6] The latter property distinguishes Andreev's reflection from the conventional specular reflection of an electron, in which only the velocity component perpendicular to the interface changes its sign. Andreev's reflection is accompanied by a current through the interface.[7]

The Andreev's scattering mechanism is most effective when an electron moves along the normal to the $N-S$ interface. When the direction of electron deviates from the normal, the Andreev's reflection probability decreases.[8,9] Dzhikaev[8] proved that excitations impinging on the $N-S$ interface at small angles undergo conventional specular reflection with a probability of the order of unity. The boundary separating the regions of Andreev's and specular reflections in the momentum space was determined. It was found that conventional specular reflection takes place for small angles of incidence $\sim(kT/\zeta)^{1/2}$.

Andreev's reflection plays a significant role in explaining excess currents of weak links.[10] The above-the-barrier reflection near the $N-S$ interface generates interference of electron- and hole-like waves in the superconductor, which forms the basis for explaining the Tomasch effect.[11,12]

Andreev[6] proved that, if a film of normal metal is in contact with superconductors on both sides, and the energy of quasiparticles does not exceed Δ, the elementary excitation spectrum of the SNS junction is quantized. The existence of the discrete spectrum of one-particle excitations was found to be closely related with the coherence of the order parameter phase. The spectrum of Andreev's energy levels for a pure SNS junction is defined by the formula

$$E_n^{(0)}=\frac{\pi\hbar v_z}{L}\left(n+\frac{1}{\pi}\arccos\frac{E}{\Delta}\pm\frac{\Phi}{2\pi}\right),\quad n=0,1,2,..., \qquad (1)$$

where v_z is the velocity of excitations along the normal to the film boundary, L the thickness of the normal layer, and Φ

the phase difference of the order parameters of two superconductors. Formula (1) taking into account the phase difference Φ was derived by Kulik.[13] There are two systems of Andreev's levels which are degenerate for $\Phi=0$. It is significant that the position of the levels is determined by the phase Φ. The change in Φ by 2π returns Andreev's levels to the initial state. The spectrum (1) was used for constructing a microscopic theory of stationary Josephson effect for impurity-free *SNS* junctions.[13–16]

The above-the-barrier reflection of quasiparticles may cause interference effects in the *SNS* structure. These effects are manifested in oscillations of the transparency coefficient of the system upon a change in the quasiparticle energy or the order parameter phase Φ.[17,18]

Apart from Andreev's reflection, an electron can also experience conventional specular reflection at the interfaces of a sandwich due to bends of energy levels, the presence of impurities at an interface, or as a result of a difference between Fermi wave vectors of contacting media. As a rule, conventional scattering at barriers can be simulated by a δ-shaped potential $V(z)=H\delta(z)$. The scattering intensity H is proportional to the dimensionless parameter $Z=H/\hbar v_z$. Blonder *et al.*[19] analyzed a transition from a perfect metal junction $(Z=0)$ to tunneling for microconstrictions of the normal metal–superconductor type.

Here we analyze quantum states of a superconductor–insulator–normal metal–insulator–superconductor system (*SINIS* structure). Layered systems (sandwiches) were studied by many authors to determine the quantum states of electrons in them. Among recent publications, Refs. 20 and 21 are the closest to the subject of this article. However, Beenakker[20] studied a different physical system which cannot be reduced by a limiting transition to an *SINIS* sandwich, and hence leads to a different electron spectrum. As regards the paper by Wendin and Shumeiko,[21] a remark will be made in the appropriate place in the text.

Our analysis is based on the Bogoliubov–de Gennes equations.[22] For energies below Δ, we have derived a dispersion equation for the quasiparticle spectrum taking into account both Andreev's reflection and conventional reflection at the boundaries of the structure. The transparency of an *SINIS* structure is calculated for a continuous spectrum, and the existence of quasi-local states in it is proved.

2. MODEL

In order to describe electron processes in an *SINIS* junction, we shall proceed from the Bogoliubov–de Gennes equations for a two-component wave function $\Psi=\binom{\psi}{\varphi}$ of quasiparticles[22]:

$$\begin{pmatrix} \hat{\mathbf{H}}_0(\mathbf{r}) & \Delta(\mathbf{r}) \\ \Delta^*(\mathbf{r}) & -\hat{\mathbf{H}}_0^*(\mathbf{r}) \end{pmatrix} \begin{pmatrix} \psi(\mathbf{r}) \\ \varphi(\mathbf{r}) \end{pmatrix} = E \begin{pmatrix} \psi(\mathbf{r}) \\ \varphi(\mathbf{r}) \end{pmatrix}, \tag{2}$$

where $\hat{\mathbf{H}}_0(\mathbf{r})=\hat{T}+V(\mathbf{r})$; $\hat{T}=(1/2m)[\hat{\mathbf{p}}-(e/c)\mathbf{A}]^2-\zeta$ is the kinetic energy operator, m the electron mass, ζ the Fermi energy, and $\mathbf{A}$ the vector potential. The Fermi energies of the normal and superconducting metals are assumed to be the same. The potential $V(\mathbf{r})$ describes conventional scattering of quasiparticles at interfaces. Metal films are assumed to be pure. We simulate the potential V and the nondiagonal potential Δ by the following expressions (see Fig. 1):

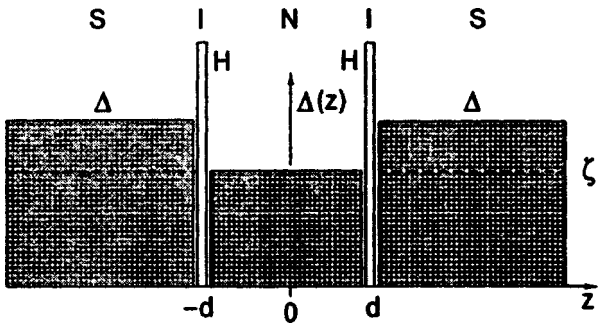

FIG. 1. Schematic diagram of a *SINIS* junction: Δ is the order parameter of the superconductor, ζ the chemical potential of metals, H the intensity of a δ-functional potential barrier, and $L=2d$ the normal layer width.

$$V(z)=H[\,\delta(z-d)+\delta(z+d)] \tag{3}$$

($L=2d$ is the width of the normal layer, the z-axis is perpendicular to the plane of the $N-S$ interface along which the structure is assumed to be translationally periodic):

$$\Delta(z)=\begin{cases} \Delta\,\exp(i\Phi_+), & z>d; \\ \Delta\,\exp(i\Phi_-), & z<-d; \\ 0, & |z|\leqslant d. \end{cases} \tag{4}$$

Here Φ_+ and Φ_- are the phases of the order parameter of two superconducting ''banks.'' For planar geometry, the problem is reduced to a one-dimensional problem through the substitution $\binom{\psi(\mathbf{r})}{\varphi(\mathbf{r})}=\exp(iq_x x)\binom{\psi(z)}{\varphi(z)}$, where the tangential component of the electron quasimomentum is chosen for simplicity in the form $\mathbf{q}(q_x,0,0)$. It can be seen from (4) that we consider the model of jump-wise variation of the order parameter at the boundary of the layers presuming the disregard of the proximity effect. The model operates the better, the more intense the electron scattering at the insulating barrier. Proximity effects in the tunnel structures *SNINS* and *SNIS* structures with a finite transparency of $S-N$ interfaces are taken into account consistently by Golubov and Kupriyanov.[23]

3. ANDREEV'S LEVELS

We shall solve the Bogoliubov–de Gennes equation for all regions of the junction, assuming that the magnetic field is equal to zero in the N layer. Let us consider the current states of quasiparticles whose energy does not exceed Δ. The solutions of Eqs. (2) has the form ($\hbar\equiv 1$)

$$\begin{pmatrix} \psi \\ \varphi \end{pmatrix} = e^{iqx}\left\{ (A_+ e^{ik_0 z}+A_- e^{-ik_0 z})\begin{pmatrix} 1 \\ 0 \end{pmatrix} + (B_+ e^{ik_1 z} + B_- e^{-ik_1 z})\begin{pmatrix} 0 \\ 1 \end{pmatrix}\right\}, \quad |z|\leqslant d, \tag{5}$$

$$\begin{pmatrix} \psi \\ \varphi \end{pmatrix} = e^{iqx}\left\{ C_+ e^{i\lambda(z-d)}\begin{pmatrix} 1 \\ \gamma_+ \end{pmatrix} + D_+ e^{-i\mu(z-d)}\begin{pmatrix} \delta_+ \\ 1 \end{pmatrix}\right\}, \quad z>d, \tag{6}$$

$$\begin{pmatrix}\psi\\ \varphi\end{pmatrix}=e^{iqx}\left\{C_-e^{-i\lambda(z+d)}\begin{pmatrix}1\\ \gamma_-\end{pmatrix}+D_-e^{i\mu(z+d)}\begin{pmatrix}\delta_-\\ 1\end{pmatrix}\right\},$$

$$z<-d. \tag{7}$$

Here we have introduced the following notation:

$$\lambda^2=\frac{k_0^2+k_1^2}{2}+2mi\sqrt{\Delta^2-E^2},$$

$$\mu^2=\frac{k_0^2+k_1^2}{2}-2mi\sqrt{\Delta^2-E^2} \tag{8}$$

(Re $\lambda>0$, Im $\lambda>0$; Re $\mu>0$; Im $\mu<0$), where k_0 and k_1 are respectively the wave vectors of a particle and a hole. The Andreev scattering probability amplitude is determined by the coefficients

$$\gamma_\pm=\frac{\Delta e^{-i\Phi_\pm}}{E+i(\Delta^2-E^2)^{1/2}};\quad \delta_\pm=\frac{\Delta e^{+i\Phi_\pm}}{E+i(\Delta^2-E^2)^{1/2}}. \tag{9}$$

Let us join the obtained solutions at the boundaries of the media by using the requirement of continuity of two-component wave functions at the points $z=\pm d$ as well as the condition

$$\frac{d\Psi(\mp d+0)}{dz}-\frac{d\Psi(\mp d-0)}{dz}=2mH\Psi(\mp d). \tag{10}$$

This gives a system of homogeneous equations to be used for finding the unknown coefficients of the problem. The requirement that the determinant of this system be equal to zero leads to the dispersion equation for the quasiparticle spectrum of the *SINIS* junction:

$$D_0\cos\Phi+\mathrm{Re}(D_1e^{2i(k_0+k_1)d})-\mathrm{Re}(D_2e^{2i(k_0-k_1)d})=0. \tag{11}$$

The quantity $\Phi=\Phi_+-\Phi_-$ is the phase difference for the order parameters of the superconductors. The coefficients D_0, D_1, and D_2 have the form

$$D_0=(\kappa_0-\kappa_0^*)(\kappa_1-\kappa_1^*)(2i\ \mathrm{Im}\ \Lambda)^2,$$

$$D_1=[\gamma^*(\kappa_0-\Lambda)(\kappa_1-\Lambda^*)-\gamma(\kappa_0-\Lambda^*)(\kappa_1-\Lambda)]^2,$$

$$D_2=[\gamma^*(\kappa_0-\Lambda)(\kappa_1^*-\Lambda^*)-\gamma(\kappa_0-\Lambda^*)(\kappa_1^*-\Lambda)]^2. \tag{12}$$

and are complex functions of the excitation energy E:

$$\kappa_0=H+\frac{ik_0}{2m},\quad \kappa_1=H+\frac{ik_1}{2m},\quad k_{0,1}=\sqrt{2m(\tilde{\zeta}\pm E)},$$

$$\Lambda=i\lambda/2m$$

$$\left(\tilde{\zeta}=\zeta-\frac{q^2}{2m},\ \lambda=\pm\sqrt{2m\tilde{\zeta}+i2m(\Delta^2-E^2)^{1/2}}\right),$$

$$\gamma=\exp[-i\ \arccos(E/\Delta)].$$

It can easily be seen that the parameter $Z=H/\hbar v_Z$ characterizing the intensity of a potential barrier does not appear in the coefficient D_0. The first term of the dispersion equation (11) is not affected by conventional scattering of quasiparticles. The second term in (11) describes Friedel type oscillations associated with the interference of quasiparticle waves in particle–particle or hole–hole scattering processes. These processes are accompanied by a strong change in quasimomentum ($\Delta k\sim k_F$) generating rapid oscillations $\sim\cos(2k_FL)$ of the density of states upon a change in the normal film thickness $L=2d$.

The third term of the dispersion equation contains oscillations of the type $\cos[(k_0-k_1)L]$ whose period is large in view of the small variation of quasimomentum during Andreev scattering. This term is associated with the interference observed in tunneling experiments.[13–24] Hahn[25] studied current states in *SN* metallic junctions taking into account both types of scattering at the film boundaries. The effect of boundary imperfections near the constriction of a superconducting point contact on its current and phase parameters was investigated in Ref. 26.

Returning to the dispersion equation, we see that the coefficients D_1 and D_2 are functions of the parameter Z. We expand all the quantities appearing in Eq. (11) into power series in the small parameter $\Delta/\zeta\ll1(E/\zeta\ll1)$ and confine our analysis only to zeroth-order terms (Andreev's approximation). Blaauboer *et al.*[27] proved that the application of Andreev's approximation for pure *SN* and *SNS* junctions with a small cross sectional area weakly affects their local density of states. In the absence of conventional scattering ($Z=0$) and in the zeroth order in the parameter Δ/ζ, Eq. (11) leads to the spectrum (1) of quantized energy levels, which was obtained by Kulik for the current state of an *SNS* junction.[15]

In the case of a finite Z, we also confine the analysis of Eq. (11) to Andreev's approximation. In the obtained expansion, the terms differ in the powers of the parameter Z. Let us first consider the case $Z\gg1$. The first term in (11) containing $\cos\Phi$ can be omitted in this case in view of the condition $|\cos\Phi|\ll Z^4$, and Eq. (11) leads to the spectrum of particles and holes, which is quantized in a ''box'':

$$\pm E=\frac{\pi^2\hbar^2n^2}{2mL^2}+\frac{q^2}{2m}-\zeta. \tag{13}$$

In the other limiting case $Z\ll1$, we retain second-order terms in the parameter Z among zeroth-order terms in Δ/ζ. Taking into account Andreev's reflection as well as conventional scattering of quasiparticles. we can write Eq. (11) for the spectrum in the form ($\zeta\sim\tilde{\zeta}$)

$$F(E)+Z^2\chi(E)=0, \tag{14}$$

$$F(E)=\cos\Phi-\mathrm{Re}\{\gamma^2(E)e^{i[k_0(E)-k_1(E)]L}\}. \tag{15}$$

$$\chi(E)=4[1-(E/\Delta)^2]\cos[(k_0(E)+k_1(E))L]$$
$$-2\ \mathrm{Re}\{(\gamma^2(E)-1)\exp[(k_0(E)-k_1(E))L]\}. \tag{16}$$

It can easily be verified that Kulik's spectrum (1) is a solution of Eq. (15) (in the zeroth order in the parameter $Z\ll1$). Substituting the expansion for energy

$$E=E_n^{(0)}+Z^2\xi$$

into Eq. (15), we can write to the required degree of accuracy

$$\xi = -\chi(E_n^0)/F'(E_n^0). \tag{17}$$

This leads to the quasiparticle spectrum (nondegenerate case $\Phi \neq 0, \pi$):

$$\varepsilon = \varepsilon_n^{(0)} \pm \frac{Z^2 t[\varepsilon^{(0)}]\delta\varepsilon^{(0)}\{2t^2[\varepsilon^{(0)}]\cos[(k_0+k_1)L]+\cos[(k_0-k_1)L]-\cos\Phi\}}{[\delta\varepsilon^{(0)}+\pi t(\varepsilon^{(0)})]\sin\Phi}. \tag{18}$$

Here we have introduced the following (dimensionless) variables: the energy $\varepsilon = E/\Delta$, the separation between Andreev's energy levels $\delta\varepsilon = \delta E_n/\Delta$ ($\delta E_n = \pi\hbar v_z/L$) and the function $t[\varepsilon^{(0)}] = [1-\varepsilon_n^{(0)2}]^{1/2}$.

While deriving formula (18), we did not impose any stringent limitations on the length of the weak link (bridge). Consequently, this expression is valid for short as well as long bridges (but also under the condition $Z \ll 1$). Wendin and Shumeiko[21] studied short bridges without imposing the stringent constraint on Z. It would be interesting to compare the results following from (18) in the limiting case of a short bridge with the results obtained by Wendin and Shumeiko for $Z \ll 1$. A transition to the limiting case of a short bridge in (18) corresponds to the conditions $mv_z L \ll \hbar$ and $\pi\hbar v_z \gg \Delta$ in dimensional units. In this case, the quasiparticle spectrum in Andreev's approximation assumes the form (the states $v_z \gtrless 0$, $\tilde{k}_F \simeq k_F$, $\cos\Phi/2 > Z$)

$$\frac{E^{(0)}}{\Delta} \equiv \varepsilon_n^{(0)} = \pm\cos\frac{\Phi}{2} \pm Z^2[1+\cos(2\tilde{k}_F L)]\,\frac{\sin^2\Phi/2}{\cos\Phi/2}. \tag{19}$$

Let us now consider expression (7) from Ref. 21:

$$E = \pm\Delta\sqrt{1 - D\,\sin^2\Phi/2},$$

where D is the penetration coefficient for the entire structure. If the reflection at the interface is weak ($Z \ll 1$), we can write the expansion of the coefficient D into a power series in this parameter. The dependence of the quasiparticle spectrum on the phase of the order parameter obtained in this case coincides with (19).

The degenerate case can also be evaluated, but the corresponding spectrum is not given here.

It was mentioned above that Andreev's approximation is often sufficient for describing current in weak links. If, however, various weak links are created by using high-temperature superconductors, the parameter Δ/ζ can be of the order of not 10^{-3}–10^{-4} (traditional superconductors), but 10^{-1}.[28] Hurd and Wendin[29] studied theoretically the Josephson current in a superconducting ballistic point contact for such large values of the parameter Δ/ζ. We also analyzed the case of a pure *SNS* junction and calculated the Andreev spectrum taking into account corrections of the order of $(\Delta/\zeta)^2$. This question will be considered in greater detail in another paper.

The application of a magnetic field parallel to the N–S interfaces complicates the energy level diagram of an *SNS* junction considerably. The local dependence of the position of Andreev's levels on the phase difference Φ is preserved, but the difference itself varies along the N–S interface. This leads to ''vanishing'' of these levels in an analysis of the density of states of an *SNS* junction in a magnetic field.[30]

4. QUASILOCAL STATES

Let us now consider the states of a continuous spectrum for which the quasiparticle energy exceeds the value of Δ. We must calculate the transparency for quasiparticles incident on a *SINIS* structure from the left. We shall use the solutions of Eqs. (2) in the form of the scattering wave functions of the problem:

$$\begin{pmatrix}\psi(z)\\ \varphi(z)\end{pmatrix} = (A_+ e^{ik_0 z} + A_- e^{-ik_0 z})\begin{pmatrix}1\\0\end{pmatrix} + (B_+ e^{ik_1 z} + B_- e^{-ik_1 z})\begin{pmatrix}0\\1\end{pmatrix}, \quad |z| \leqslant d; \tag{20}$$

$$\begin{pmatrix}\psi(z)\\ \varphi(z)\end{pmatrix} = C_+ e^{i\lambda_1(z+d)}\begin{pmatrix}1\\ \gamma_-\end{pmatrix} + D_- e^{-i\lambda_1(z+d)}\begin{pmatrix}1\\ \gamma_-\end{pmatrix} + D_+ e^{i\lambda_2(z+d)}\begin{pmatrix}\delta_-\\1\end{pmatrix}, \quad z < -d; \tag{21}$$

$$\begin{pmatrix}\psi(z)\\ \varphi(z)\end{pmatrix} = E_+ e^{i\lambda_1(z-d)}\begin{pmatrix}1\\ \gamma_+\end{pmatrix} + F_- e^{-i\lambda_2(z-d)}\begin{pmatrix}\delta_+\\1\end{pmatrix}, \quad z > d, \tag{22}$$

where $\gamma_\pm = \gamma e^{-i\Phi_\pm}$, $\delta_\pm = \gamma e^{i\Phi_\pm}$, $\gamma = \Delta/[E+(E^2-\Delta^2)^{1/2}]$ the quantities k_0, k_1, and $\tilde{\zeta}$ are defined as before, and $\lambda_{1,2} = [2m\tilde{\zeta} \pm 2m(E^2-\Delta^2)^{1/2}]^{1/2}$.

For joining the solutions, we use the condition of continuity of the wave functions at the interfaces between the media and condition (10). This leads to a nonhomogeneous system of eight equations for determining the unknown coefficients, which makes it possible to calculate the coefficient of transmission of quasiparticles through a two-barrier structure:

$$W_{SINIS} = \frac{1+|\tilde{F}_-|^2}{|\tilde{C}_+|^2}, \tag{23}$$

where $\tilde{F}_- = F_-/E_+$, $\tilde{C}_+ = C_+/E_+$, $\tilde{C}_+ = M_2/M_0$, $\tilde{F}_- = M_1/M_0$, a M_0, M_1, M_2 are the determinants given in Appendix. Using these determinants, we can write formula (23) in the form

$$W_{SINIS}=\frac{|M_0|^2+|M_1|^2}{|M_2|^2}. \tag{24}$$

Substituting expressions (A1), (A2), and (A3) from Appendix, we obtain the following expression for the numerator of (24):

$$\begin{aligned}|M_0|^2+|M_1|^2=256[1-\gamma^2(x)]^2\{&[1+\gamma^4(x)][1+2S(1+S)]+4\gamma^2(x)S(1+S)+2[1+\gamma^2(x)]S(1-S)[\gamma^2(x)\cos 2k_0L+\cos 2k_1L]-2\gamma^2(x)(1+2S)\cos[(k_0-k_1)L'+\Phi]+4[1+\gamma^2(x)]S^{3/2}[\gamma^2(x)\sin 2k_0L+\sin 2k_1L]\\&-4\gamma^2(x)S\cos\Phi\{2(1-S)\cos[(k_0+k_1)L]+(1+2S)\cos[(k_0-k_1)L]+4S^{1/2}\sin[(k_0+k_1)L]\}\}.\end{aligned} \tag{25}$$

The denominator of (24) is given by

$$\begin{aligned}|M_2|^2=256\{&2[1-\gamma^2(x)]^4S^2(1+S^2)^2+\alpha^2(x)+\beta^2(x)+2\alpha(x)\beta(x)\cos[2(k_0-k_1)L]+2[1-\gamma^2(x)]^4S^2\{(1+S^2-6S)\cos[2(k_0+k_1)L]+4S^{1/2}(1-S)\sin[2(k_0+k_1)L]\}+2[\alpha(x)+\beta(x)][1-\gamma^2(x)]^2S(1-S)(\cos 2k_0L+\cos 2k_1L)+S^{3/2}[\alpha(x)+\beta(x)][1-\gamma^2(x)]^2(\sin 2k_0L+\sin 2k_1L)\\&+4\gamma^2(x)\cos^2\Phi-4\gamma^2(x)\cos\Phi\{\{[\alpha(x)+\beta(x)]\cos[(k_0-k_1)L]+2[1-\gamma^2(x)]^2S(1-S)\cos[(k_0+k_1)L]+4[1-\gamma^2(x)]^2S^{3/2}\sin[(k_0+k_1)L]\}\},\end{aligned} \tag{26}$$

where the following notation has been introduced:

$$\alpha(x)=[\gamma^2(x)-\{1-\gamma^2(x)\}S]^2,\quad S=Z^2/(1-Q^2),$$

$$\beta(x)=[1+\{1-\gamma^2x)\}S]^2,\quad Q=q/k_F.$$

The energy of scattering states satisfies the condition $2E\gg\Delta$, i.e., the parameter $\gamma\ll 1$. Consequently, we can write the expansions of the numerator and denominator in (24) in this small parameter. Retaining only the terms of the order of γ^2, we obtain

$$W_{SINIS}=\frac{f_0+\gamma^2f_1}{f_2+\gamma^2f_3}, \tag{27}$$

where

$$\begin{aligned}f_0=&1+2S(1+S)+2S(1-S)\cos 2k_1L+4S^{3/2}\sin 2k_1L;\\f_1=&-2+2S(1-S)(\cos 2k_0L-\cos 2k_1L)-2(1+2S)\cos[(k_0-k_1)L+\Phi]+4S^{3/2}(\sin 2k_0L-\sin 2k_1L)-4S\cos\Phi\{2(1-S)\cos[(k_0+k_1)L]+(1+2S)\cos[(k_0-k_1)L]+4S^{1/2}\sin[(k_0+k_1)L]\};\\f_2=&S^4+(1+S)^4+4S^2(1+S)^2\cos^2[(k_0-k_1)L]+2S^2\{[1+S^2-6S]\cos[2(k_0+k_1)L]+4S^{1/2}(1-S)\sin[2(k_0+k_1)L]\}+2S(1-S)[S^2+(1+S)^2]\times(\cos 2k_0L+\cos 2k_1L)+4S^{3/2}[S^2+(1+S)^2]\times(\sin 2k_0L+\sin 2k_1L);\\f_3=&-8S^2(1+S)^2-4S^3(1+S)-4S(1+S)^3-4S(1+S)[(1+S)^2+S^2]\cos[2(k_0-k_1)L]-8S^2\{(1+S^2-6S)\cos[2(k_0+k_1)L]+4S^{1/2}(1-S)\sin[2(k_0+k_1)L]\}-8S^2(1-S^2)(\cos 2k_0L+\cos 2k_1L)-4S(1-S)[S^2+(1+S)^2](\cos 2k_0L+\cos 2k_1L)-16S^{5/2}(1+S)(\sin 2k_0L+\sin 2k_1L)-8S^{3/2}[S^2+(1+S)^2](\sin 2k_0L+\sin 2k_1L)-4\cos\Phi\{[S^2+(1+S)^2]\cos[(k_0-k_1)L]+2S(1-S)\cos[(k_0+k_1)L]+4S^{3/2}\sin[(k_0+k_1)L]\}.\end{aligned}$$

The value $\gamma=0$ defines the position of resonant levels for a completely normal structure. It can be seen that, after a transition of the ''banks'' of the sandwich to the superconducting state, the relative displacement of these levels is determined by the small parameter γ^2.

Using formula (24), we can construct numerically the dependence of the transparency of an *SINIS* structure on the reciprocal energy $x=\Delta/E(x\leqslant 1)$ for the values of the parameters $\Phi=\pi/3$, $Q=0.1$, $Z=0.1$, $\Delta/\zeta=5\times10^{-3}$ (Fig. 2a), $Z=0.1$, $\Delta/\zeta=10^{-3}$ (Fig. 2b), and $Z=0.5$, $\Delta/\zeta=5\times10^{-4}$ (Fig. 2c). It can be seen that the transparency of the *SINIS* structure becomes equal to unity for certain energy values (resonant transparency levels of a two-barrier system).

The patterns of resonant spikes on the energy curves are also shown for comparison in the case of zero energy gap $\Delta=0$ (Fig. 3a) and for a finite gap $\Delta=10^{-4}$ eV (Fig. 3b) for the same values of other parameters of the structure (for example, we have chosen the values $Z=0.1$ and $\zeta=1$ eV). It can be seen that the period of oscillations increases when a finite gap is formed.

Let us consider various special cases of expression (24).

(1) Let us suppose that $Z=0$ (*SNS* junction). In this case, $\kappa=\kappa^*=1$, and formula (24) is transformed into the following expression[19–31]:

$$W_{SNS}=\left\{1+\frac{4\gamma^2}{(1-\gamma^2)^2}\sin^2[(k_0-k_1)L/2-\Phi/2]\right\}^{-1}. \tag{28}$$

Here the resonant spikes appear due to above-the-barrier reflection of quasiparticles at the gap edges.

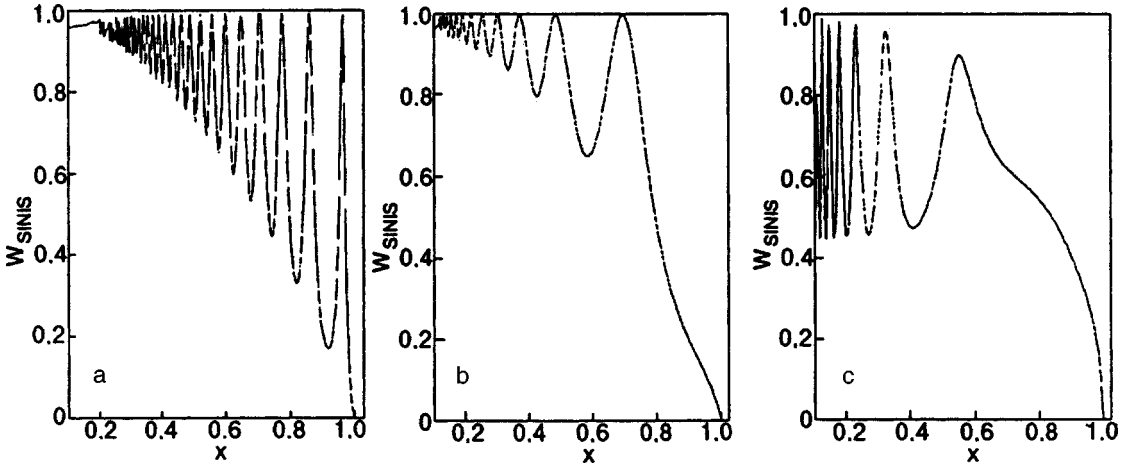

FIG. 2. Numerical calculation of the transparency coefficient W_{SINIS} as a function of $x=\Delta/E$. The chosen values of parameters: $\Phi=\pi/3$, $Q=0.1$, $Z=0.1$, $\Delta/\zeta=5\times10^{-3}$ (a), $Z=0.1$, $\Delta/\zeta=10^{-3}$ (b), and $Z=0.5$, $\Delta/\zeta=5\times10^{-4}$ (c).

(2) We put $\Delta=0$ ($\gamma=0$) (*NININ* structure). In this case, the transparency is given by[32,33]

$$W_{NININ}=\left\{1+4\left(\frac{mH}{k_0}\right)^2\left[\cos k_0L+\frac{mH}{k_0}\sin k_0L\right]^2\right\}^{-1}. \tag{29}$$

The ''quasi-local levels'' are defined by the equation

$$\tan k_0L=-k_0\hbar^2/mH.$$

The energy values of this structure are defined as $E=\hbar^2k_0^2/2m$.

(3) We put $d=0$ (*SIS* structure). The potential $V(z)$ in Eq. (3) assumes the form $2H\delta(z)$. As a result, the transparency of the system becomes

$$W_{SIS}=-\frac{1+4Z^2+2\gamma^2(1-\cos\Phi)(1+8Z^2)(1-\gamma^2)^{-2}}{[1+4Z^2+2\gamma^2(1-\cos\Phi)/(1-\gamma^2)^2]^2}. \tag{30}$$

In the case under consideration, there are no quasi-local states, but the transparency of the system is a function of the phase of the order parameter.

5. CONCLUSION

We studied the electron quantum states of a superconductor–insulator–normal metal– insulator–superconductor sandwich (*SINIS* structure). Metal films we assumed to be pure. The analysis was carried out on the basis of the Bogoliubov–de Gennes equations. We used the model of step-wise variation of the order parameter at film interfaces, which means that we disregarded the proximity effect. The model operates the better, the higher the intensity of electron scattering by an insulating barrier.

The main result obtained in this research is the derivation of the dispersion equation (11) for the quasiparticle spectrum of the *SINIS* sandwich, the quasiparticle energy

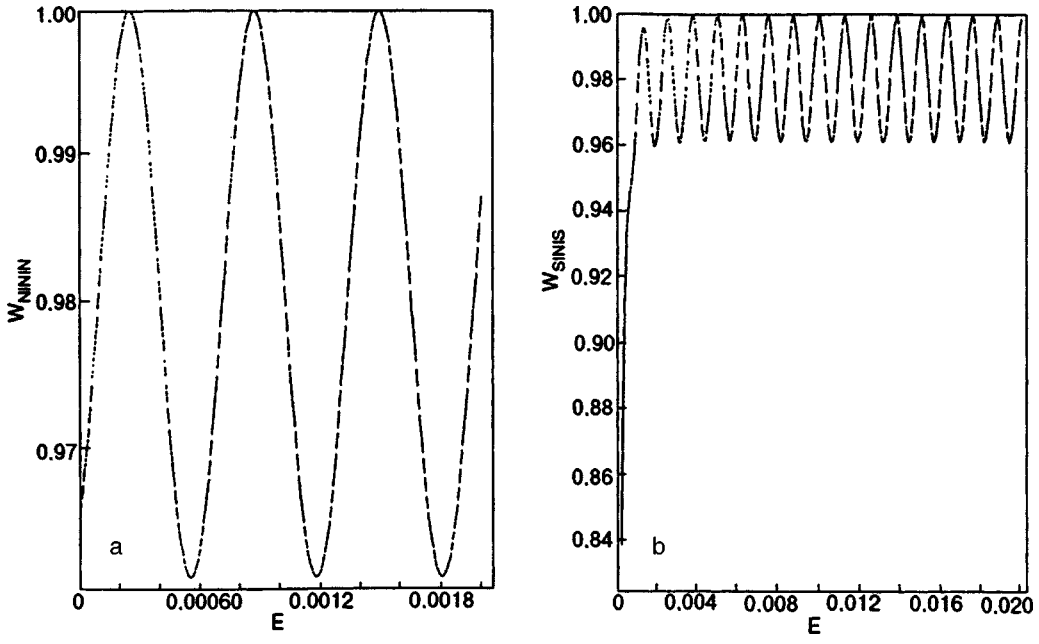

FIG. 3. Transparency coefficient as a function of energy E for $Z=0.1$, $\zeta=1$ eV, and different values of Δ, eV: 0 (a) and 10^{-4} (b).

being lower than the energy gap Δ of the superconductor. This equation describes interference effects induced by Andreev's scattering as well as by conventional reflection of quasiparticles at the interfaces between contacting media. The coefficients D_0, D_1, and D_2 are complex functions of the excitation energy. In the presence of current through the structure, the phase difference Φ of the order parameters appears only in the first term of the equation. The coefficient D_0 of this term does not depend on the parameter Z characterizing the intensity of the potential barrier, i.e., conventional scattering processes do not affect its value. The second term of the dispersion equation (11) describes rapid oscillations of the Friedel type, which emerge during particle–particle (or hole–hole) scattering. The third term in (11) describes oscillations with a large period, which are associated with Andreev's scattering mechanism.

If we confine the analysis of Eq. (11) only to Andreev's approximation and assume that conventional scattering does not take place ($Z=0$), the solution of this equation gives the spectrum of Kulik's quantized energy levels for the current state of an *SNS* junction. We derived an analytic expression for the quasiparticle spectrum in the case of a small $Z \ll 1$. It was noted that the dispersion equation (11) makes it possible to go beyond Andreev's approximation and calculate the quasiparticle spectrum taking into account corrections of the order of $(\Delta/\zeta)^2$, which is important for high-T_c superconductors.

We also studied the states of the continuous spectrum of quasiparticles for which the transparency coefficient W_{SINIS} for an *SINIS* sandwich is calculated as a function of E. The form of W_{SINIS} was obtained numerically for various values of the parameters of the problem. The plots of the dependences show that the transparency coefficient of the *SINIS* structure becomes equal to unity for certain energy values (resonant transparency levels of the two-barrier system).

The authors are grateful to A. N. Omelyanchouk for fruitful discussions and to D. V. Abraimov for his help in numerical calculations.

This research was carried out under financial support of the Ukrainian State Foundation for Fundamental Studied, grant No. 2.4/165.

APPENDIX

$$M_0 = -4(1-\gamma^2)\{e^{ik_1L}(1+\kappa)^2[1-e^{i(k_0-k_1)L}\gamma^2 e^{i\Phi}] + e^{-ik_1L}(1-\kappa)(1-\kappa^*)[1-e^{-i(k_0-k_1)L}\gamma^2 e^{i\Phi}]\}; \tag{A1}$$

$$M_1 = 4(1-\gamma^2)\gamma_+(1-\kappa^*)\{e^{ik_1L}(1+\kappa)[1 - e^{i(k_0-k_1)L}e^{i\Phi}] + e^{-ik_1L}(1+\kappa^*)[1 - e^{-i(k_0-k_1)L}e^{i\Phi}]\}; \tag{A2}$$

$$\begin{aligned} M_2 = {} & 32\gamma^2 \cos\Phi - e^{i(k_0+k_1)L}(1-\gamma^2)^2(1-\kappa^2)(1-\kappa^*) \\ & \times(1+\kappa) - e^{-i(k_0+k_1)L}(1-\gamma^2)^2(1-\kappa^{*2})(1+\kappa^*) \\ & \times(1-\kappa) - 2e^{i(k_0-k_1)L}\gamma^2(1+\gamma^2)(1+\kappa)(1+\kappa^*) \\ & + 2e^{-i(k_0-k_1)L}\gamma^2(1+\gamma^2)(1-\kappa)(1-\kappa^*) \\ & + 2e^{i(k_0-k_1)L}(1+\gamma^2)(1-\kappa^*)(1-\kappa) \\ & - 2e^{-i(k_0-k_1)L}(1+\gamma^2)(1+\kappa^*)(1+\kappa) \\ & + e^{-i(k_0-k_1)L}\gamma^2(1-\gamma^2)(1+|\kappa|^2)(1-\kappa)(1-\kappa^*) \\ & + e^{i(k_0-k_1)L}\gamma^2(1-\gamma^2)(1+|\kappa|^2)(1+\kappa)(1+\kappa^*) \\ & - e^{i(k_0-k_1)L}(1-\gamma^2)(1+|\kappa|^2)(1-\kappa^*)(1-\kappa) \\ & - e^{-i(k_0-k_1)L}(1-\gamma^2)(1+|\kappa|^2)(1+\kappa^*)(1+\kappa). \end{aligned} \tag{A3}$$

Here $\kappa = 1 - i2Z$.

*E-mail: gogadze@ilt.kharkov.ua

[1] L. V. Iogansen, Zh. Éksp. Teor. Fiz. **45**, 207 (1963) [Sov. Phys. JETP **18**, 146 (1963)].
[2] J. C. Penley, Phys. Rev. **128**, 596 (1962).
[3] R. Tsu and L. Esaki, Appl. Phys. Lett. **22**, 562 (1973).
[4] L. L. Chang and L. Esaki, Appl. Phys. Lett. **24**, 593 (1974).
[5] A. G. Aleksanyan, E. M. Belenov, I. N. Kompanets *et al.*, Zh. Éksp. Teor. Fiz. **83**, 1389 (1982) [Sov. Phys. JETP **56**, 799 (1982).
[6] A. F. Andreev, Zh. Éksp. Teor. Fiz. **46**, 1823 (1964) [Sov. Phys. JETP **19**, 1228 (1964)].
[7] R. Kummel, Z. Phys. **218**, 472 (1969).
[8] Yu. K. Dzhikaev, Zh. Éksp. Teor. Fiz. **68**, 295 (1975) [Sov. Phys. JETP **41**, 144 (1975)].
[9] R. Kummel, Phys. Rev. B **16**, 1979 (1977).
[10] S. N. Artemenko, A. F. Volkov, and A. V. Zaĭtsev, Pis'ma Zh. Éksp. Teor. Fiz. **76**, 1816 (1978) [*sic*].
[11] W. J. Tomasch, Phys. Rev. Lett. **16**, 16 (1966).
[12] W. J. McMillan and P. W. Anderson, Phys. Rev. Lett. **16**, 85 (1966).
[13] I. O. Kulik, Zh. Éksp. Teor. Fiz. **57**, 1745 (1969) [Sov. Phys. JETP **30**, 944 (1969)].
[14] C. Ishii, Prog. Theor. Phys. **44**, 1525 (1970).
[15] J. Bardeen and J. L. Johnson, Phys. Rev. B **5**, 72 (1972).
[16] A. V. Svidzinsky, T. N. Antsygina, and E. N. Bratus, J. Low Temp. Phys. **10**, 131 (1973).
[17] J. Demers and A. Griffin, Can. J. Phys. **49**, 285 (1971).
[18] A. Griffin and J. Demers, Phys. Rev. B **4**, 2202 (1971).
[19] G. E. Blonder, M. Tinkham, and T. M. Klapwijk, Phys. Rev. B **25**, 4515 (1982).
[20] C. Beenakker, Phys. Rev. Lett. **67**, 3876 (1991).
[21] G. Wendin and V. Shumeiko, Superlattices Microstruct. **20**, 569 (1996).
[22] P. G. de Gennes, *Superconductivity of Metals and Alloys*, Benjamin, New York (1966).
[23] A. A. Golubov and M. Yu. Kupriyanov, Zh. Éksp. Teor. Fiz. **96**, 1420 (1989) [Sov. Phys. JETP **69**, 805 (1989)].
[24] J. M. Rowell and W. J. McMillan, Phys. Rev. Lett. **16**, 453 (1966).
[25] A. Hahn, Phys. Rev. Lett. **B31**, 2816 (1985).
[26] A. N. Omelyanchouk, R. de Bruyn Ouboter, and C. J. Muller, Fiz. Nizk. Temp. **20**, 501 (1994) [Low Temp. Phys. **20**, 398 (1994)].
[27] M. Blaauboer, R. T. W. Koperdraad, A. Lodder, and D. Lenstra, Phys. Rev. B **54**, 4283 (1996).
[28] K. Karrai, E. J. Choi, F. Dunmore, *et al.*, Phys. Rev. Lett. **69**, 152 (1992).
[29] M. Hurd and G. Wendin, Phys. Rev. B **49**, 15258 (1994).
[30] G. A. Gogadze and I. O. Kulik, Zh. Éksp. Teor. Fiz. **60**, 1819 (1971) [Sov. Phys. JETP **33**, 984 (1971)].
[31] G. A. Gogadze, Fiz. Nizk. Temp. **12**, 1102 (1986) [Sov. J. Low Temp. Phys. **12**, 622 (1986).
[32] D. Bohm, *Quantum Theory* [Russian transl.], Moscow (1961).
[33] V. M. Galitskiĭ, B. M. Karnakov, and V. I. Kogan, *Problems in Quantum Mechanics* [in Russian], Nauka, Moscow (1981).

Translated by R. S. Wadhwa

Pulsed differential calorimetry of Zn-doped LSCO cuprates

G. G. Basilia, G. A. Kharadze, K. A. Kvavadze, and M. M. Nadareishvili

*Institute of Physics, Georgian Academy of Science, Tbilisi, Georgia**

D. F. Brewer, G. Ekosipedidis, and A. L. Thomson

*University of Sussex, Falmer, Brighton BN1 9QJ, U.K.***

(Submitted February 11, 1998)
Fiz. Nizk. Temp. **24**, 726–730 (August 1998)

The low temperature heat capacity measurements on LSCO samples containing Zn impurities have been performed by means of pulsed differential calorimetry technique. The interpretation of the Zn-concentration dependence of the residual γ-coefficient in the linear temperature part of $C_{\rm el}(T)$ at $T \ll T_c$ is consistent with a model based on the assumption of the *d*-wave symmetry of the order parameter of these superconducting copper oxides.
 [S1063-777X(98)00308-9]

1. INTRODUCTION

A great deal of effort has been applied to establish the symmetry properties of the ordered superconducting states of high-T_c cuprates. In contrast to the superfluid phases of liquid ^{3}He, for which the symmetries of the order parameters were established almost immediately after their discovery, the symmetry properties of the ordered states of high-T_c superconductors are still under debate after ten years of considerable experimental and theoretical activity. What is, however, now firmly established is that the Cooper pairs in high-T_c cuprates are in a spin-singlet state, and the main focus has become concentrated on the orbital structure of the order parameter.[1]

A considerable amount of information accumulated during recent years has clearly shown that the magnitude of the gap function $|\Delta(\mathbf{k})|$ of the high-T_c superconducting copper oxides is highly anisotropic in $\mathbf{k}$-space, but it is still necessary to explore the behavior of its phase which distinguishes, in particular, the *s*-wave-like and the *d*-wave-like properties of the Cooper-pair wave functions. Accordingly, phase-sensitive experiments on the order parameter have acquired special importance and among these the performance of Josephson-type measurements has proved to be the most direct way to establish the order parameter phase behavior. During the last few years these experiments have given valuable information about the orbital symmetry of $\Delta(\mathbf{k})$ in high-T_c superconductors[2] with strong support for the proponents of the $d_{x^2-y^2}$-type behavior of the Cooper-pair wave-function, although some controversy is still present, possibly connected with distortion of the pure *d*-wave-like order parameter near the crystal boundaries.[3]

Among other order-parameter phase-sensitive properties a response of the superconducting state to pair-breaking scattering events on various pointlike defects, localized on the conducting CuO_2 planes of the high-T_c superconducting cuprates, has also proved to be of great value. In contrast to the *s*-wave-like case the non-magnetic scattering centers strongly destroy the ordered state with $d_{x^2-y^2}$ symmetry.[4–7] This fact is intimately connected to the quantity $\langle\Delta(\mathbf{k})\rangle$—i.e., the average value of the superconducting gap function across the Fermi surface. In the case of Cooper pairing in the $d_{x^2-y^2}$ channel, we have

$$\Delta_d(\mathbf{k}) = \Delta(T)(\cos\, ak_x - \cos\, ak_y) \tag{1}$$

and $\langle\Delta(\mathbf{k})\rangle = 0$. This property of the *d*-wave state opens the way to a strong suppression of T_c by non-magnetic impurities (compare with Ref. 8)—an effect observed for various kinds of scattering centers introduced into high-T_c cuprates, including those which are generated as a result of a radiation damage.[9]

Another important effect of non-magnetic scattering centers on the properties of the *d*-wave paired state is the gradual filling of quasiparticle density of states near the Fermi level with increase in concentration of impurities. The gap function given by the Eq. (1) possesses nodes, $\Delta(\mathbf{k}) = 0$, along four lines on the cylindrical Fermi surface and due to this property the density of states N_f at the Fermi level is zero in the pure limit with the infinite quasiparticle mean free path. In the presence of an impurity scattering (at a finite value of the mean-free path l) the Fermi-level density of states $N_f \neq 0$ and increases with a decrease of l, as has been predicted in a number of theoretical investigations.[5–7] These observations are in a sharp contrast with what is expected in the case of an *s*-wave-like Cooper pairing with $\langle\Delta(\mathbf{k})\rangle \neq 0$. This state may also have very pronounced anisotropy in the (k_x, k_y) plane with a large difference between $\Delta_{\max}$ and $\Delta_{\min}$. One can even imagine an *s*-wave-like state with ''accidental'' zeros $\Delta_{\min} = 0$ along the same nodal lines on the Fermi surface as in the $d_{x^2-y^2}$ pairing case. This rather artificial (but instructive) situation is described by a gap function with the form

$$\Delta_s(\mathbf{k}) = \Delta(T)|\cos\, ak_x - \cos\, ak_y| \tag{2}$$

which again has $N_f = 0$ in the pure limit. In spite of the similar magnitudes of the gap functions in Eqs. (1) and (2), the response to impurity scattering of a superconducting state with even symmetry, corresponding to Eq. (2), is radically

different from what has just been described for the $d_{x^2-y^2}$ state, whose symmetry is odd. This happens because the impurity scattering events probe the phase properties of the order parameter and the phases of the gap functions given by Eqs. (1) and (2) behave quite differently. It can be shown[6,7] that, for a superconductor with an *s*-wave-like pairing described by Eq. (2), instead of filling the quasiparticle states at the Fermi level, a finite gap ε_g in the density of states grows up as a result of impurity scattering. In a more realistic *s*-wave-like case with $\Delta_{\min}\neq 0$ the impurity scattering pushes the gap to a value $\varepsilon_g > \Delta_{\min}$ which simply means that in this case the impurities tend to smear out any initial in-plane anisotropy of the superconducting states. These very different responses of superconductors with conventional (*s*-wave-like) and unconventional (*d*-wave-like) order parameters to the phase-sensitive impurity scattering events have proved to be a good probe of the symmetry of the order parameter in the high-T_c cuprates.

A drastic difference in the quasiparticle spectral density near the Fermi energy for impurity-containing *s*-wave-like and *d*-wave-like ordered states has an immediate influence on the character of the low temperature behavior of the specific heat of superconductors providing one more possibility of exploring the symmetry properties of the high-T_c copper oxide systems.[10,11] Although heat capacity measurements contain less direct information than Josephson experiments, they probe bulk properties of samples and are not sensitive to possible distortions of the order-parameter symmetry near the crystal boundaries.

2. EXPERIMENTAL METHOD

We have performed low temperature heat capacity measurements on a family of LSCO samples doped with Zn by means of pulsed differential calorimetry technique. When using a differential method one measures the difference ΔC of the heat capacities of the sample of interest and the reference sample with known $C(T)$. Continuous and pulsed heating regimes can be used. The former method has been successfully applied in recent investigations of fundamental properties of a number of high-T_c superconductors (see, for example, Refs. 12 and 13). The pulsed differential calorimeter designed by us[14] combines the high sensitivity of the continuous heating type differential calorimeter and the high accuracy of a classical pulsed calorimeter.

The measuring unit consists of two identical cells holding the sample of interest and the reference sample. The cells are connected by means of a thermal link so that before application of a heat pulse of duration Δt, as well as after some relaxation time $\tau \gg \Delta t$, the two samples are in thermal equilibrium. At all stages adiabatic conditions are maintained.

The time evolution of the sample temperature is given by the equations

$$T_1(t)-T_i=\frac{1}{C_1}\int_0^t \dot{Q}(t')dt', \qquad T_2(t)-T_i=\frac{1}{C_2}\int_0^t \dot{Q}(t')dt', \tag{3}$$

where $T_1(0)=T_2(0)=T_i$ is an initial temperature (before the heat pulse) and the heat-power input $Q=IV$ is supplied simultaneously to both samples by means of an electric heater. From (3) it is seen that

$$C_1\Delta T=IV\Delta t-\Delta\dot{Q}, \quad C_2\Delta T=IV\Delta t+\Delta Q, \tag{4}$$

where $\Delta T=T_f-T_i$ and $\Delta Q=K\int_0^\infty \delta T(t)dt$ is an amount of heat transferred between the samples through the thermal link (with thermal conductivity K) due to the temperature difference $\delta T(t)$ present between the two thermal equilibrium states. Finally, the measured heat capacity difference $\Delta C=2\Delta Q/\Delta T$.

3. LOW-TEMPERATURE CALORIMETRY OF $La_{2-x}Sr_xCu_{1-y}Zn_yO_4$

We have investigated a zinc-doped LSCO series of samples by carrying out accurate measurements on their specific heats using our pulsed differential calorimetry techniques. Six samples of $La_{2-x}Sr_xCu_{1-y}Zn_yO_4$ were studied, all with an optimal level of hole doping ($x=0.16$), and with Zn concentrations of $y=0.00$; 0.01; 0.02; 0.033; 0.045 and 0.06. The sample containing 6 at.% of Zn was used as the reference sample since it was certainly not a superconductor and, indeed, was in a metallic state. The samples were fabricated by a standard solid-state reaction in which the initial combination of the constituent chemical compounds was done via solid state mixing and then the samples were sintered at a temperature of 1030 K while being subjected to a high pressure. The resulting sample pill was then ground up and the sinter process was repeated again in the presence of a high pressure. Subsequent measurements of the susceptibility showed that the samples with Zn concentrations of 0.00, 0.01 and 0.02 had superconducting transition temperatures of ~38 K, ~26 K and ~15 K, respectively. The samples with concentrations of 0.033 and 0.045, on the other hand, displayed no superconducting transitions for temperatures down to 4.2 K, which was the lowest temperature of our susceptibility measurements.

In the results reported below, the differential specific heat

$$\Delta C(y,T)=C(y,T)-C(0.06,T) \tag{5}$$

of the five samples with $y=0.00$; 0.01; 0.02; 0.033 and 0.045 were measured over the temperature interval 2–60 K, where the sample with the 0.06 Zn concentration was being used as the reference sample. As an example, the raw data for the sample which contained no zinc, $\Delta C(0,T)$, are presented in Fig. 1 where a pronounced peak at the superconducting transition temperature, $T_c\cong 37$ K, for this nominally pure sample ($y=0$) is evident.

The specific heat difference ΔC can be represented as a sum of electronic and phonon contributions:

$$\Delta C=\Delta C_{\rm el}+\Delta C_{\rm ph}. \tag{6}$$

Since Zn is isoelectronic with the Cu for which it is substituted, we may assume that the contribution $\Delta C_{\rm el}$ will, in the normal state, depend only upon the hole concentration x (and not upon y). This contribution is a term which is linear in

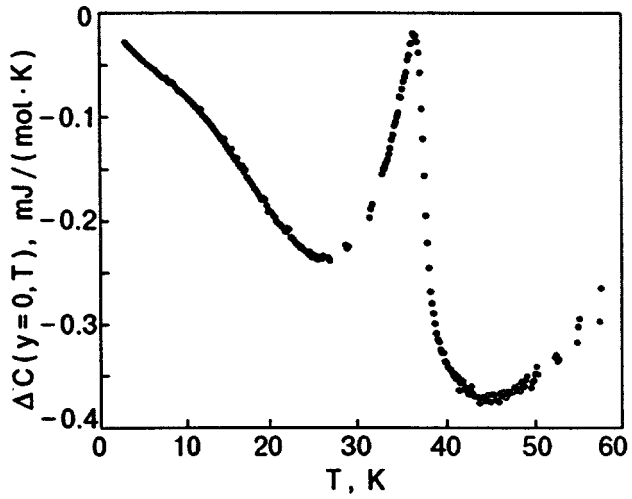

FIG. 1. Raw data for $\Delta C(y=0,T)$. A pronounced peak is clearly seen at $T_c \approx 37$ K.

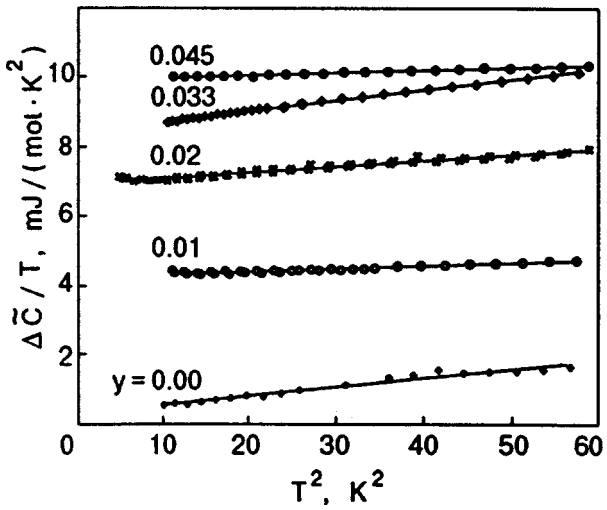

FIG. 3. Plots of $\Delta\tilde{C}/T$ as a function of T^2 in the low-temperature region ($T<8$ K).

temperature, $\gamma_N T$, where γ_N is the Sommerfeld coefficient, and it is convenient to eliminate this contribution from the measured values of the quantity $\Delta C(y,T)/T$. For the reference sample, in its metallic state, the Sommerfeld coefficient γ_N, which could be obtained from the linear term in the specific heat, can be considered to remain constant over the whole temperature range and, therefore, for the sample of concentration $x=0.16$ we have put $\gamma_N = 10$ mJ/(mol·K^2), in accordance with known results. Then, having settled upon this value for γ_N, we are able to obtain values for the function $\Delta\tilde{C}/T = \Delta C/T + \gamma_N$, which are presented in Fig. 2 for the samples with concentrations $y=0.00$, 0.01 and 0.02, and these clearly show the suppression produced in the transition temperature T_c by the addition of Zn impurities.

As was mentioned in the introduction, besides the suppression of T_c, the impurity scattering has a profound influence on the low temperature ($T \ll T_c$) properties of a superconducting state with strong anisotropy of the gap function $\Delta(\mathbf{k})$ especially in the case of an unconventional (singular) behavior of its phase (as for *d*-wave Cooper pairing). In the low temperature domain $\Delta\tilde{C}/T$ can be represented as

$$\frac{\Delta\tilde{C}}{T} = \gamma(y) + \Delta\beta T^2, \tag{7}$$

where the residual $\gamma(y)$ should be zero for $y=0$ in the case of the $d_{x^2-y^2}$ symmetric order parameter since $\gamma(y) \propto N_f(y)$ and $N_f(0)=0$ due to the nodes of $\Delta(\mathbf{k})$ on the Fermi surface. The T^2 term in (7), in addition to the phonon contribution, is expected to have an electronic contribution in the case of a *d*-wave like order parameter.[5]

Having plotted $\Delta\tilde{C}/T$ as a function of T^2, as shown in Fig. 3, we are able to find $\gamma(y)$ from the intercepts on this graph. The dependence of γ at low temperatures on the Zn concentration is shown in Fig. 4. It is seen that $\gamma(y)$ increases rapidly with y and then levels out for $y>0.04$. This behavior is consistent with the earlier measurements[10,11] which have been interpreted in terms of the $d_{x^2-y^2}$-wave Cooper pairing model, predicting a gradual filling of the density of states at the Fermi level.

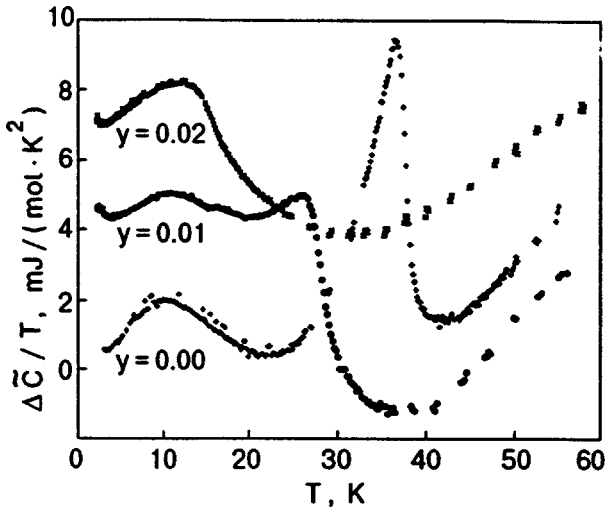

FIG. 2. Temperature dependence of $\Delta\tilde{C}/T = \Delta C/T + \gamma_N$ for three samples with Zn concentration $y=0.00$; 0.01 and 0.02.

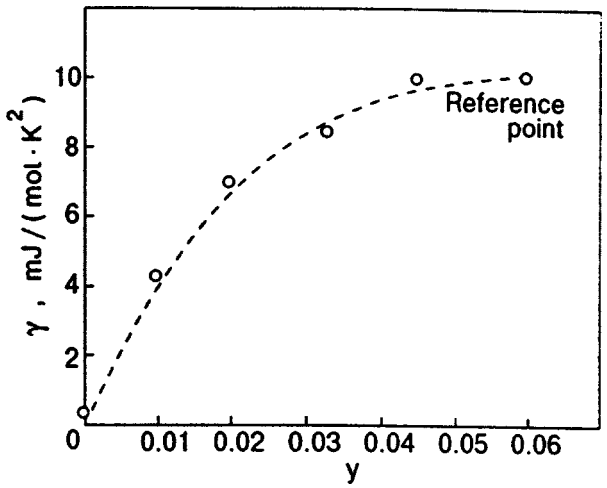

FIG. 4. Dependence of γ-coefficient on the Zn concentration.

We have to keep in mind that, according to the *d*-wave pairing scenario, the temperature dependence given by Eq. (7) is expected for temperatures $T<T^*$, where T^* is a disorder-dependent crossover temperature. In the temperature range $T^*<T\ll T_c$ a term with a linear dependence on T should appear in Eq. (7) due to a linear dependence of the quasiparticle density of states on the excitation energy $\varepsilon=|E-E_F|$ at low values for these energies ($\varepsilon^*<\varepsilon\ll\Delta$). Below T^* the impurity induced deviation from this linear dependence takes over.[15] In the case of a sample with no impurities we should have $\gamma(0)=0=T^*$ and a contribution with a linear dependence on temperature should be present for temperatures $T\ll T_c$ ($\Delta\tilde{C}/T=\alpha T+\Delta\beta_{\rm ph}T^2$). We note that, according to our data, $\gamma(0)\neq 0$ (although it is rather small) indicating that in our nominally pure sample ($y=0$) there is some amount of disorder and $T^*\neq 0$. This could be the cause of optimal hole doping where the α-coefficient is expected to be the smallest and T^* should be the largest at a given impurity scattering rate.

In conclusion, using pulsed differential calorimetry technique we have confirmed that the scattering of quasiparticles on Zn impurities present in LSCO high-T_c superconductor has a pronounced influence on low-temperature thermodynamic properties. An interpretation of the Zn-concentration dependence of the residual γ-coefficient of the linear temperature part of $C_{\rm el}(T)$ is consistent with a model based on the assumption of the *d*-wave symmetry of the order parameter of these superconducting copper oxides.

This work was partly supported by the INTAS Grant N1010-CT93-0046.

The authors are indebted to J. W. Loram for discussion of our experimental results and for providing us with the results of his own measurements prior to publication.

*E-mail: gogi@iph.hepi.edu.ge
**E-mail: d.f.brewer@sussex.ac.uk

[1] D. J. Scalapino, Phys. Rep. **250**, 331 (1995).
[2] D. J. Van Harlingen, Rev. Mod. Phys. **67**, 515 (1995).
[3] S. R. Bahcall, Phys. Rev. Lett. **76**, 3634 (1996).
[4] R. J. Radtke, K. Levin, H. B. Schuttler, and M. R. Norman, Phys. Rev. B **48**, 653 (1993).
[5] T. Hotta, J. Phys. Soc. Jpn. **62**, 274 (1993).
[6] L. S. Borkovski and P. J. Hirschfeld, Phys. Rev. B **49**, 15404 (1994).
[7] R. Fehrenbacher and M. R. Norman, Phys. Rev. B **50**, 3495 (1994).
[8] A. I. Larkin, JETP Lett. **2**, 130 (1965).
[9] E. M. Jackson, B. D. Weaver, G. P. Summers, P. Shapiro, and E. A. Burke, Phys. Rev. Lett. **74**, 3033 (1995); S. K. Tolpygo, J.-Y. Lin, M. Gurvitch, S. Y. Hou, and J. M. Phillips, Phys. Rev. B **53**, 12454 (1996).
[10] N. Momono and M. Ido, Physica C **264**, 311 (1996); N. Momono, M. Ido, T. Nakano, M. Oda, Y. Okajima, and K. Yamaya, Physica C **233**, 395 (1994).
[11] M. Hiroi, H. Sato, M. Sera, and S. Kobayashi, Physica C **235/240**, 1779 (1994).
[12] J. W. Loram, K. A. Mirza, J. R. Cooper, and W. Y. Liang, Phys. Rev. Lett. **71**, 1740 (1993).
[13] J. W. Loram, K. A. Mirza, J. R. Cooper, N. Athanassopou, and W. Y. Liang, *10th Anniversary HTS Workshop*, Houston, March (1996).
[14] K. A. Kvavadze and M. M. Nadareishvili, Patent N1610415 (1991).
[15] P. J. Hirschfeld, W. O. Putikka, and D. J. Scalapino, Phys. Rev. Lett. **71**, 3705 (1993); P. J. Hirschfeld and N. Goldenfeld, Phys. Rev. B **48**, 4219 (1993).

This article was published in English in the original Russian journal. It was edited by R. T. Beyer.

Quasiperiodic superconducting V/Zr multilayers: critical magnetic fields and crossover

N. Ya. Fogel, V. G. Cherkasova, M. Yu. Mikhaĭlov, Yu. V. Bomze, O. I. Yuzephovich, and I. M. Dmitrenko

*B. Verkin Institute for Low Temperature Physics and Engineering, National Academy of Sciences of the Ukraine, 310164 Kharkov, Ukraine**

A. N. Stetsenko

State Polytechnic University, 310002 Kharkov, Ukraine
(Submitted March 10, 1998)
Fiz. Nizk. Temp. **24**, 731–736 (August 1998)

Critical magnetic fields parallel and perpendicular to the planes of quasiperiodic superconducting Fibonacci multilayers (ML) consisting of vanadium and zirconium are measured. The temperature dependence of the parallel critical field $H_{c\|}$ displays two crossovers. The $H_{c\|}(T)$ dependence is of square-root type in the vicinity of the transition temperature T_c and linear at low temperatures. Between these temperature intervals, the dependence follows a power law: $H_{c\|}\sim(1-T/T_c)^{\alpha}$, $\alpha=0{,}78\pm0{,}02$. The complex nature of this dependence can be explained in the framework of the Ginzburg–Landau theory for a quasiperiodic ML, as well as by the scaling theory for fractal multilayers which takes into account the different structure length scales in the case of ML with a complex sequence of layers. © *1998 American Institute of Physics.* [S1063-777X(98)00408-3]

1. INTRODUCTION

Investigations of the properties of superconducting multilayers (ML) have been carried out for a number of years. The majority of publications concerns the structural, normal and superconducting properties of periodic ML. Many experimental data and theoretical models for these ML have been systematized in a number of reviews.[1–7]

In addition to the standard periodic ML, layered systems of simpler (superconducting sandwiches)[8–10] as well as more complicated types (ML with a double periodicity, random and fractal ML,[11,12] and quasiperiodic ML[13,14]) were also studied. The use of other structural patterns leads to a significant variation of the results for critical fields as compared to the results for periodic ML. In particular, the temperature dependence of the critical field $H_{c\|}(T)$ parallel to the layers of fractal and quasiperiodic ML can be represented in the form

$$H_{c\|}\sim(T_c-T)^{\alpha}. \tag{1}$$

The exponent α lies in the interval $0.5<\alpha<1$, does not coincide with any of the limiting values[1)] and depends on fractal dimensionality[11] or on the characteristic wavelength Λ_F of the quasiperiodic multilayer,[13] the coupling constant for the materials used, and the layer thickness.[15,16] On the other hand, periodic multilayers are characterized by the limiting values 1 and 0.5 of the exponent α, corresponding to the three- and two-dimensional behavior, respectively.[6,17]

In this work, we present the results of investigation of the critical fields for quasiperiodic V/Zr multilayers, which indicate that the difference in the behavior of the $H_{c\|}(T)$ dependence for quasiperiodic and periodic ML may be more pronounced than that following from the works of Karkut *et al.*[13] and Cohn *et al.*[14] In particular, one cannot rule out the oscillatory temperature dependence of $H_{c\|}$ associated with the spatial inhomogeneity of a quasiperiodic ML at different scales of length.[18] Similarities in the dependence of quasiperiodic and fractal ML are also discussed.

2. SAMPLE PREPARATION AND MEASURING TECHNIQUE

Fibonacci type quasiperiodic multilayers were obtained by successive condensation of Zr and V vapor from two electron-beam vaporizers on (001) substrates of fluorophlogopite (FP) and Al_2O_3, heated to a temperature of 600 °C in a vacuum of $(2-6)\times10^{-5}$ Pa. We believe that as in the case of periodic ML,[19] multilayers deposited on fluorophlogopite are most perfect from the structural point of view. The layer thickness was monitored during the process of deposition by a quartz resonator. In order to decrease the roughness associated with the island mechanism of growth, some of the layers were deposited on a Zr sublayer of thickness 400 Å deposited preliminarily on the substrate. These samples were also covered by a thick Zr layer to prevent possible manifestation of surface superconductivity (in the case of a magnetic field applied parallel to the layers) which may mask the peculiarities in the behavior of $H_{c\|}$ associated with the internal structure of the sample.

The method of fabrication of Fibonacci-type quasiperiodic ML was described by Merlin *et al.*[20] Such a multilayer structure is formed by two blocks A and B. In our case, each block consists of a layer of vanadium and a layer of zirconium. All Zr layers have the same thickness $d_{Zr}=20$ Å, while the V layers had a thickness 60 Å in block A and 29 Å in block B. The thickness of individual layers was chosen in such a way that the ratio of thicknesses of the blocks is equal to the ''golden'' number $G=(1+\sqrt{5})/2$. The alternation of

blocks was determined by the Fibonacci quasiperiodic sequence $ABAABABAABAAB\ldots$.[20] The characteristic wavelength of the quasiparticle multilayer is defined as $\Lambda_F = Gd_A + d_B$ (here d_A and d_B are the thicknesses of blocks A and B respectively). For the multilayers investigated by us, $\Lambda_F = 180$ Å. If such a method is used for constructing multilayers, the sequence of layers is self-similar. Such a ML is shown schematically in Ref. 13. All samples contain 43 layers.

The electron-microscopic and electron-diffraction studies of samples revealed an axial texture in the layers with the axis [001] for Zr and [110] for V, oriented along the normal to the layer plane. The crystallites in ML had a size ~ 200 Å.

The technique used for measuring critical fields was the same as that used for periodic multilayers.[17,21] The critical fields H_c were defined at the middle of the resistive transitions $R(H)$. The magnetic field was oriented parallel to the layers to within $\sim 0.2°$, while the error in temperature measurement did not exceed $\sim 10^{-3}$ K. The superconducting transition temperatures T_c of samples deposited on different substrates do not differ significantly. The width ΔT of the resistive transition $R(T)$ for $H=0$ is quite small. The lowest value $\Delta T/T_c \simeq 1\times 10^{-2}$ was registered for the sample deposited on a fluorophlogopite substrate (the value ΔT describes the broadening of resistive transition between the points $0.1R_n$ and $0.9R_n$). Owing to the small broadening of the transition, the values of T_c are determined with a fairly high degree of accuracy, which is essential for calculating the reduced temperature $\tau = (T_c - T)/T_c$ which plays a significant role in the analysis of experimental data.

3. EXPERIMENTAL RESULTS AND DISCUSSION

Figure 1 shows the temperature dependence of parallel and perpendicular critical fields for ML deposited on FP. The dependence $H_{c\perp}(T)$ for quasiperiodic ML is qualitatively similar to that for periodic ML or films, while it can be seen from Figs. 1 and 2 that the dependence of $H_{c\parallel}$ is nontrivial. In the vicinity of T_c, this dependence is square-root-like while the dependence at the lowest temperatures attained experimentally becomes linear. These two regions of the $H_{c\parallel}(T)$ dependence are separated by a quite broad temperature interval in which $H_{c\parallel} \sim (T_c - T)^{\alpha}$, $\alpha = 0.78 \pm 0.02$. Thus, the temperature dependence of $H_{c\parallel}$ displays two crossovers. Samples deposited on sapphire substrates also reveal two crossover points, but the linear region of the dependence $H_{c\parallel}(T)$ for these samples begins at a lower temperature. The presence of the upper and lower Zr layers does not affect the form of the dependence $H_{c\parallel}(T)$, i.e., surface superconductivity is obviously not observed in samples without protective Zr layers either. Samples deposited on different substrates have practically the same value of α, which means that the smoothness of the interfaces for layer thicknesses used by us does not affect the dependence of the critical field $H_{c\parallel}$ significantly. It must be mentioned that Cohn *et al.*[14] also observed double crossover on the dependence $H_{c\parallel}(T)$ for some quasiperiodic Nb/Ta samples.

Kitaev and Levitov[15,18] studied theoretically the behavior of critical fields of quasiperiodic ML by using the Ginzburg–Landau approximation. Their results show that the same exponent is retained for the perpendicular field $H_{c\perp}(T)$ as for periodic ML: the coherence length $\xi_{\parallel} \sim \tau^{-1/2}$; $H_{c\perp} - \tau$; $\xi_{\parallel}(\tau) = [\varphi_0/2\pi H_c(\tau)]^{1/2}$ where φ_0 is the magnetic flux quantum and $\tau = (T_c - T)/T_c$. In the field parallel to the layers, the dependence for different ML is not universal, and the exponent α for the critical field $H_{c\parallel}(T) \sim \tau^{\alpha}$ varies in the interval $0.5 < \alpha < 1$ depending on the structure and superconducting parameters of quasiperiodic ML. It is pointed out that since the scaling for Fibonacci layers at the second-order

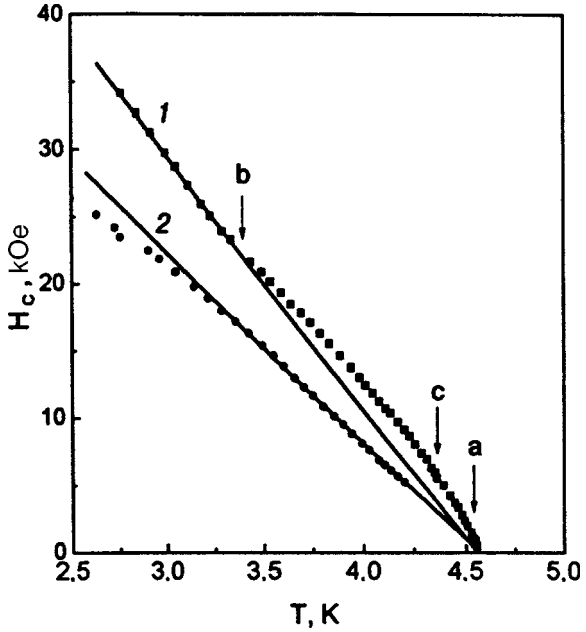

FIG. 1. Temperature dependence of critical magnetic fields parallel (*1*) and perpendicular (*2*) to the layers in quasiperiodic ML V/Zr. *a* and *b* are crossover points. The meaning of point *c* is described in the text.

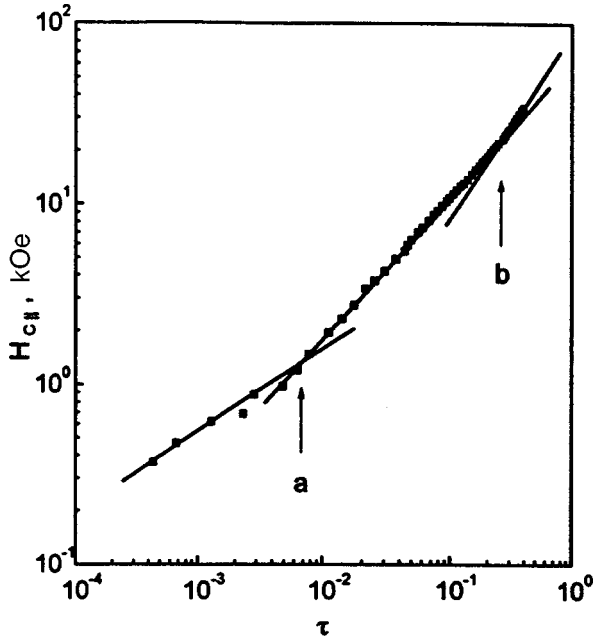

FIG. 2. Dependence of parallel critical magnetic field $H_{c\parallel}$ on the reduced temperature $\tau = (T_c - T)/T_c$. *a* and *b* are crossover points.

phase transition points should be observed only upon an increase in the scale by a factor Φ ($\Phi=[(1+\sqrt{5})/2]^2$ is the square of the golden number), the $H_{c\|}(T)$ dependences may be more complicated than power dependences. The $H_{c\|}(\tau)$ dependence may display singularities with a period $2\gamma \ln \Phi(\gamma=1/(2\alpha-1))$.[18,22] An analysis of the data obtained by Karkut *et al.*[13] for one of the samples was carried out by Kitaev and Levitov who obtained the value $\alpha=0.74$. Some departures from this dependence may be observed at higher temperatures.[15]

Let us compare the experimental results with the above-mentioned theory of quasiperiodic layered structures.[15,18] According to the calculations made by Kitaev and Levitov,[15] the $H_{c\perp}(T)$ dependence was found to be linear for the investigated ML. However, the $H_{c\|}(T)$ dependence is much more complicated. According to Figs. 1 and 2, the main features of this dependence can be described as follows. There are three well-defined temperature intervals with different types of $H_{c\|}(T)$ dependence. The exponent for $H_{c\|}$ is close to 0.5 (0.43) in the immediate vicinity of T_c. At the lowest temperatures for which the $H_{c\|}(T)$ dependence was measured, the exponent is equal to unity, and the linear dependence $H_{c\|}(T)$ is extrapolated to the same critical temperature that was obtained from the $R(T)$ measurements in zero magnetic field. A power dependence of $H_{c\|}$ with an exponent 0.78 was observed between these two intervals. The $\ln \tau$ interval between the two crossover points (a and b in Figs. 1 and 2) is 3.64. This value differs by just 8% from the parameter $2\gamma \ln \Phi$ which is equal to 3.37 for the sample under consideration. However, it would not be proper to state that the experimentally observed dependence $H_{c\|}(T)$ reflects the oscillatory dependence predicted by Kitaev and Levitov,[18] since one cannot speak of any periodicity in the narrow temperature interval over which the experimental results were obtained. It should be remarked that the large value of the period makes it difficult to detect such a periodicity in experiments. Measurements of $H_{c\|}$ at lower temperatures are not very promising since the crossover point b is ''too close'' to $T=0$ if we take into consideration the expected periodicity in $\ln \tau$. On the other hand, measurements at temperatures close to T_c are too complicated for the existing facilities for temperature measurement. For our samples, one may expect to observe an additional period on the oscillatory dependence $H_{c\|}(\tau)$ only if a sufficiently large number of experimental points are obtained in an interval 10^{-3} K in the vicinity of T_c. There are better chances of detecting oscillations in samples with comparatively smaller values of γ.

Although the double crossover situation has not been interpreted unambiguously so far, it is obvious that the experimental results are consistent with the theoretical predictions.[15,16,18]

On the other hand, the behavior of quasiperiodic ML is similar in certain respects to the expected behavior of fractal ML. According to calculations made by using the scaling theory,[11] fractal ML must display a number of crossovers corresponding to the conditions

$$\xi_{\perp n}(T)=S_n.$$

Here $S_n=2^{(n-1)/D}S_1$ are the characteristic scales of length in the fractal lattice, S_1 is the smallest scale of length in a given ML, D the fractal dimensionality, n the number of various scales, and $\xi_{\perp n}(T)$ the coherence length in the direction perpendicular to the layers for each scale of lengths. According to calculations,[11] the dependence $H_{c\|}(T)$ must be close to linear away from T_c (i.e., at low temperatures where the smallest scale of lengths in fractal ML is significant), while the two-dimensional situation should prevail in the vicinity of T_c, i.e., for large length scales. In the intermediate temperature interval, the behavior of $H_{c\|}$ (i.e., the value of α) is determined by fractal dimensionality. In our experiments, a similar situation is observed in quasiperiodic ML. In some respects, the quasiperiodic ML are more ordered than fractal ones, but we can single out in such ML not only the period Λ_F, but also a number of structurally determined characteristic lengths associated with the size of solitary blocks and their combinations. As in the case of any ML system, the transverse coherence length in such a ML is defined by the relation

$$H_{c\|}(T)=\varphi_0/2\pi\xi_{\|}(T)\xi_{\perp}(T).$$

The temperature dependence of the critical field $H_{c\perp}$ (see Fig. 1) can be used to determine the value of $\xi_{\|}(0)$ for the sample under investigation. This parameter is found to be equal to 71 Å. Using the value of the critical fields $H_{c\|}$ in the region of their linear variation with temperature, we arrive at the value $\xi_{\perp}(0)=54$ Å. Accordingly, we obtain the value $\xi_{\perp 1}(T)=101$ Å at the crossover temperature T_1 (point b in Figs. 1 and 2). This value is close to the size of the BB block (98 Å). Obviously, the dependence $H_{c\|}(T)$ cannot display smaller structural lengths, i.e., sizes of the blocks A and B separately, since their characteristic length $d_A, d_B<\xi_{\perp}(0)$.

On the other hand, it follows from the theory[11] that in the immediate vicinity of T_c, where large characteristic lengths are significant, the behavior of the fractal ML must be close to two-dimensional, and

$$H_{c\|}\sim \tau^{1/2}/-\ln\ \tau. \tag{2}$$

Here, the small logarithmic correction is connected with the influence of three-dimensional long-range interaction.

We observed just such a behavior for the investigated quasiperiodic ML in the vicinity of T_c. According to the data shown in Fig. 2, we obtain the dependence $H_{c\|}\sim\tau^{0.43}$ in the interval of temperatures close to T_c. Plotting the data in coordinates $H_{c\|}$ vs. $\tau^{1/2}/-\ln\tau$ (Fig. 3), we find that the interval of $2D$ behavior is even broader. In the interval between the two regions discussed above, the index α differs from 0.5 and 1. Note that the dependence $H_{c\|}(T)$ described by formula (2) is in better agreement with the experimental data than the power dependence with index 0.5, and is observed over a much broader temperature interval than the latter. The point of crossover from the dependence (2) to the dependence $H_{c\|}\sim\tau^{\alpha}$ is marked by letter c in Fig. 1. It should also be noted that the value of index α obtained in this way for the interval between points c and b is equal to 0.763 ± 0.002, and differs slightly from that obtained in the interval between the points a and b (the value of α was determined in both cases by the method of least squares), but has a much lower dispersion.

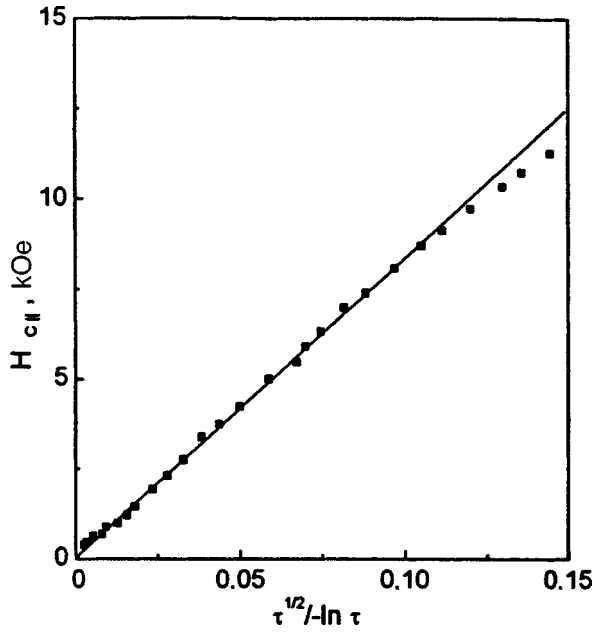

FIG. 3. Dependence of parallel critical magnetic field $H_{c\|}$ on $\tau^{1/2}/-\ln\tau$.

Thus, the behavior of the dependence $H_{c\|}(T)$ in quasiperiodic V/Zr multilayers, which is characterized by the existence of a double crossover, is described quite adequately by the theory developed by Kitaev, Burlachkov, and Levitov[15,16,18] for such systems. On the other hand, the existence of two crossover points and the peculiarities of the temperature dependence of $H_{c\|}$ can also be explained by the Matijasevic-Beasley theory[11] for fractal ML. The possibility of interpretation of experimental results by using quite different approaches does not carry any inherent contradictions since quasiperiodic and fractal ML contain structural elements with different scales of lengths, which is quite significant in the case when the magnetic field is oriented parallel to the layers.

In conclusion, the authors are pleased to express their thanks to L. I. Glazman and especially to L. S. Levitov for discussion of the results and for providing information about some unpublished results, as well as for recommending the choice of materials constituting the ML aa well as the film thickness.

*E-mail: fogel@ilt.kharkov.ua

[1)]Quasiperiodic ML with small values of Λ_F,[13] which display a nearly two-dimensional behavior, i.e. for which the value of $\alpha\sim 0.5$, are an exception to this rule.

[1] M. R. Beasley, in *Inhomogeneous Superconductors* [Berkeley Springs Conf., Ed. by H. C. Wolfe], New York (1979).
[2] M. R. Beasley, in *Percolation, Localization, and Superconductivity* [Ed. by A. M. Goldman and S. A. Wolf], Plenum Press, N.Y., London (1983).
[3] S. T. Ruggiero and M. R. Beasley, in *Synthetic Modulated Structures*, Academic Press, New York (1985).
[4] V. Matijasevic and M. R. Beasley, in *Artificially Structured Materials*, Amsterdam (1987).
[5] B. Ya. Shapiro, Metallofizika **9**, 3 (1987).
[6] B. Y. Jin and J. B. Ketterson, Adv. Phys. **38**, 189 (1989).
[7] I. K. Schuller, Solid State Commun. **92**, 141 (1994).
[8] N. Ya. Fogel' and V. G. Cherkasova, Zh. Éksp. Teor. Fiz. **109**, 223 (1996) [JETP **82**, 118 (1996)]
[9] V. G. Cherkasova, N. Ya. Fogel', and A. S. Pokhila, Fiz. Nizk. Temp. **20**, 1245 (1994) [Low Temp. Phys. **20**, 975 (1994)].
[10] D. Neerinck, K. Temst, C. Van Haesendonck *et al.*, Phys. Rev. B **43**, 8676 (1991).
[11] V. Matijasevic and M. R. Beasley, Phys. Rev. B **35**, 3175 (1987).
[12] A. Sidorenko, C. Sürgers, T. Trappman, and H. v. Löhneysen, Phys. Rev. B **53**, 11751 (1996).
[13] M. G. Karkut, J. M. Triscone, D. Ariosa, and O. Fisher, Phys. Rev. B **34**, 4390 (1986).
[14] L. Cohn, J. J. Lin, F. J. Lamelas *et al.*, Phys. Rev. B **38**, 2326 (1988).
[15] A. Yu. Kitaev and L. S. Levitov, Pis'ma Zh. Eksp. Teor. Fiz. **45**, 83 (1987) [JETP Lett. **45**, 67 (1987)].
[16] L. I. Burlachkov and L. S. Levitov, Physica C **158**, 88 (1989).
[17] L. I. Glazman, I. M. Dmitrenko, V. L. Tovazhnyanskiĭ *et al.*, Zh. Éksp. Teor. Fiz. **92**, 1461 (1987) [Sov. Phys. JETP **65**, 821 (1987)].
[18] A. Yu. Kitaev and L. S. Levitov, Zh. Éksp. Teor. Fiz. **95**, 311 (1989) [Sov. Phys. JETP **68**, 176 (1989)].
[19] V. L. Tovazhnyanskiĭ, A. N. Stetsenko, A. I. Fedorenko *et al.*, Fiz. Nizk. Temp. **15**, 828 (1989) [Sov. J. Low Temp. Phys. **15**, 459 (1989)].
[20] R. Merlin, K. Bajema, R. Clarke *et al.*, Phys. Rev. Lett. **55**, 1768 (1984).
[21] E. I. Bukhshtab, V. Yu. Kashirin, N. Ya. Fogel' *et al.*, Fiz. Nizk. Temp. **19**, 704 (1993) [Low Temp. Phys. **19**, 506 (1993)].
[22] L. S. Levitov, Private Communication.

Translated by R. S. Wadhwa

Influence of mechanisms of nonequilibrium quasiparticle scattering on the properties of phase-slip centers

G. E. Churilov, A. B. Agafonov, D. A. Dikin, and V. M. Dmitriev

*B. Verkin Institute for Low Temperature Physics and Engineering, National Academy of Sciences of the Ukraine, 310164 Kharkov, Ukraine**

(Submitted March 27, 1998)
Fiz. Nizk. Temp. **24**, 737–749 (August 1998)

Electrical characteristics of homogeneous superconducting tin films with phase-slip centers (PSC) and with structures of the superconductor–normal metal–superconductor (SNS) type are studied experimentally. It is found that near the superconducting transition temperature, elastic scattering of nonequilibrium quasiparticles can play a significant role in PSC by reducing the effective charge disbalance time, and hence the diffusion length for quasiparticles as compared to similar processes in the SNS structure. The application of an external electromagnetic field of frequency $\sim 10^{10}$ Hz in the vicinity of the superconducting transition temperature reduces the resistance of the SNS structure to zero, indicating a superconducting transition in the N region. An increase in the transport current results in the formation of the first PSC just in this region. Non-Josephson oscillations appear in this region at certain temperatures, currents, and radiation power. © *1998 American Institute of Physics.* [S1063-777X(98)00508-8]

INTRODUCTION

Long quasi-one-dimensional superconductors (narrow films or filaments with transverse dimensions smaller than the coherence length $\xi(T)$), in which the critical density j_c of the Ginzburg–Landau pair-breaking current[1] is attained, display a dynamic resistive state,[2,3] characterized by the formation of phase-slip centers (PSC) distributed along the sample at temperatures below the superconducting transition temperature T_c (Fig. 1a). In the regions of their formation, the modulus of the complex order parameter $|\psi|$ of Cooper pairs vanishes periodically with the Josephson frequency ω_J, its phase χ experiencing a jump by a magnitude multiple of 2π. At the instance when the modulus of the order parameter (the energy gap Δ of the superconductor) vanishes at the PSC (Fig. 1c), this region of the generally superconducting film becomes a source of excess quasiparticle excitations involves in the charge transport (normal current) through the sample. As a result, the time-averaged transport current contains both superconducting (j_S) and the normal (j_N) components (Fig. 1d). The presence of the latter component leads to energy dissipation in the resistive state. The structure of a solitary PSC has been studied in detail both theoretically[4] and experimentally.[5–7] However, many aspects (especially the nonstationary dynamics of PSC) remain unclear.

A PSC is a symmetric one-dimensional spatial structure consisting of several nonequilibrium regions in which certain dynamic processes dominate. It was found theoretically[4] and experimentally[6] that three spatial regions embedded into one another can be singled out in a PSC (Fig. 1b). These regions are mutually connected, and hence the designations of individual parts of PSC are conditional and reflect the dominating processes.

The central and the smallest region in the PSC structure is its core having a size of the order of the coherence length $\xi(T)$ in the superconductor. This region is a source of excess quasiparticles, leading to disbalance of the electron- and hole-like branches in the excitation spectrum of the nonequilibrium superconductor, and remains least comprehensively studied in view of technological difficulties involved in preparing the required samples. It has been found experimentally that the chemical potential μ_s of Cooper pairs in this region undergoes an abrupt jump,[5] while the currents j_N and j_S as well as the energy gap Δ oscillate with the Josephson frequency ω_J.[2,6] At the center of this region, the gap Δ vanishes periodically, remaining small outside this region. Energy gap oscillations induce balanced oscillations of the superconducting and normal currents at the Josephson frequency[7] (the so-called Carlson–Goldman mode[8]) at the core and in its neighborhood. Thus, the core is a source of strong deviations from equilibrium and stability of the entire PSC structure.

The second region of the PSC extends from the core in both directions to distances of the order of $d_n(T) = [\xi(T) l_E(T)]^{1/2}$,[4] where l_E is the depth of penetration of a weak longitudinal electric field in the superconductor. The Josephson oscillation amplitude of Δ decreases rapidly, and the superconducting component j_S of transport current remains small so that the entire current is carried practically by normal excitations. For this reason, the given region can be referred to as quasi-normal. It was proved that the deviations from stability in the electric potential due to non-Josephson oscillation (NJO) at the boundaries of this region is characterized by a much lower frequency than in the PSC core.[9,10] In this research, this instability will be considered most thoroughly.

In the third PSC region extending on both sides from the core over distances of the order of the depth $l_E(T)$ of penetration of a longitudinal electric field into the superconductor, the superconducting (j_S) and the normal (j_N) cur-

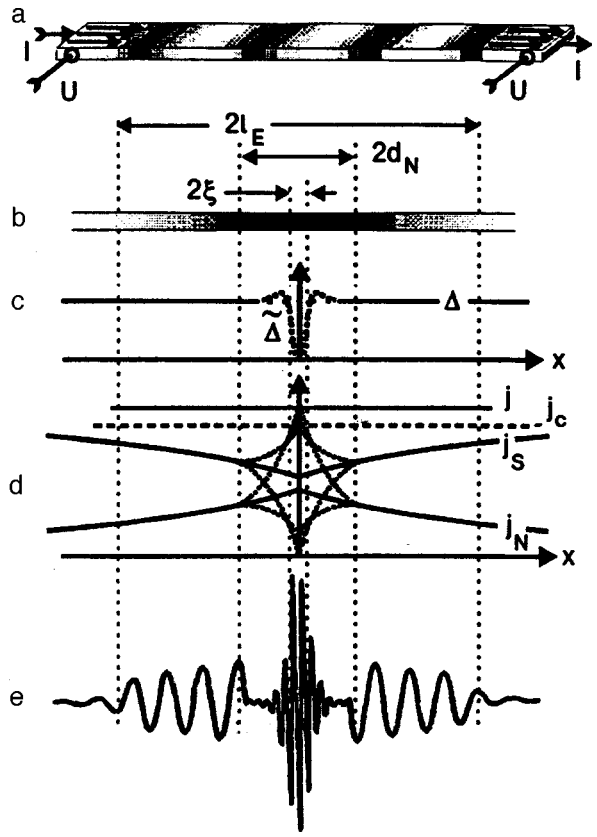

FIG. 1. Structure of a phase-slip center: schematic diagram of a narrow superconducting film with PSC emerging for current $I>I_c$ (a), the structure of a solitary PSC, where $2l_E=2l_E(T)$ is the length of the nonequilibrium region, $2\xi=2\xi(T)$ the core size, and $2d_N=2[\xi(T)l_E(T)]^{1/2}$ the length of the quasi-normal region (b), the distribution of energy gap Δ along PSC and its oscillations $\tilde{\Delta}$ in the core region (c), distribution of total current j and time-averaged normal (j_N) and superconducting (j_S) currents along PSC; dotted curves in the quasinormal region $2d_N$ mark the boundaries in which the superconducting and normal currents oscillate (d), and schematic diagram of plasma oscillations excited in individual parts of PSC, i.e., high-frequency (Carlson–Goldman mode) in the core and low-frequency (NJO mode) in nonequilibrium regions (e).

rents coexist as before, but the amplitudes of their oscillations are insignificant. This nonequilibrium region of the PSC is the longest. All relaxation process occur in this region and practically terminate at its boundaries. For this reason, the time-averaged voltage drop across a film with a single PSC is mainly determined (if we neglect the contribution from the core) by the length $2L_E(T)$ of the nonequilibrium region. The size of this region is determined by various relaxation mechanisms in the superconductor.[11]

It has been established reliably that inelastic electron–phonon scattering with the characteristic time τ_ε determining $l_E(T)$ plays a significant role in a superconductor near T_c. At lower temperatures, when the energy gap width differs from zero considerably, much stronger current is required for creating a resistive state. It was proved theoretically[12,13] that the motion of Cooper pair condensate at a large velocity becomes itself a source of elastic scattering of quasiparticles. This reduces the relaxation time as compared to τ_ε, and accordingly changes the electric field penetration depth $l_E(T)$,[14] which was confirmed experimentally.[15,16]

Nevertheless, we shall prove that relaxation of quasiparticles in PSC at sample temperatures very close to the superconducting transition temperature can be due to both scattering mechanisms described above.

Moreover, a PSC becomes a source of NJO in a narrow range of temperatures and currents (see above). This points to the emergence of special processes of relaxation of nonequilibrium quasiparticles in PSC leading to excitation of low-frequency potential oscillations. According to the model[17,18] proposed on the basis of a large number of experimental results, the emergence of the low-frequency instability of PSC is due to relaxation to the level of energy gap Δ of quasiparticles that have acquired a certain energy ε_1 as a result of multiple Andreev's reflections inside the quasinormal region $2d_N(T)$.[6] If the level ε_1 in the region of the $N-S$ interface is at the edge of the energy gap Δ in the range of operation of weak high-frequency (Josephson) oscillations, so that $(\varepsilon_1-\Delta)\sim\Delta\gamma^{3/2}$, the probability of relaxation of nonequilibrium quasiparticles with such an energy due to photon bremsstrahlung is much higher than the probability of the phonon scattering mechanism.[18,19] Here the depairing factor[4] $\gamma=\hbar/(2\tau_\varepsilon\Delta)$ and is approximately equal to 10^{-2} for tin. The fulfillment of these conditions for the PSC structure (and hence the existence of NJO) is possible only in a very narrow interval of temperatures and currents. The energy liberated for such a relaxation excites weakly attenuating collective plasma oscillations[20] of superconducting electrons at frequency $\omega_0\approx(\varepsilon_1-\Delta)/\hbar$ much lower than the Josephson frequency in the third nonequilibrium region of the PSC. This determines the small amplitude of such low-frequency plasma oscillations. The electron–phonon scattering remains the main relaxation mechanism for the remaining nonequilibrium quasiparticles being injected.

The penetration of a longitudinal electric field into a superconductor to a depth $l_E(T)$, i.e., the coexistence of the superconducting and normal current components, is also observed for the transport of electric charge through the junction between a normal metal and a superconductor.[21] In an SNS structure with two $N-S$ interfaces, nonequilibrium regions of the size $l_E(T)$ each are formed on both sides of the N layer. At first sight, these are the same nonequilibrium regions as in a PSC, which is hence similar to an SNS structure. However, the difference is that the energy gap as well as the superconducting and normal currents in the core of a PSC oscillate with the Josephson frequency, while only normal current exists in the N region of length larger than $2\xi_N(T)$ of an SNS structure, and there is no energy gap. Moreover, the time-averaged supercurrent in a PSC is approximately equal to $0.6j_c$, always tending to the critical value at a distance $l_E(T)$ from the core, i.e., at the edge of the nonequilibrium region.[2] On the other hand, the supercurrent in an SNS structure (in which the superconducting current within the normal layer is equal to zero) can attain its critical value at the boundary between the nonequilibrium region and the superconductor only when the total transport current is equal to or larger than the critical current. Consequently, the nonequilibrium regions of a PSC are always under the conditions of higher density of the condensate of Cooper pairs than in an SNS structure.

Taking into account what has been said above, it is necessary to compare PSC and *SNS* structures created (if possible) in the same sample under the same external conditions (temperature and transport current) and to find out in which cases and which relaxation mechanism for nonequilibrium quasiparticles play a decisive role in their resistive behavior. We have made an attempt to excite NJO in an *SNS* structure in a high-frequency electromagnetic field, thus simulating PSC with the help of the *SNS* structure.

1. EXPERIMENTAL RESULTS

1.1. Experimental methods and technique

The resistive state of narrow films is usually studied at temperatures close to the superconducting transition temperature ($T/T_c = 0.95-0.999$) in order to eliminate overheating and hysteresis processes. Besides, a PSC becomes a source of NJO just in this temperature range under certain voltage across the PSC (see above). In the tin films under investigation at the same temperatures, $\xi(T) \cong 1$ μm, and the size $2d_N(T)$ of the quasi-normal region of the PSC amounts to several micrometers, while $2l_E(T)$ can be as large as 20–30 μm.

For this reason, a correct comparison of PSC (including those under the NJO conditions) and *SNS* structures can be compared correctly at these temperatures if we place an insert of a normal metal of length from one to a few micrometers in a narrow superconducting film of width of the order of $\xi(T)$ and length not smaller than $2l_E(T)$ across the current. It is also important that the $N-S$ interfaces are ''clean'' and not lead to additional mechanisms of inelastic scattering during charge transport. This problem can be solved most easily by reducing locally the superconducting transition temperature of the superconducting film due to the proximity effect[22] in its contact with a normal metal.

The samples for the experiments described here were prepared as follows. A filamentary indium single crystal (whisker) of diameter 6–8 μm was pressed across a narrow tin film (having a width of the order of 1 μm) (see the inset to Fig. 2). Since the value of T_c for In is approximately 0.3 K lower than superconducting transition temperature for Sn, a region with a smaller energy gap due to the proximity effect was formed in the region of their contact. The diffusion of In into Sn led with time to an additional suppression of superconductivity in the region of junction. Continued diffusion of

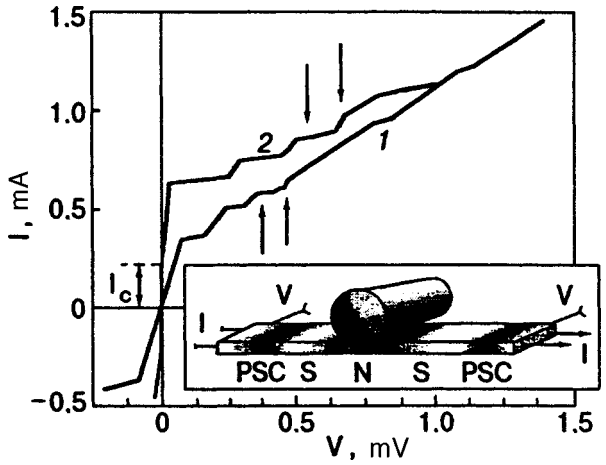

FIG. 2. Typical current–voltage characteristics of a superconducting film with an insert of a normal metal (curve *1*) and with a phase-slip center (curve *2*) in the ''weak'' region. The arrows on the two IVC mark the regions in which NJO are excited for definite currents. The inset shows schematic diagram of the sample under investigation carrying current I. Here PSC are the phase-slip centers formed in the superconducting part of the film and N is the normal region formed due to proximity effect due to the normal whisker lying across the film.

In increased its local concentration, and gradually penetrated on both sides of the junction. As a result, the length of the region with the lower superconducting transition temperature (the length of the normal insert) increased. This allowed us to investigate *SNS* structures with different length of the N region on the same sample in the temperature range between the values of T_c of Sn and In.

The experiments on such samples revealed that they possess another interesting property. The superconducting temperature of the In–Sn alloy can change from the value of T_c for In to temperatures exceeding the value of T_c for Sn depending on the In concentration. For example, an alloy containing 30% In and 70% Sn has a superconducting transition temperature near 7.3 K.[23] For this reason, we could also study *NSN* structures in the course of In diffusion into a Sn film.

All the experiments discussed here were made on superconducting Sn films with a normal metal insert and without it; the basic parameters of the samples are given in Table I. Here d, w and L are the thickness, width, and length of the film. The superconducting transition temperature T_c, the film resistance R_{300} and $R_{4.2}$ at 300 and 4.2 K, as well as

TABLE I. Physical parameters of superconducting Sn films under investigation.

Sample number	d, nm	w, μm	L, μm	T_c, K	R_{300}, Ω	$R_{4.2}$, Ω	$\xi(0)$, nm	$l_E(0)$, μm	l_{eff}, nm
1*	58	1.4	47	3.822	82	7.5	101	1.69	94.4
2*	174	1.5	34	3.779	17.5	0.72	127.2	2.59	221.4
3*	294	1.8	43	3.802	11	0.41	130.1	2.73	245.4
4	378	1.8	76	3.789	15	0.42	138	3.16	330
5	684	2.4	63	3.76	5.1	0.089	148	4.03	535
6*	698	1.8	84	3.767	8.9	0.173	198.8	3.8	479.2
7	850	1.4	68	3.825	7.9	0.43	123	3.6	190
8	950	2.6	54	3.77	2.9	0.037	153	4.72	735

Remark: Asterisks on sample numbers indicate samples without normal inserts.

$\xi(0), l_E(0)$, and the effective mean free path l_{eff} were measured before the formation of the N insert in the film.

An analysis of the resistive state on the samples carrying direct current was carried out by the traditional four-probe method with analog recording of current–voltage characteristics (IVC) and a high accuracy of the choice and stabilization of temperature ($\delta T \leqslant 2\times 10^{-4}$ K).

Besides, we tried to simulate nonstationary dynamics of PSC in a non-Josephson *SNS* structure to a certain extent by placing it in an external rf electromagnetic field. The radiation frequency varied from 10^9 to 10^{10} Hz, and the power of the external rf generator was supplied to the sample along a coaxial line through a coupling capacitor, i.e., in the preset current mode.

1.2. DC experiments

The transition of the samples from the normal to the superconducting state was determined from their current–voltage characteristics (IVC). At first, the superconducting transition occurred at a certain temperature T_c in a long tin film except in the ''weak'' region (N-insert). The N inset became superconducting upon cooling to T_c^0.

In the general form, the IVC of samples with an N insert at temperatures $T_c > T > T_c^0$ at which an *SNS* structure is formed is a superposition of the IVC of two series-connected parts of the sample: the superconducting film and a part of the same film in the normal state. A typical IVC has the form shown by curve *1* in Fig. 2. The initial slope for small currents is determined by the residual ohmic resistance of the normal part of the film, which determines its size. A further increase in direct current leads to a transition of the main part of the long narrow film to the resistive state. In this case, the IVC (curve *1* in Fig. 2) first displays a voltage jump at a certain current, indicating the attainment of the critical current for the formation of the first PSC, followed by the step structure at large currents, which is typical of samples with several PSC.

At temperatures below T_c^0, the IVC displays the critical current (curve *2* in Fig. 2) which is much smaller than the current corresponding to the formation of the remaining PSC. It can be seen from the figure that the differential resistance of the sample at small currents, which is determined by the first PSC (the initial slope on curve *2*) is smaller than the resistance of the *SNS* structure (the initial segment of curve *1*). This decrease in resistance has the form of a jump in a narrow temperature interval $\sim 10^{-2}$ K during a transition through T_c^0. It was proved experimentally for a large number of samples that such a difference in the differential resistances of PSC and *SNS* structures emerges and increases in the films upon a decrease in the mean free path (other conditions being the same).

A typical resistive transition for a sample with a normal insert is depicted in Fig. 3.

It was mentioned above that the diffusion of indium into a tin film increases the length of the normal region and the residual resistance of the sample, For this reason, the temperature dependences $R(T)$ measured with an interval of about a few weeks after sample preparation remain functionally similar for a certain time (curves *1* and *2* in Fig. 4), and only a slight decrease in T_c^0 and an increase in the residual resistance were observed. The normal Sn–In region became more and more inhomogeneous with time, and the resistive transition changed significantly (curve *3* in Fig. 4). Such a sample displayed complete superconducting transition only at a temperature close to T_c for In (3.5 K). The onset of the superconducting transition was not displaced for all the three curves, indicating the invariability of the superconducting transition temperature of the matrix Sn film. We do not give any temporal characteristics of the rate of sample ageing since this process is determined by many factors like temperature, film thickness, and thermal cycling.

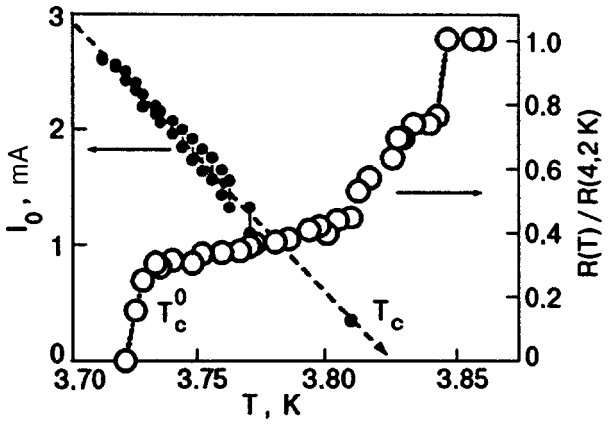

FIG. 3. Temperature dependences of the film resistance $R(T)$ during a transition of the sample from the normal to the superconducting state and of the current corresponding to generation of NJO, measured in sample No. 7 with an insert of a normal metal.

The samples with a normal insert studied by us also displayed NJO. It was found that low-frequency oscillations of the potential are induced only for a transport current exceeding the current of PSC formation in a pure Sn film, their characteristics being independent of the state (N or S') of the ''weak'' region. This is illustrated in Fig. 2 where the region of emergence of NJO on IVC is marked by vertical

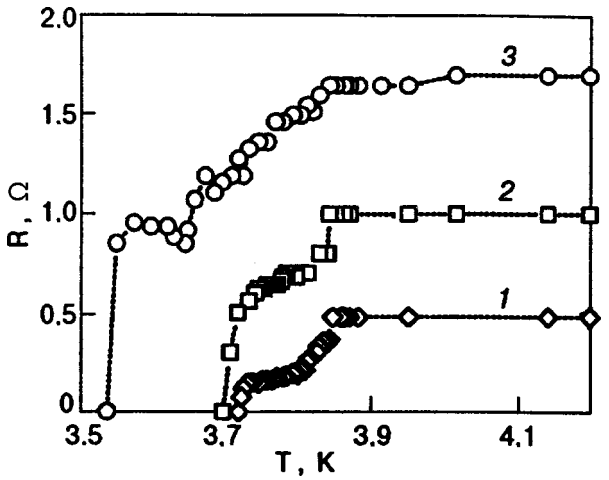

FIG. 4. Time variation of the resistive transition $R(T)$ in a sample with a normal insert. Curves *2* and *3* were measured 5 and 110 days respectively after the first measurement.

arrows. Moreover, Fig. 3 shows the temperature dependence $I_0(T)$ of the current corresponding to the region of existence of NJO together with the resistive transition curve for a sample with a normal insert. The point of intersection of the former curve with the temperature axis determined the local value of the superconducting transition temperature of the Sn film in the region of emergence of NJO. This method was developed and verified in our previous experiments on a large number of samples.[24] Thus, NJO are generated beyond the junction between the In whisker and the Sn film, i.e., in the resistive part of the sample which is a pure tin film.

1.3. Analysis of IVC in external electromagnetic field

In order to simulate high-frequency dynamics of PSC, we made experiments to determine the effect of electromagnetic field on the characteristics of samples with an *SNS* structure. The oscillation frequency of the order parameter in PSC measured near the superconducting transition temperature lies between 10^9 and 10^{10} Hz. For this reason, we choose the frequency of external radiation in the same frequency range. In the temperature interval corresponding to the existence of an *SNS* structure ($T_c > T > T_c^0$) under the effect of rf radiation in a certain power interval, we observed superconductivity stimulation in the homogeneous region of the film as well as the emergence of superconductivity in the ''weak'' region during a transition of the normal part to the superconducting state. In the former case, IVC displayed an increase in the critical current corresponding to the formation of PSC in the homogeneous part of the Sn film, while in the latter case we observed the vanishing of resistance for a small transport current and the emergence of the critical current. This current increased with the rf power, attained a certain maximum value, and then decreased to zero starting from certain values of power. The results of these experiments are shown in Fig. 5 presenting IVC measured for different radiation levels on one of the samples. The emergence of the critical current in the ''weak'' region and the voltage jump associated with it indicated the formation of a PSC in this region under the action of the electromagnetic field.

In this case, the samples becomes a source of NJO in narrow intervals of rf power, direct current, and temperature. It is important to note that in the absence of an external electromagnetic field, the film became a source of NJO at temperatures $T < T_c^0$ for the same values of the critical current of the ''weak'' region as in the case of superconductivity stimulation, but for much larger transport currents.

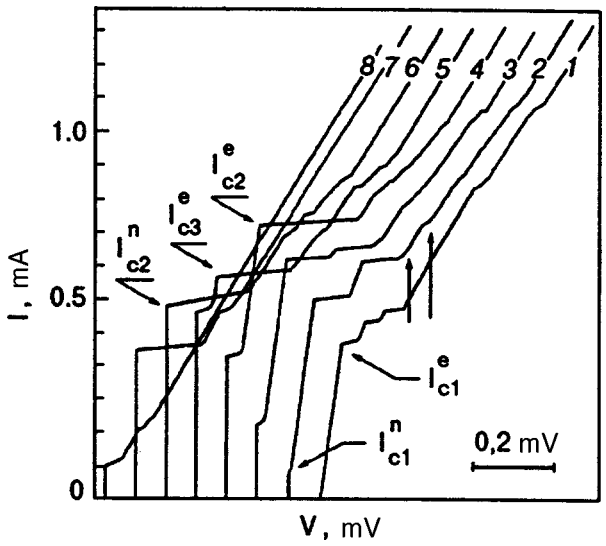

FIG. 5. IVC of a sample with an insert of a normal metal, measured at different irradiation levels (a larger number of IVC corresponds to a higher power). The arrow mark the region of existence of NJO, I^e_{c1} and I^n_{c1} are critical currents for the homogeneous part of the sample and weak region respectively, and I^n_{c2} is the maximum value of the ''weak'' link current attained in the superconductivity stimulation mode.

2. DISCUSSION OF RESULTS

2.1. Electrical properties of *SNS* structure and PSC in direct current

The dc analysis of the temperature dependence of the resistance for samples with an *N* insert revealed that a transition from the normal to the superconducting state in them occurs in two stages, which follows from the presence of two steps on the $R(T)$ curves for a sample shown in Figs. 3 and 4.

The first abrupt decrease in the sample resistance at $T = 3.845$ K (see Fig. 3) is associated with the onset of a superconducting transition in the homogeneous tin film. The sample resistance ultimately vanishes at $T = 3.72$ K. This temperature is lower than T_c of the Sn film, but is still much higher than the superconducting transition temperature for In (3.41 K). Consequently, we can assume that the normal region formed in the film at $3.72\ \text{K} < T < 3.845\ \text{K}$ is mainly due to the local suppression of T_c of the film due to the proximity effect exerted by the In whisker. In this temperature range, the sample had the form of an *SNS* structure in which parts of the long superconducting film of width $\sim 1\ \mu$m were superconducting ''banks,'' and the role of the normal insert was played by the part of the same film in the normal state. For this reason, the residual resistance of the sample is determined by the normal segment a few micrometers long, depending on the size of the contact region between the film and the whisker, as well as nonequilibrium segment of the superconductor adjoining it on both sides.

The depth $l_E(T)$ of penetration of a weak longitudinal electric field in the superconductor at the $N-S$ interface is determined in the general case by the length of diffusion of quasiparticles into the superconductor:[25]

$$l_E(T) = \sqrt{D\tau_Q(T)}. \tag{1}$$

Here $D = l_{\text{eff}} v_F/3$ is the diffusion coefficient for quasiparticles with the mean free path l_{eff} and the Fermi velocity v_F, and τ_Q is the charge disbalance relaxation time. Charge imbalance in a superconductor can relax due to various mechanisms. According to the theory[26] if we take into account all known relaxation processes in a nonequilibrium superconductor, the effective relaxation time of charge disbalance is defined as

$$\tau_Q = \frac{4kT_c}{\pi\Delta}\sqrt{\tau_\varepsilon/(2\Gamma)}, \tag{2}$$

where

$$\Gamma = \frac{1}{2\tau_\varepsilon} + \frac{1}{\tau_s} + \frac{D(2mv_s)^2}{2\hbar^2} + \frac{D}{2\Delta}\left(-\frac{\partial^2\Delta}{\partial r^2}\right). \tag{3}$$

Expression (3) takes into account electron scattering mechanisms characterized by the time τ_ε of inelastic scattering at the Fermi surface, the time τ_s of scattering by magnetic impurities with spin flip, the time of elastic scattering in the presence of a superfluid momentum $2\mathbf{m}v_s$, and gap anisotropy along the coordinate.

The Sn films under investigation contain no magnetic impurities, and hence the second term in formula (3) is equal to zero. In addition, the contribution to relaxation of excitations due to anisotropy of Δ is negligibly small since the variation of Δ at the $N-S$ interface occurs at a distance of the order of the coherence length ξ which is much smaller than the penetration depth l_E for a longitudinal electric field. If the resistive transition is studied with a small measuring current (much smaller than the critical current), the contribution of pair breaking mechanism due to velocity v_s of the superconducting component can be neglected also. As a result, the factor Γ is equal to $1/(2\tau_\varepsilon)$, and the effective relaxation time depends only on inelastic electron–phonon scattering. In this case, according to (2), τ_Q can be expressed in terms of the energy gap Δ and the time τ_ε of the electron–phonon interaction:

$$\tau_Q(T) = \frac{4kT_c}{\pi\Delta(T)}\,\tau_\varepsilon. \tag{4}$$

This expression for the charge disbalance relaxation time, which was mentioned by several authors, is a particular case of (2) taking into account the electron–phonon scattering alone.

For superconductors with a weak link (including tin), the energy gap near T_c can be defined as in Ref. 27:

$$\Delta(T) = 1{,}74\Delta(0)\sqrt{1-T/T_c}. \tag{5}$$

If we take into account the fact that $\Delta(0) = 1.76kT_c$, the value of effective relaxation time for charge disbalance in a nonequilibrium superconductor adjoining the $N-S$ boundary is defined as

$$\tau_Q(T) = 0{,}42\tau_\varepsilon(1-T/T_c)^{-1/2}. \tag{6}$$

Using formulas (1) and (6), we can write the temperature dependence $l_E(T)$ of the size of the nonequilibrium region in the form

$$l_E(T) = l_E(0)(1-T/T_c)^{-1/4}. \tag{7}$$

It can be seen from Fig. 3 that a transition from the normal to the superconducting state starts at 3.845 K, followed by a small plateau extending to $T = 3.825$ K. In this interval, individual segments of the film obviously go over to the superconducting state, and the entire film becomes superconducting at $T_c = 3.825$ K. The fact that this is the critical point was confirmed by the measurements of the temperature dependence of transport current corresponding to the emergence of NJO and its extrapolation to zero. The temperature T_c which is critical for the region of emergence of NJO coincides with the temperature corresponding to the end of the first short plateau on the $R(T)$ curve. Upon a further decrease in temperature ($T_c^0 < T < T_c$), the sample resistance is determined by the resistance $R_N(T)$ of the normal insert as well as the resistance $R_E(T)$ of nonequilibrium regions. If we assume that R_N is independent of temperature, the shape of the resistive transition curve $R(T)$ must reflect the temperature dependence of the depth $l_E(T)$ of penetration of a longitudinal electric field into the superconductor. The total length of the nonequilibrium region is equal to $2l_E(T)$ since the resistive state is formed on both sides of the normal insert, and the temperature dependence is determined only by the relaxation mechanism.

For the length $L = 68\ \mu$m of the film whose resistive transition is depicted in Fig. 3, the contribution of the purely normal region to the sample resistance in the absence of In diffusion along the film is much smaller than the contribution from nonequilibrium regions $l_E(T)$ since the length of these regions near the superconducting transition temperature can be of the order of tens of micrometers. We compared the experimental dependence $R(T)$ depicted in Fig. 3 with the calculated value of the resistance $R_{SNS}(T)$ in a region of length $[l_N + 2l_E^{\rm ph}(T)]$, where L_N is the length of its purely normal part, and $l_E^{\rm ph}(T)$ is the depth of penetration of a longitudinal electric field into the superconductor in the case of inelastic electron–phonon relaxation, which is determined from (1) and (4). Since the sample is a film of uniform cross section, we calculated the contribution to the resistance from the region $2l_E^{\rm ph}(T)$ by multiplying the residual resistance per unit length R_r/L at 3.845 K by the length of the nonequilibrium region: $R_E(T) = (R_r/L)2l_E^{\rm ph}(T)$. This resistance is supplemented with the contribution of the resistance of the normal insert, which is equal to $(R_r/L)l_N$. Thus, the $R_{SNS}(T)$ dependence was calculated by using the formula

$$R_{SNS}(T) = \frac{R_r}{L}\,(2l_E^{\rm ph}(T) + l_N). \tag{8}$$

While calculating $R_{SNS}(T)$, we used the value of $l_E^{\rm ph}(0) \cong 3.6\ \mu$m determined from the electrical parameters of the sample and the critical temperature $T_c = 3.825$ K determined from the $I_0(T)$ dependence (see Fig. 3). If we assume that the normal insert has the length $l_N = 5\ \mu$m, we obtain the solid curve in Fig. 6. The fact that the calculated temperature dependence exactly coincides with the experimental points confirms the fact that the electron–phonon mechanism of quasiparticle relaxation plays a decisive role in the nonequilibrium superconductor adjoining the $N-S$ interface near T_c, where the critical current is small.

As the temperature is lowered below $T_c^0 = 3.72$ K, the IVC displays the critical current (curve *2* in Fig. 2) indicating a transition of the ''weak'' region (normal insert) to the superconducting state. The superconductivity of this ''weak'' region is suppressed in the same way as the formation of a PSC in the homogeneous part of the sample, i.e., jump-wise, with the emergence of excess current. Apart from critical current, the main difference between IVC depicted in Fig. 2

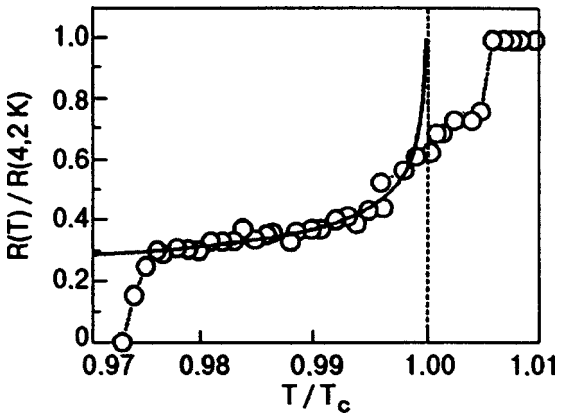

FIG. 6. Normalized temperature dependences of the resistance $R(T)$ of a film with a normal insert during its transition from the normal to the superconducting state. Experimental values are marked by circles and the solid curve is obtained as a result of calculations using formula (8).

(curves *1* and *2*) is different slopes of the initial linear segments, indicating that the films carrying small currents have different differential resistances. It can be seen from the figure that the resistance of the sample with a normal insert (curve *1*) is considerably larger than in the case of PSC (curve *2*). Such a difference cannot be explained only by the elimination of the resistance of the normal insert of length $l_N=5\ \mu$m from formula (8) used for calculating $R_{SNS}(T)$.

It was mentioned above that the diffusion length of quasiparticles in a superconductor depends on the effective time τ_Q of charge disbalance relaxation, which is determined on the static $N-S$ boundary by inelastic scattering mechanism, and hence by the time τ_ε. In the case of PSC, the conditions for nonequilibrium regions differ considerably from the previous case. In the nonequilibrium region of PSC, the time-averaged supercurrent changes from $\sim 0.6 j_c$ at the center to the critical value at the edges. This is due to the fact that a PSC is formed in the film when the critical pair-breaking current is attained. On the other hand, in an *SNS* structure with current, the supercurrent is equal to zero in its normal region, while at the edge of the nonequilibrium region it tends to the value of preset transport current. If we increase the total current to the critical current of the superconducting film, the supercurrent of the *SNS* structure averaged over the nonequilibrium region is smaller than in the case of PSC. A further increase in the current through the sample leads to the formation of PSC in its superconducting regions at distances longer than $l_E(T)$ from the $N-S$ interface.

Thus, we can expect that the fraction of superfluid current in the total transport current increases considerably upon an insignificant decrease in temperature as a result of the formation of PSC in the nonequilibrium region of an *SNS* structure. For this reason, in the expression (3) for Γ, we must take into account the contribution from the third term, viz., elastic scattering of quasiparticles at the momentum of the condensate of Cooper pairs. In this case, $\Gamma=\Gamma_{\rm PSC}$ near T_c is determined by the contribution of two relaxation mechanisms:

$$\Gamma_{\rm PSC}=\frac{1}{2\tau_\varepsilon}+\frac{Dp_c^2}{2\hbar^2}=\frac{1}{2\tau_\varepsilon}+\frac{1}{6\tau_{\rm GL}}, \tag{9}$$

where $\tau_{GL}=(\pi\hbar/8k_B)(T_c-T)^{-1}$ is the Ginzburg–Landau time. For a superconductor at zero temperature, we have $\tau_{\rm GL}=3\times10^{-12}T_c^{-1}$[s]. Expression (9) shows that, at high current densities (of the order of critical current), the relaxation mechanism of charge disbalance is determined by the relation between relaxation times. For example, for $\tau_\varepsilon \ll \tau_{\rm GL}$, inelastic scattering dominates in the superconductor, while the factor $\Gamma_{\rm PSC}$ for $\tau_\varepsilon \gg \tau_{\rm GL}$ is mainly determined by the second term in (9), which corresponds to elastic scattering under the effect of current. Since τ_ε is constant for a given metal, while the value of $\tau_{\rm GL}$ depends of the closeness of the working temperature to the critical value, scattering mechanism may change with temperature in the course of experiments. The temperature corresponding to such a ''crossover'' can be determined from formula (9) by equating the contributions of elastic and inelastic scattering mechanisms ($2\tau_s=6\tau_{\rm GL}$):

$$t=\frac{T}{T_c}=1-\frac{3\pi\hbar}{8k_BT_c\tau_\varepsilon}. \tag{10}$$

PSC experiments are usually made in the temperature range $10^{-2}>T/T_c>5\times10^{-4}$. In this temperature range, inelastic scattering prevails in Nb, Pb, and In, while the main contribution to scattering in Zn and Al comes from elastic processes. Stuivinga *et al.*[16] used this to explain the fact that the size of PSC observed in Al and its resistance is smaller than follows from the assumption concerning the presence of inelastic scattering alone. It should be noted that none of the terms in (9) cannot be neglects in the temperature range corresponding to crossover since both mechanisms make their contribution to relaxation of quasiparticles. This is manifested in the shape of the IVC. Let us estimate the possible reason behind the difference in the initial segments of characteristics shown in Fig. 2 from this point of view.

We shall first determine the crossover temperature taking into account formula (10). Since the PSC in this case is formed in the region with a smaller energy gap, i.e., at the intersection of the In whisker with Sn film, we choose $T_c^0=3.72$ K as the critical temperature. The available data and the results of our experiments suggest that the electron–phonon interaction time is $\tau_\varepsilon=3\times10^{-10}$ s. Then the reduced crossover temperature can be obtained for a given sample from formula (10) ($t=T/T_c^0=0.992$). The current–voltage characteristic (2) depicted in Fig. 2 was measured for $T/T_c^0=0.987$, which is quite close to the crossover temperature. Hence we can expect a strong influence of the additional elastic scattering due to the superconducting current component. This leads to a reduced effective relaxation time as compared to formula (4):

$$\tau_Q=\frac{4kT\tau_\varepsilon}{\pi\Delta}\left(\frac{3\tau'_{\rm GL}}{\tau_\varepsilon+3\tau_{\rm GL}}\right)^{1/2}. \tag{11}$$

As a result, the effective length of the PSC, and hence its resistance, decreases.

Taking into account (11), we can write, in analogy with (8), the following expression for the differential resistance of nonequilibrium regions of PSC:

$$R_{\rm PSC}=\frac{R_r}{L}\,2l_E(T)=\frac{R_r}{L}\,2l_E^{\rm ph}(T)\left(\frac{3\tau_{\rm GL}}{\tau_\varepsilon+3\tau_{\rm GL}}\right)^{1/4}. \qquad (12)$$

Using formulas (8) and (12), we can define the ratio of the resistance R_{SNS} for inelastic scattering to the dynamic resistance $R_{\rm PSC}$ of the PSC for elastic and inelastic scattering through the ratio of relaxation times:

$$\frac{R_{SNS}}{R_{\rm PSC}}=\frac{l_N+2l_E^{\rm ph}(T)}{2l_E^{\rm ph}(T)}\left(\frac{3\tau_{\rm GL}+\tau_E}{3\tau_{\rm GL}}\right)^{1/4}. \qquad (13)$$

The ratio of the initial differential resistance of the *SNS* structure to the differential resistance of the first PSC determined from the IVC in Fig. 2 is equal to 1.66. The calculation of this ratio by using (13) and $\tau_\varepsilon=3\times10^{-10}$ s for the corresponding reduced temperatures for *SNS* and PSC and the normal region length $l_N=5\ \mu$m gives a value differing from the experimental result only by 15%. The reason behind such a discrepancy can be the increase in the critical temperature in the nonequilibrium region of the PSC emerging in the film in place of the *SNS* from the value of T_c^0 of the ''weak'' region, which is used in calculations, to the value of T_c for a homogeneous tin film. The choice of the length of the normal insert does not affect significantly the calculated ratio of the resistance in contrast to the choice of the critical temperature. However, we can say that the results of calculations are in accord with the experimental results even for the existing difference in the ratios $R_{SNS}/R_{\rm PSC}$.

Thus, we can state that elastic processes of quasiparticle scattering in the presence of the superfluid component of transport current play a significant role in the region of the ''crossover'' temperature in PSC along with inelastic electron–phonon scattering.

It was mentioned above that low-frequency oscillations of potential (NJO) are generated in superconducting samples in a certain range of transport current. In Fig. 2, the boundaries of the regions of existence of NJO on IVC are marked by arrows. It was proved in previous investigations that PSC becomes a source of NJO at definite temperatures and bias voltages across the PSC.[6] In the present work, we tried to analyze peculiarities in NJO in the presence of a purely normal region as well as at temperatures $T<T_c^0$, at which the normal insert becomes superconducting. As in the case of homogeneous samples, a decrease in temperature leads to a displacement of the region of existence of NJO towards strong currents. The dependence of the NJO region on current is illustrated in Fig. 3. A transition through T_c^0 does not lead to noticeable changes in the current and temperature dependences of excitation of NJO. Besides, we did not detect noticeable changes in the spectrum of the signal upon a transition of the *N* insert to the superconducting state while studying the amplitude–frequency characteristics of the NJO signal.

2.2. *SNS* structure in an external electromagnetic field

We carried out a large number of experiments on long Sn films with an *SNS* structure. The length of the normal region in the *SNS* structures in the temperature range under investigation was lager than the coherence length $\xi(T)$ by a factor of several units. As a result, such structures did not display the overlapping of the wave functions $|\psi|$ of the complex order parameter for Cooper pairs, which is essential for an experimental observation of the stationary Josephson effect, i.e., high-frequency oscillations of energy gap were not observed. Thus, the *SNS* structures under investigation differ significantly from PSC in the absence of oscillations of Δ near the $N-S$ boundary in the former structures. It was mentioned in Introduction, however, that a constituent part of the model of emergence of NJO used by us is the relaxation of nonequilibrium (in energy) quasiparticles injected from the *N* to the *S* region near the edge of the energy gap at small high-frequency oscillations of the potential Δ. Such a mechanism of scattering of quasiparticles must lead to the emergence of low-frequency photons in the nonequilibrium region of a superconductor.

For this reason, we decided to compensate the absence of Δ oscillations in an *SNS* structure at the $N-S$ interface by their excitation induced by an external electromagnetic field applied to the sample, thus simulating the processes occurring in PSC.

It is very important to choose correctly the frequency of the electromagnetic field, which determines the response of the superconductor. Under actual experimental conditions, Josephson's frequencies f of gap oscillations in PSC near the critical temperature are of the order of 10^{10} Hz, while the width of the energy gap Δ in a homogeneous channel is much larger than $\hbar\omega$. For this reason, we made our experiments at external radiation frequencies of this range.

It was found that the application of the field of frequency $\sim10^{10}$ Hz to the samples near the superconducting transition temperature reduces the resistance of the normal insert with increasing radiation power P. At a certain value of the power, this resistance vanishes, and its further increase leads to the emergence of a critical current whose magnitude increased with P. The electrical parameters of the samples changed qualitatively under the action of the applied electromagnetic field in the same way as in the case of superconductivity stimulation in heterogeneous bridges.[28] The only difference is that our samples are geometrically homogeneous, and the electrical nonuniformity is due to the normal insert going over to the superconducting state under irradiation. In this connection, it would be interesting to analyze the mechanism of superconductivity stimulation in such samples.

The IVC depicted in Fig. 5 were recorded for different levels of power at a temperature at which the sample under investigation had the form of an *SNS* structure. In the absence of radiation and for small transport currents, the sample resistance is a finite value determined (see above) by the resistance of the normal insert and two nonequilibrium resistive regions of length $l_E(T)$ (curve *1* in Fig. 5). The same curve shows the current I_{c1}^e corresponding to the for-

mation of the first PSC. It is the Ginzburg–Landau equilibrium pair-breaking current for the homogeneous long superconducting part of the sample, viz., the ''bank'' in the weak link under investigation. Under the action of the increasing power of external rf radiation, IVC display the increasing critical current I_{c1}^n of the weak link (curve *2* in Fig. 5). This means that the normal region of the film created by us due to the proximity effect becomes superconducting under irradiation. At the same time, the critical current in the banks increases noticeably with the rf power and attains its maximum value I_{c2}^e at a certain power. Such a behavior for a homogeneous superconducting channel can be explained by the superconductivity stimulation mechanism proposed by Eliashberg.[29] Although the critical current increases with P in the region of the normal insert, it remains smaller than the equilibrium current of the banks up to a certain level of power ($I_{c1}^n < I_{c1}^e$). This means that a weak link of the $SS'S$ type is formed in the sample. In this case, superconductivity is probably stimulated due to the Eliashberg mechanism as well as due to the Aslamazov–Larkin mechanism[30] for heterogeneous superconducting structures. In the latter case, stimulation is localized directly in the region of a weak link, for which a potential well is formed on the dependence of Δ on the longitudinal coordinate. At certain levels of rf power (curves *5* and *6* in Fig. 5), the critical current of the weak link becomes larger than the equilibrium critical current of the banks ($I_{c2}^n > I_{c1}^e$). In this case, we can state that the Eliashberg stimulation mechanism plays a decisive role since the superconducting parameters can exceed their equilibrium values only due to the operation of this mechanism.

Consequently, a rf electromagnetic field transforms an SNS structure to an $SS'S$ structure. For this reason, the first PSC in which nonequilibrium processes leading to the generation of NJO developed for a certain value of current was formed just in the region with a lower order parameter. Two vertical arrows on curve *2* in Fig. 5 indicate the region on the IVC in which NJO exist. If, however, the intensity and/or frequency of the external signal were below the values required for the emergence of the critical current of a ''weak'' link, no NJO were detected in this region. Non-Josephson oscillations were found to be also very sensitive to the rf power level. An insignificant increase in this power leads to the suppression of the conditions of NJO excitation in the sample. Sample cooling in zero electromagnetic field to temperatures $T < T_c^0$, at which the same value of critical current of the weak link is attained as in the case of superconductivity stimulation (curve *2* in Fig. 5), makes it possible to excite NJO in the sample, but the value of transport current in this case is much larger than the current corresponding to NJO excitation under the conditions of superconductivity stimulation.

The above results indicate that we cannot create the conditions in an SNS placed in a uniform electromagnetic field similar to those existing in PSC in which NJO are excited. This is probably due to the fact that high-frequency oscillations of energy gap occur along the entire film and are not localized in its quasi-normal region as in the case of PSC (see Fig. 1).

CONCLUSIONS

We investigated experimentally the electrical parameters of the resistive state of homogeneous superconducting Sn films with PSC as well as SNS structures. It is found that elastic scattering processes reducing the effective time of relaxation of charge imbalance to the equilibrium state, and hence the diffusion length of quasiparticle, play a significant role in PSC near the superconducting transition temperature. The reason behind this effect is that the values of the averaged supercurrent in nonequilibrium PSC regions is closer to the critical current than in similar regions of an SNS structure. For small transport currents, this leads to a lower dynamic resistance of nonequilibrium regions of PSC as compared to that of a similar SNS structure.

The application of an external electromagnetic field of frequency $\sim 10^{10}$ Hz to an SNS structure near the superconducting transition temperature reduces to zero the resistance of the N region and causes its transition to the superconducting state and the emergence of critical current in the sample. In this site, a superconducting region with an energy gap value smaller than for the remaining film is formed, and the first PSC is formed just in this region upon an increase in the transport current through the sample. Under certain values of temperature, current, and level of external radiation power, NJO are excited in this region.

We failed to excite experimentally NJO in an SNS structure by applying a rf signal in the absence of the critical current through the sample. This means that it is impossible to create conditions in an SNS structure in a uniform electromagnetic field, which are completely similar to those existing in PSC.

This research was partly financed by the Ministry of Sciences from the State Foundation for Fundamental Studies, project No. 2.4/136.

The authors are privileged to present this work as their contribution to the publications dedicated to the jubilee of Igor Mikhailovich Dmitrenko. Two of the authors (V.M.D. and G.E.Ch.) began their scientific career under the guidance of Igor Mikhailovich and cherish fond memories of those years. The younger authors (D.A.D.) and (A.B.A) took up and developed the creative traditions of Acad. Dmitrenko's school. We wish Igor Mikhailovich sound health and the joy brought by his pupils.

*E-mail: churilov@ilt.kharkov.ua

[1] V. L. Ginzburg and L. D. Landau, Zh. Éksp. Teor. Fiz. **20**, 1064 (1950).
[2] W. J. Skocpol, M. R. Beasley, and M. Tinkham, J. Low Temp. Phys. **16**, 145 (1974).
[3] V. P. Galaiko, V. M. Dmitriev, and G. E. Churilov, Fiz. Nizk. Temp. **3**, 1010 (1977) [Sov. J. Low Temp. Phys. **3**, 491 (1977)].
[4] B. I. Ivlev and N. B. Kopnin, Usp. Fiz. Nauk **142**, 435 (1984) [Sov. Phys. Usp. **27**, 206 (1984)].
[5] R. Tidecks and Th. Werner, J. Low Temp. Phys. **67**, 225 (1987).
[6] G. E. Churilov, D. A. Dikin, V. M. Dmitriev, and V. N. Svetlov, Fiz. Nizk. Temp. **17**, 185 (1991) [Sov. J. Low Temp. Phys. **17**, 96 (1991)].
[7] A. M. Kadin, L. N. Smith, and W. J. Skocpol, J. Low Temp. Phys. **38**, 497 (1980).
[8] R. V. Carlson and A. M. Coldman, Phys. Rev. Lett. **34**, 11 (1975).
[9] G. E. Churilov, V. N. Svetlov, and V. M. Dmitriev, Fiz. Nizk. Temp. **13**, 241 (1987) [Sov. J. Low Temp. Phys. **13**, 137 (1987)].

[10] G. E. Churilov, V. M. Dmitriev, and A. P. Beskorsyi, Pis'ma Zh. Éksp. Teor. Fiz. **10**, 231 (1969) [JETP Lett. **10**, 146 (1969)].
[11] M. Stuwinga, C. L. Ham, T. M. Klapwijk, and J. E. Mooij, J. Low Temp. Phys. **53**, 633 (1983).
[12] V. P. Galaiko, Zh. Éksp. Teor. Fiz. **68**, 223 (1975) [Sov. Phys. JETP **41**, 108 (1975)].
[13] A. Schmidt and G. Schon, J. Low Temp. Phys. **20**, 207 (1975).
[14] V. P. Galaiko, J. Low Temp. Phys. **26**, 483 (1977).
[15] V. M. Dmitriev and E. V. Khristenko, Fiz. Nizk. Temp. **3**, 1210 (1977) [Sov. J. Low Temp. Phys. **3**, 587 (1977)].
[16] M. Stuwinga, J. E. Mooij, and T. M. Klapwijk, J. Low Temp. Phys. **46**, 555 (1982).
[17] G. A. Gogadze, V. M. Dmitriev, V. N. Svetlov, and G. E. Churilov, in *Abstracts of Papers to 24th All-Union Cong. on Low Temp. Phys.*, Tbilisi (1986).
[18] G. A. Gogadze, Fiz. Nizk. Temp. **12**, 1102 (1986) [Sov. J. Low Temp. Phys. **12**, 622 (1986)].
[19] G. A. Gogadze, Fiz. Nizk. Temp. **16**, 790 (1990) [Sov. J. Low Temp. Phys. **16**, 466 (1990)].
[20] G. A. Gogadze, Fiz. Nizk. Temp. **14**, 196 (1988) [Sov. J. Low Temp. Phys. **14**, 108 (1988)].
[21] A. B. Pippard, J. G. Shepherd, and D. A. Tindall, Proc. R. Soc. London, Ser. A **324**, 17 (1971).
[22] P. G. de Gennes, Rev. Mod. Phys. **36**, 225 (1964).
[23] V. V. Kravchenko, E. A. Golovanov, and S. I. Bondarenko, Fiz. Met. Metalloved. **43**, 430 (1973).
[24] G. E. Churilov, V. N. Svetlov, and V. M. Dmitriev, Fiz. Nizk. Temp. **12**, 425 (1986) [Sov. J. Low Temp. Phys. **12**, 242 (1986)].
[25] J. R. Waldram, Proc. R. Soc. London, Ser. A **345**, 231 (1975).
[26] A. Schmid, *Proceedings of NATO Advan. Study Inst. on Nonequilibrium Superconductivity, Phonons and Kapitza Boundaries* (ed. by K. E. Gray), Plenum Press, New York (1981).
[27] M. Tinkham, *Introduction to Superconductivity*, McGraw-Hill, New York (1975).
[28] V. M. Dmitriev, V. N. Gubankov, and F. Ya. Nad', in *Nonequilibrium Superconductivity* (ed. by D. N. Langenberg and A. L. Larkin), Elsevier, Amsterdam (1985).
[29] G. M. Eliashberg, Pis'ma Zh. Éksp. Teor. Fiz. **11**, 186 (1970) [JETP Lett. **11**, 114 (1970)].
[30] L. G. Aslamazov and A. I. Larkin, Zh. Éksp. Teor. Fiz. **74**, 2184 (1978) [Sov. Phys. JETP **47**, 1136 (1978)].

Translated by R. S. Wadhwa

LOW-TEMPERATURE MAGNETISM

Low temperature spin-glass magnetic behavior of $Ce_3Pd_{20}Ge_6$

Yu. P. Gaidukov, V. N. Nikiforov, and Yu. A. Koksharov

Low Temp. Dep., Faculty of Physics, M. V. Lomonosov Moscow State University, Russia

R. Szymczak and H. Szymczak

Institute of Physics, Polish Academy of Sciences, 02-668 Warsaw, Poland

A. V. Gribanov

Faculty of Chemistry, M. V. Lomonosov Moscow State University, Russia

(Submitted October 14, 1997; revised March 3, 1998)
Fiz. Nizk. Temp. **24**, 750–753 (August 1998)

A polycrystalline sample of $Ce_3Pd_{20}Ge_6$ is investigated using a dc SQUID magnetometer. A noticeable difference between ZFC and FC magnetic susceptibility is found below ≈60 K. The temperature dependence of the magnetic susceptibility demonstrates an anomaly near approximately 2.8 K below which a remanent magnetic moment exists. Two characteristic temperatures detected support the assumption that there are different cerium magnetic subsystems in $Ce_3Pd_{20}X_6$ (X=Ge, Si) compounds. Unusual magnetic behavior observed in $Ce_3Pd_{20}Ge_6$ is discussed within the framework of the ''molecular magnetism'' model which predicts a frustration of exchange interactions.
[S1063-777X(98)00608-2]

1. INTRODUCTION

The problem of the coexistence of magnetic and Kondo ground states in *f*-electron systems has been discussed intensively over the past decade (Ref. 1). In our previous works[2,3] we reported on a Kondo-like dependence of electrical resistivity and unusual magnetic behavior in polycrystalline samples of $Ce_3Pd_{20}X_6$ (X=Ge, Si). The electrical resistivity of these compounds demonstrates logarithmic increasing below characteristic temperatures of 10 K ($Ce_3Pd_{20}Ge_6$) and 50 K ($Ce_3Pd_{20}Si_6$). In addition a magnetic anomaly was found in $Ce_3Pd_{20}Si_6$ below ≈50–60 K. Though the crystal structures of $Ce_3Pd_{20}Ge_6$ and $Ce_3Pd_{20}Si_6$ are very similar, no magnetic anomalies were detected in the former compound above the helium temperature.[2,3] However, an antiferromagnetic-like peculiarity of ac-susceptibility in $Ce_3Pd_{20}Ge_6$ was found at 1 K (Ref. 4). In the presented work a polycrystalline sample of $Ce_3Pd_{20}Ge_6$ has been investigated using a dc SQUID magnetometer in the temperature range from 2 to 200 K and at magnetic fields (2–50) kOe. The sample of $Ce_3Pd_{20}Ge_6$ was prepared using a melting technique in an arc furnace in the argon atmosphere as described in Ref. 5. Annealing in the argon atmosphere (at the pressure of 1.1×10^5 Pa) was performed at 600 °C during about 700 h. The crystal structure of the sample determined by the x-ray analysis is the same as reported in Ref. 5. The temperature dependence of the electrical resistivity of the sample being studied as a test shows a logarithmic increase below 10 K that accords with results obtained in Refs. 2 and 3.

2. EXPERIMENTAL RESULTS

Figure 1 represents the temperature dependences of a static magnetic susceptibility at low (12 Oe) and high (50 kOe) magnetic fields (χ_{low} and χ_{high}, respectively). At high temperatures the following relationship takes place: $\chi_{low}>\chi_{high}$. Below approximately 10 K χ_{high} is almost equal to χ_{low}. It is interesting to note that the electrical resistivity has a Kondo minimum at the same temperature.[2,3] The solid line in Fig. 1 shows the Curie law's magnetic susceptibility χ_{free} of Ce^{3+} ions in $Ce_3Pd_{20}Ge_6$ if they would be free of exchange interactions. The curves $\chi_{low}(T)$ and $\chi_{free}(T)$ cross each other at the temperature ≈50 K. It is likely that this temperature is characteristic of $Ce_3Pd_{20}Ge_6$ as well as of $Ce_3Pd_{20}Si_6$.[2,3] The low temperature magnetic susceptibility (at 12 and 2 Oe) is displayed in Fig. 2. Curves $\chi(T)$ clearly demonstrate a magnetic anomaly near $T_1\approx2.8$ K. Below T_1 the increase in the susceptibility slows down noticeably which excludes a ferromagnetic type of this anomaly. Moreover, no evidence of the magnetic hysteresis was observed in magnetization curves measured at 2 K. Furthermore, as may be seen from Fig. 3, the effective magnetic moment M (per Ce^{3+} ion) decreases with lowering of the temperature from 10 to 2.4 K.

It should be noted that increase of the magnetic field at low temperatures suppresses the magnetic susceptibility [see Fig. 2, compare M/H at 12 and 2 Oe (inset)]. This is a characteristic feature of spin-glass systems. In addition, a distinct remanent magnetic moment (RMM) was detected at low temperatures. The inset of Fig. 4 demonstrates the tem-

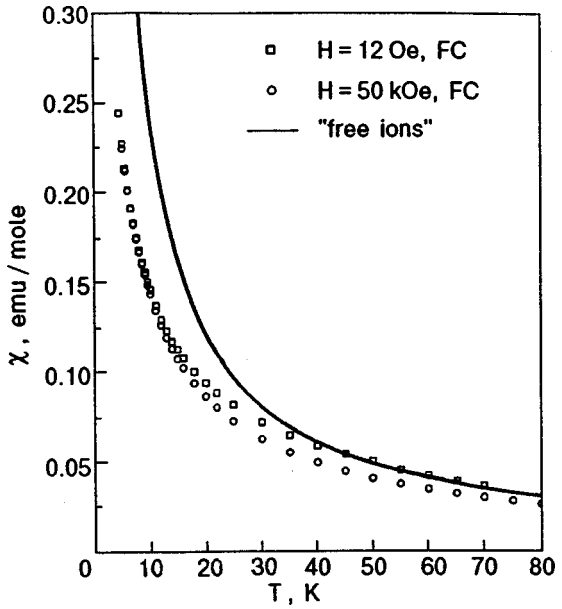

FIG. 1. Temperature dependences of the $Ce_3Pd_{20}Ge_6$ magnetic susceptibility at different magnetic fields. The solid line represents the calculated ''free ions'' magnetic susceptibility which follows the Curie law.

perature dependence of RMM in $Ce_3Pd_{20}Ge_6$ near T_1. To obtain these data the sample was cooled down to 2 K at the zero external magnetic field, then the magnetic field of 100 Oe was applied for a short time and next it was turned off. On subsequent heating, the RMM of the sample quickly falls down in the temperature range from 2.4 to 3 K and falls down lower at temperatures above 3 K. The existence of the RMM also could indicate a ''spin-glass'' (SG) nature of low

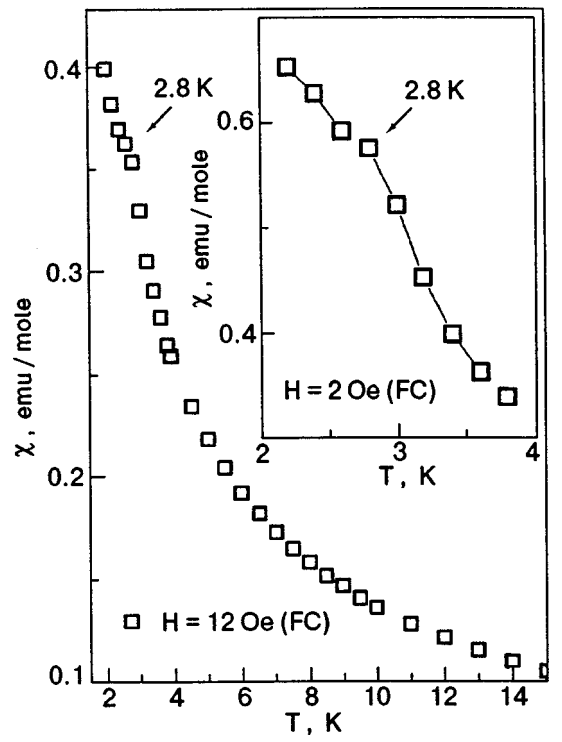

FIG. 2. The low temperature magnetic susceptibility of $Ce_3Pd_{20}Ge_6$ at 12 Oe. The inset shows the magnetic susceptibility at 2 Oe.

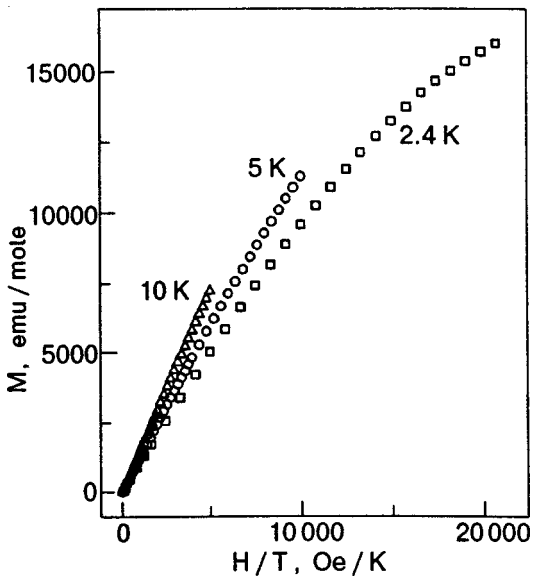

FIG. 3. Magnetization curves of $Ce_3Pd_{20}Ge_6$ at different temperatures.

temperature magnetism in $Ce_3Pd_{20}Ge_6$. This point of view is supported by Fig. 4 which shows the difference ΔM between magnetic moments of $Ce_3Pd_{20}Ge_6$ measured during zero field cooling (ZFC) and field cooling (FC) procedures. The value of ΔM clearly tends to zero at temperatures above $T_2 \approx 60$ K.

3. DISCUSSIONS

Since 1995, when $Ce_3Pd_{20}X_6$ (X=Ge, Si) was synthesized,[5] magnetic properties of this compound have been investigated in works.[2–4,6–8] It was found that the possibility of detecting magnetic anomalies depends strongly on the applied magnetic field. Thus, the cusp in the ac-magnetic

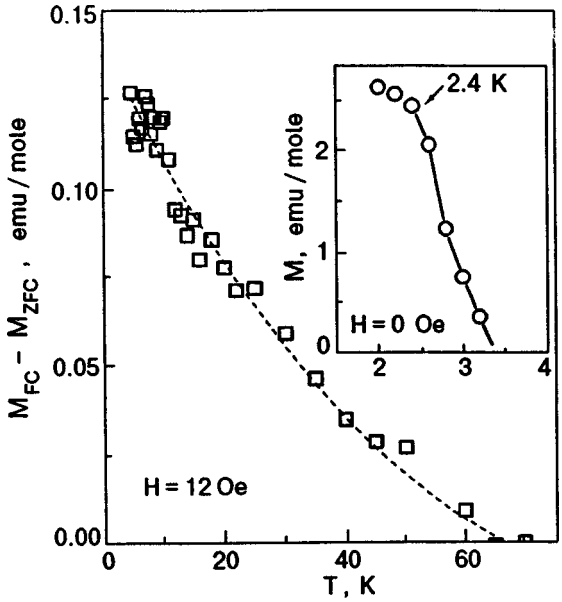

FIG. 4. The difference between the FC and ZFC magnetic moment of $Ce_3Pd_{20}Ge_6$ versus the temperature. The inset shows the temperature dependence of the remanent magnetic moment below 4 K.

susceptibility of $Ce_3Pd_{20}Si_6$ at 0.15 K is suppressed by the weak static magnetic field.[7] The magnetic behavior of $Ce_3Pd_{20}Si_6$ at high temperatures (4–100 K) is also sensitive to the static magnetic field.[3] This evident field-dependence on the applied magnetic field explains why the magnetic anomaly at 50 K in $Ce_3Pd_{20}Si_6$[3] and that at 2.7 K in $Ce_3Pd_{20}Ge_6$, observed in this work, were undetected at the magnetic field 3 kOe used in Refs. 4 and 8.

The marked field sensitivity of magnetic susceptibility in $Ce_3Pd_{20}Si_6$ was analyzed within the framework of the ''molecule magnetism'' model.[3] This model could explain also a ''spin-glass'' magnetic behavior in $Ce_3Pd_{20}Ge_6$. According to Ref. 5 and the ''molecular magnetism'' model, there are two non-equivalent Ce positions (Ce1 and Ce2) in the crystal lattice of $Ce_3Pd_{20}X_6$.[3] First type (Ce1) ions form face-centred ''large'' cube and second type (Ce2) ones make up a ''small'' cube inside the ''large''. If Ce2–Ce2 ferromagnetic exchange interactions dominate over others, this could result in the formation of ''superparamagnetic cubes'' (SPC) containing eight Ce2 ions.[3] Anomaly at 50–60 K in $Ce_3Pd_{20}Si_6$ can be attributed to antiferromagnetic (AF) ordering of SPC.[3] In this case Ce1 moments, placed between two SPC, undergo magnetic frustration. It is well known that magnetic frustration and spin-glass behavior are intimately related.[9] Non-freezing cerium magnetic moments are capable of being effective Kondo's scattering centers.[3] Analogous frustration of exchange interactions may also take place in $Ce_3Pd_{20}Ge_6$. Within the framework of this model in the temperature range 50–60 K there may occur the magnetic transition of SPC to antiferromagnetic state in $Ce_3Pd_{20}Si_6$ and to the ''freezing'' state (partial or complete) in $Ce_3Pd_{20}Ge_6$. This characteristic temperature is determined mainly by Ce2–Ce2 exchange interactions which should be close in both compounds. From this point of view the second magnetic anomaly at T_1 in $Ce_3Pd_{20}Ge_6$ is due to ''freezing'' of some Ce1 magnetic moments (see below).

Figure 5 shows the unit cell of $Ce_3Pd_{20}Ge_6$ crystal structure (only Ce positions are presented). The analysis of an arrangement of cerium atoms relative to SPC reveals two different positions of Ce1 ions. These are Ce1′ positions, which are located at corners of the ''large'' cube, and Ce1″ ones—at centers of the faces. Because of their unequivalent location near SPC these Ce1 subsystems may undergo magnetic ordering at different temperatures. It is possible that T_1 is the temperature of ''freezing'' in one of these subsystem. This could result in the termination of Kondo-like increase of the electrical resistivity near 2 K.[4] Other Ce1 subsystem could have a transition to the antiferromagnetic phase under cooling below 1 K.[4]

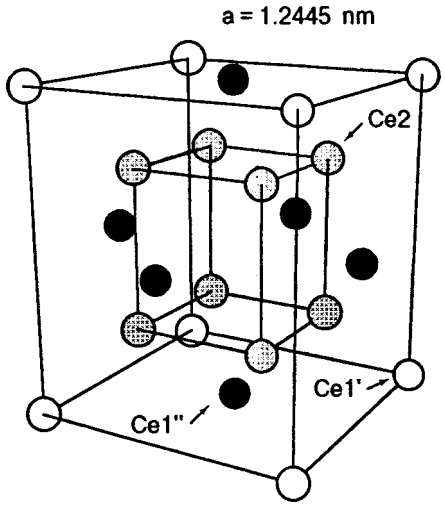

FIG. 5. The unit cell of $Ce_3Pd_{20}Ge_6$ crystal structure. Only Ce positions are shown.

In conclusion, we suppose that $Ce_3Pd_{20}X_6$ (X=Ge, Si) system could be considered as antiferromagnetic with a few $4f$ magnetic subsystems and a strong frustration of exchange interactions. This could explain the anomalous magnetic behavior (including ''spin-glass'' one) and coexistence of magnetic and Kondo-like properties at the same temperature region.

This work was partially supported by the Russian Fundamental Research Foundation (Grant 95/02/04340 and 95/03/09647).

[1] Yu. Izyumov, M. Katsnelson, and Yu. Skryabin, *Itinerant Electron Magnetism*, Nauka, Moscow (1994).
[2] Yu. P. Gajdukov, Yu. A. Koksharov, Yu. V. Kochetkov, J. Mirkovic, and V. N. Nikiforov, JETP Lett. **61**, 381 (1995).
[3] V. N. Nikiforov, Yu. A. Koksharov, J. Mirkovic, and Yu. V. Kochetkov, J. Magn. Magn. Mater. **163**, 184 (1996).
[4] J. Kitagawa, N. Takeda, and M. Ishikawa, Phys. Rev. B **53**, 5101 (1996).
[5] A. V. Gribanov, Yu. D. Seropegin, and O. I. Bodak, J. Alloys Compd. **204**, L9 (1994).
[6] J. Kitagawa, N. Takeda, M. Ishikawa, T. Yushida, A. Ishiguro, and T. Komatsubara, in *Proceedings of Conference on Strongly Correlated Electron Systems*, August 19–22, Zurich (1996) (in print).
[7] N. Takeda, J. Kitagawa, and M. Ishikawa, in *Conference on Strongly Correlated Electron Systems*, August 19–22, Zurich (1996) (in print).
[8] N. Takeda, J. Kitagawa, and M. Ishikawa, J. Phys. Soc. Jpn. **64**, 387 (1995).
[9] S. Ozeroff and P. Keezom, in *Semiconductors and Semimetals, Diluted Magnetic Semiconductors Volume*, V. 25, Jacek K. Furdyna and Jacek Kossut (Eds.), Academic Press Inc. (1988).

This article was published in English in the original Russian journal. It was edited by R. T. Beyer.

Anisotropy of local and hyperfine magnetic fields in ^{57}Fe nuclei in the hexaferrite $SrFe_{12}O_{19}$

S. P. Kuntsevich

Kharkov State University, 310077 Kharkov, Ukraine
(Submitted April 15, 1997; revised March 10, 1998)
Fiz. Nizk. Temp. **24**, 754–758 (August 1998)

Local magnetic fields and their anisotropy in ^{57}Fe nuclei are measured in the domain boundaries for the sites $4f_1$ of Fe^{3+} ions of the hexaferrite $SrFe_{12}O_{19}$ in the temperature range 4.2–295 K. The anisotropy of the magnetic moment moduli of Fe^{3+} ions is determined at low temperatures. The anisotropy of the magnetic moment moduli is considered as the physical factor responsible for the hyperfine field anisotropy. The connection between the anisotropy of magnetic moment moduli and the magnetic characteristics of the ferrite is considered in the molecular field approximation. © *1998 American Institute of Physics.* [S1063-777X(98)00708-7]

INTRODUCTION

The analysis of low-temperature properties of magnetically ordered materials is carried out most frequently by using the semiclassical approach. This approach is based on the constancy of the moduli of magnetic moments of ions and hence the magnetization of a magnet. This condition is used to determine the equilibrium orientation of the magnetization and its small oscillations. The semiclassical approximation is inadequate for studying a number of phenomena. For example, by rejecting the condition of conservation of magnetization modulus, Baryakhtar[1] created a phenomenological theory of magnetic relaxation which correctly explains the difference between the relaxation constants in the Landau–Lifshitz equation obtained from the mobility of domain walls (DW), and the data on ferromagnetic resonance (FMR). Hence the experimental measurement of the magnetization anisotropy and the magnetic moment moduli of ions acquires a considerable significance. For highly anisotropic rare-earth compounds, the anisotropy of the magnetic moment moduli can be determined from the experimental dependence of magnetization on the applied magnetic field along easy and difficult magnetization directions.[2] For the oxide ferrimagnets containing $3d$ magnetic ions and having a lower anisotropy, the effect should be less pronounced, and it has not been possible so far to observe the anisotropy of the moduli of magnetic moments of ions and the magnetization. Special experimental techniques have to be worked out in this connection. The considerable progress made in the technique of growth of perfect crystals of ferrimagnets, and in the methods for studying local characteristics of magnetic ions by the NMR technique[3] allows us to use the NMR technique for determining the anisotropy of the moduli of magnetic moments of ions. At temperatures close to absolute zero, the hyperfine field $H_{\rm hf}$ at the nucleus of a magnetic ion in the magnetically ordered state is determined by the modulus of the magnetic moment of the ion.[4] Hence the dependence of $H_{\rm hf}$ on the magnetization orientation relative to the crystallographic axes can provide experimental information about the anisotropy of magnetic moment moduli. The following circumstance must be taken into consideration in this connection. The local field at a nucleus is the superposition of the hyperfine field $H_{\rm hf}$ and the dipole field H_d produced by the magnetic ions surrounding the nucleus. The dipole field may change as a result of reorientation of local magnetic moments. Hence it is preferable to study this effect in multisublattice ferrimagnets for nuclei in crystallographic positions with a small anisotropy of dipole fields. For M-type hexaferrites, such positions correspond to $4f_1$ for Fe^{3+} ions in the c-sublattice. According to the data presented in Ref. 5, the theoretical value of the dipole field anisotropy in $4f_1$ positions is about an order of magnitude lower than for the other crystallographically nonequivalent positions of Fe^{3+} ions. The local field anisotropy δH_l at the nuclei can be determined experimentally by NMR studies in DW nuclei using the steady-state method.

In M-type uniaxial magnetic crystals, NMR signals are observed from ^{57}Fe at the edge of the DW with a frequency ν_d and from the nuclei in the middle of the DW with a frequency ν_w.[3] For nuclei at the edge of the DW, the magnetic moments are oriented along the light magnetization axis, which coincides with the **c**-axis, while the magnetic moments of nuclei in the middle of the DW lie in the basal plane. Thus the difference $\delta\nu=\nu_w-\nu_d$ in frequencies characterizes the anisotropy of local frequencies, and hence the anisotropy $\delta H_l=H_w-H_d$ of local fields upon a reorientation of magnetic moments from the **c**-axis towards the basal plane.

In this work, we report on the measurements of local fields and their anisotropy at ^{57}Fe nuclei of Fe^{3+} ions at $4f_1$ positions in the hexaferrite $SrFe_{12}O_{19}$ (SrM) in the temperature range 4.2–295 K. The hyperfine field anisotropy, which is treated as a consequence of the anisotropy of magnetic moment moduli of Fe^{3+} ions, is determined at low temperatures. The connection between the anisotropy of magnetic moment moduli and the magnetic characteristics of a ferrite is considered in the molecular field approximation.

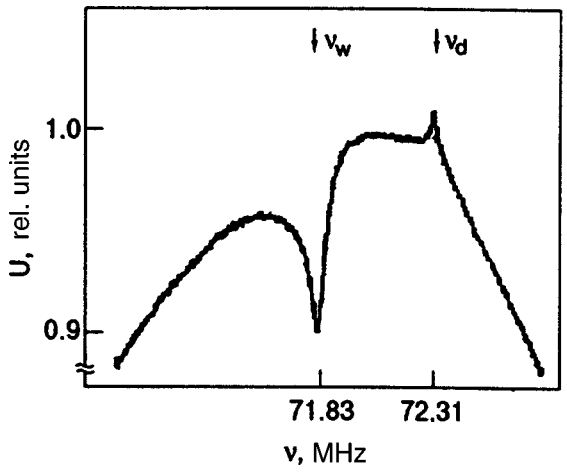

FIG. 1. Dependence of the voltage U across the *pickup-circuit* on frequency at 77 K.

SAMPLES AND MEASURING TECHNIQUE

Crystals of $SrFe_{12}O_{19}$ (SrM) grown from solution in the molten flux $SrO \cdot B_2O_3$ were used as samples. The crystals were synthesized in the temperature interval 1180–1050 °C. The samples were enriched in the isotope ^{57}Fe to 95%. The phase composition of crystals was checked by x-ray crystallography. At room temperature, the crystal lattice constants had the following values: $a=0.588$ nm, $c=2.299$ nm. The NMR of DW nuclei was observed in the steady state by using a device consisting of a rf amplifier with the *pickup-circuit* containing the sample connected to its input, and a frequency-characteristic meter X1-42. The NMR was detected from the resonance peaks on the frequency characteristic of the *pickup-circuit*. The voltage across the circuit did not exceed 10^{-2} V. The crystal was oriented in the *pickup-circuit* in such a way that the rf field was oriented along the **c**-axis while the signal intensity was the highest. NMR of nuclei in the domains was observed by using a noncoherent spin-echo spectrometer which made it possible to find the dependence of the echo signal amplitude on the duty factor of rf pulses.

DISCUSSION OF RESULTS

Two NMR lines were observed for ^{57}Fe nuclei in a DW in the $4f_1$ positions of Fe^{3+} ions. Streever[7] provided an identification of NMR spectral lines for various crystallographic positions of Fe^{3+} ions in an M-type hexaferrite. Figure 1 shows the frequency characteristic of the pickup circuit recorded at 77 K with the help of a plotter. Two peaks at frequencies ν_d and ν_w can be seen. The frequency values are given in Table I. For identifying the peaks, we used the fact that the NMR signal frequencies for nuclei at the edge of a DW should not differ significantly from the NMR frequencies of nuclei in the domains. The signal frequency $\nu_\parallel$ for nuclei in $4f_1$ positions of domains was determined by the spin-echo technique. The value of $\nu_\parallel$ differs insignificantly from the frequency ν_d which was attributed to the nuclei at the DW edge. The identification of signal from nuclei in the middle of a DW requires a knowledge of the anisotropy of local frequencies upon a reorientation of the magnetization vector from the **c**-axis to the basal plane in the one-domain state

$$\delta\nu' = \nu_\perp - \nu_\parallel, \tag{1}$$

where $\nu_\perp$ corresponds to the magnetization orientation in the basal plane and $\nu_\parallel$ to the orientation along the **c**-axis.

The quantity $\delta\nu'$ was determined by the spin-echo technique in a field 1.75 MA/m using the method described by us earlier.[3] The values of $\delta\nu'$ and the theoretical value of $\nu_\perp$ are shown in Table I. It can be seen from the Table that the value of $\nu_\perp$ differs only slightly from that of ν_w which was attributed to the nuclei in the middle of the DW. The steady-state technique used for observing NMR made it possible to trace the temperature variation of ν_d and ν_w. The data of these temperature dependences were used to find the temperature variation of local fields H_d and H_w at the nuclei. These variations are shown in Fig. 2. It follows from the

TABLE I. Characteristic frequencies of NMR spectra of the hexaferrite $SrFe_{12}O_{19}$ at 77 K.

ν_d, MHz	ν_ω, MHz	$\delta\nu$, MHz	$\delta\nu'$, MHz	$\nu_\parallel$, MHz	$\nu_\perp$, MHz
72.28	71.83	−0.45	−0.32	72.29	71.97

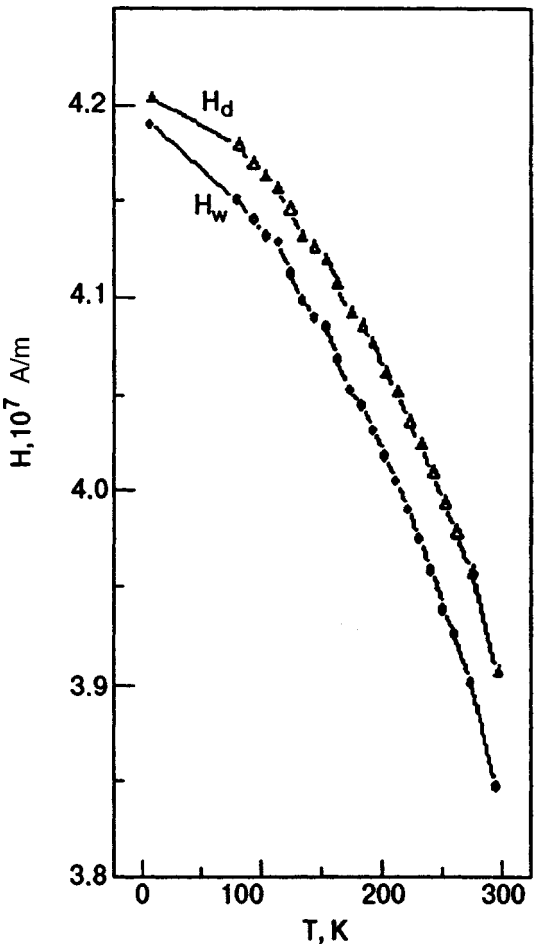

FIG. 2. Temperature dependence of local fields on ^{57}Fe nuclei H_w in the middle and H_d at the edge of a DW, respectively.

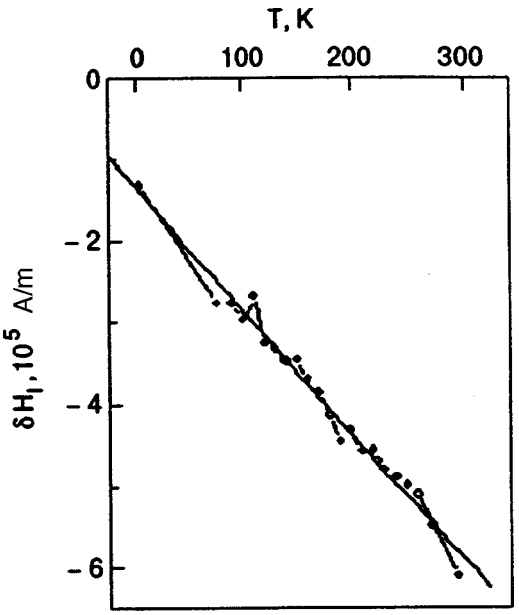

FIG. 3. Temperature dependence of the anisotropy δH_l on ^{57}Fe nuclei.

figure that the local field anisotropy $\delta H_l = H_w - H_d$ increases with temperature. The excitation of magnons inside a DW must lead to a sharper decrease in the local field H_w with increasing temperature as compared to the field H_d.[4,6] This should lead to an increase in δH_l since $H_w < H_d$. Figure 3 shows the temperature dependence of the local field anisotropy δH_l. It can be seen that δH_l increases linearly with temperature. The linear dependence indicates that the main contribution to the temperature variation of δH_l comes from the mechanism associated with a decrease in the local magnetization in the middle of the DW as compared to the edges on account of thermal excitation of magnons within the DW. According to the calculations carried out by Winter,[6] the difference in local magnetizations must increase linearly with temperature. Extrapolation of $\delta H_l(T)$ to $T = 0$ K allows us to find the local field anisotropy $\delta H_l(0) = -144$ kA/m. The expression for $\delta H_l(0)$ has the form

$$\delta H_l(0) = \delta H_{hf}(0) + \delta H_d(0), \tag{2}$$

where $\delta H_{hf}(0)$ is the hyperfine field anisotropy, and $\delta H_d(0)$ the dipole field anisotropy.

According to the computational data obtained by Stepankova *et al.*,[5] $\delta H_d(0) = 95$ kA/m for $4f_1$ positions in the c-sublattice of Fe^{3+} ions in an M-type hexaferrite at low temperatures. Hence we obtain from formula (2) $\delta H_{hf}(0) = -239$ kA/m. In magnetically ordered ferrimagnets, $H_{hf}(0) \gg H_d(0)$, and it can be assumed that $H_{hf}(0) \approx H_l(0) = 41.9$ MA/m, while the relative variation $\delta H_{hf}/H_{hf} = -5.7 \times 10^{-3}$. In the analysis of hyperfine interaction anisotropy, it is usually assumed that the hyperfine field and the magnetic moment of an ion are connected through a tensor relation.[9] This approach corresponds to an approximation in which relativistic interactions are disregarded and it is assumed that the modulus of magnetic moment of an ion is conserved during reorientation. In the review article by Loktev and Ostrovskii,[8] it is shown that the interaction of all degrees of freedom in a highly anisotropic magnet leads to a non-conservation of the modulus of the magnetic moment of ions and the magnetization modulus during reorientation of the magnetic moments. This conclusion is confirmed by the experimental results on the measurement of anisotropy of the magnetization modulus of intermetallic compounds at low temperatures.[2] Hence it would be quite appropriate to consider that the hyperfine field anisotropy follows from the anisotropy of moduli of magnetic moments of Fe^{3+} ions in $4f_1$ positions, and to assume that the decrease in hyperfine field due to reorientation of magnetic moments from light to difficult magnetization direction is associated with the decrease $\delta\mu$ in the modulus of the magnetic moment of the Fe^{3+} ion, where $\delta\mu/\mu \approx \delta H_{hf}/H_{hf} = -5.7 \times 10^{-3}$. It should be interesting to use this approach for estimating the observed effect. In the expression for the energy W of an Fe^{3+} ion in the $4f_1$ position in a DW, we consider two largest terms, viz., the exchange energy $W_{\rm exc}$ and the anisotropy energy W_a:

$$W = W_a + W_{\rm exc}. \tag{3}$$

Considering that the ferromagnet is not subjected to an external agency and treating it as a closed system, we obtain $\delta W = 0$ and $\delta W_{\rm exc} = -\delta W_a$ for spin reorientation. This leads to the relation

$$\delta W_{\rm exc}/W_{\rm exc} = -\delta W_a/W_{\rm exc}. \tag{4}$$

In $4f_1$ positions, the Fe^{3+} ions in the c-sublattice have three exchange bonds with Fe^{3+} ions in the $12k$ position of the a sublattice and six exchange bonds with Fe^{3+} ions in the $2a$ position of the b sublattice.[10] Hence in the molecular field approximation, the exchange field $H_{\rm exc}$ and the exchange energy $W_{\rm exc}$ for Fe^{3+} ions in the $4f_1$ positions may be presented in the form[11]

$$H_{\rm exc} = 2\mu(3J_{ac} + 6J_{bc})(g\beta)^2,$$
$$W_{\rm exc} = -\mu^2(3J_{ac} + 6J_{bc})(g\beta)^2, \tag{5}$$

where μ is the magnetic moment of the Fe^{3+} ion, g the electron g- factor, β the Bohr magneton, and J_{mn} the absolute values of the integrals of indirect exchange between ion of sublattices b, a and c. Using relations (4) and (5), we obtain

$$\frac{2\delta\mu}{\mu} + \frac{\delta J_{ac} + 2\delta J_{bc}}{J_{ac} + 2J_{bc}} = -\frac{\delta W_a}{W_{\rm exc}}. \tag{6}$$

In the approximation considered by us, it is assumed that the change $\delta\mu$ in the magnetic moments in the positions $4f_1$, $12k$ and $2a$ is practically the same. For ions in the middle of the DW, the change in the anisotropy energy is numerically equal to the anisotropy energy, and hence

$$-\delta W_a/W_{\rm exc} = -W_a/W_{\rm exc} \approx H_a/H_{\rm exc}, \tag{7}$$

where H_a is the anisotropy field of the ferrite SrM. The quantity $-\delta W_a/W_{\rm exc} > 0$, since a reorientation of magnetic moments from the light to difficult magnetization direction gives $\delta W_a > 0$, while $W_{\rm exc} < 0$. The value of the anisotropy field for the ferrite under consideration at low temperatures (77 K) is $H_a = 1.37 \cdot 10^6$ A/m. Using expressions (5), quan-

tities J_{ac} and J_{bc} from Ref. (10), and $\mu = g\beta s$ ($s = 5/2$), we obtain for the exchange field $H_{\text{exc}} = 464 \times 10^6$ A/m. Hence formula (7) gives $W_a / W_{\text{exc}} \approx 3 \times 10^{-3}$. The value of $-\delta W_a / W_{\text{exc}}$ is of the same order as $|\delta\mu|/\mu$, but the signs of $-\delta W_a / W_{\text{exc}}$ and $\delta\mu/\mu$ are opposite. It should be observed that Rozenfeld *et al.*[2,12] mentioned such a peculiarity in their works, but without considering the sign. They found experimentally that the relative anisotropy of magnetization in intermetallic compounds has the same order of magnitude as the ratio of the anisotropy energy to the exchange energy. Using the values of $-\delta W_a / W_{\text{exc}}$ and $\delta\mu/\mu$ as well as the relation (6), we obtain $(\delta J_{ac} + 2\delta J_{bc})/(J_{ac} + 2J_{bc}) = 14.4 \cdot 10^{-3}$ which gives $\delta J_{ac} + 2\delta J_{bc} > 0$. According to Eqs. (5) this corresponds to a decrease in the exchange energy and a change in the separation and angles between exchange bonds in the chain of interactions $Fe^{3+}(4f_1) - O^{2-} - Fe^{3+}(12k)$ and $Fe^{3+}(4f_1) - O^{2-} - Fe^{3+}(2a)$.

The above analysis can be summed up as follows. An increase in the anisotropy energy during reorientation of magnetic moments is compensated by a decrease in the exchange energy. This is accompanied by an increase in the indirect exchange integrals and a change in the separation between magnetically active ions. The variation of ion separation is accompanied by a redistribution of the spin and electron densities with a corresponding decrease in the magnetic moment moduli of Fe^{3+} ions.

[1] V. G. Bar'yakhtar, Zh. Éksp. Teor. Fiz. **87**, 1501 (1984) [Sov. Phys. JETP **60**, 863 (1984)].
[2] E. V. Rozenfel'd and A. V. Korolev, Zh. Éksp. Teor. Fiz. **108**, 862 (1995) [JETP **81**, 471 (1995)].
[3] S. P. Kuntsevich, A. A. Bezlepkin, and Yu. A. Popkov, Zh. Éksp. Teor. Fiz. **88**, 1820 (1985) [Sov. Phys. JETP **61**, 1079 (1985)].
[4] E. A. Turov and M. P. Petrov, *Nuclear Magnetic Resonance in Ferro- and Antiferromagnets* [in Russian], Nauka, Moscow (1969).
[5] H. Stepankova, J. Englich, and B. Sedlak, Czech. J. Phys. **B33**, 816 (1983).
[6] J. M. Winter, Phys. Rev. **124**, 452 (1961).
[7] R. L. Streever, Phys. Rev. **186**, 286 (1969).
[8] V. M. Loktev and V. S. Ostrovskii, Fiz. Nizk. Temp. **20**, 983 (1994) [Low Temp. Phys. **20**, 775 (1994)].
[9] M. I. Kurkin and E. A. Turov, *Nuclear Magnetic Resonance in Magnetically Ordered Materials and its Application* [in Russian], Nauka, Moscow (1990).
[10] M. P. Petrov and A. V. Kuntsevich, Zh. Éksp. Teor. Fiz. **63**, 2239 (1972) [Sov. Phys. JETP **36**, 1184 (1972)].
[11] J. Smart, *Effective Field Theories of Magnetism*, Philadelphia (1966).
[12] A. S. Ermolenko and E. V. Rozenfel'd, Fiz. Met. Metalloved. **48**, 505 (1979).

Translated by R. S. Wadhwa

Quantum spin liquid in the 2*D* anisotropic Heisenberg model with frustrated next nearest neighbor exchange

S. S. Aplesnin

*L. V. Kirenskii Institute of Physics, Siberian branch of the Russian Academy of Sciences, 660036 Krasnoyarsk, Russia**

(Submitted April 22, 1997; revised November 17, 1997)
Fiz. Nizk. Temp. **24**, 759–766 (August 1998)

The two-dimensional ($2D$) Heisenberg model with anisotropic exchange ($\Delta = 1 - J_x/J_z$) and with negative next nearest neighbor exchange (J_2) with $S = 1/2$ is investigated by using the quantum-mechanical Monte-Carlo method. The energy, magnetic moment at a site, heat capacity, and spin-spin correlation functions are calculated. The stability regions for Néel ordering of spins as well as the strip-phase and gapless quantum spin liquid are determined in the interval $\Delta/2 \leqslant J_2/J_1 \leqslant 1/(2\Delta)$. © *1998 American Institute of Physics.* [S1063-777X(98)00808-1]

Over the recent years, a large number of publications have been devoted to the theoretical and experimental studies of $2D$ Heisenberg antiferromagnets (AF) in a square lattice with spin $S = 1/2$. Following the discovery of high-temperature superconductivity in metal oxides, considerable attention has been paid to the investigations of frustrated antiferromagnets with a negative next nearest neighbor interaction. Several elegant theories have been proposed for new types of magnetic states. These are the resonant valence bond (RVB) states proposed by Anderson,[1] which are formed as a result of superposition over all realizations of singlet pairs. Calculations for a 4×4 lattice[2] confirm the closeness of the energies E_{RVB} to the exact value. The N-Fermi approach, in which N different flavors are introduced instead of the two projections of the electron spin S,[3,4] leads to a 1/2-flux state with gapless spin excitation and a power attenuation of the spin–spin correlation function. In the strong frustration region $J_2/J_1 \sim 0.6$, where J_α is the energy of antiferromagnetic exchange interaction between nearest or next nearest neighbors, the existence of gap magnetic states is assumed with an energy gap $\sim (0.1-0.2)J$. These states include that of a quantum spin liquid (SL) with scalar and vector chiral ordering,[4,5] and an ordered dimeric (spin-Peierls) state.[6,7] in the $1/N$ approximation (N is the number of flavors),[6] the energy of the dimeric state is slightly lower than the energy of the chiral spin state: $E_{\mathrm{chiral}}/E_{\mathrm{dimer}} = 0.994$. The exact diagonalization in small lattices[8] gives opposite results: the vector chiral order parameter is double the dimeric parameter. The latter states are described by fractional statistics and have a specific spectrum of spinon, holon, and anyon excitations described in detail by Izyumov *et al.*[9]

Most works devoted to investigation of the Heisenberg model with frustrations assume a long-range AF order at $T = 0$ and $J_2 = 0$. The critical value of J_2/J_1 corresponding to the violation of long-range magnetic order depends on the technique and approximations used in analytic computations and varies between 0.1 and 0.4.[7,10–12] The more precise the uncoupling of spin correlation functions, the smaller the critical value for the frustrated bond. For values of J_2/J_1 in the interval 0.6–0.8, a four-sublattice AF is formed.[7,11] All these investigations are based on Heisenberg's isotropic model although quasi-two-dimensional compounds have an exchange anisotropy $\sim (10^{-4}-10^{-2})J$. For example, CaV_3O_7 with an exchange $J_2/J_1 \approx 1.3$ has a temperature-independent static structural factor $S(q)$ above the Néel temperature.[13] The anisotropy lowers quantum fluctuations and minimizes computational error associated with the finite size of the lattice.

In an earlier work,[14] we studied the dimeric state in an antiferromagnetic Heisenberg chain with four-spin interaction and with a spin $S = 1/2$. The four-spin exchange may be a result of interaction of spins with lattice vibrations (phonons). Expanding the exchange integral in powers of atomic displacements, we obtain the spin–phonon interaction in first-order perturbation theory. Transforming the phonon operators through a displacement by a certain constant[15] determined by the condition of vanishing of terms linear in phonon operators, we obtain the four-spin exchange. Thus the bilinear and four-spin exchange correspond effectively to a spin-Peierls system with a spin-Peierls phase transition in the one-dimensional Heisenberg model.[16] Such a transition corresponds to the formation of spin pairs that are in singlet states with ordered centers of mass relative to one another. In this work, we study the properties of the dimeric state and calculate the dimeric state–paramagnet phase transition temperature as a function of the four-spin interaction. The transition vanishes in the absence of a four-spin interaction, and the calculated properties for the antiferromagnetic chain are in good agreement with the results of computations, e.g., the correlation radius varies according to a power law $\xi = A/T$ in the entire range of temperature T.

Thus, we can single out two problems. The first one concerns the possibility of existence of a quantum spin liquid in an anisotropic frustrated AF and the effect of exchange anisotropy on the stability region of long-range antiferromagnetic order and the quantum spin liquid. The second problem concerns the existence of an energy gap in the excitation spectrum of a quantum spin liquid. The value of the

gap in the SL can be determined from the temperature dependence of heat capacity, susceptibility, and from the dependence of magnetization on the applied magnetic field. We shall use the trajectory algorithm[17] in the Monte-Carlo (MC) method. The basic idea underlying this algorithm is the transformation of a quantum D-dimensional problem into a classical $(D+1)$-dimensional problem by introducing ''time sections'' in the space of imaginary time $0<\tau<1/T$, and the realization of the MC procedure in the ''imaginary time-coordinate'' space.

1. MODEL AND COMPUTATIONAL TECHNIQUE

Let us consider an anisotropic Heisenberg AF with the next nearest neighbor antiferromagnetic interaction in a square lattice with spins $S=1/2$ localized at its sites and directed along the Z-axis coinciding with the direction of the applied field. The Hamiltonian can be presented in the form

$$H=-\sum_{\alpha=1}^{2}\sum_{h_a=1}^{4}\sum_{i=1}^{N}\{J_{\alpha}^{zz}(h_\alpha)S_i^zS_{i+h_\alpha}^z + J_{\alpha}^{x,y}(h_\alpha)(S_i^xS_{i+h_\alpha}^x+S_i^yS_{i+h_\alpha}^y)\} - H^z\sum_{i=1}^{N/2}(S_i^z+S_{i+h_\alpha}^z), \quad (1)$$

where $J\alpha<0$, the summation over h_α is carried out over all neighbors in the αth coordination sphere, $\Delta=1-J^{x,y}/J^z$ is the ''easy axis'' type exchange anisotropy, H^z is external magnetic field, and N the total number of spins.

The algorithm and the MC method were described in detail in an earlier publication.[18] The Hamiltonian is divided into clusters of four spins on a plaquette, and commutation between them is taken into consideration using Trotter's formula. In the MC procedure adopted in our work, we use periodic boundary conditions along Trotter's direction and over the lattice. The linear dimensions of the lattice are $L=40$, 48, 64 and 80, and $m=16$, 32, 48 (where m is a positive integer called Trotter's number). The number of MC steps per spin varies from 3000 to 10000. One MC step involves the rotation of all spins in a lattice of size $L\times L\times 4m$. The energy E and the heat capacity C are defined by formulas

$$E=\left\langle (1/2)\sum_{i,j,r}F_{i,j}^r\right\rangle,\quad F_i^r=-\partial/\partial\beta(\ln\rho_i^r),\quad C=dE/dT. \quad (2)$$

Here $\rho_{i,j}^r$ are matrix elements of the local density matrix $(i,j=1,\ldots,L,\ r=1,\ldots,m)$, and $\beta=1/(k_BT)$. Summation is carried out over eight spin clusters $L\times L\times m$, and the angle brackets indicate thermodynamic averaging. Magnetization M and longitudinal susceptibility χ are defined as

$$M=\left\langle\sum_{i,j,r}M_{i,j}^r\right\rangle,$$

$$M_{i,j}^r=\frac{1}{4m}\sum_{h_x h_y=0}^{1}(S_{i+h_x,j+h_y}^r+S_{i+h_x,j+h_y}^{r+1}),$$

$$(S_i=\pm 1/2),\quad \chi=M/H. \quad (3)$$

We calculated the longitudinal $R(r)=\langle S_0^zS_r^z\rangle$ spin-spin and four-spin $\langle S_0^zS_1^zS_r^zS_{r+1}^z\rangle$ correlation functions and their Fourier transform along the sides and diagonal of a square lattice. The thermodynamic mean of the spin at a site is defined as $\sigma=\lim_{r\to\infty}[\mathrm{abs}(\langle S_0^zS_r^z\rangle)]^{1/2}$. The correlation radius ξ of spin interaction and the pre-exponential index η are defined through the relation

$$R(r)=A/r^{\eta}\exp(-r/\xi), \quad (4)$$

where $R(r)$ is the normalized correlation function $R(r)=\langle S^z(0)S^z(r)\rangle-\langle S^z\rangle^2$. In the model with competing interactions in the absence of a magnetization-type order parameter, a possible characteristic of the system may be the correlation function of locally calibrated operator over an elementary plaquette. These plaquettes may turn out to be ordered, and the type of this order may be determined from the eight-spin correlation function

$$\langle S^z(0)S^z(h_x)S^z(h_y)S^z(h_x+h_y)S^z(r)S^z(r+h_x)\times S^z(r+h_y)S^z(r+h_x+h_y)\rangle. \quad (5)$$

Chiral order may exist in the region of strong frustrations $(J_2\sim 0.5J_1)$. Let us determine the vector parameter of chirality over the smallest triangle

$$\mathbf{F}_{ijk}=(\mathbf{S}_i\times\mathbf{S}_j+\mathbf{S}_j\times\mathbf{S}_k+\mathbf{S}_k\times\mathbf{S}_i) \quad (6)$$

and calculate its z-projection F^z

$$F_{ijk}^z=i[(S_i^+S_j^--S_i^-S_j^+)+(S_j^+S_k^--S_j^-S_k^+)+(S_k^+S_i^--S_k^-S_i^+)]. \quad (7)$$

We calculate the correlation functions of normal and anomalous types of spin operators $\langle S^+(0)S^-(r)\rangle$, $\langle S^+(0)S^+(r)+S^-(0)S^-(r)\rangle$. by using the Hirsch technique.[19] The idea underlying this technique is that the world lines are ruptured at a distance $r=m$ in the Trotter direction, and the wave functions in the S^z representation become equal at this distance. The computation of these correlations requires a new MC procedure with free boundary conditions in the Trotter direction and a doubling of the computation time.

The statistical error in MC computation was determined by using the standard technique. The mean value was computed, the instantaneous value memorized, and the mean square deviation determined after completion of the MC procedure. This error lies in the interval (0.1–2)%. The systematic error arises due to a finite value of the number m and is proportional to $\sim A/(mT)^2$.

In a frustrated AF, the matrix elements in a 16×16 matrix corresponding to a four-spin cluster on a plaquette may assume negative values. However, the probability of local and closed rotations is an even function of negative matrix elements. The probability of global rotations is equal to the product of matrix elements from 1 to m, which may be negative. The statistical weight of these configurations is small and is determined as follows. The number of configurations in the space of negative (positive) weights $Z_-(Z_+)$ is determined by the MC procedure, and the quantity $Z_-/(Z_+$

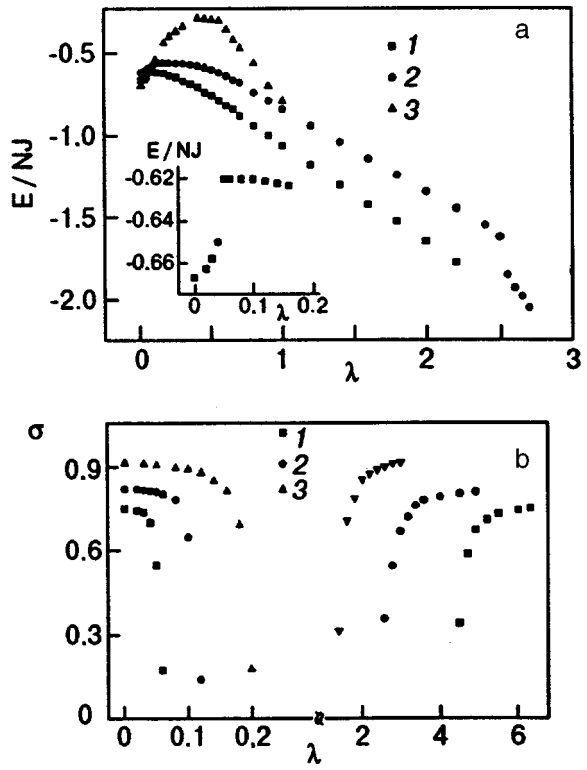

FIG. 1. Dependences of the energy E/NJ of an anisotropic AF with $\Delta=0.05$ (curve *1*), 0.2 (curve *2*), and an isotropic AF[11] (curve *3*) ($\Delta=0.1$ in the inset) (a) and of the magnetization σ at the site for an AF with $\Delta=0.1$ (curve *1*), 0.2 (curve *2*), and 0.4 (curve *3*) (b) on the normalized next nearest neighbor exchange $\lambda=J_2/J_1$.

$+Z_-)=0.02-0.044$ decreases with increasing temperature. This leads to a systematic error of the same order of magnitude in the computed values:

$$\langle A\rangle \approx A_+\{1+Z_-/(Z_+-Z_-)\}. \tag{8}$$

Here A_+ is the sum of physical quantities in the space of positive weights. To improve convergence of thermodynamic means, the sign of the statistical weight of the configuration was not taken into consideration. This is valid if the ratio $(Z_+-Z_-)/(Z_++Z_-)$ tends to a constant value as $T\to 0$.[20] In the region of strong frustrations ($J_2/J_1=0.5$), the difference in the values of energy calculated by taking into account the sign of transition probability $W>0$ and without it abs(W) is $\sim 5\%$.

2. DISCUSSION OF RESULTS

While calculating the thermodynamic characteristics of an anisotropic AF with frustrated next nearest neighbor exchange in the ground state, we shall use the technique of asymptotic continuation of these quantities (calculated at finite temperatures) to $T=0$. The dependence of energy, magnetization at a lattice site, and spin correlation functions on the next-nearest neighbor exchange was calculated for several values of exchange anisotropy $\Delta=0.05$, 0.1, 0.2, 0.3, 0.4, 0.6, 0.75 and 0.8. The critical values of $\lambda_{c1,2}$ corresponding to the vanishing (emergence) of long-range order are determined from the kinks on the energy dependence $E(\lambda)$ and the vanishing of magnetization at a lattice site (Fig. 1).

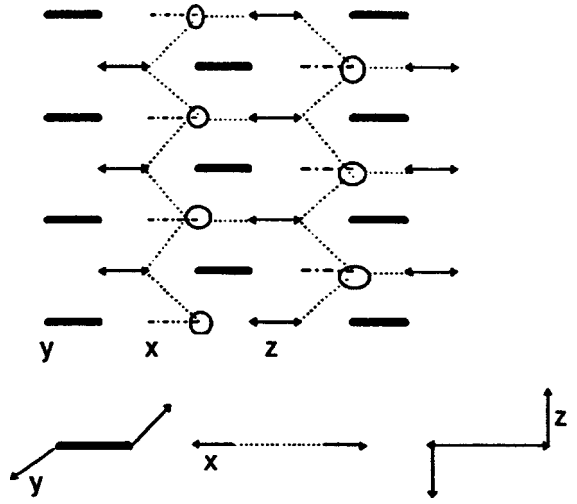

FIG. 2. Magnetic structure of a spin liquid: spin pairs directed along the X-axis (dashed line), Y-axis (solid line), and Z-axis (arrowed line). The dotted line indicates correlations along the longitudinal spin components.

Frustration decreases the absolute value of the energy of an AF by 5–8%. For $\lambda>\lambda_{c1}$, a dimeric state is formed in which dimers are arranged in a particular order. Such a structure can be presented schematically in the form of three types of dimers with a mutually orthogonal arrangement. The fine lines in Fig. 2 show pairs of spins directed along the X-axis, while the thick lines and lines with double arrows indicate respectively the spin pairs directed along the Y- and Z-axes. Spins directed along the Z-axis induce polarization along the longitudinal spin components on the nearest neighbors marked by circles in Fig. 2. The spin–spin correlations along longitudinal components are shown by dashed lines. In this region, the correlation functions along the diagonal of the square [110] at a distance $r=\sqrt{2}a$ are negative for longitudinal components and zero along transverse components as shown in Fig. 2.

Figure 3a shows the spin correlation functions varying with the exchange J_2 in accordance with the magnetic structure presented in Fig. 2. For the critical value $\lambda_1=(1+\Delta)/4$, the sign of $\langle S^z(0)S^z(r=\sqrt{2})\rangle$ varies from positive to negative, and the signs of spin correlation functions of nearest and next nearest neighbors coincide with the signs of the exchange, and the frustration disappears. This leads to an increase in the absolute value of energy. The theoretical value of the energy of the disordered state exceeds all energy values obtained by other methods. Thus, for $\lambda=1/2$ the exact diagonalization gives $E/J=-0.53$,[21] the spherically-symmetric spin-wave theory gives $E/J=-0.26$,[11] while the $1/N$- fermion representation gives $E/J=-0.23$.[4]

Upon a further increase in the exchange J_2, the short-range order in transverse spin components along the diagonal decreases by $r=\sqrt{2}a$ and becomes equal to zero $\langle S^+(0)S^-(r=\sqrt{2})\rangle\approx 0$ (Fig. 3b) for $\lambda=\lambda_2$. Spin correlation functions have a power dependence on distance $\langle S^z(0)S^z(r)\rangle\sim 1/r^\eta$, and can be approximated quite well by a straight line on the logarithmic scale (Fig. 3c) where the exponent η varies in the interval 2.5–3.5 for $\lambda_1<\lambda<\lambda_2$. The chirality parameter calculated over the entire lattice ac-

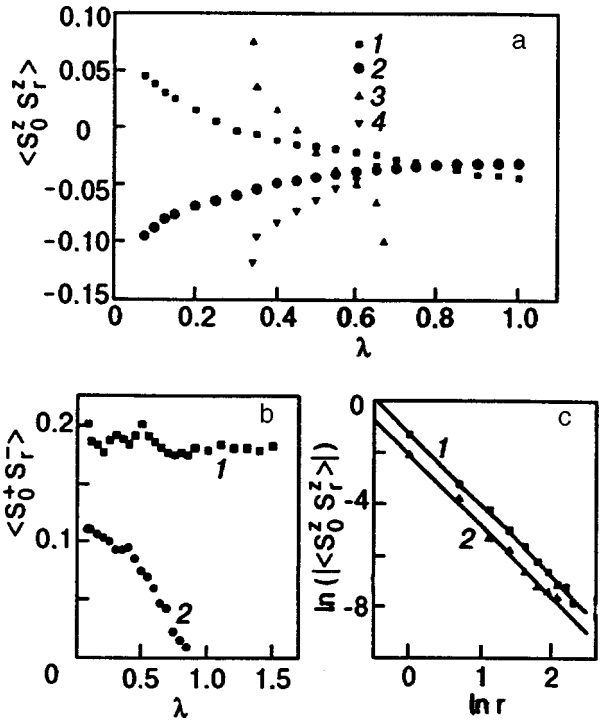

FIG. 3. Spin–spin correlation functions along the longitudinal spin components $\langle S_0^z S_r^z\rangle$ in an SL with $\Delta=0.1$ (*1,2*), 0.75 (*3,4*) at $r=1$ (*2,4*), $\sqrt{2}$ (*1,3*) (a) along transverse spin components $\langle S_0^+ S_r^-\rangle$ with $\Delta=0.1$, $r=1$ (*1*), $r=\sqrt{2}$ (*2*) (b), (c) shows the dependence of the correlation function of an SL with $\Delta=0.05$, $\lambda=0.25$ (*1*), 0.8 (*2*) on logarithmic scale.

cording to formula (8) is equal to zero ($F=0$), i.e., there is no chiral order. The proposed[7] ordering of dimers over sublattices embedded into one another in a staggered manner can be calculated by using the four-spin correlation function defined in these sublattices. The MC computation of four-spin correlation functions along the sides, diagonals and sublattices $\langle S_0 S_1 S_r S_{r+1}\rangle \approx 0$ for $r=L/2$, and does not lead to a long-range order of singlet pairs. There is no correlation between spin plaquettes described by formula (5). At distances $r>a$, the function (5) tends to zero. Hence the long-range order parameter for chiral and singlet ordering of pairs is equal to zero in this state.

The dependence of magnetization on the external magnetic field is linear (Fig. 4c). the critical field $H_c=0$, and hence there is no energy gap between the ground and triplet excited states. The susceptibility is independent of temperature and applied magnetic field in SL. The temperature dependence of heat capacity can be approximated quite well by a power law $C(T)\sim AT^n$, where the exponent n varies between 2 and 3 depending on the value of the exchange J_2. For an exchange anisotropy $\Delta=0.05$, $J_2/J_1=3$ in an SL, the MC results are approximated correctly by a power dependence $C(T)\sim AT^{2.7(2)}$ (Fig. 4a). It was mentioned above that the negative sign of the matrix elements of transition probability leads to a small error of $\sim 3\%$ in the energy values for $\lambda=0.3$. Figure 4b shows the energy values calculated by taking into account the sign of the transition probability (curve *1*) and without taking the sign into consideration (curve *2*). The computational error decreases with increasing temperature.

Let us emphasize the basic characteristics of this state. The thermodynamic mean of the spin is equal to zero, a short-range order exists with a sharp attenuation of spin correlation functions according to a power law, and the energy gap between the ground state and the excited state is equal to zero, which corresponds to the definition of a gapless quantum spin liquid.[22] The magnetic properties of a quantum spin liquid are analogous to those of a ''tomographic'' Luttinger liquid for the two-dimensional case.[23] The existence of a gapless SL in the $2D$-Heisenberg model with frustrations is in accord with the general theorem of Lieb, Schultz and Mattis[24] applied to the two-dimensional case.[25] According to this theorem, the disordered phase of an antiferromagnet containing an arbitrary half-integral spin in a unit cell must have a broken symmetry or gapless excitations.

The energy of an SL in the isotropic case can be presented in the form of the energy of singlets in J_1 and the energy along longitudinal spin components with J_2 (the Ising component $\sim 2S^2J_2$): $E=-0.687-0.5\lambda$, which is in good agreement with the MC results for $\lambda>\lambda_2$ where the correlation functions along the longitudinal components become equal at distances $r=1$ and $r=\sqrt{2}$ (Fig. 3a). The exponent η begins to decrease with increasing exchange J_2 to $\eta\approx 1$ for

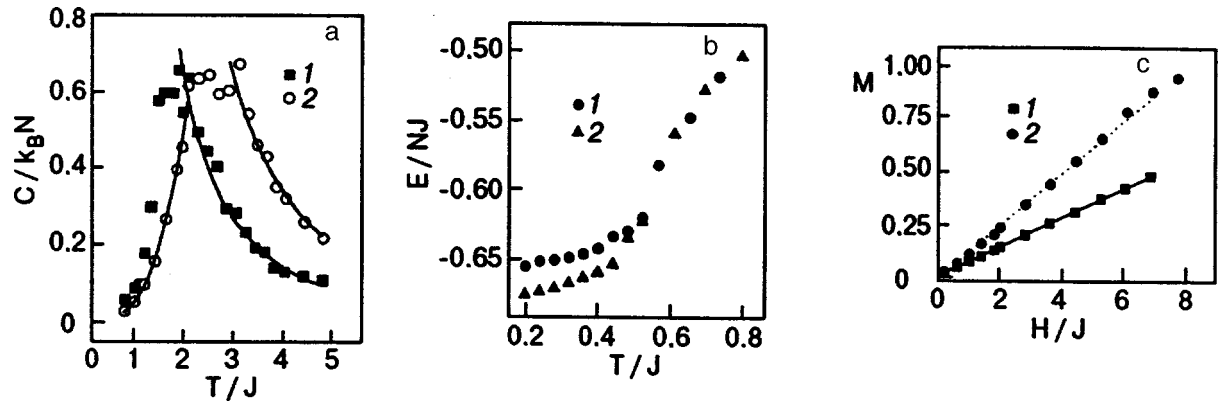

FIG. 4. (a) Temperature dependence of the heat capacity C/k_BN of a spin liquid for $\Delta=0.05$, $\lambda=2$ (curve *1*) and 3 (curve *2*); (b) temperature dependence of energy E/NJ calculated without taking (curve *2*) and taking (curve *1*) into consideration the sign of transition probability for $\Delta=0.05$, $\lambda=0.3$; (c) dependence of the magnetization M on the applied field in a spin liquid with $\Delta=0.05$, $\lambda=1$ (curve *1*) and 2 (curve *2*).

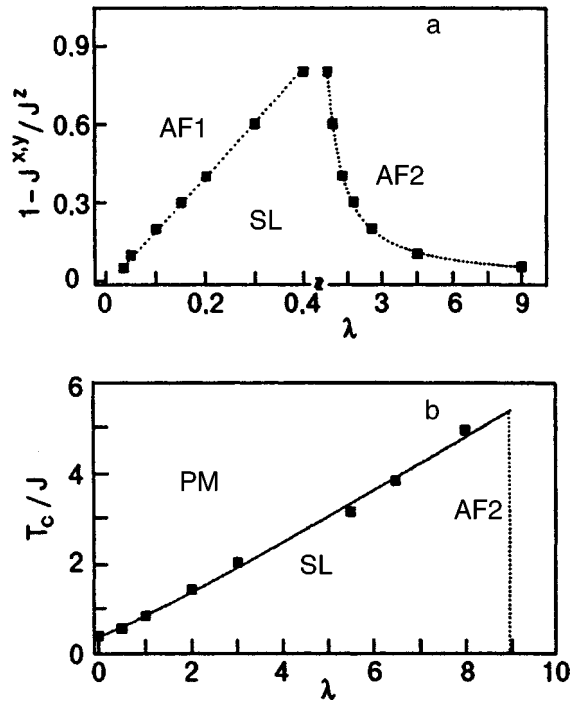

FIG. 5. Phase diagram of the ground state of a Néel antiferromagnet (AF1), strip-phase (AF2) and quantum spin liquid (SL) in the coordinates exchange anisotropy vs. normalized nearest neighbor interaction (a), and of a paramagnet (PM), AF2 and SL in the temperature vs. λ coordinates for $\Delta = 0.05$ (b).

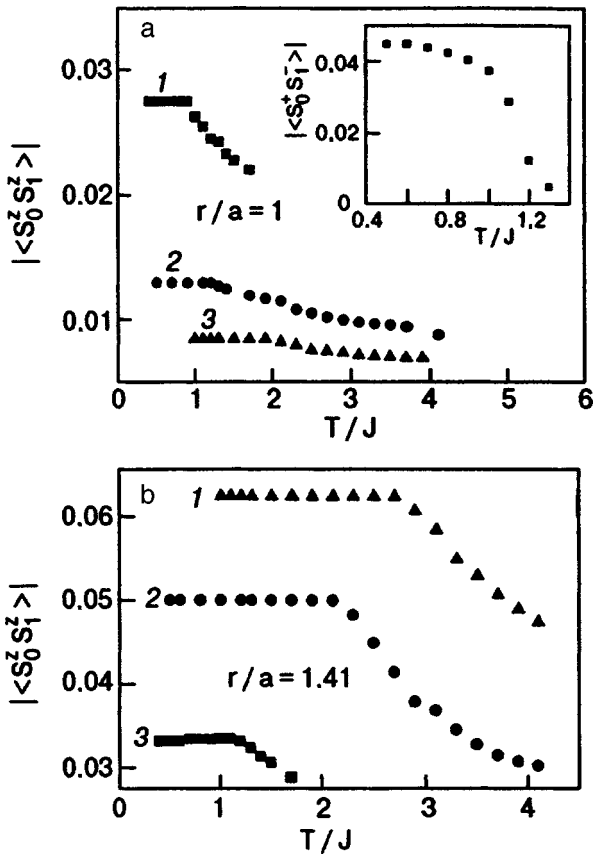

FIG. 6. Temperature dependence of spin correlation functions along longitudinal components in a spin liquid with $\Delta = 0.05$, $\lambda = 1$ (*1*), 2 (*2*), and 3 (*3*) at a distance $r/a = 1$ (a) and $\sqrt{2}$ (b). The inset shows the same dependence for $r/a = 1$ with $\lambda = 2$ along the transverse components.

$\lambda = \lambda_{c2}$. A four-sublattice AF structure obtained by the method of exact diagonalization[12,21] or analytically[11,26] can be singled out over several nearest neighbors. This structure is formed by two spin sublattices with a staggered ordering and a unit cell size $\sqrt{2}a$ embedded one into the other. On account of an inadequate consideration of spin correlations in analytic computations and the small size of lattice in an exact diagonalization, the variation in the short-range order for $\lambda_1 = (1+\Delta)/4$ and λ_2 is naturally associated with the violation of the Néel state and the emergence of a strip phase (AF2) with a ferromagnetic ordering of spins along one side of a square, and an antiferromagnetic ordering along the other side. The strip phase, determined from the Fourier spectrum $\langle S_{-q}S_q\rangle$ in MC computations, is degenerate for two vectors $\mathbf{Q}(0,\pi/a)$ and $\mathbf{Q}(\pi/a,0)$, and a spontaneous breaking of symmetry occurs along one of these vectors for $\lambda \geqslant \lambda_{c2}$. The interpolation of the critical values λ_{c1} and λ_{c2} calculated by the MC technique leads respectively to a linear $\lambda_{c1} = \Delta/2$ and inverse $\lambda_{c2} = 1/2\Delta$ dependence on exchange anisotropy. An asymptotic continuation for the isotropic case reveals the absence of a long-range order of the strip-phase type. Figure 5a shows the phase diagram of the ground state of an anisotropic Néel antiferromagnet (AF1), strip phase (AF2), and of a quantum spin liquid. Only one line corresponding to the isotropic case $\Delta = 0$ was investigated earlier. Our computations reveal the absence of a long-range order for all values of the exchange $J_2 < 0$, and two types of short-range order for $\lambda < 0.25$ and $\lambda > 0.75$ with a power dependence of the spin correlation functions on distance. In the interval $0.25 < \lambda < 0.75$, the spin–spin correlation function decreases sharply with distance: $\langle S^z(0)S^z(r)\rangle \sim 1/r^{3.5(3)}$.

For the order parameters in a quantum spin liquid, we can take correlation functions at distances $r = 1, \sqrt{2}$. The correlation functions along the longitudinal components are independent of temperature (in contrast to those along the transverse components). Since the excitations in SL are spinons, a singlet pair is transformed into a triplet with $S^z = 0$. The static structural factor $s(Q)$, viz., the Fourier harmonic of the pair correlation function at $Q = \pi/a$ for $\lambda < \lambda_2$ and $Q = \pi/(\sqrt{2}a)$ for $\lambda > \lambda_2$, has a temperature dependence analogous to the dependence $\langle S^z(0)S^z(r = 1,\sqrt{2}a)\rangle$ shown in Fig. 6. Two temperature transitions appear in the spin liquid for $\lambda > \lambda_2$. The first transition is associated with the violation of the dimeric order at $T = T_{1c}$, where the relation $\langle S^+(0)S^-(r=1)\rangle - \langle S^z(0)S^z(r=1)\rangle$, characteristic for an AF with Néel ordering of spins is satisfied. The developed long-range magnetic order in longitudinal components shown by a dashed line in Fig. 2 is preserved for $T > T_{1c}$, and is transformed into a paraphrase at $T = T_{2c}$. The spin correlation function $\langle S^z(0)S^z(r=\sqrt{2})\rangle$ has a singularity at this temperature (Fig. 6b), and the dependence of the spin–spin correlation function on distance changes from power to exponential. In the temperature interval $T_{1c} < T < T_{2c}$, the heat capacity (Fig. 4) and susceptibility have their maximum values. For $T > T_{2c}$, the temperature dependence of heat capacity is analogous to that for a paramagnet:

$C(T) \sim A/T^2$ (Fig. 4). Figure 5b shows the range of existence of the spin liquid on the temperature-exchange (normalized to next nearest neighbor) plane. The long-range magnetic order[13] is formed in CaV_3O_7 due to a weak interaction between planes. Above $T_N = 2$ K, the magnetic static structural factor $s(Q)$ is independent of temperature up to $T = 40$ K, and has a noncommensurate vector $\mathbf{Q} \sim 0.7\pi(1,1)$ in the basal plane. A quantum spin liquid is probably formed in this temperature interval.

Summarizing the results of this research, we can conclude that for the anisotropic frustrated $2D$-Heisenberg model with antiferromagnetic interactions, a gapless spin liquid exists in the interval $\Delta/2 < \lambda < 1/2\Delta$. For $\lambda > (1+\Delta)/4$, the spin-spin correlation functions for the nearest and next-nearest neighbors are negative and frustration vanishes. Long-range chiral and dimeric order do not exist in a quantum spin liquid. The spin–spin correlation function has a power dependence on distance in SL.

*E-mail: gap@iph.krasnoyarsk.su

[1] P. W. Anderson, Mater. Res. Bull. **8**, 153 (1973).
[2] J. Richter, Phys. Lett. A **140**, 81 (1989).
[3] I. Affleck and J. B. Marston, Phys. Rev. B **37**, 3774 (1988).
[4] D. Poilblanc, Phys. Rev. B **42**, 4049 (1990).
[5] S. Spielman, K. Fesler, C. B. Eom *et al.*, Phys. Rev. Lett. **65**, 123 (1990).
[6] X. G. Wen, F. Wilczek, and A. Zee, Phys. Rev. B **39**, 11413 (1989).
[7] M. P. Gelfand, R. P. Singh, and D. A. Huse, Phys. Rev. B **40**, 10801 (1989).
[8] J. Richter, Z. Phys. B **79**, 403 (1990).
[9] Yu. A. Izyumov, M. I. Katsnel'son, and Yu. N. Skryabin, *Magnetism of Collectivized Electrons* [in Russian], Fizmatlit, Moscow (1994).
[10] A. V. Mikheenkov, E. L. Nagaev, and E. V. Zhasinos, Phys. Lett. A **205**, 101 (1995).
[11] A. F. Barabanov and V. M. Beresovsky, Phys. Lett. A **186**, 175 (1994).
[12] H. J. Shulz, T. A. L. Ziman, and D. Poilblanc, J. Physiol. (Paris) **6**, 675 (1996).
[13] H. Harashina, K. Kodama, and S. Shamoto *et al.*, J. Phys. Soc. Jpn. **65**, 1570 (1996).
[14] S. S. Aplesnin, Fiz. Tverd. Tela (St. Petersburg) **38**, 1868 (1996) [Phys. Solid State **38**, 1031 (1996)].
[15] È. L. Nagaev, *Magnets with a Complex Exchange Interaction* [in Russian], Fizmatlit, Moscow (1988).
[16] L. N. Bulaevskii, A. I. Buzdin, and D. I. Khomskii, Solid State Commun. **27**, 5 (1978).
[17] H. Raedt and A. Lagendijk, Phys. Rep. **127**, 233 (1985).
[18] S. S. Aplesnin, Zh. Eksp. Teor. Fiz. **112**, 2184 (1997) [JETP **85**, 1196 (1997)].
[19] J. E. Hirsch and R. L. Sugar, Phys. Rev. B **26**, 5033 (1982).
[20] J. E. Hirsch, P. J. Scalapino, R. L. Sugar, and R. Blankenbecler, Phys. Rev. Lett. **47**, 1628 (1981).
[21] J. Richter, Phys. Rev. B **47**, 5794 (1993).
[22] F. D. M. Haldane, Phys. Rev. Lett. **50**, 1153 (1983).
[23] P. W. Anderson, Phys. Rev. B **42**, 2624 (1990).
[24] E. Lieb, T. Schultz, and D. Mattis, Ann. Phys. **16**, 407 (1961).
[25] I. Affleck, Phys. Rev. B **37**, 5186 (1988).
[26] H. A. Schulz and T. A. Ziman, Europhys. Lett. **18**, 355 (1992).

Translated by R. S. Wadhwa

LOW-DIMENSIONAL AND DISORDERED SYSTEMS

Order parameter fluctuations and superconducting transition temperature in quasi-2*D* metals with arbitrary carrier density

V. M. Loktev

*N. N. Bogolyubov Institute of Theoretical Physics, National Academy of Sciences of the Ukraine, 252143 Kiev, Ukraine**)

V. M. Turkowski

T. G. Shevchenko University, 252127 Kiev, Ukraine

(Submitted March 17, 1998)
Fiz. Nizk. Temp. **24**, 767–772 (August 1998)

It is shown that the order parameter fluctuations result in a power dependence of the superconducting transition temperature in quasi-2*D* metals on the probability of fermion hopping between layers. The dependence of this temperature on the carrier concentration is determined for a model with indirect attraction between carriers. It is found that the transition takes place at temperatures lower than those expected from the BCS theory. © *1998 American Institute of Physics.* [S1063-777X(98)00908-6]

INTRODUCTION

The problem of crossover from superfluidity (Bose–Einstein condensation) of compound bosons to BCS-type superconductivity has acquired considerable importance over the last few years. This is due to well-manifested peculiarities of the superconducting transition in high-temperature superconductors (HTSC) whose behavior depends significantly on the concentration n_f of free carriers in them (see, for examples, Refs. 1–5). However, even if we disregard the earlier (before the creation of the BCS theory) attempts to associate the phenomenon of superconductivity with Bose–Einstein condensation (see Ref. 6 for an excellent account of the history and physics of superconductivity by I. M. Dmitrenko), it is worthwhile to note that the problem of crossover began to be studied intensively at the end of the sixties following the observation of anomalies in the conductivity of metal–ammonia solutions. In order to explain these anomalies, Dmitrenko and Kulik[7] used the idea of tunneling and superfluidity of local pairs whose formation was associated with a strong nonretarded interaction U (Hubbard's model with $U<0$ was used), while the superconducting transition temperature T_c was found to be proportional to $n_f^{2/3}$, which corresponds to a possible Bose condensation of pairs formed in a $3D$-system at $T>T_c$. Dmitrenko and Kulik[7] did not calculate the chemical potential μ of Fermi particles (carriers) which must be negative in such situations,[8,9] i.e., there must be no Fermi surface.

Under the same assumptions (disregarding fluctuations), $T_c \propto n_f$ in $2D$-systems, which is indeed observed with a considerable degree of precision[1,10–12] if we take into consideration weakly doped HTSC samples. Since copper oxides can be treated as $2D$-systems to a good approximation, it would seem that such a concentration dependence of T_c should indicate Bose condensation of local pairs which is used for interpreting some other experimental data also[13] (see also our review.[5]) This, however, is not in accord with the photoelectron spectra ARPES[14,15] which point towards the presence of a Fermi surface in metallic phases of HTSC, and hence a positive value of μ and thus the absence of pairs in the **r**-space. Moreover, real copper oxides are quasi-two-dimensional, strictly speaking, and this circumstance is extremely important from the point of view of the possible formation of a uniform (including superconducting) order parameter in them. Finally, it is unlikely that the attractive fermion–fermion interaction in conductors of any dimensionality can occur without retardation effects.

Hence, in this publication dedicated to the 70th birth anniversary of I. M. Dmitrenko in July 1998, we shall endeavor to consider crossover on the basis of a more real model than in Ref. 7, i.e., the model with an indirect attraction between fermions (in the framework of the simplest Fröhlich Hamiltonian). We shall also generalize the approach to obtaining the $T-n_f$ phase diagram of $2D$ metals with an arbitrary charge carrier, which was developed in Refs. 16 and 17, to the $3D$ case which emerges when the interlayer (Josephson) tunneling is taken into account. It will be proved that when the probability of the emergence of the third direction is low, the value of T_c is much smaller than the mean-field value ($T_c^{MF} \equiv T_c^{BCS}$) which follows formally from the BCS theory. In contrast to the case of nonretarded attraction, retardation is responsible for different behavior of T_c and T_c^{MF} upon a change in n_f even in the concentration region in which the generally accepted assumption (see Refs. 3 and 5) of the BCS theory concerning the validity of the equality $\mu=\varepsilon_F$ (ε_F is the Fermi energy) is valid. Another unsolved problem remaining in the HTS physics is the behavior of the function $T_c(n_f)$ in the range of large n_f (strong

doping), in which it rapidly drops to zero for most cuprate compounds.[18–20] We propose that such a behavior can be due to doping-induced degradation of intermediate long-wave bosons (which are henceforth referred to as Einstein's phonons) whose exchange causes attraction between charge carriers.[1)]

FORMULATION OF THE MODEL

Let us consider a system of parallel planes. One-electron states in each plane are characterized by a quasimomentum and spin, while the probability of hops between planes is low. The system defined in this way is basically similar to that studied for the first time by Efetov and Larkin[23] (see also Ref. 24) who analyzes a quasi-1D case in the BCS approximation. In the case of quasi-2D electrons interacting with phonons, the density of the Hamilton system can be written in the form ($\hbar=1$)

$$H=-\sum_{i,\sigma}\left[\psi_\sigma^+(x_j)\left(\frac{\nabla^2}{2m}+\mu\right)\psi_\sigma(x_j)+g_{\rm ph}\psi_\sigma^+(x_j)\psi_\sigma(x_j)\varphi(x_j)\right]+H_{\rm ph}+t_J\sum_j\psi_\uparrow^+(x_j)\psi_\downarrow^+(x_j)\psi_\downarrow(x_{j-1})\psi_\uparrow(x_{j-1}),$$

$$x_j\equiv(\mathbf{r}_j^{2D},t). \tag{1}$$

In this expression, the notation is adopted, according to which j labels conducting planes, $\psi_\sigma(x_j)$ and $\varphi(x_j)$ are the operators of electron and phonon fields of the jth plane, $g_{\rm ph}$ is their coupling constant, m and $\sigma=\uparrow,\downarrow$ are the fermion mass and spin, $t_J\sim|t_{\rm coh}|^2/W$ is the constant of Josephson's (two-particle) tunneling whose role in the transverse (relative to cuprate layers) transport in HTSC is regarded as significant in spite of its weakness (see Ref. 25), $t_{\rm coh}$ is the amplitude of coherent electron transition between adjacent planes, W the width of conduction band, and $H_{\rm ph}$ the Hamiltonian of a free Bose field which will be regarded as nondispersive and characterized by frequency ω_0 for the sake of simplicity. It should be noted that in view of the ionic nature of HTSC compounds, it is optical weakly dispersive phonon branches that are often regarded as probable intermediate bosons ensuring attraction sufficient to attaining high T_c.[26–30]

The propagator of free bosons, which determines this attraction, has the standard form[31]

$$D(\omega)=\frac{2\omega_0}{\omega^2-\omega_0^2+i\delta},\quad \delta\to0, \tag{2}$$

which will be slightly modified artificially in order to take into account the following physical circumstances: we assume that as the value of n_f increases, long-wave bosons with $\mathbf{k}\lesssim\mathbf{k}_{\rm min}$ become strongly attenuating and cease to be carriers of fermion–fermion interaction. Here the boundary momentum $\mathbf{k}_{\rm min}$ is proportional to the Fermi momentum $\mathbf{k}_F$ so that $k_{\rm min}=\alpha k_F\equiv\alpha\sqrt{2m\varepsilon_F}$, where α is a free parameter. It should be recalled that $\varepsilon_F=\pi n_f/m$ for free 2D fermions with a quadratic energy–momentum relation.[22] Formally, such an assumption boils down to the replacement of (2) by the propagator

$$D(\omega,\mathbf{k})=D(\omega)\,\theta(k-k_{\rm min}), \tag{3}$$

which obviously coincides with $D(\omega)$ for $n_f=0$.

Knowing (1) and (3) and introducing the order parameter $\Phi_j(x,y)=\omega_0\langle\psi_\uparrow(x_j)\psi_\downarrow(y_j)\rangle$, we can easily calculate the density of the effective thermodynamic potential Ω of the system by using the method proposed in Refs. 16 and 17 (see also Ref. 5 and 32), which can help in an analysis of the superconducting properties of the system. This method is based on the phase–modulus concept for the function $\Phi_j(x,y)=\Delta_j(x,y)\exp[i\theta_j(x,y)]$, which is regarded as inhomogeneous since long-range uniform ordering in a pure 2D system at finite temperatures is impossible. Such a parametrization is also convenient and physically justified since the absence of this ordering is due to just thermal fluctuations of the order parameter phase.

However, we cannot determine Ω under such quite general assumptions. For this reason, an admissible approximation is the disregard of nonuniformity and fluctuations of the modulus of the order parameter, leading to the equality $\Delta_j(x,y)\Delta(n_f,T)\equiv\Delta$. The other assumption concerns the smoothness of phase fluctuations, or the smallness of the quantity $\nabla_j\theta_j(x,y)$, which allows us to calculate the value of Ω to within $[\nabla_j\theta_j(x,y)]^2$ (long-wave approximation).

Carrying out the appropriate calculations which in fact are the same as in Ref. 16, we can arrive at the expression

$$\frac{\Omega}{N_{\mathbf{c}}}=\Delta^2-\int\frac{d\omega d\mathbf{k}}{(2\pi)^3}\left[2T\,\ln\cosh\frac{\sqrt{\xi^2(\mathbf{k})+\Delta^2}}{2T}-\xi(\mathbf{k})\right]\times D(\omega,\mathbf{k})+\int_0^{1/T}d\tau\int d\mathbf{r}^{2D}J(\mu,\Delta,T)(\nabla\theta)^2-\frac{t_J\Delta^2}{N_{\mathbf{c}}}\int dx\{1-\cos[\theta_j(x,x)-\theta_{j-1}(x,x)]\}, \tag{4}$$

in which the coefficient

$$J(\mu,\Delta,T)=\frac{1}{16\pi}\left\{\sqrt{\mu^2+\Delta^2}+\mu+2T\,\ln\left[1+\exp\left(-\frac{\sqrt{\mu^2+\Delta^2}}{T}\right)\right]\right\}-\frac{T}{8\pi}\left[1-\left(\frac{\Delta}{2T}\right)^2\frac{\partial}{\partial(\Delta/2T)}\right]\times\int_{-\mu/2T}^{\infty}dx\,\frac{x+\mu/2T}{\cosh^2\sqrt{x^2+(\Delta/2T)^2}} \tag{5}$$

is a quantity playing the role of stiffness relative to nonuniform ''shear'' deformations of the order parameter in the plane of its definition, and $\xi(\mathbf{k})=\mathbf{k}^2/2m-\mu$. While writing expressions (4) and (5), we have omitted the subscript j on the terms where it is insignificant and introduced the number $N_{\mathbf{c}}$ of planes per unit length along the **c**-axis perpendicular to the planes. Thus, the expression obtained for Ω is the starting expression for deriving equations describing the behavior of

characteristic temperatures as functions of n_f. It should be noted that the form of effective potential is in accord with the expression derived by Abrikosov,[24] who assumed that interplanar tunneling occurs through resonant two-level centers which are always present in finite quantity between conducting layers of real HTSC samples. In addition, coefficient (5) in Ref. 24 was assumed to be equal to the density of superconducting condensate.

PHASE DIAGRAM OF THE SYSTEM

It should be mentioned above all that the quasi-$2D$ model under consideration (as well as the $2D$ model) has two, and not one, characteristic temperatures[16,23]: T_c^{BCS} at which the modulus of the order parameter Δ (which naturally depends on T as well as on n_f) emerges and starts being ''ordered,'' and T_c which is the true superconducting transition temperature appearing as a result of the quasi-two-dimensional nature of the system (in the $2D$ case, the Berezinskii–Kosterlitz–Thouless temperature plays the role of the critical temperature).[5,16] No spontaneous breaking of continuous symmetry of operator (1) at T_c^{BCS}, and this temperature is not critical since it is typical of relatively fast formation of the quantity Δ. Below this temperature, the modulus of $\Delta \neq 0$, but there is no nondiagonal long-range order down to the point $T = T_c$ in view of well-developed long-wave transverse fluctuations. This, in turn, indicates that the wave functions of pairs of incoherent in the region $T_c \lesssim T \lesssim T_c^{BCS}$, and their phases are random in different regions and planes.

Although T_c^{BCS} is not critical, its behavior can easily be determined by writing an equation for Δ in the self-consistent field (BCS) approximation:

$$\Delta = -ig_{\rm ph}^2 \int \frac{d\omega\, d\mathbf{k}}{(2\pi)^3} \frac{D(\omega,\mathbf{k})\Delta}{\omega^2 - \xi^2(\mathbf{k}) - \Delta^2 + i\delta}, \tag{6}$$

which is a direct consequence of the fulfillment of the condition

$$\left.\frac{\partial\Omega}{\partial\Delta}\right|_{\nabla\theta=0, t_J=0} = 0$$

of the minimum of effective potential disregarding hops between the layers. Expression (6) contains unknown chemical potential whose expression can be derived from the standard definition

$$\left.\frac{\partial\Omega}{\partial\mu}\right|_{\nabla\theta=0, t_J=0} = -n_f$$

and has the form

$$\sqrt{\mu^2+\Delta^2} + \mu + 2\ln\left[1 + \exp\left(-\frac{\sqrt{\mu^2+\Delta^2}}{T}\right)\right] = 2\varepsilon_F. \tag{7}$$

Thus, Eqs. (6) and (7) form a closed self-consistent system of equations whose solutions are analyzed in Ref. 16. The explicit dependences $T_c^{BCS}(n_f)$ and $\mu(T_c^{BCS}, n_f)$ follow directly (6) and (7) if we use the criterion $\Delta \to 0$ specifying the critical line in the same approximation.

The temperature T_c can be obtained by using the same expression (4) taking into account the last term since it corresponds to the global $(3D)$ ordering. In the case of weak tunneling assumed by us and apparently corresponding to HTSC compounds, the required temperature is the temperature of stabilization of the unified phase $\theta_j(x,y) = \theta$ in all the layers, which can be attributed, following Refs. 23 and 24, to the universal value of $\langle\cos\theta\rangle \neq 0$, thus becoming the order parameter that can be determined from the equation[23]

$$\langle\cos\theta\rangle = \left\{\int D\theta \exp\left[-\frac{\Omega^{MF}(\theta)}{T}\right]\right\}^{-1} \times \int D\theta \cos\theta \exp\left[-\frac{\Omega^{MF}(\theta)}{T}\right], \tag{8}$$

where

$$\Omega^{MF}(\theta) = N_{\mathbf{c}} \int d\mathbf{r}^{2D}[J(\mu,\Delta,T)(\nabla\theta)^2 - t_J\Delta^2\langle\cos\theta\rangle\cos\theta] \tag{9}$$

is the total effective potential of unit volume of a quasi-$2D$ system, which is actually taken in the self-consistent (or mean) field approximation, but with θ-fluctuations taken into consideration. However, the thermodynamic potential (9) and Eq. (8) corresponding to it take into account only classical fluctuations of the field $\Phi_j(x,y)$. At the same time, quantum fluctuations requiring special consideration must be significant either for extremely low temperatures, or for very small values of n_f. Both cases can be difficult for an experimental verification since copper oxides whose conductivity is determined by a heterovalent doping undergo a metal–insulator transition for $n_f \lesssim 0.05$ and become nonsuperconducting.

An explicit expression for T_c can be obtained from the condition for the existence of a nonzero solution of Eq. (8) taking into account (6) and (7). Assuming, as usual, that $\langle\cos\theta\rangle \ll 1$ at the point of transition and carrying out the required expansion on the right-hand side of (8), after calculating the functional integral (even for $t_J \to 0$) we arrive at the final expression

$$T_c^3 = N_{\mathbf{c}}^3 t_J J^2(\mu,\Delta,T_c)\left(\frac{\Delta}{\omega_0}\right)^2, \tag{10}$$

where $J(\mu,\Delta,T)$ is defined in (5). It will be proved below that this formula gives a dependence $T_c(n_f)$ differing from those obtained earlier for quasi-$1D$[23] and $3D$[7] cases. Moreover, expression (10) shows, first, that $T_c = 0$ for $t_J = 0$ as expected, and second, this formula is also valid in the limit of large n_f for which $\mu = \varepsilon_F$, and Cooper (and not local) pairing is formed in the system.

We can easily derive the asymptotic forms for both temperatures T_c^{BCS} an T_c. Indeed, in the range of small n_f where $\varepsilon_F/\omega_0 \ll 1$, the temperature T_c^{BCS} satisfies the equation $T_c^{BCS}\ln(T_c^{BCS}/\varepsilon_F) = \omega_0 \exp(-4\pi/g_{\rm ph}^2 m)$ which directly implies that $\partial T_c^{BCS}/\partial\varepsilon_F \to \infty$, for $\varepsilon_F \to 0$. In the same range, we have

$$T_c = \frac{N_{\mathbf{c}}}{2}\left[\frac{1}{\pi^2}\frac{t_J}{\omega_0}\exp(-4\pi/g_{\rm ph}^2 m)\right]^{1/3} \varepsilon_F \sim N_f, \tag{11}$$

where N_f is the volume concentration of free charge carriers. In other words, the critical temperature is a linear function of n_f, while the quantity $2\Delta(T=0)/T_c \sim n_f^{-1/2}$, for example, is much larger than its canonical (BCS) value ≈ 3.5. Naturally, the power of n_f differing from those determined in Refs. 7 and 23 is actually a consequence of the $2D$ nature of the system since the tunneling constant was assumed to be a small parameter in the analysis of (8) and in the derivation of (10). It follows from (11) that an increase in this parameter increases T_c on one hand, while on the other hand it can lead (if the smallness criterion is violated) to corrections which ''replace'' the linear dependence (11) by the dependence $T_c \propto N_f^{2/3}$ obtained by Dmitrenko and Kulik.

In the region of large values of n_f, the temperature $T_c^{BCS} \sim \Delta(T=0) = \text{const}$ if $\varepsilon_F/\omega_0 \gg 1$ and $\mu = \varepsilon_F$, and the dependence $T_c^{BCS}(n_f)$ corresponds to the BCS–Eliashberg theory. Since the density of states in this theory is independent of energy in the $2D$ case, $T_c^{BCS}(n_f)$ turns out to be constant. At the same time, it follows directly from (10) that T_c continues to increase, approaching T_c^{BCS} only asymptotically so that $T_c^{BCS} - T_c \to 0$, and such a behavior is preserved for all $\alpha \leqslant 1$ (see (3)). The inequality $\alpha > 1$ appears to be more interesting: in this case, a point $\varepsilon_F^{\rm cr}$ (or, which is the same $n_f^{\rm cr}$) exists at which $T_c^{BCS} = T_c = 0$. In other words, for $n_f \geqslant n_f^{\rm cr}$, a quasi-$2D$ metal with degrading long-wave intermediate bosons must lose its superconducting properties. Then it can be concluded from (4) that if $\varepsilon_F \leqslant \varepsilon_F^{\rm cr} = \omega_0(\alpha-1)\exp(-4\pi/g_{\rm ph}^2 m)$, we have

$$T_c^{BCS} = \omega_0 \ln^{-1} \frac{2\varepsilon_F^{\rm cr}}{\varepsilon_F^{\rm cr} - \varepsilon_F};$$

$$T_c = \omega_0 \left[\frac{3^5}{2^{12}\pi^2} N_{\mathbf{c}}^3 \frac{t_J(\varepsilon_F^{\rm cr})^{12}}{\omega_0^{13}} (\alpha-1)^{10} \left(1 - \frac{\varepsilon_F}{\varepsilon_F^{\rm cr}} \right)^5 \right]^{1/11}. \tag{12}$$

In all cases, $T_c < T_c^{BCS}$, i.e., the region $T_c \leqslant T \leqslant T_c^{BCS}$ is actually a pseudogap as in the $2D$ case since $\Delta \neq 0$ in it. An analysis of this region was carried out in Refs. 5 and 16. It should be borne in mind, however, that $\Delta(T_c^{BCS}) = 0$ only in the BCS approximation and that in actual practice the value of $\Delta(T)$, or pseudogap, can in principle be finite in the range of $T > T_c^{BCS}$.

CONCLUSION

Thus, the finite temperature of stabilization of a uniform order parameter is completely controlled by tunneling between layers (the stronger the tunneling, the higher the value of T_c which in turn is always smaller than T_c^{BCS}). The pseudogap phase possessing peculiar properties can also exist in quasi-$2D$ systems. Many thermodynamic parameters (e.g., the paramagnetic susceptibility)[17] exhibit a peculiar behavior and are smooth in the range of the true superconducting transition temperature T_c. Naturally, the model under investigation, which describes the crossover from superconductivity at low carrier concentrations (superfluidity of local pairs) to the BCS superconductivity, fails to give a complete idea of the behavior of HTSC systems which, strictly speaking, cannot be described by the models with free (and not strongly correlated) charge carriers. A generalization of the theory to the case of strong (Hubbard) electron–electron correlations will be carried out in a separate publication.

It is with a sense of deep satisfaction and responsibility that we dedicate this research to the jubilee of Academician Igor Mikhailovich Dmitrenko (National Academy of Sciences of the Ukraine), who is a leading light and an enthusiast of low-temperature physics and technology. The generally recognized experimental investigations carried out by him for many years created the foundations and stimulated the formation of a large number of fundamental trends in superconducting physics and its applications, such as Josephson and point-contact spectroscopy, nonequilibrium superconductivity, analysis of the properties of the resistive state and quantum interference effects.

*)E-mail: vloktev@gluk.apc.org

1)By way of an analogy, we can mention low-frequency spin fluctuations whose spectrum becomes diffusive upon an increase in n_f.[21,22] This, in turn, points towards the suppression of the long-range magnetic order in the initially AFM ordered copper oxide layers in HTS. On the other hand, the disregard of the intermediate boson dispersion allows us to solve the obtained equations analytically. However, the complete self-consistent solution of the problem is hardly possible at present.

[1] Y. I. Uemura, in *Proceedings Workshop in Polarons and Biopolarons in High-T_c Superconductors and Related Materials*, Cambridge, 1994 (ed. by E. Salje), University Press, Cambridge (1995).
[2] V. J. Emery and S. Kivelson, Nature (London) **374**, 434 (1995).
[3] V. M. Loktev, Fiz. Nizk. Temp. **22**, 3, 490 (1996) [Low Temp. Phys. **22**, 1, 376 (1996)].
[4] D. Pines, Tr. J. Physics **20**, 535 (1996).
[5] V. M. Loktev and S. G. Sharapov, Cond. Mat. Phys. No. 11, 131 (1997).
[6] I. M. Dmitrenko, *In the Realm of Superconductivity* [in Russian], Naukova Dumka, Kiev (1981).
[7] I. M. Dmitrenko and I. O. Kulik, Phys. Status Solidi B **64**, K13 (1974).
[8] A. I. Akhiezer, S. V. Peletminskii, and A. A. Yatsenko, Ukr. Fiz. Zh. **39**, 1852 (1993).
[9] M. Randeria, in *Bose–Einstein Condensation* (ed. by A. Griffin, D. W. Snoke, and S. Stringari), Cambridge, University Press, New York (1995).
[10] J. B. Torrance, Y. Tokura, A. I. Nazzal *et al.*, Phys. Rev. Lett. **61**, 1127 (1988).
[11] S. Uchida, T. Ido, H. Tagaki *et al.*, Phys. Rev. B **43**, 7942 (1991).
[12] Y. I. Uemura, Preprint Cond. Mat./9706151 (1997).
[13] D. Mihailovic, B. Podobnic, J. Demsar *et al.*, Preprint Cond. Mat./9801049 (1998).
[14] H. Ding, T. Yokoya, J. C. Campuzano *et al.*, Nature (London) **382**, 51 (1996).
[15] B. G. Levi, Phys. Today **49**, 17 (1996).
[16] V. P. Gusynin, V. M. Loktev, and S. G. Sharapov, Pis'ma Zh. Éksp. Teor. Fiz. **65**, 170 (1997) [JETP Lett. **65**, 182 (1997)]; Fiz. Nizk. Temp. **23**, 816 (1997) [Low Temp. Phys. **23**, 612 (1997)].
[17] V. P. Gusynin, V. M. Loktev, and S. G. Sharapov, Fiz. Nizk. Temp. **23**, 1247 (1997) [Low Temp. Phys. **23**, 936 (1997)].
[18] B. Keimer, N. Belk, R. J. Birg *et al.*, Phys. Rev. B **46**, 14034 (1992).
[19] H. Takagi, R. J. Cava, M. Marezio *et al.*, Phys. Rev. Lett. **68**, 3777 (1992).
[20] T. Nagano, Y. Tomioka, Y. Nakayama *et al.*, Phys. Rev. B **48**, 9689 (1993).
[21] M. A. Ivanov, V. M. Loktev, and Yu. G. Pogorelov, Zh. Éksp. Teor. Fiz. **101**, 596 (1992) [Sov. Phys. JETP **74**, 317 (1992)].
[22] V. M. Loktev, Sverkhprovodimost' Fiz., Khim., Tekh. **4**, 2293 (1991).
[23] K. Efetov and A. I. Larkin, Zh. Éksp. Teor. Fiz. **66**, 2290 (1974) [Sov. Phys. JETP **39**, 1129 (1974)].
[24] A. A. Abrikosov, Phys. Rev. B **55**, R6149 (1997).
[25] P. W. Anderson, Science **268**, 1154 (1995).
[26] V. L. Ginzburg and E. G. Maksimov, Sverkhprovodimost': Fiz., Khim., Tekh. **5**, 1543 (1992).
[27] N. M. Plakida and V. S. Udovenko, Mod. Phys. Lett. B **6**, 541 (1998).

[28] A. S. Aleksandrov and A. B. Krebs, Usp. Fiz. Nauk **162**, 1 (1992) [Sov. Phys. Usp. **35**, 1 (1992)].
[29] I. V. Stasyuk, A. M. Shvaika, and E. Schachinger, Physica C **213**, 57 (1993).
[30] V. A. Moskalenko, Teor. Mat. Fiz. **111**, 439 (1997); *ibid.* **113**, 432 (1997).
[31] A. A. Abrikosov, L. P. Gor'kov, and I. E. Dzyaloshinskii, *Methods of Quantum Field Theory in Statistical Physics*, Prentice Hall, Englewood Cliffs, NJ, 1963.
[32] Yu. M. Ivanchenko and Yu. V. Medvedev, Preprint Donetsk. Physicotechnical Inst. No. 84-4(79), Donetsk (1984).

Translated by R. S. Wadhwa

LATTICE DYNAMICS

Localization of vibrational defects in one-dimensional structures with a complex unit cell

M. A. Mamalui, E. S. Syrkin, and S. B. Feodosyev

B. Verkin Institute for Low Temperature Physics and Engineering, National Academy of Sciences of the Ukraine, 310164, Kharkov, Ukraine[*)]

(Submitted March 16, 1998)
Fiz. Nizk. Temp. **24**, 773–785 (August 1998)

Exact analytic expressions are obtained for Green's functions of a linear chain with a diatomic unit cell containing an isotopic substitutional impurity. An infinite chain as well as a semi-infinite chain with an impurity at the free end are considered. The total change in the phonon spectrum and the spectral densities of vibrations of the impurity and its nearest neighbors are investigated. The conditions for the formation and characteristics of local and gap vibrations are analyzed. A general method of obtaining exact solutions by using Jacobi matrices is proposed for a wide class of one-dimensional systems. © *1998 American Institute of Physics.* [S1063-777X(98)01008-1]

The derivation of exact analytic expressions for vibrational characteristics of linear chains is an important problem in the crystal lattice dynamics. Exactly solvable one-dimensional models are traditionally used for determining basic regularities in the behavior of phonon spectra of real three-dimensional crystals and are often used to control and interpret the asymptotic and numerical results obtained for more complex and realistic models (see, for example, Refs. 1–3). This is the more so since quasi-one-dimensional behavior of quasiparticle excitations is observed not only for quasi-one-dimensional systems. It is also displayed by individual low-frequency modes split in layered crystals,[4,5] Such modes take place even in three-dimensional crystalline structures whose macroscopic properties are far from being low-dimensional and which exhibit the suppression of the long-range order in the arrangement of atoms in the crystal and considerable local anisotropy of atomic interaction.[6] For example, the results of experiments[7,8] on the low-frequency dynamics of complex multilayered crystals $KDy(MoO_4)_2$ and $CsDy(MoO_4)_2$ were interpreted successfully by using the phonon spectrum of a linear chain with a diatomic unit cell. The presence of separated quasi-one-dimensional modes in the phonon spectra of the lattices with a large number of atoms in a unit cell can be an argument supporting the application of one-dimensional models for studying nonlinear properties of high-temperature superconductors[9] and other anharmonic crystals. This circumstance also explains increasing interest in obtaining exact solutions for harmonic vibrations of linear chains with more than one atom in the unit cell as the zeroth approximation for an analysis of nonlinear properties of crystals with a gap in the vibrational spectrum.

The interest to one-dimensional models (especially those with a complex unit cell) arose in connection with considerable advances in the synthesis of virtually one-dimensional structures that can be used in microelectronics as an element of ultra-miniature semiconducting devices.[10] The interpretation of processes occurring in such systems involves an analysis of the behavior of quasi-particle (including phonon) spectra of linear chains with a polyatomic unit cell, which contain various defects (e.g., chains with impurities, semi-infinite chains, and finite chains). Such problems were considered in a number of recent publications. For example, Bass *et al.*[11] obtained asymptotic analytic expressions for frequencies and amplitudes of atomic vibrations in a diatomic linear chain with an isotopic substitutional impurity. Vibrational modes of a finite linear chain were studied by Glushko and Khrisanov.[12] Special attention in these publications was paid to vibrations localized in the gap or beyond the quasi-continuous spectrum of the chain, which are important for an analysis of quasi-one-dimensional behavior of three-dimensional structure as well as for characteristics of synthesized one-dimensional systems. The method of Jacobi matrices (recursive technique) is a powerful and effective tool for calculating vibrational parameters of crystals with broken regularity (especially for describing localized vibrations).[13–15] The application of this method made it possible to derive exact analytic expressions for the conditions of formation and characteristics of localized vibrations formed by various defects in a linear chain with a monatomic unit cell and to determine the total change in the continuous spectrum of the chain by a defect as well as the frequency spectra of individual atoms.[16,17]

In the present paper, the method of Jacobi matrices is used for obtaining exact analytic expressions for the conditions of formation and parameters of local and gap vibrations in a linear chain with a diatomic unit cell containing an isotopic substitutional impurity. An infinite and semi-infinite chains with an impurity at the free end are considered. A

general method of obtaining exact solutions is proposed for a wide class of one-dimensional systems.

EXACT SOLUTIONS FOR ONE-DIMENSIONAL VIBRATIONAL SYSTEMS BY THE METHOD OF JACOBI MATRICES

In the method of Jacobi matrices, we present the entire space H of displacements of atoms of a chain [by choosing appropriately the generating vectors $\mathbf{h}_0^{(i)}$] in the form of a direct sum of orthogonal subspaces $H^{(i)}$ invariant to the operator $\mathbf{L}$ describing chain vibrations:

$$\mathbf{L}(\mathbf{r},\mathbf{r}')=\frac{\Phi(\mathbf{r},\mathbf{r}')}{\sqrt{m(\mathbf{r})m(\mathbf{r}')}}$$

(so-called cyclic subspaces). These subspaces are linear envelopes stretched on the sequence $\{\mathbf{L}^n\cdot\mathbf{h}_0^{(i)}\}_{n=0}^{\infty}$ of linearly independent vectors. Orthonormalization of this sequence gives the orthogonal basis $\{\mathbf{h}_n^{(i)}\}_{n=0}^{\infty}$ in which the operator $\mathbf{L}^{(i)}$ induced by the operator $\mathbf{L}$ in the subspace $\mathbf{H}^{(i)}$ can be presented in the form of three-diagonal Jacobi matrix (**J**-matrix). We shall denote by $a_n^{(i)}$ $(n=0,1,2,\ldots)$ its diagonal matrix elements and by $b_n^{(i)}$ the nondiagonal matrix elements and use the superscript (i) labeling the subspaces only when different cyclic subspaces have to be distinguished.

Frequency distributions of atomic vibrations of the system are usually expressed in terms of the matrix elements of Green's operator $\mathbf{G}=(\lambda\mathbf{I}-\mathbf{L})^{-1}$ (λ, which is the square of the frequency, is the eigenvalue of the operator $\mathbf{L}$). If we use the displacement $\mathbf{u}$ of an atom with the radius vector $\mathbf{r}$ as a generating vector $\mathbf{h}_0=|\mathbf{r}|\mathbf{u}\rangle\in H$, the matrix element $G_{00}(\lambda)\equiv(\mathbf{h}_0,\mathbf{G}\mathbf{h}_0)$ will contain complete information on the frequency characteristics of system vibrations in which the given atom is displaced along $\mathbf{u}$. The conditions for the presence of an imaginary component in $G_{00}(\lambda)$ determine the boundaries of the continuous vibrational spectrum, while the imaginary component itself characterizes the frequency distribution of the vibrations of this atom in these bands. The spectral density normalized to unity is given by

$$\rho_0(\lambda)=\frac{1}{\pi}\,\mathrm{Im}\,G_{00}(\lambda). \tag{1}$$

The distribution function $g(\lambda)$ for squares of the frequency is equal to the arithmetic mean of spectral densities associated with linearly independent generating vectors $\mathbf{h}_0^{(i)}$.

The function $G_{00}(\lambda)$ may have poles only outside the continuous spectrum, i.e., in the region where it is purely real function. These poles λ_d determine the squares of discrete frequencies of (local or gap) vibrations. The residues at these poles, i.e.,

$$\mu_{d,0}=\mathrm{r\acute{e}s}_{\lambda=\lambda_d}G_{00}(\lambda) \tag{2}$$

are the intensities (weights) of these vibrations.

The time-averaged square of the amplitude of vibrations for an atom with the radius vector $\mathbf{r}$ as a function of the squared frequency and temperature is proportional to $\rho(\lambda)$ for vibrations at the same frequency lying in a band of the continuous spectrum and to $\mu_{d,0}$ for vibrations with a discrete frequency.

If a region of the continuous spectrum is simply connected and has no ''hatches'' the matrix elements of the **J**-matrix tend with increasing number to certain limiting values depending on the values of the upper and lower boundaries of the continuous band.[13] Equating all a_i and b_i for $i\geqslant n$ to these limiting values, we obtain the following expression for the Green's function[14,15]:

$$G_{00}(\lambda)=\frac{Q_n(\lambda)-b_{n-1}Q_{n-1}(\lambda)K_\infty(\lambda)}{P_n(\lambda)-b_{n-1}P_{n-1}(\lambda)K_\infty(\lambda)}, \tag{3}$$

where the function $K_\infty(\lambda)$ can be expressed in terms of the limiting values of matrix elements, $P_m(x)$ are polynomials defined by the recurrence relation

$$b_mP_{m+1}(x)=(x-a_m)P_m(x)-b_{m-1}P_{m-1}(x) \tag{4}$$

under the initial conditions $P_{-1}(x)\equiv 0$, $P_0(x)\equiv 1$, and the polynomials $Q_m(x)$ are defined by the same recurrence relation, but under the initial conditions $Q_0(x)\equiv 0$, $Q_1(x)\equiv 1/b_0$.

It can easily be verified that the vectors of the orthonormal basis $\{\mathbf{h}_n^{(i)}\}_{n=0}^{\infty}$ are connected through the relation which is important for the further analysis, i.e.,

$$\mathbf{h}_n=P_n(\mathbf{L})\mathbf{h}_0. \tag{5}$$

If the continuous spectrum region is multiply connected, the matrix elements of the **J**-matrix may exhibit a quite complex asymptotic behavior.[19] However, for models of linear chains with polyatomic unit cells, the asymptotic behavior of such elements is frequently found to be periodic:

$$\lim_{m\to\infty}a_{i+mk}=\alpha_i;\quad \lim_{m\to\infty}b_{i+mk}=\beta_i. \tag{6}$$

In this case, we obtain from Eq. (3)

$$K_\infty(\lambda)=\frac{\tilde{P}_k(\lambda)+\beta_{k-1}\tilde{Q}_{k-1}(\lambda)\pm\sqrt{[\tilde{P}_k(\lambda)-\beta_{k-1}\tilde{Q}_{k-1}(\lambda)]^2-4}}{2\beta_{k-1}\tilde{P}_{k-1}(\lambda)}, \tag{7}$$

where the polynomials $\tilde{P}_n(\lambda)$ and $\tilde{Q}_n(\lambda)$ are constructed with the help of matrix elements α_i and β_i.

From relations (1) and (3), we obtain the following expression for the spectral density $\rho_0(\lambda)$:

$$\rho(\lambda)=\frac{1}{\pi}\frac{\mathrm{Im}\,K_\infty(\lambda)}{|P_n(\lambda)-b_{n-1}P_{n-1}(\lambda)K_\infty(\lambda)|^2}. \tag{8}$$

It can easily be seen that this function is analytic. Hence

it is called the analytic approximation of the spectral density. If this expression is exact for some system, the true spectral density is an analytic function of the square of frequency. This is a characteristic feature of one-dimensional structures. For lattices with a higher dimensionality, the total phonon density always has Van Hove singularities. For such structures, formula (8) is an approximation of the spectral density describing exactly the behavior of its first $2n-1$ moments.

Formulas (3), (7) and (8) for Green's function and the spectral density will be exact if the elements of the **J**-matrix assume their limiting values starting from a certain number n. Such a behavior of matrix elements reflects a periodic repetition of atomic displacements in the base vectors $\{\mathbf{h}_n^{(i)}\}_{n=0}^{\infty}$ and a periodic dependence of the moduli of these vectors on the number n. This is possible if the number of atoms excited in them does not increase indefinitely upon an increase in the value of n, and is also a periodic function of the number, which is a characteristic feature of vibrations in the wave band. Obviously, the base vectors in a linear chain with interaction between the nearest neighbors will exhibit such a behavior if

(a) the chain is semi-infinite; in this case, the displacement of the terminal atom should be chosen as the generating vector;[17]

(b) the chain extends indefinitely on both sides, but does have a center of symmetry. We make the center of symmetry coincide with the origin of coordinates and enumerate the atoms on either side of this center as $\{\pm n_n^{(i)}\}_{n=0}^{\infty}$.

Two different situations can arise in this case:

(1) An atom is located at the center of symmetry. In this case,
$$H=H^{(0)}\oplus H^{(\pm 1)}, \tag{9}$$
where the base $\{\mathbf{h}_n^{(0)}\}_{n=0}^{\infty}$ in the subspace $H^{(0)}$ is formed as a result of displacement of this atom $(n=0)$ and synphase (antisymmetric) displacements of atoms with numbers $\pm n$, while the base $\{\mathbf{h}_n^{(\pm 1)}\}_{n=0}^{\infty}$ is formed by the antiphase (symmetric) displacements of atoms with numbers $\pm(n+1)$ (the atom $n=0$ is stationary in this subspace).

(2) There is no atom at the center of symmetry, i.e., there is no atom with number $n=0$. In this case,
$$H=H^{(+)}\oplus H^{(-)}, \tag{10}$$
where the bases $\{\mathbf{h}_n^{(+)}\}_{n=0}^{\infty}$ and $\{\mathbf{h}_n^{(-)}\}_{n=0}^{\infty}$ are formed respectively by synphase and antiphase displacements of atoms with numbers $\pm(n+1)$ (a particular case of such symmetry was considered earlier by us.[17]).

It can easily be verified that relation (5) is valid for each of the four bases considered above, and that each subspace is cyclic. Since the displacement of an atom with number $\pm n$ is equal to the arithmetic mean of the vectors belonging to mutually orthogonal subspaces ($\mathbf{h}_n^{(0)}$ and $\mathbf{h}_{n-1}^{(\pm 1)}$ in the first case, and $\mathbf{h}_{n-1}^{(+)}$ and $\mathbf{h}_{n-1}^{(-)}$ in the second case), Green's function for the vibrations of this atom may be expressed in terms of arithmetic means of the corresponding diagonal elements of Green's operator **G** of the system written in the above bases.

Using formula (5), we can easily write

$$\rho_n(n)\equiv\frac{1}{\pi}\,\mathrm{Im}\;G_{nn}(\lambda)=P_n^2(\lambda)\rho_0(\lambda); \tag{11}$$

$$\mu_{d,n}\equiv \mathrm{r\acute{e}s}_{\lambda=\lambda_d}G_{nn}(\lambda)=P_n^2(\lambda_d)\mu_{d,0}. \tag{12}$$

Among other things, it follows from these expressions that the imaginary parts of the functions $G_{nn}(\lambda)$ (i.e., the continuous spectral bands) are the same for any n, and the poles of the functions $G_{nn}(\lambda)$ describing the squares of frequencies of discrete vibrations (local or gap) λ_d are also the same for all n. Formula (12) can be used to determine the extent of localization and the characteristic features of attenuation of such vibrations.

INFINITE DIATOMIC LINEAR CHAIN CONTAINING AN ISOTOPIC SUBSTITUTIONAL IMPURITY

Let us consider the variation of the phonon spectrum of a linear chain with a diatomic unit cell as a result of introduction of an isotopic substitutional impurity, and analyze the conditions of emergence of localized states in such a system, as well as their characteristics.

Suppose that we have a periodic linear chain having a diatomic unit cell with atoms of masses m_1 and m_2. Each of the atoms may be a center of symmetry, hence we can use formula (9) to break the space of atomic displacements into cyclic subspaces. We make the origin of coordinates coincide with an atom of mass m_1, and choose its displacement as the generating vector $\mathbf{h}_0^{(0)}$. Such a choice does not entail any loss of generality. The generating vector $\mathbf{h}_0^{(\pm 1)}$ will be the symmetric displacement of nearest neighbors of the given atom (i.e., of the atoms with mass m_2). In this case,

$$\mathbf{h}_n^{(0)}=\frac{(-1)^n}{\sqrt{2}}\left|\begin{matrix} n \\ -n\end{matrix}\right|\begin{matrix}1\\1\end{matrix}\Big\rangle;\quad \mathbf{h}_{n-1}^{(\pm 0)}=\frac{(-1)^n}{\sqrt{2}}\left|\begin{matrix} n \\ -n\end{matrix}\right|\begin{matrix}1\\-1\end{matrix}\Big\rangle. \tag{13}$$

The operator **L** can be presented in the form

$$\mathbf{L}(|n-n'|)=\begin{cases}\dfrac{1}{2}\sqrt{\lambda_1\lambda_2}; & |n-n'|=1;\\ \lambda_1; & n=n'=2k;\\ \lambda_2; & n=n'=2k+1;\\ 0; & |n-n'|>1,\end{cases} \tag{14}$$

where $\lambda_i=2\alpha/m_i$ $(i=1,2)$.

If at the origin of coordinates there is an isotropic impurity of mass m' in place of the atom of mass m, (see Fig. 1), the vibrations of a chain containing an impurity will be described by the operator $\mathbf{L}+\mathbf{\Lambda}^{(i)}$, where the perturbation operator $\Lambda^{(i)}$ has the following form in the coordinate space:

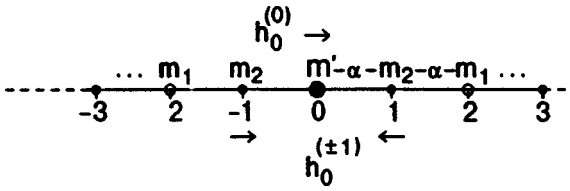

FIG. 1. Schematic diagram of a model of an infinite one-dimensional chain with a local defect.

$$\Lambda^{(i)}=\frac{-\varepsilon\lambda_1}{1+\varepsilon}\,\delta_{n,0}+\left(\frac{1}{\sqrt{1+\varepsilon}}-1\right)\times\left(\frac{\lambda_1\lambda_2}{2}\right)^{1/2}(\delta_{n,-1}+\delta_{n,1}) \tag{15}$$

[$\varepsilon\equiv(m'-m_1)/m_1$; $\delta_{i,k}$ is the Kronecker delta].

It can be shown easily that in the cyclic subspace $H^{(\pm1)}$, the operator $\mathbf{\Lambda}^{(i)}$ induces the zeroth operator, while the operator $\mathbf{L}$ can be represented in terms of a $\mathbf{J}$-matrix with elements

$$a_{2k}^{(\pm1)}=\lambda_2;\quad a_{2k+1}^{(\pm1)}=\lambda_1;\quad b_n^{(\pm1)}=\frac{\sqrt{\lambda_1\lambda_2}}{2}, \tag{16}$$

($k,n=0,1,2,3,\ldots$).

In the cyclic subspace $H^{(0)}$, the operator $\mathbf{L}+\mathbf{\Lambda}^{(i)}$ has the form of the Jacobi matrix

$$\tilde a_0^{(0)}=\frac{\lambda_1}{1+\varepsilon};\quad a_{2k}^{(0)}=\lambda_1;\quad a_{2k+1}^{(0)}=\lambda_2;$$

$$\tilde b_0^{(0)}=\left(\frac{\lambda_1\lambda_2}{2(1+\varepsilon)}\right)^{1/2};\quad b_n^{(0)}=\frac{\sqrt{\lambda_1\lambda_2}}{2}, \tag{17}$$

where $k,n=1,2,3,\ldots$, and the tilde over a letter indicates matrix elements that depend on the perturbation introduced by the impurity:

$$\{\tilde a,\tilde b\}_0^{(0)}=\{\tilde a,\tilde b\}_0^{(0)}(\varepsilon),$$

and the corresponding matrix elements of the unperturbed operator $\mathbf{L}$ are defined as

$$\{\tilde a,\tilde b\}_0^{(0)}=\{\tilde a,\tilde b\}_0^{(0)}(0).$$

Using formulas (3) and (7), we can obtain from the given matrix elements expressions for Green's functions in both cyclic subspaces (the sign before the radical in formula (7) is chosen in such a way that the spectral density is positive).

In the subspace $H^{(0)}$, we have

$$G_{00}^{(0)}(\lambda,\varepsilon)=\frac{1+\varepsilon}{R^{(0)}(\lambda,\varepsilon)}\left\{\varepsilon(\lambda-\lambda_2)+\mathscr{L}(\Theta)\times\left(\left|\frac{(\lambda-\lambda_1)(\lambda-\lambda_2)(\lambda_1+\lambda_2-\lambda)}{\lambda}\right|\right)^{1/2}\right\}, \tag{18}$$

where

$$R^{(0)}(\lambda,\varepsilon)\equiv-\lambda^2(1-\varepsilon^2)+\lambda[\lambda_2(1-\varepsilon^2)+2\lambda_1]-\lambda_1(\lambda_1+\lambda_2), \tag{19}$$

while $\mathscr{L}(\Theta)$ denotes a combination of Heaviside functions defining the continuous spectral bands:

$$\mathscr{L}(\Theta)\equiv i[\Theta(\lambda)\Theta(\lambda_1-\lambda)+\Theta(\lambda-\lambda_2)\Theta(\lambda_1+\lambda_2-\lambda)]+\Theta(\lambda-\lambda_1)\Theta(\lambda_2-\lambda)-\Theta(\lambda-\lambda_1-\lambda_2). \tag{20}$$

In the subspace $H^{(\pm1)}$, we can write

$$G_{00}^{(\pm1)}(\lambda)=\frac{2}{\lambda_1\lambda_2}\left\{(\lambda-\lambda_2)+\mathscr{L}(\Theta)\times\left[\left|\frac{\lambda(\lambda-\lambda_1)(\lambda_1+\lambda_2-\lambda)}{\lambda-\lambda_2}\right|\right]^{1/2}\right\}. \tag{21}$$

It follows hence that the continuous spectrum of the chain under consideration (with or without an impurity) consists of two bands of the same width $\Omega_0^2\equiv\{\lambda_1,\lambda_2\}_{\min}$, separated by a gap of width $\{\lambda_1,\lambda_2\}_{\max}-\{\lambda_1,\lambda_2\}_{\min}\equiv\omega_0^2-\Omega_0^2$. The upper boundary of the continuous spectrum is $\lambda_{\max}=\lambda_1+\lambda_2$.

The spectral densities defined in the continuous spectral bands can be represented as follows:

$$\rho_0^{(0)}(\lambda,\varepsilon)=\frac{1}{\pi R^{(0)}(\lambda,\varepsilon)}\,(1+\varepsilon)\times\left[\left|\frac{(\lambda-\lambda_1)(\lambda-\lambda_2)(\lambda_1+\lambda_2-\lambda)}{\lambda}\right|\right]^{1/2}; \tag{22}$$

$$\rho_0^{(\pm1)}(\lambda)=\frac{2}{\pi\lambda_1\lambda_2}\left[\left|\frac{\lambda(\lambda-\lambda_1)(\lambda_1+\lambda_2-\lambda)}{\lambda-\lambda_2}\right|\right]^{1/2}. \tag{23}$$

Let $\mathbf{n}=|n|1\rangle$ be the unit displacement vector for an atom with number m. It was mentioned above that this vector is equal to the sum of two mutually orthogonal vectors $\mathbf{h}_n^{(0)}$ and $\mathbf{h}_{n-1}^{(\pm1)}$. Hence we obtain from (17) and (18)

$$\rho(n,\lambda,\varepsilon)=\frac{1}{2}\{\rho_n^{(0)}(\lambda,\varepsilon)+\rho_{n-1}^{(\pm1)}(\lambda)\}$$

$$=\frac{1}{2}\{[P_n^{(0)}(\lambda,\varepsilon)]^2\rho_0^{(0)}(\lambda,\varepsilon)+[P_{n-1}^{(\pm1)}(\lambda)]^2\times\rho_0^{(\pm1)}(\lambda)\},$$

$$\mu_d(n,\varepsilon)=\frac{\mu_{d,n}^{(0)}}{2}=\frac{1}{2}\,[P_n^{(0)}(\lambda_d,\varepsilon)]^2\mu_{d,0}^{(0)} \tag{24}$$

(since the perturbation operator under consideration does not act in the cyclic subspace $H^{(\pm1)}$, there are no vibrations with discrete frequencies in this subspace).

For an ideal chain, the function $R^{(0)}(\lambda,0)=(\lambda-\lambda_1)\times(\lambda_1+\lambda_2-\lambda)$ and the spectral density $\rho(2k,\lambda)$ generated as a result of displacement of an atom of mass m_1 is

$$\rho(2k,\lambda)=\rho_0^{(0)}=\frac{1}{\pi}\left[\left|\frac{\lambda-\lambda_2}{\lambda(\lambda-\lambda_1)(\lambda_1+\lambda_2-\lambda)}\right|\right]^{1/2} \tag{25}$$

(note that $\mathrm{Re}\,G_{00}^{(0)}(\lambda,0)=0$).

For an ideal linear chain, this result can also be obtained quite easily by using the ''traditional'' approach, i.e., by expansion in plane waves. Seeking the solution of the equation of motion

$$\ddot{u}^{(i)}(na,t)=-\lambda_{(i)}[2u^{(i)}(na,t)-u^{(3-i)}((n+1)a,t) - u^{(3-i)}(n-1)a,t]$$

$[u^{(i)}(na,t)\ (i=1,2)]$ is the displacement of the ith sublattice atom at the nth lattice site) in the form

$$u^{(i)}(n,t)=\frac{1}{\sqrt{m_i}}\sum_{k,\sigma} e^{(i)}(k,\sigma)\exp\, i[kna-t\sqrt{\lambda_\sigma(k)}]$$

(the index σ is used to enumerate the vibrational branches), we obtain

$$(\lambda_i-\lambda)\left[\frac{1}{\sqrt{m_i}}e^{(i)}(k,\sigma)\right] - \lambda_{3-i}\cos ka\left[\frac{1}{\sqrt{m_{3-i}}}e^{(3-i)}(k,\sigma)\right]=0. \quad (26)$$

It should be noted at the very outset that Eqs. (26) are invariant to sign reversal of k, hence the eigenvalues and eigenfunctions will be even functions of this variable. In other words, the spectrum will be simple and $e^{(i)}(k,\sigma)=e^{(i)}(\lambda_\sigma)$.

The squares of eigenfrequencies satisfy the following dispersion relations:

$$\lambda_\sigma(k)=\frac{\lambda_1+\lambda_2}{2}\pm\left[\left(\frac{\lambda_1-\lambda_2}{2}\right)^2+\lambda_1\lambda_2\cos^2 ka\right]^{1/2} \quad (27)$$

(the minus sign preceding the radical corresponds to the acoustic branch, and the plus sign to the optical branch). The eigenfunctions $e^{(i)}(\lambda_\sigma)$ corresponding to these eigenvalues and normalized by the condition $\sum_i[e^{(i)}(\lambda_\sigma)]^2=1$, can be written in the form

$$e^{(i)}(\lambda_\sigma)=\left[\left|\frac{\lambda_\sigma-\lambda_{3-i}}{2\lambda_\sigma-(\lambda_1+\lambda_2)}\right|\right]^{1/2}. \quad (28)$$

Note that the squares of the eigenfrequencies λ_1 and λ_2 have the value $ka=\pi/2$ corresponding to them, i.e., the vibrations of atoms of a unit cell are displaced in phase by a quarter of a period. The atom with mass m_1 is at rest for $\lambda=\lambda_2$, while the atom of mass m_2 has its maximum amplitude. Conversely, the atom with mass m_1 has its maximum amplitude for $\lambda=\lambda_1$, while the atom of mass m_2 is at rest.

The distribution function for the squares of frequencies for an ideal diatomic chain normalized to unity has the form

$$g(\lambda)=\frac{1}{2\pi}\frac{|\lambda_1+\lambda_2-2\lambda|}{\sqrt{\lambda(\lambda-\lambda_1)(\lambda-\lambda_2)(\lambda_1+\lambda_2-2\lambda)}}. \quad (29)$$

The spectral density generated by the displacement of an atom from the sublattice i in the crystallographic direction l can be presented in the form[3,13,20]

$$\rho_l^{(i)}=\frac{V_0}{(2\pi)^q}\sum_\sigma \oint_{\lambda_\sigma(\mathbf{k})=\lambda}\frac{dS}{\nabla_{\mathbf{k}}\lambda_\sigma(\mathbf{k})}|e^{(i)}(\mathbf{k},\sigma)|^2$$

(q is the dimensionality of space, and V_0 is the q-dimensional volume of the unit cell). For the one-dimensional system under consideration, we obtain

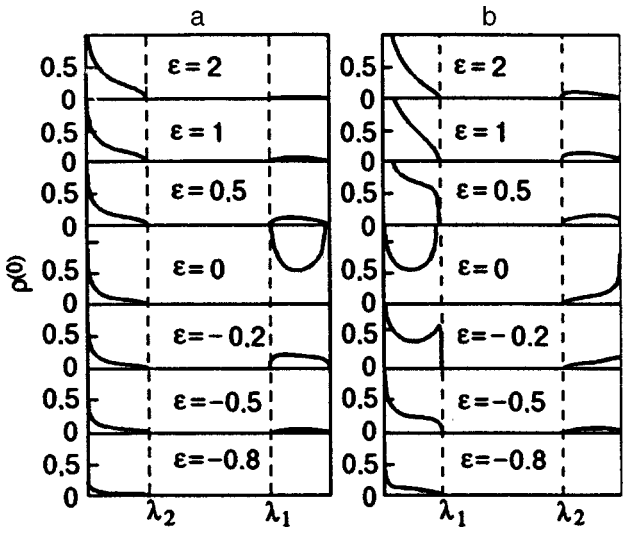

FIG. 2. Evolution of the spectral densities of an impurity atoms with a change in mass defect: the impurity in the light sublattice ($\lambda_1>\lambda_2$) (a) and in the heavy sublattice ($\lambda_2>\lambda_1$) (b).

$$\rho^{(i)}(\lambda)=2g(\lambda)[e^{(i)}(\lambda_\sigma)]^2. \quad (30)$$

For the spectral density generated by the displacement of an atom of mass m_1, expressions (30) and (25) coincide. Obviously, the spectral density generated by the displacement of an atom of mass m_2 [the function $\rho(2k+1,\lambda)$] ia obtained by interchanging λ_1 and λ_2 in (25) or (30). The same result is obtained from (23)–(25). The distribution function (29) of the squares of frequencies for the chain under consideration is equal[13] to the arithmetic average of $\rho(2k,\lambda)$ and $\rho(2k+1,\lambda)$.

Each of the above spectral densities has root singularities at the edges of the continuous spectrum for $\lambda=0$ and $\lambda=\lambda_1+\lambda_2$ (see Fig. 2 for $\varepsilon=0$). The spectral density generated by the displacement of a heavy atom has a root singularity at the upper boundary of the acoustic band (Ω_0^2) and tends to zero $\sim\sqrt{\lambda}$ at the lower boundary of the optical band (ω_0^2). Conversely, the spectral density generated by the displacement of a light atom tends to zero $\sim\sqrt{\lambda}$ for $\lambda\to\Omega_0^2$ and has a root singularity at $\lambda=\omega_0^2$. Hence the formation of local vibrations with frequencies higher than $\sqrt{\lambda_1+\lambda_2}$ by a light isotopic impurity must take place without a threshold, i.e., for $\varepsilon<0$ irrespective of whether the impurity is in heavy or light sublattice (the highest vibrational frequency corresponds to the simultaneous antiphase displacements of atoms in both sublattices).

Similarly, the gap vibrations must be detached from the top of the acoustic band without threshold due to the presence of a light impurity in the heavy sublattice and from the bottom of the optical band due to the presence of a heavy impurity in the light sublattice.

It was mentioned above that the vibrational amplitudes of heavy sublattice atoms vanish at the frequency ω_0, while the vibrational amplitudes of light sublattice atoms vanish at the frequency Ω_0. Hence the isotopic impurity will not affect the vibrations of the sublattice atoms at such frequencies. Consequently, the splitting of gap vibrations from the top of the acoustic band under the effect of an isotopic im-

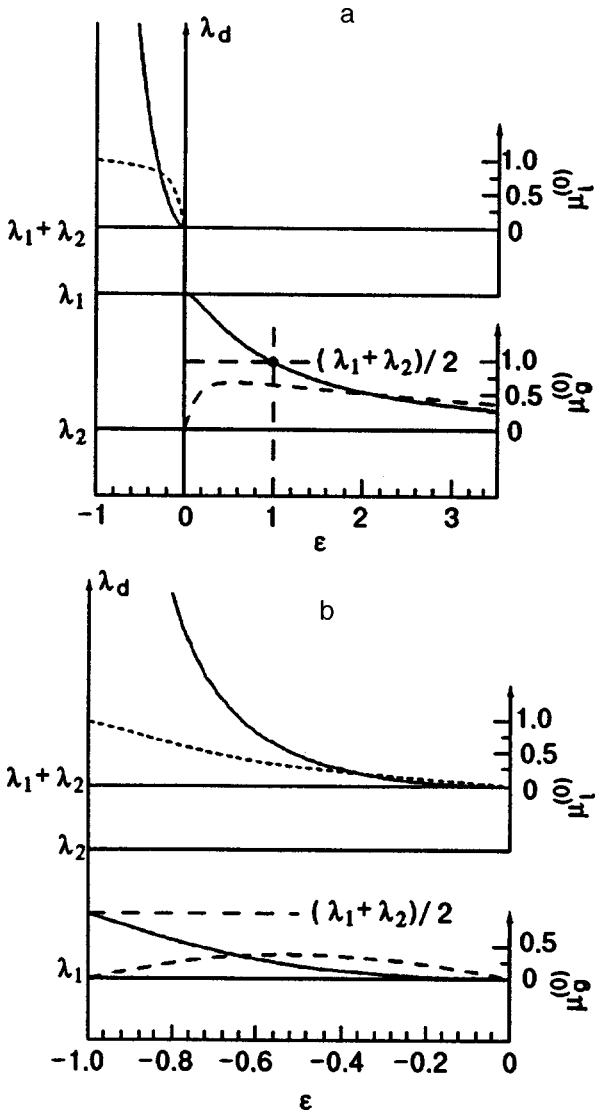

FIG. 3. Squared frequencies and intensities of local and gap vibrations associated with an isotopic impurity in an infinite chain as functions of ε: $\lambda_1>\lambda_2$ (a) and $\lambda_2>\lambda_1$ (b).

purity in the light sublattice and from the bottom of the optical band under the effect of an isotopic impurity in the heavy sublattice must be quite difficult at least.

The computation of poles of Green's function (18) [i.e., the roots of the quadratic trinomial (19)] leads to the following result:

$$\lambda_{l,g}=\frac{1}{2}\left\{\lambda_2+\frac{2\lambda_1}{1-\varepsilon^2}\pm\left[\lambda_2^2+\left(\frac{2\lambda_1\varepsilon}{1-\varepsilon^2}\right)^2\right]^{1/2}\right\}. \tag{31}$$

The pole corresponding to the plus sign before the radical is equal to $\lambda_1+\lambda_2$ for $\varepsilon=0$ and decreases with increasing ε. Consequently, it corresponds to a local vibration with square of the frequency $\lambda_l>\lambda_1+\lambda_2$. The pole corresponding to the minus sign before the radical also decreases with increasing ε, but is equal to λ_1 for $\varepsilon=0$. It corresponds to a gap vibration with square of the frequency $\lambda_g\in[\Omega_0^2,\omega_0^2]$.

The residue of the function (18) at the points $\lambda_{l,g}$, i.e., the intensity of local or gap vibrations, can be presented in the form

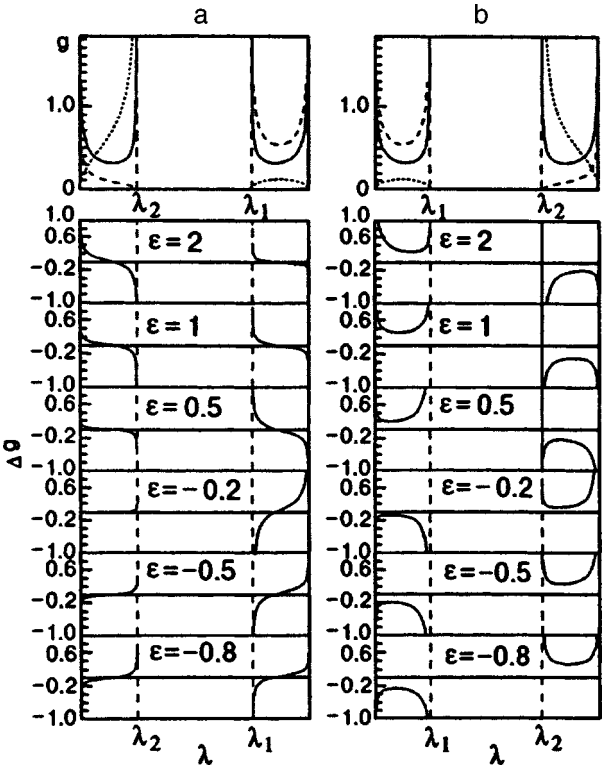

FIG. 4. Formation of total phonon density $g(\lambda)$ of a diatomic linear chain by spectral densities $\rho^{(0)}(\lambda)$ (dashed curves) and $\rho^{(\pm1)}(\lambda)$ (dotted curves) and the function $\Delta g(\lambda)$ for various values of mass defect for $\lambda_1>\lambda_2$ (a) and $\lambda_2>\lambda_1$ (b).

$$\mu_{l,0}=\frac{|\varepsilon|-\varepsilon}{2(1-\varepsilon)}\left[1+\frac{2\lambda_1-\lambda_2(1-\varepsilon^2)}{\sqrt{4\lambda_1^2\varepsilon^2+\lambda_2^2(1-\varepsilon^2)^2}}\right]; \tag{32}$$

$$\mu_{g,0}=\begin{cases}\dfrac{|\varepsilon|+\varepsilon}{2(1-\varepsilon)}\left[\dfrac{2\lambda_1-\lambda_2(1-\varepsilon^2)}{\sqrt{4\lambda_1^2\varepsilon^2+\lambda_2^2(1-\varepsilon^2)^2}}-1\right]; & \lambda_1>\lambda_2;\\ \dfrac{|\varepsilon|-\varepsilon}{2(1-\varepsilon)}\left[1-\dfrac{2\lambda_1-\lambda_2(1-\varepsilon^2)}{\sqrt{4\lambda_1^2\varepsilon^2+\lambda_2^2(1-\varepsilon^2)^2}}\right]; & \lambda_1<\lambda_2.\end{cases} \tag{33}$$

Figure 2 shows the evolution of the spectral densities $\rho_0^{(0)}(\lambda,\varepsilon)$ upon a variation of the parameter ε, while Fig. 3 shows the dependence of the square of discrete frequencies and intensities of the corresponding vibrations on ε.

If $\lambda_1>\lambda_2$ (impurity in the light sublattice), local and gap vibrations are formed without a threshold (see above), being split from the top of the optical band for $\varepsilon<0$ and from its bottom for $\varepsilon>0$, respectively. The squared frequency of local vibrations tends to infinity $\sim(1-\varepsilon^2)^{-1}$ as $\varepsilon\to-1$ (i.e., for $m'/m_1\to0$), while the intensity tends to unity. In other words, vibrations become more and more localized. As $\varepsilon\to\infty$, the squared frequency of the gap vibration tends to the upper boundary of the acoustic band ($\Omega_0^2=\lambda^2$) also as $\sim(1-\varepsilon^2)^{-1}$. The intensity of this vibration increases abruptly at first, then decreases slowly, and this vibration becomes delocalized further and further as Ω_0^2 is approached. It should be noted that for $\varepsilon=1$ (impurity is twice as heavy as an atom in the light sublattice), the square of the fre-

quency of the gap vibration is exactly at the middle of the gap irrespective of the relation between m_1 and m_2:

$$\lambda_g(1)=\frac{\lambda_1+\lambda_2}{2}\equiv\frac{\lambda_{\max}}{2}. \tag{34}$$

The intensity of this vibration is given by

$$\mu_{g,0}(1)=\frac{\lambda_1-\lambda_2}{\lambda_1}\equiv\frac{\omega_0^2-\Omega_0^2}{\omega_0^2}. \tag{35}$$

A light impurity in the heavy sublattice ($\lambda_1<\lambda_2$) leads to simultaneous thresholdless formation of local as well as gap vibrations. In this case, local vibrations become more and more localized with decreasing $\varepsilon(\mu_{l,0}\to 1$, and $\lambda_l\to\infty)$. On the other hand a gap vibration separated in this case from the top of the acoustic band is localized weakly. The $\mu_{g,0}(\varepsilon)$ dependence is nearly symmetric in the interval $\varepsilon\in[-1,0]$ and vanishes for $\varepsilon=-1$. The square of the frequency of this vibration reaches the middle of the gap, and gap vibrations cannot be formed in the upper half of the gap in this case.

A heavy impurity in the heavy sublattice does not lead to the formation of discrete vibrations. In this case, an increase in ε leads to the ''pumping'' of phonons in the spectral density $\rho^{(0)}(\lambda,\varepsilon)$ from the optical to the acoustic band.

The complete change in the phonon spectrum of a linear chain with a diatomic unit cell due to an isotopic substitutional impurity can be describe by using the displacement function $\xi(\lambda,\varepsilon)$ introduced by Lifshitz[1]:

$$\Delta g(\lambda)=\frac{2\xi(\lambda,\varepsilon)}{\partial\lambda}.$$

The shear function can be easily evaluated by using Jacobi matrices[13] and for the problem under consideration has the form

$$\xi(\lambda,\varepsilon)=\pm\frac{1}{\pi}\arctan\left\{\varepsilon\left[\frac{\lambda(\lambda-\lambda_2)}{(\lambda-\lambda_1)(\lambda_1+\lambda_2-\lambda)}\right]^{1/2}\right\}, \tag{36}$$

where the ''plus'' sign corresponds to the acoustic band in which the dispersion of vibrations is positive and the ''minus'' sign corresponds to the optical band (dispersion is negative). The evolution of the dependences

$$\Delta g(\lambda)=\pm\varepsilon g(\lambda)$$
$$\times\frac{\lambda_1[2\lambda_2-2\lambda(\lambda_1+\lambda_2)+\lambda(\lambda_1+\lambda_2)]}{|2\lambda-\lambda_1-\lambda_2|[|\lambda-\lambda_1|(\lambda_1+\lambda_2-\lambda)+\varepsilon^2\lambda(\lambda-\lambda_2)]}$$

with a change in the parameter ε is shown in Fig. 4. In the approximation linear in the impurity concentration p, the total phonon density is given by $g(\lambda,\varepsilon)=g(\lambda)+p\Delta g(\lambda)$.

It can easily be seen that $\xi(\lambda)|_0^{\Omega_0}=\mathrm{sgn}(\varepsilon)\Theta(\lambda_2-\lambda_1)$, and $\xi(\lambda)|_{\omega_0^2}^{\lambda_1+\lambda_2}=-1$, which coincides with the results of the above analysis of the redistribution of vibrations between the bands.

With increasing number n (i.e., the distance from an impurity atom), the intensity of the vibration with a discrete frequency decreases according to the law (12). It can easily be proved by mathematical induction that the amplitudes of discrete vibrations form a decreasing geometric progression with increasing distance between the unit cell and the impurity atom. The common ratio q of this progression is given by

$$q_{l,g}=\frac{P_4(\lambda_{l,g})}{P_2(\lambda_{l,g})}=\frac{P_3(\lambda_{l,g})}{P_1(\lambda_{l,g})}$$
$$=\frac{2\lambda_1\varepsilon\pm\sqrt{4\lambda_1^2\varepsilon^2+\lambda_2^2(1-\varepsilon^2)^2}}{\lambda_2(1-\varepsilon^2)}, \tag{37}$$

where, as in (31), the ''plus'' and ''minus'' signs in front of the radical corresponds to local and gap vibrations, respectively. The intensities of discrete vibrations form a geometric progression with the common ratio q^2 and the sum equal to unity.

It should be noted that if the elements of the Jacobi matrix of the operator $\mathbf{L}+\mathbf{\Lambda}$ in a system of an arbitrary dimensionality tend to limiting values with increasing n, the attenuation of the amplitudes of discrete vibrations for large n is determined by (37), i.e., is exponential. For example, the attenuation of local vibrations in a lattice with a monatomic unit cell at large distances from a defect can only be exponential.

The amplitude of vibrations of an impurity atom itself at a discrete frequency is larger than the amplitude of vibrations of a neighboring atom if

$$|P_1(\lambda_d,\varepsilon)|<\left(\frac{2\lambda_1}{\lambda_2(1+\varepsilon)}\right)^{1/2}. \tag{38}$$

This inequality holds identically for a local vibration associated with a light impurity in the light sublattice. For a local vibration associated with a light impurity in the heavy sublattice, this inequality is satisfied for

$$\frac{\lambda_1}{\lambda_2}>\frac{(1+\varepsilon)(1-2\varepsilon)}{1-3\varepsilon} \tag{39}$$

(in this case, $\varepsilon<0$ and $\lambda_1<\lambda_2$). According to (37), the violation of (39) means that the amplitude of vibrations of a light atom at a discrete frequency in each unit cell is larger than for a heavy atom, although the light atom is separated from the defect by a larger distance. In other words, the exponential decrease of the amplitude of the vibrations is ''modulated'' by certain oscillations. For the gap vibration associated with a light impurity in the heavy sublattice, the inequality (38) never holds. This vibration is mainly localized at the nearest neighbors of the impurity (light atoms).

For the gap vibration associated with the heavy impurity in the light sublattice, inequality (38) also holds under the condition (39), but $\varepsilon>0$ and $\lambda_1>\lambda_2$ in this case. Inequality (39) is violated when λ_g is near the top of the acoustic band, where the amplitudes of atomic vibrations in the light sublattice become zero. Heavy atoms mainly vibrate at frequencies close to Ω_0, and hence the amplitudes of vibrations with the gap frequency for heavy atoms at large distances from the defect are larger than for less remote atoms.

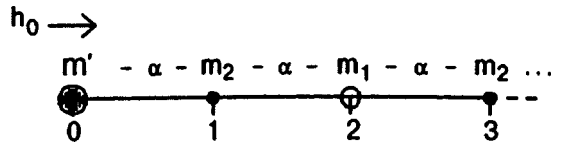

FIG. 5. Schematic diagram of a model for a semi-infinite one-dimensional chain.

SEMI-INFINITE DIATOMIC LINEAR CHAIN WITH AN ISOTOPIC SUBSTITUTIONAL IMPURITY AT THE FREE END

Let us consider a semi-infinite chain ($n \geqslant 0$) with a diatomic unit cell. The atom of mass m_1 at the free end of the chain ($n=0$) is replaced by an isotopic impurity of mass m'. In this case, the perturbation operator $\mathbf{\Lambda}^{(si)}$ in the coordinate representation has the form

$$\Lambda^{(si)} = -\mathbf{L}\Theta(-n) - \frac{1+\varepsilon\lambda_1}{2(1+\varepsilon)}\,\delta_{n,0} + \left(\frac{1}{\sqrt{1+\varepsilon}} - 1\right)\frac{\sqrt{\lambda_1\lambda_2}}{2}\,\delta_{n,1}, \tag{40}$$

where the unperturbed operator $\mathbf{L}$ is chosen in the form of a dynamic operator (14) of a perfect infinite diatomic chain, and the notation λ_i ($i=1,2$) and ε corresponds to (15).

Having chosen $\mathbf{h}_0 = |0|1\rangle$ as the generating displacement vector (see Fig. 5) and using the procedure $\{\mathbf{L}^n\mathbf{h}_0\}_{n=0}^{\infty}$, we obtain the family of the basis vectors $\{\mathbf{h}_n\}_{n=0}^{\infty} = \{|n| \times (-1)^n\rangle\}_{n=0}^{\infty}$. The linear envelope stretched on these vectors coincides with the complete displacement space H for atoms in the given system. The **J**-matrix of the operator $\mathbf{L} + \mathbf{\Lambda}^{(si)}$ in this basis has the form

$$\tilde{a}_0 = \frac{1}{2}\frac{\lambda_1}{1+\varepsilon}; \quad a_{2k} = \lambda_1; \quad a_{2k-1} = \lambda_2;$$

$$\tilde{b}_0 = \frac{1}{2}\left(\frac{\lambda_1\lambda_2}{1+\varepsilon}\right)^{1/2}; \quad b_n = \frac{\sqrt{\lambda_1\lambda_2}}{2}; \quad k,n = 1,2,3,\ldots. \tag{41}$$

The Green's function of the given system can be written as

$$G_{00}^{(si)}(\lambda,\varepsilon) = \frac{2(1+\varepsilon)}{R^{(si)}(\lambda,\varepsilon)}\left\{(1+2\varepsilon)(\lambda-\lambda_2) + \mathscr{S}(\Theta) \times \left(\left|\frac{(\lambda-\lambda_1)(\lambda-\lambda_2)(\lambda_1+\lambda_2-\lambda)}{\lambda}\right|\right)^{1/2}\right\}, \tag{42}$$

where $\mathscr{S}(\Theta)$ is defined by (20), and

$$R^{(si)}(\lambda,\varepsilon) = 4\varepsilon(1+\varepsilon)\lambda^2 + 2\lambda[\lambda_1 - 2\lambda_2\varepsilon(1+\varepsilon)] - \lambda_1(\lambda_1+\lambda_2). \tag{43}$$

At the points

$$\lambda_{l,g}(\varepsilon) = \frac{1}{2}\left\{\lambda_2 + \frac{\lambda_1}{2\varepsilon(1+\varepsilon)} \mp \mathrm{sgn}(\varepsilon)\left(\lambda_2^2 + \lambda_1^2\left[\frac{1+2\varepsilon}{2\varepsilon(1+\varepsilon)}\right]^2\right)^{1/2}\right\} \tag{44}$$

this function has poles with the residues

$$\mu_{l,g} = \frac{(1+2\varepsilon) \mp |1+2\varepsilon|[\Theta(\lambda_1-\lambda_2) \pm \Theta(\lambda_2-\lambda_1)]}{4\varepsilon} \times \left\{1 \pm \frac{\lambda_1 + 2\lambda_2\varepsilon(1+\varepsilon)}{\sqrt{\lambda_1^2(1+2\varepsilon)^2 + 4\lambda_2^2\varepsilon^2(1+\varepsilon)^2}}\right\} \tag{45}$$

(in all the combinations $\pm$ or $\mp$, the upper sign corresponds to local and the lower sign to gap vibrations). For $\varepsilon = 0$, Eq. (43) assumes the form

$$R^{(si)}(\lambda,0) = \lambda_1[2\lambda - (\lambda_1+\lambda_2)],$$

and its only root corresponding to a gap vibration is given by

$$\lambda_g(0) = \frac{\lambda_1+\lambda_2}{2}. \tag{46}$$

The intensity of this vibration at the terminal atom has the form

$$\mu_g^{(0)}(0) = \frac{\lambda_1-\lambda_2}{\lambda_1}\,\Theta(\lambda_1-\lambda_2), \tag{47}$$

and a gap vibration is formed only when $\lambda_1 > \lambda_2$, i.e., an atom from the light sublattice is located at the end of the chain. The squared frequency of this vibration is exactly at the middle of the gap. It should be noted that this is completely in accord with the characteristics of the gap vibration associated with the presence of a heavy isotope with $m'/m_1 = 2$ in the light sublattice of an infinite chain (see (34) and (35)).

It can easily be verified that $\lim_{\varepsilon\to-0}\lambda_l(\varepsilon) = -\infty$ and expressions (44) and (45) for gap vibrations with $\varepsilon = 0$ are transformed into (46) and (47), respectively.

The spectral density of the vibrations of the terminal atom, which is defined in the bands of the continuous spectrum, has the form

$$\rho^{(si)}(\lambda,\varepsilon) = \frac{2(1+\varepsilon)}{\pi R^{(si)}(\lambda,\varepsilon)}\left(\left|\frac{(\lambda-\lambda_1)(\lambda-\lambda_2)(\lambda_1+\lambda_2-\lambda)}{\lambda}\right|\right)^{1/2}, \tag{48}$$

which also coincides with (25) for $\varepsilon = 1$. The root singularity at $\lambda = 0$ typical of the phonon spectrum of one-dimensional structures is preserved for all values of ε. For $\varepsilon = -1/2$, the function

$$R^{(si)}(\lambda,\varepsilon) = R^{(si)}\left(\lambda, -\frac{1}{2}\right) = (\lambda-\lambda_1)(\lambda_1+\lambda_2-\lambda)$$

and (48) coincides with the spectral density (25) of the corresponding atom in a perfect infinite chain, i.e., the mass defect compensates the effect of the free surface. In other words, the effect of the free end of a linear chain on its phonon spectrum and vibrational parameters is completely similar to the effect of an isotopic impurity with a mass twice as large as the mass of the end-point atom of the chain.

Finally, comparing (18) with (42), we obtain the expression

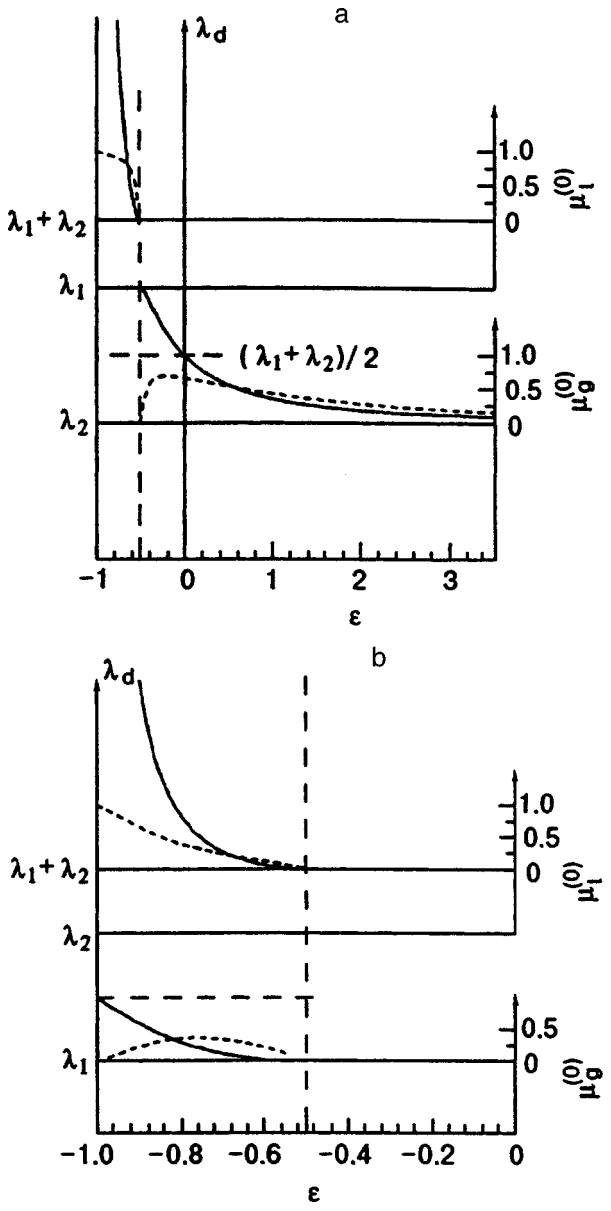

FIG. 6. Squared frequencies and intensities of discrete vibrations in a semi-infinite chain as functions of ε: $\lambda_1>\lambda_2$ (a) and $\lambda_2>\lambda_1$ (b).

$$G_{00}^{(si)}(\lambda,\varepsilon)=G_{00}^{(0)}(\lambda,1+2\varepsilon), \tag{49}$$

leading to similar relations for spectral densities and parameters of discrete vibrations.

Figure 6 shows the characteristics of discrete vibrations as functions of the parameter ε. Irrespective of the relation between λ_1 and λ_2, $\mu_l(-1/2)=\mu_g(-1/2)=0$, i.e., $\varepsilon=-1/2$ is the threshold value of discrete vibrations. The local vibrations with the squared frequency $\lambda_l(\varepsilon)$ splits from the upper boundary $\lambda_1+\lambda_2$ of the optical band for $\varepsilon<-1/2$. A further decrease in ε ($\varepsilon\in[-1/2,1]$), the frequency and intensity of this vibration increase $[\lambda_l(\varepsilon)\to\infty,\mu_l(\varepsilon)\to 1]$. The value $\lambda_g(1/2)=\lambda_1$, i.e., for $\lambda_1<\lambda_2$ a gap vibration whose squared frequency tends to the lower boundary $\omega_0^2=\lambda_2$ splits from the top $\Omega_0^2=\lambda_1$ of the acoustic band, and the intensity decreases nonmonotonically to zero (for $\varepsilon=-1$). This gap vibration ''coexists'' with the local vibration as in the case of a light impurity in the heavy sublattice of an infinite chain.

It was noted above [see (46) and (47)] that for $\lambda_1>\lambda_2$ the gap vibration exists for $\varepsilon=0$ also. It can be easily verified from (44) and (45) that for $\varepsilon>0$, the frequency of this vibration decreases with increasing impurity mass to the upper boundary of the acoustic band $[\lim_{\varepsilon\to\infty}\lambda_g(\varepsilon)=\Omega_0^2=\lambda_2]$, and the intensity tends to zero, For $\varepsilon\in[0,-1/2]$, the frequency of the gap vibration increases to the lower boundary of the optical band $[\lambda_g(-1/2)=\omega_0^2=\lambda_1]$, and the intensity decreases to zero. A further decrease in the impurity mass lads to the disappearance of the gap vibration and to the formation of a local vibration.

CONCLUSION

Exact analytic solutions for Green's function can be obtained for infinite linear chains with a periodic arrangement of atoms (with an infinitely large, but finite period) and with disordered defect clusters by using the method of Jacobi matrices in the case when the system has a symmetry center. An exact solution is obtained by splitting the entire displacement space into the complete system of two cyclic subspaces formed by displacements that are symmetric and antisymmetric about the given center. For a semi-infinite chain, such an exact solution can be obtained in all cases. The corresponding unique cyclic subspace (which is a complete system) is generated by a displacement of the terminal atom of the chain.

The imaginary components of diagonal elements of Green's function and the residues at the poles of the given function, which characterize the vibrational amplitudes of atoms at frequencies lying in the region of the continuous spectrum and at discrete frequencies respectively depend on the number of this diagonal element as $P_n^2(\lambda)$. The amplitudes of discrete vibrations associated with the defects outside of the defect cluster form a decreasing geometric progression, i.e., attenuate exponentially.

The continuous spectrum of the squared eigenfrequencies for a linear chain with a diatomic unit cell in which each atom is a symmetry center consists of two bands of the same width. The spectral densities of both atoms (and hence their vibrational amplitudes) have root singularities at zero and at the upper boundary of the entire spectrum. The amplitude of vibrations of the heavy atom has another root singularity at the upper boundary Ω_0^2 of the acoustic band and vanishes at the lower boundary ω_0^2 of the optical band. On the contrary, the amplitude of vibrations of the light atom vanishes for $\lambda=\Omega_0^2$ and has a root singularity for $\lambda=\omega_0^2$.

The presence of a light isotopic substitutional impurity in such a chain leads to the thresholdless formation of local vibrations splitting from the upper boundary of the optical band irrespective of the sublattice containing the impurity. Moreover, if the light impurity is in the heavy sublattice, a gap vibration localized mainly at the nearest neighbors of the impurity splits from the upper boundary of the acoustic band.

A heavy impurity in the light sublattice leads to the formation of a gap vibration splitting from the lower boundary of the optical band. A heavy impurity in the heavy sublattice

does not form vibrations with discrete frequencies, but causes the ''pumping'' of phonons from the optical to the acoustic band.

The effect of the free end of a chain on the vibrational parameters is completely similar to the effect of a heavy isotope with $m'/m=2$. The vibrational characteristics of a semi-infinite chain with an isotopic impurity at the end can be obtained from the corresponding characteristics of an infinite chain through the substitution $\varepsilon \to 1+2\varepsilon$.

The authors are pleased to express their gratitude to A. M. Kosevich, the author of classical results and classical works on lattice dynamics, for his continued interest in our work. Naturally, the results of the present research were discussed in detail with Arnold Markovich whose 70th birth anniversary is being celebrated in July 1998. In the course of discussions, he made a number of valuable remarks and suggestions which were gratefully taken into account.

*)E-mail: syrkin@ilt.kharkov.ua

[1] I. M. Lifshits, Zh. Éksp. Teor. Fiz. **17**, 1076 (1947).
[2] A. Maradudin, E. Montroll *et al.*, *Theory of Lattice Dynamics in the Harmonic Approximation*, New York (1963).
[3] A. M. Kosevich, *Theory of Crystal Lattice* [in Russian], Vishcha Shkola, Kharkov (1988).
[4] A. M. Kosevich, E. S. Syrkin, and S. B. Feodosyev, Phys. Low-Dimens. Semicond. Struct. **3**, 47 (1994).
[5] E. S. Syrkin, S. B. Feodosyev, and O. Ya. Shamfarova, Fiz. Nizk. Temp. **17**, 746 (1991) [Sov. J. Low Temp. Phys. **17**, 393 (1991)].
[6] S. B. Feodosyev, I. A. Gospodarev, A. M. Kosevich, and E. S. Syrkin, Phys. Low-Dimens. Semicond. Struct. **10/11**, 209 (1995).
[7] V. I. Kut'ko, Yu. N. Kharchenko, N. M. Nesterenko, and A. A. Gurskas, Fiz. Nizk. Temp. **22**, 785 (1996) [Low Temp. Phys. **22**, 603 (1996)].
[8] V. I. Kut'ko, Fiz. Nizk. Temp. **24**, 383 (1998) [Low Temp. Phys. **24**, 291 (1998)].
[9] N. M. Plakida, V. L. Aksenov, and S. L. Drecsler, Europhys. Lett. **4**, 1309 (1987).
[10] *Proceedings of the IInd NATO ASI Conf. ''Quantum Dot Materials for Nonlinear Optic Applications''*, Sept. 15–26, Bressanone, Italy (1996).
[11] F. G. Bass, V. L. Fal'ko, and S. I. Khankina, Ukr. Fiz. Zh. **38**, 901 (1993).
[12] E. Ya. Glushko and V. A. Khrisanov, Fiz. Nizk. Temp. **23**, 1215 (1997) [Low Temp. Phys. **23**, 910 (1997)].
[13] V. I. Peresada, in *Physics of Condensed State* [in Russian], Kharkov (1968).
[14] V. I. Peresada, V. N. Afanas'ev, and V. S. Borovikov, Fiz. Nizk. Temp. **1**, 461 (1975) [Sov. J. Low Temp. Phys. **1**, 227 (1975)].
[15] R. Haydock, in Solid State Phys. Vol. 35 (ed. by H. Ehrenreich, F. Seitz, and D. Turnbull), Academic Press, New York (1980).
[16] E. S. Syrkin and S. B. Feodosyev, Fiz. Nizk. Temp. **20**, 586 (1994) [Low Temp. Phys. **20**, 463 (1994)].
[17] M. A. Mamalui, E. S. Syrkin, and S. B. Feodosyev, Fiz. Tverd. Tela (St. Petersburg) **38**, 3683 (1996) [Phys. Solid State **38**, 2006 (1996)].
[18] N. I. Akhiezer, *Classical Problem of Moments* , Amer. Math. Soc., Providence, RI, 1968.
[19] Yu. Ya., Tomchuk. Ph.D. thesis, Kharkov State University, Kharkov (1964).
[20] A. M. Kosevich, E. S. Syrkin, and S. B. Feodosyev, Phys. Lett. A **167**, 94 (1992).

Translated by R. S. Wadhwa

Low-temperature plasticity of Pb–Bi alloys: the role of thermal activation and inertial effects

N. V. Isaev, V. D. Natsik, V. V. Pustovalov, V. S. Fomenko, and S. E. Shumilin

*B. Verkin Institute for Low Temperature Physics and Engineering, National Academy of Sciences of the Ukraine, 310164 Kharkov, Ukraine**

(Submitted March 6, 1998)
Fiz. Nizk. Temp. **24**, 786–796 (August 1998)

Detailed studies of temperature dependences of critical shear stress and strain-rate sensitivity of deforming stress of Pb–Bi single crystals with 0.1–6.0 at. % Bi are carried out in the temperature range 0.5–295 K. The deforming stress decrease during a superconducting transition of the sample is studied and the concentration dependence of the effect is measured. The ideas of a gradual transition (upon cooling) from thermally activated motion of dislocations through impurity barriers to the thermoinertial mechanism in the temperature range 10–25 K and further to the quantum-inertial motion at temperatures $\lesssim 1$ K are developed. A detailed thermoactivation analysis of experimental data is carried out, and empirical estimates of internal stresses, dislocation–impurity interaction parameters, electron and phonon components of dynamic drag coefficient for dislocations are obtained. © *1998 American Institute of Physics.* [S1063-777X(98)01108-6]

1. INTRODUCTION

The theory of yield stress of solid solutions based on the concepts of thermoactivated overcoming of local impurity barriers by dislocations predicts a monotonic increase of effective stress upon cooling.[1,2] It was proved earlier[3,4] that, in the case of solid solutions of Sn and Sb in Pb, this theory successfully describes the main peculiarities of plastic flow, which are detected in experiments in the range of moderately low temperatures. The thermoactivation analysis of experimental data carried out in these publications according to the algorithm proposed in Refs. 1 and 5 makes it possible to estimate the empirical parameters of the theory and to determine the statistics of barrier distribution along the dislocation line.

However, the low-temperature singularities (anomalies) in plasticity observed in the range of hydrogen and helium temperatures cannot be explained by using simple thermofluctuation concepts. Above all, this concerns the complex temperature dependence of the yield stress, athermal creep, and the stress jump in the superconducting transition. These effects were studied in many experimental works whose review is given in Ref. 6. Several hypotheses proposed for explaining low-temperature anomalies take into account specific features of dynamic and activated motion of dislocations at low temperatures. For example, the decisive role of inertial[7,8] and quantum-mechanical[3,9,10] effects in overcoming of impurity barriers by dislocations was proved for alloys based on fcc and hcp metals. However, the mechanisms of low-temperature anomalies of plasticity are not completely clear as yet.

It has become clear recently[11,12] that experimental data can be interpreted correctly only under a number of conditions the chief ones of which are listed below:

(1) A wide temperature interval in which plastic deformation occurs through dislocation slip and is not affected significantly by diffusion;
(2) An analysis of temperature dependences of differential parameters of plasticity such as strain rate and temperature sensitivity of deforming stress, that must be carried out along with an analysis of temperature dependence of yield stress;
(3) A range of concentration of impurity barriers as wide as possible, which is responsible for dislocation drag;
(4) A variety of local barrier heights obtained by varying the types of doping elements.

The fulfillment of these conditions and the use of modified procedure of thermoactivated analysis[11,12] make it possible to obtain rich information on dynamic parameters of dislocations and dislocation–impurity interaction, i.e., to determine the statistics of impurity distribution along dislocation lines and to estimate the height of impurity barriers, the characteristic level of internal stresses, and the dynamic drag coefficient for dislocations.

Single crystals of Pb-based solid solutions are most convenient objects of investigation that satisfy all the conditions listed above. In this paper, the kinetics of low-temperature plastic deformation of Pb–Bi single crystals with a wide set of concentration values of Bi impurity is studied in detail. The application of the rigorous procedure of thermoactivation analysis of the experimental data makes it possible to enrich and clarify the knowledge of dynamic effects exhibited in the motion of dislocations at low temperatures. The interest in Pb–Bi alloys is also due to peculiar variations of their thermal properties during the superconducting transition, which is important for determining the possible role of thermal effects in low-temperature peculiarities in plasticity of metals.

2. EXPERIMENTAL TECHNIQUE

We investigated Pb–Bi alloys with Bi concentrations 0.1, 0.5, 1.0, 3.0, and 6 at. %. The purity of starting materials for sample preparation was 99.9999% for Pb and 99.997% for Bi. Single crystals were grown by using the Bridgmann method in a dismountable graphite mold,[13] which made it possible to obtain a batch of 10 samples from one seed. The size of the working part of the sample was $15\times3\times1$ mm. The extension axis was oriented close to the [110] direction. The stress–strain curves $\tau(\varepsilon)$ for extension at a constant strain rate $\dot{\varepsilon}=1.1\times10^{-4}$ s^{-1} (τ is the shear stress and ε the shear strain) were recorded in the temperature range 0.5–295 K. The experiments were made on a low-temperature deforming setup with a ^{4}He cryostat at temperatures $T\geqslant4.2$ K and on a setup with a ^{3}He cryostat at 0.5–4.2 K.[14] Temperature variation was carried out by evacuation of ^{4}He and ^{3}He vapor. The temperature was monitored by three resistance thermometers fixed at different points of the sample. The relative error of temperature measurements did not exceed 10^{-2}.

The critical shear stress τ_0 was determined from the deviation of the initial segment of the $\tau(\varepsilon)$ curve from Hooke's law. In some cases, the sample was unloaded near the stress τ_0, cooled, and loaded again. The values of τ_0 obtained by sample loading at 3–4 different temperatures taking into account strain-hardening at each loading corresponded to the values determined from the $\tau(\varepsilon)$ curve at a fixed temperature.

At $T<T_c$ ($T_c\approx7.2$ K is the superconducting transition temperature for Pb), the measurements were made on samples in the superconducting and normal states: a transition to the normal state was induced by switching on the magnetic field of a superconducting solenoid containing the sample. In these experiments, we recorded the deforming stress jump $\Delta\tau_{SN}$. Weakly doped alloys did not display the effect of magnetic flux trapping distorting the jump $\Delta\tau_{SN}$. In the case of strongly doped alloys, the effect of magnetic flux trapping on the parameters being measured was eliminated by recording their values only during the first destruction of superconductivity by the applied magnetic field.

Apart from τ_0, we also recorded the sensitivity of deforming stress $[\Delta\tau(\varepsilon)]_T$ to an increase in the strain rate $\dot{\varepsilon}$ from $1.1\cdot10^{-5}$ s^{-1} by a factor of 10 and 100 during deformation at a fixed temperature. In order to plot the temperature dependence $\Delta\tau(T)$, the value of $\Delta\tau$ was determined by extrapolating the dependence $\Delta\tau(\tau)$ to the point $\tau=\tau_0$, which allowed us to minimize the uncontrollable influence of deformation defects. The error in stress measurements was ±2 kPa.

3. DISCUSSION OF EXPERIMENTAL RESULTS

3.1. Temperature dependence of plasticity parameters

The experimentally measured temperature dependences $\tau_0(T)$ and $\Delta\tau(T)/\ln\dot{\varepsilon}$ of the critical shear stress and the strain-rate sensitivity of deforming stress recorded in experiments for all the alloys under investigation are shown in Figs. 1, 2, 3, and 4.

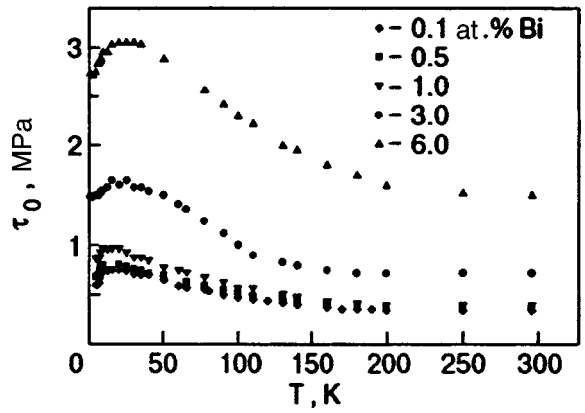

FIG. 1. Temperature dependence of the critical shear stress $\tau_0(T)$ for Pb–Bi single crystals with different Bi concentrations; the extension axis is oriented approximately along the [110] direction.

For all the five values of impurity concentration, we can distinguish four segments on the $\tau_0(T)$ curves (see Figs. 1 and 2): the absence of any temperature dependence (athermal region) at $T>150-200$ K, an increase in τ_0 upon sample cooling to a certain temperature $T_{m1}\approx10-30$ K, a noticeable decrease in the value of τ_0 during sample cooling below T_{m1}, and the formation of one more athermal segment at $T<5$ K. The temperature boundaries of these regions, the height of the peak on the $\tau_0(T)$ curve, and the values of τ_0 in high- and low-temperature athermal segments depend significantly on the concentration C of impurity atoms.

Below the superconducting transition temperature T_c, the well-known effect of plasticity variation is observed[6]: the transition of the samples from the superconducting to the normal state induced by a magnetic field is accompanied by an increase in the critical shear stress by $\Delta\tau_{NS}=\tau_{0N}(T)-\tau_{0S}(T)>0$ (see Fig. 2). It is worth noting that the relative

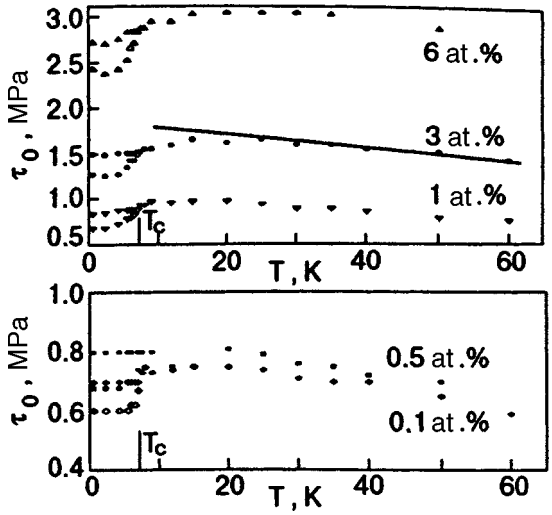

FIG. 2. Anomaly of critical shear stress $\tau_0(T)$ for Pb–Bi single crystals in the normal and superconducting states (low-temperature specification of dependences presented in Fig. 1): dark symbols correspond to the normal state and light symbols to the superconducting state, and T_c is the superconducting transition temperature. The solid curve describes the theoretical dependence (3) corresponding to purely thermoactivated slip of dislocations in the alloy Pb–3 at. %Bi obtained for the values of parameters from Table I.

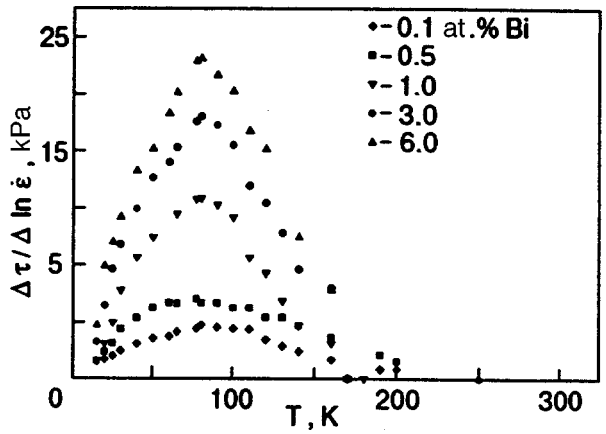

FIG. 3. Temperature dependence of the sensitivity of deforming stress to the variation of strain rate $\dot{\varepsilon}$ from 1.1×10^{-5} to 1.1×10^{-4} s^{-1} for Pb–Bi alloys with different concentrations of Bi.

magnitude of the stress decrease is quite large ($\Delta\tau_{NS}/\tau_{0N} \approx 10-15\%$), and the value of $\Delta\tau_{NS}$ considerably depends on the impurity concentration.

For all the alloys under investigation, the dependence $\Delta\tau(T)/\Delta \ln\dot{\varepsilon}$ (see Figs. 3 and 4) is a curve with a peak at $T_{m2}\approx 80-90$ K. The peak temperature T_{m2} is independent of the impurity concentration, while the value of $\Delta\tau(T_{m2})/\Delta \ln\dot{\varepsilon}$ increases significantly with concentration. The strain-rate sensitivity of deforming stress virtually vanishes in the regions $T\approx 180-200$ K and $T<12-15$ K (to within the error of measurements of $\Delta\tau\approx 2$ kPa). It should be noted that the value of $\Delta\tau(T)/\Delta \ln\dot{\varepsilon}$ becomes negative at $T>200$ K, and stress-strain curves display a decrease in the stage of linear strain-hardening and first features of unstable (jump-wise) plastic flow. These observations indicate a significant role of impurity diffusion and dislocation–diffusion effects of deformation ageing in inelastic deformation processes at $T>200$ K.

The dependences $\Delta\tau(T)/\Delta \ln\dot{\varepsilon}$ depicted in Figs. 3 and 4 were obtained by changing the strain rate by a factor of 10. Similar values of $\Delta\tau(T)/\Delta \ln\dot{\varepsilon}$ were observed in the case when the strain rate was decreased by a factor of 100.

Figure 4 shows (on a magnified scale on the temperature axis) the low-temperature anomaly of the strain-rate sensitivity $[\Delta\tau(T)/\Delta \ln\dot{\varepsilon}]_T$: the rate of decrease in this quantity increases abruptly upon cooling at $T<20-30$ K. The anomaly can be seen more clearly on the temperature dependence of activation volume (see Fig. 4b):

$$V(T)=kT(\Delta \ln\dot{\varepsilon}/\Delta\tau)_T.$$

The general regularities in the temperature dependences $\tau_0(T)$ and $\Delta\tau(T)/\Delta \ln\dot{\varepsilon}$ for Pb–Bi alloys are qualitatively similar to those observed for other alloys based on fcc metals.[3,4,8]

3.2. Thermally activated plasticity

The experimentally observed temperature and impurity concentration dependences $\tau_0(T)$ and $\Delta\tau(T)/\Delta \ln\dot{\varepsilon}$ of the critical shear stress and the strain-rate sensitivity of flow

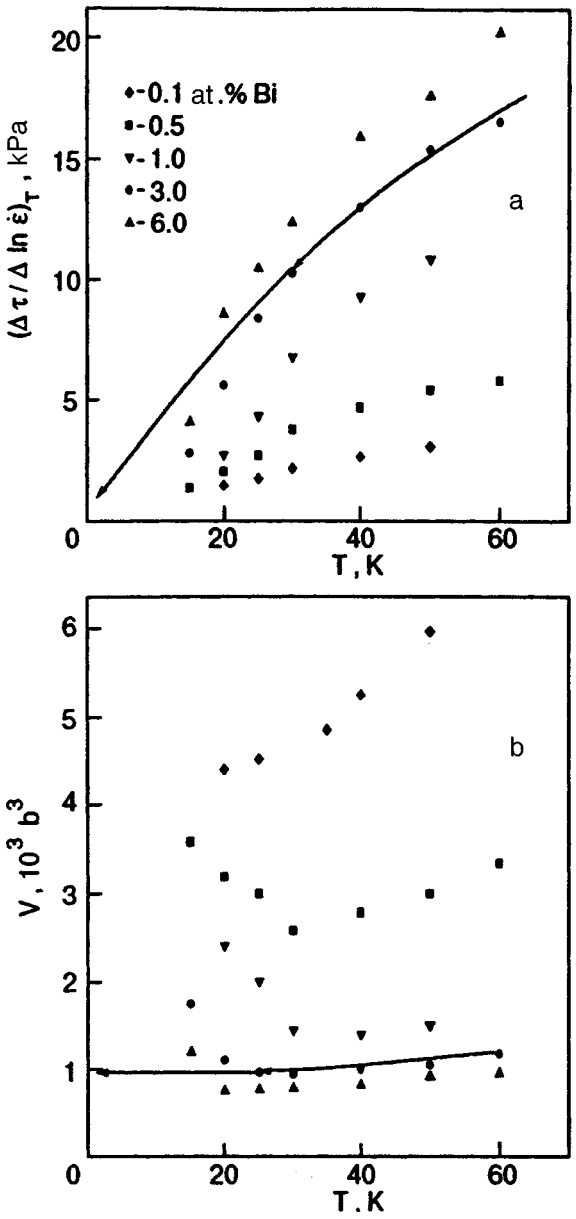

FIG. 4. Low-temperature anomalies of the strain-rate sensitivity of deforming stress (a) and activation volume (b). Solid curves are theoretical dependences corresponding to purely thermoactivated dislocation slip in the alloy Pb–3 at. % Bi plotted for the values of parameters from Table I.

stress for Pb–Bi single crystals at $30\text{ K}<T<150$ K possess all the features typical of dislocation-type plastic deformation determined by thermoactivated motion of dislocations through local barriers formed by impurity atoms. In such cases, the relation between the plastic strain rate $\dot{\varepsilon}$, the deforming stress τ, and temperature T is determined by the classical Arrhenius equation

$$\dot{\varepsilon}=\dot{\varepsilon}_0 \exp[-H(\tau^*)/kT]. \quad (1)$$

Here $\tau^*=\tau_0-\tau_i$ is the effective stress equal to the difference between the deforming stress τ_0 and the long-range (internal) stress τ_i, and $H(\tau^*)$ is the effective activation energy (enthalpy) whose form is determined by the power

law governing the interaction of a dislocation with the pinning center and the statistics of distribution of such centers along a dislocation line.

In various models of solid-state strain hardening, the stress dependence of activation enthalpy is successfully approximated by the universal expression[1]

$$H(\tau^*)=H_0[1-(\tau^*/\tau_c)^p]^q, \tag{2}$$

where H_0 is the energy parameter of dislocation–impurity interaction typical of a given impurity, and τ_c the critical stress of activationless motion of a dislocation through impurity barriers. The exponents p and q in formula (2) are numerical parameters of the order of unity. The value of the parameter q is determined by the shape of a barrier, while the parameter p and τ_c are determined by the properties of the barrier itself and the statistics of barrier distribution along the dislocation line.

Relations (1) and (2) readily lead to explicit expressions for the experimentally studied parameters of plasticity:

$$\tau_0(T)=\tau_i+\tau_c[1-(T/T_0)^{1/q}]^{1/p}, \tag{3}$$

$$\left(\frac{\Delta\tau}{\Delta\ \ln\dot{\varepsilon}}\right)_T=\frac{\tau_c}{pqA}\left(\frac{T}{T_0}\right)^{1/q}\left[1-\left(\frac{T}{T_0}\right)^{1/q}\right]^{(1-p)/p}. \tag{4}$$

Here we have used the following notation: $A=\ln(\dot{\varepsilon}_0/\dot{\varepsilon})$; $T_0=H_0/kA$.

A comparison of relations (3) and (4) with the experimental curves presented in Figs. 1, 2, 3, and 4 allows us to determine the empirical values of the parameters p, q, τ_i, τ_c, A, and H_0 of the theory. In the general case, we must take into account the fact that the parameters τ_c, τ_i, and H_0 are directly proportional to the shear modulus G, and hence are functions of temperature in accordance with the dependence $G(T)$. The disregard of this fact can lead to significant errors in the estimates of the parameters of the theory in the cases when formulas (3) and (4) are used for describing experimental data in a very wide temperature range.[11] However, this interval for Pb-based alloys does not exceed 200 K as a rule, and the corrections associated with the temperature dependence $G(T)$ are small.

Additional difficulties are also encountered when the temperature dependence of the parameter τ_i appearing in formula (3) is taken into account correctly. This is due to low reliability of the method of measurement of $\tau_i(T)$ in the low-temperature range.[15] The thermoactivation analysis proposed in Ref. 11 makes it possible to avoid possible errors associated with the above circumstances.

First of all, we must analyze the temperature dependence of the strain-rate sensitivity of stress $(\Delta\tau/\Delta\ \ln\dot{\varepsilon})_T$ whose theoretical expression (4) does not contain the parameter τ_i. Using this dependence, we can obtain empirical values of the parameters p, q, and T_0 as well as the ratio τ_c/A. Then we can calculate τ_c after determining the parameter A independently. This can be done by finding the empirical values of the derivative $d\tau_0/dT$ by numerical differentiation of the curves shown in Fig. 1 and using the relation

$$A=-T\left(\frac{\Delta\tau}{\Delta\ \ln\dot{\varepsilon}}\right)_T^{-1}\left(\frac{d\tau_0}{dT}\right)_{\dot{\varepsilon}}. \tag{5}$$

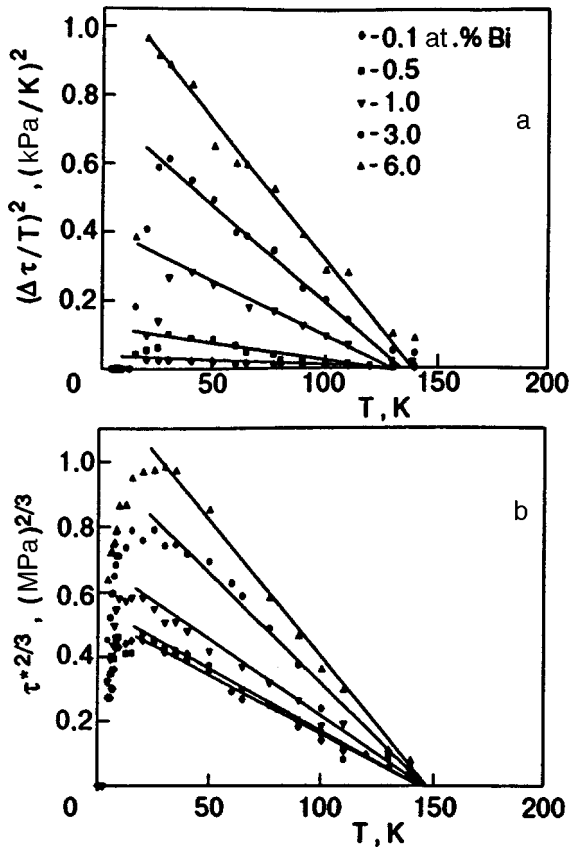

FIG. 5. Comparison of experimental temperature dependences of $(\Delta\tau/T)^2$ (a) and $\tau^{*2/3}$ (b) with formulas (3) and (4) (solid lines) for the values of the parameters $p=2/3$ and $q=1$.

provided that $d\tau_i/dT \ll d\tau_0/dT$. Under the above assumptions concerning the impurity nature of barriers overcome by a dislocation through thermal activation and a weak dependence $\tau_i(T)$, the value of A calculated from formula (5) should not depend significantly on the impurity concentration and temperature. Athermal empirical values of the parameter A is a criterion of applicability of Eq. (1) and relation (2) for describing a plastic flow.

In order to match expressions (3) and (4), we must take the values of $\tau_i=\tau_0(T_0)$ as an empirical estimate of internal stresses. Then we must find the empirical values of effective stress $\tau^*(T)=\tau_0(T)-\tau_i=\tau_0(T)-\tau(T_0)$ for each concentration and verify the correspondence of the chosen values of p and q to experimental dependences shown in Fig. 1.

While processing the experimental data according to the above algorithm, we considered all possible combinations of the values of exponents appearing in formula (2): $p=1$, 2/3 and $q=2$, 3/2, and 1. In each case, we analyzed the correlation between the experimental data and the theoretical dependences (3) and (4) as well as temperature and concentration dependences of the parameters of the theory appearing in these expressions. It was found as a result of analysis that the optimal values of the parameters are $p=2/3$ and $q=1$. For these values, the dependence $(\Delta\tau/\Delta\ \ln\dot{\varepsilon})_T$ in the $(\Delta\tau/T)^2$ vs. T coordinates is linear for all the alloys under investigation in the temperature range $T=30-140$ K (Fig. 5a). In the same temperature range, the dependence $\tau_0(T)$ is

TABLE I. Empirical values of the parameters of the theory.

C, at. %	T_0, K	τ_c, MPa	τ_i, MPa	A	H_0, eV	f_m, $H\cdot10^{-11}$	T_i, K	$\Delta\tau_{NS}/\tau_c$
0.1	141	0.30	0.40	20	0.25	2.0	12	0.31
0.5	140	0.37	0.45	20	0.25	2.0	15	0.31
1.0	138	0.57	0.50	20	0.25	2.0	17	0.28
3.0	137	0.99	0.80	20	0.25	2.0	22	0.24
6.0	140	1.35	1.95	23	0.27	2.2	25	0.24

linear in the coordinates $(\tau^*)^{2/3}$ vs. T, where $\tau^*(T) = \tau_0(T) - \tau_0(T_0)$ (Fig. 5b).

The empirical values of the parameters T_0, τ_c, and τ_i calculated by using the curves in Figs. 1, 2, 5a and b and expressions (3) and (4) are given in Table I. The values of the parameter A obtained as a result of numerical differentiation of $\tau_0(T)$ (Fig. 1) as well as from formula (5) and the data presented in Fig. 2 were found to be independent of temperature in the interval 30–140 K. The values of A averaged over this temperature interval and the values of $H_0 = kT_0A$ corresponding to them are also given in Table I. It can be seen that only the critical stress τ_c and the internal stress τ_i display a considerable dependence on the impurity concentration. The effect of impurities on the internal stress τ_i is insignificant for low concentrations and becomes noticeable only for $C>0.01$.

The correctness of the above analysis and obtained estimates is confirmed additionally by the following circumstances. The value of the parameter $A\approx20$ is typical of most fcc metals.[1,2] This parameter is virtually independent of temperature in a fairly wide temperature range 30–140 K, which means that the role of the dependences $G(T)$ and $\tau_i(T)$ is insignificant. The temperature T_0 corresponding to the upper limit of applicability of Eq. (1) is approximately the same for all the alloys. According to formula (2), this means that the type and parameters of the barriers responsible for dislocation drag do not change upon an increase in the Bi concentration.

The characteristic energy parameter H_0 also behaves in analogy with T_0. The empirical value of H_0 corresponds to the case when solitary impurity atoms play the role of the effective barrier for dislocations in a fcc crystal. The average value of $H_0\simeq0.26$ eV is close to the corresponding value obtained in Refs. 3 and 4 as a result of thermoactivation analysis for Pb–Sn alloys (0.27 eV) and is much lower than for Pb–Sb alloys (0.31 eV). The value of H_0 is in accord with the data on the height of impurity barriers in Pb, which were obtained by using other methods.[16–18]

Another important test that makes it possible to estimate the correctness of the choice of the numerical values for p and q is the verification of correlation between the values of temperature T_{m2} and T_0 following from formula (4). An analysis of formula (4) for maximum leads to the relation $T_{m2}=p^qT_0$. It can easily be seen that this relation holds to within $\sim10\%$ for the values $p=2/3$ and $q=1$.

The value of the parameter p and the form of the $\tau_c(C)$ dependence give an idea about the statistics of barrier distribution along a dislocation line. The value $p=2/3$ corresponds to the case when the average length L of dislocation segments is a function of the stress τ^* acting on a dislocation (Friedel statistics). In this case, in the first approximation the value of L is determined by the formula[19]

$$L\approx(2E_Lb/\tau^*C)^{1/3}, \tag{6}$$

where E_L is the linear tensile force acting on the dislocation and b the Burgers vector. In the Friedel statistics, the stress corresponding to activationless depinning of the dislocation from a barrier is defined as

$$\tau_c=(2E_L/b^2)\delta^{2/3}C^{1/2}, \tag{7}$$

where $\delta=f_m/2E_L$ is the dimensionless barrier strength (f_m is the maximum force required for overcoming a barrier without thermal activation). Figure 6 shows that the values of τ_c obtained for alloys with different impurity concentrations satisfies relation (7) indeed. The slope of the straight line in Fig. 6 makes it possible to estimate the parameter f_m:

$$\frac{2E_L}{b^2}\,\delta^{2/3}=\frac{f_m^{3/2}}{b^2}\,\sqrt{2E_L}=7\cdot10^6\ \text{Pa}. \tag{8}$$

Using this relation, the standard estimate of $2E_L=Gb^2$, the values of the shear modulus $G=10^{10}$ Pa and Burgers vector $b=3.5\times10^{-10}$ m for the easy slip system in Pb, we obtain the values of f_m given in Table I. The value of f_m obtained for Bi impurities is slightly smaller than for doping Pb with Sn[3] and Sb.[4] This is in good agreement with the data on the effect of Bi, Sn, and Sb impurities on solid-solution hardening of Pb.[16–18]

It should be noted that the empirical value of the parameter $q=1$ for Bi impurities differs from the value of $q=3/2$ obtained for Sn and Sb impurities.[3,4] In the case of Bi impurities, the values of $q=3/2$ or 2 do not satisfy formulas (3) and (4) or lead to unexpectedly high values of the parameters H_0, T_0, and f_m. This indicates the difference in the profiles of potential barriers created by these impurities.

Thus, the optimal value of the parameter $p=2/3$ and the form of concentration dependences $\tau_c(C)$ indicate that the barrier distribution along a dislocation line in these alloys corresponds to the Friedel statistics. The values of the energy parameter H_0 of the barrier, the maximum force f_m, and the

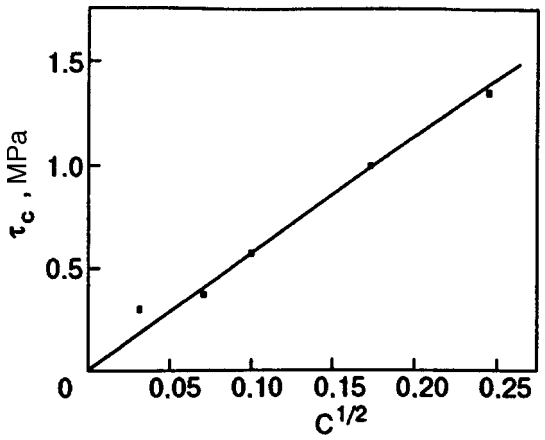

FIG. 6. Concentration dependence of the critical stress for activationless flow of dislocations.

limiting temperature T_0 are typical of barriers formed by individual substitutional atoms in Pb. At $T>140$ K, the effective contribution to the deforming stress comes only from long-range obstacles.

All the regularities of plastic flow in Pb–Bi alloys described above change significantly for $T<30$ K: the temperature dependences of the measured parameters of plasticity deviate from regularities typical of a thermoactivation process described by the Arrhenius equation. Such deviations are known as low-temperature anomalies of plasticity.

3.3. Low-temperature anomalies of plasticity

The departure of experimental data from the theoretical dependences (3) and (4) at $T<30$ K is clearly seen from Figs. 2 and 4. When the sample is cooled below a certain characteristic temperature T_i, the temperature sensitivity $(d\tau_0/dT)_{\dot\varepsilon}$ and the strain-rate sensitivity $(\Delta\tau/\Delta\ln\dot\varepsilon)_T$ of deforming stress decrease more rapidly than what is predicted by the dependences (3) and (4). The derivative $(d\tau_0/dT)_{\dot\varepsilon}$ reverses its sign and becomes positive, while $(\Delta\tau/\Delta\ln\dot\varepsilon)_T$ decreases to zero (to within the error in stress measurements $\Delta\tau\sim 2$ kPa). In the region of the peak $\tau_0(T)$, the temperature dependence of activation volume has a clearly manifested minimum (see Fig. 4b). The temperature T_i corresponding to the beginning of the anomaly increases with the impurity concentration (see Table I).

At a temperature $T<T_c$, where T_c is the superconducting transition temperature, all the alloys under investigation go over to the superconducting state. This is accompanied by a characteristic jump-wise change in τ_0 by $\Delta\tau_{NS}$.[6] It can be seen from Fig. 2 that the value of $\Delta\tau_{NS}(T)$ increases upon cooling, while $\Delta\tau_{NS}(0)$ depends on the impurity concentration.

The physical mechanisms whose action can explain low-temperature anomalies of plasticity were considered by Dotsenko *et al.*[20] Taking into account the type of anomalies observed by us here, which are typical of fcc alloys, we shall consider in greater detail the theoretical hypotheses which were recently confirmed in experiments.

Under the action of high effective stresses in the low-temperature region, dislocations can be accelerated to high velocities. In this case, a transition to the above-the-barrier motion of dislocations can be made, for which the following relations must hold[21]:

$$\tau^*=\gamma\dot\varepsilon \quad \text{and} \quad \delta\tau/\delta\dot\varepsilon=\gamma\dot\varepsilon, \tag{9}$$

where γ is a parameter proportional to the dynamic drag coefficient for dislocations. In our case (see Sec. 3.1), the measured values of the strain-rate sensitivity of deforming stress are in noticeable contradiction with relations (9). For example, it can be seen from Figs. 2 and 4 that the temperature dependences $\tau_0(T)$ and $(\Delta\tau(T)/\Delta\ln\dot\varepsilon)_T$ are different, while these dependences should be identical according to (9). Thus, the anomalous nature of plasticity parameters observed in our experiments cannot be explained by a transition from the thermofluctuation to the above-the-barrier motion of dislocations.

A possible reason behind the anomalies can be associated with a transition from the thermoactivated to quantum-mechanical motion of dislocations through barriers. Osetskii *et al.*[22] explained the creep of pure Pb at $T<10$ K by quantum effects, while it was proved[22,23] that the limiting temperature Θ below which the quantum mechanism plays a decisive role must be of the order of $0.1\Theta_D$ (Θ_D is the Debye temperature). The inclusion of quantum effect in a description of motion of a dislocation through local barriers boils down to the replacement of temperature T in Eq. (1) by the ''effective'' temperature $T^*(T)$:

$$T^*(T)=\begin{cases}(\Theta/2)(1+T^2/\Theta^2), & T<\Theta\\ T, & T>\Theta\end{cases}. \tag{10}$$

After the substitution $T\to T^*(T)$ in (1), relations (3) and (4) with the obtained values of p and q become

$$\tau_0(T^*)=\tau_i-\tau_c(1-T^*/T_0)^{3/2}, \tag{11}$$

$$\left(\frac{\Delta\tau}{\Delta\ln\dot\varepsilon}\right)_T=\frac{3\tau_c}{2A}\sqrt{1-T^*/T_0}\,(T^*/T_0). \tag{12}$$

These formulas make it possible to explain the athermal nature of plastic flow at $T<5$ K if we put $\Theta\approx 10$ K.[22] However, the emergence of a peak on the $\tau_0(T)$ curve at $T=20-30$ K cannot be explained by expressions (11) and (12).

It was proved earlier[3,4] that more unambiguous conclusions on the influence of quantum effects on the motion of dislocations through impurity barriers can be made from an analysis of the temperature dependence of $(\Delta\tau/\Delta\ln\dot\varepsilon)_T$. However, the strain-rate sensitivity in our case vanishes at $T<12$ K in view of limited sensitivity of measuring instruments. Thus, we can only state that the plasticity parameters studied by us at $T<30$ K have anomalies that cannot be explained only by quantum effects.

The effect of inertial properties of dislocations is considered to be one of possible reasons behind manifestation of low-temperature anomalies of plasticity.[7,8,24] In the low-temperature region, dislocation segments go over from a damped to an undamped state due to an increase in the effective stress $\tau^*(T)$ and a decrease in the phonon component $B_{\rm ph}(T)$ of the dynamic drag coefficient $B(T)=B_{\rm ph}(T)+B_e$ (B_e is the athermal contribution of conduction electrons to dislocation drag). The time of attenuation of natural vibrations of the dislocation segment in this case constitutes a considerable part of the time of expectation of a favorable thermal of quantum fluctuation. As a result, quantum depinning from an individual barrier is accompanied by the motion of the dislocation through a large number of neighboring barriers (unzipping). The conditions for the existence of undamped dislocations is the simultaneous fulfillment of the two inequalities

$$\tau_0-\tau_i=\tau^*>0{,}5\tau_c, \tag{13}$$

$$BL<2\pi(ME_L)^{1/2}, \tag{14}$$

where M is the linear mass density of a dislocation.

The assumption concerning successive transition from the purely activated to the thermoinertial mechanism follows

by a transition to the quantum–inertial mechanism of motion of dislocations through impurity barriers upon cooling has made it possible to describe completely the low-temperature anomaly of plasticity for Pb–Sn and Pb–Sb alloys.[3,4] According to Table I and Fig. 1, condition (13) is satisfied for Pb–Bi alloys even at $T<60$ K. In order to verify condition (14), we can use the rough estimates $E_L \approx 0.5Gb^2$, $M \approx 0.5\rho b^2$ (ρ is the crystal density), and take the value of the drag coefficient $B=4\times10^{-5}$ N·m^{-2}·s typical of Pb-based alloys in the low-temperature range.[25] Putting $G\simeq10^{10}$ Pa, $\rho\approx10^4$ kg/m^3, and $b\approx3.5\times10^{-10}$ m, we obtain the following condition for the fulfillment of (14): $L<10^{-7}$ m. According to relation (7) taking into account (9), the length of the segment $L\approx10^{-7}$ m for $\tau^*\approx0.5\tau_c$ even for the alloy with the minimum impurity concentration $C=0.001$. Thus, at $T\approx T_i$ condition (14) holds for all the five alloys under investigation.

The combined influence of inertial effects and thermal fluctuations on the motion of dislocations through obstacles was analyzed by using computer simulation methods.[26] The features of such an influence following from the thermoinertial model are (a) a decrease of the derivative $d\tau^*/dT$ to zero and its sign reversal; (b) a sharp increase in the activation volume V upon cooling as a result of quasi-dynamic nature of motion, and (c) the emergence of anomalies only in the presence of impurity barriers and an increase in the threshold temperature of the anomaly with the impurity concentration. The regularities in manifestations of low-temperature peculiarities in plasticity parameters observed by us are in accord with the features of thermoinertial model listed above. Consequently, the low-temperature anomalies in plasticity of Pb–Bi alloys are determined by the same physical mechanisms as those used for explaining the anomalies in plasticity of Pb–Sn and Pb–Sb alloys[3,4]: the thermoinertial mechanism is realized at $T<20$–30 K, while at $T<10$ K the motion of dislocations through impurity barriers is governed by the quantum–inertial mechanism.

3.4. Dynamic drag coefficient for dislocations

Experimental recording of the threshold temperature T_i of the low-temperature anomaly and the application of the basic concepts of the theory of thermoinertial motion of dislocations provide information on the characteristic value and temperature dependence of the dynamic drag coefficient $B(T)$ for dislocations.[12]

According to the theory of thermoinertial effects, the threshold temperature T_i increases with the concentration of impurity barriers. When the inequality $\tau^*>0.5\tau_c$ is satisfied, the $T_i(C)$ dependence must be described by the condition $B(T)L(\tau^*,C)=2\pi(ME_L)^{1/2}$, in which the temperature dependence $B(T)$ is determined by the phonon component. At $T<\Theta_D$, the phonon contribution to dynamic drag of dislocations is correctly approximated by a power function,[27] and hence we can use the following expression for $B(T)$:

$$B(T)=B_e+\eta(T/\Theta_D)^{\nu}, \tag{15}$$

where $\eta=$const, and the value of the exponent ν is determined by the interaction between dislocations and phonons.

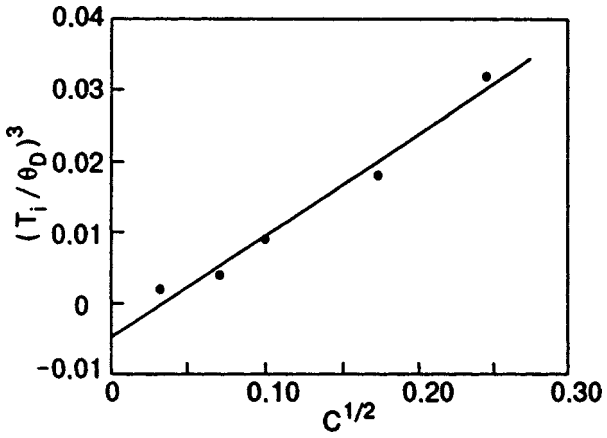

FIG. 7. Concentration dependence of the threshold temperature T_i of the low-temperature anomaly, illustrating the validity of formula (16) for $\nu=3$.

Considering that $L(\tau^*,C)$ in the given case is determined by formula (7), putting $\tau^*\approx\tau_c$, and taking into account the dependence $\tau_c(C)$ [see (9)], we can expect that the following relations hold:

$$\eta(T/\Theta)^{\nu}=\alpha C^{1/2}-B_e,$$

$$\alpha=2\pi\delta^{2/9}(ME_L/b^2)^{1/2}. \tag{16}$$

The results presented in Fig. 7 indicate that relation (16) holds for all values of T_i if we assume that the Debye temperature $\Theta_D=94$ K[19] and put $\nu=3$ and $\eta=7\alpha$. The value $\nu=3$ in formula (16) corresponds qualitatively to the case when the contribution to dislocation drag is determined by inelastic scattering of thermal phonons by dislocation lines (Flatter effect).[27] Extrapolating the straight line in Fig. 7 to its intersection with the ordinate axis, we can obtain the empirical value of the electron drag coefficient $B_e=3.5\times10^{-5}$ N·m^{-2}·s. This value is in good agreement with the empirical estimates of the electron drag coefficients B_{eN} in the normal state, which were obtained from an analysis of other experimental data for Pb and its alloys,[25] but is approximately an order of magnitude higher than theoretical estimates.[28]

For the coefficient η in formula (15), we obtain the empirical estimate $\eta=7\alpha\approx7\times10^{-3}$ N·m^{-2}·s.

3.5. Variation of stress in the course of superconducting transition

The effect of the electron state of the sample on the critical shear stress is known to be a common property of superconductors.[6] A transition from the N to the S state in solid solutions causes a jump-wise variation of stress by $\Delta\tau_{NS}=\tau_{0N}-\tau_{0S}$, and the magnitude of the effect depends considerably on temperature, concentration, and the barrier height: $\Delta\tau_{NS}=\Delta_{NS}(T,C)$. At temperatures below $0.5T_c$, the temperature dependence of $\Delta\tau_{NS}$ attains saturation. In order to clarify the mechanism of stress jump, we must take into account the form of the concentration dependence

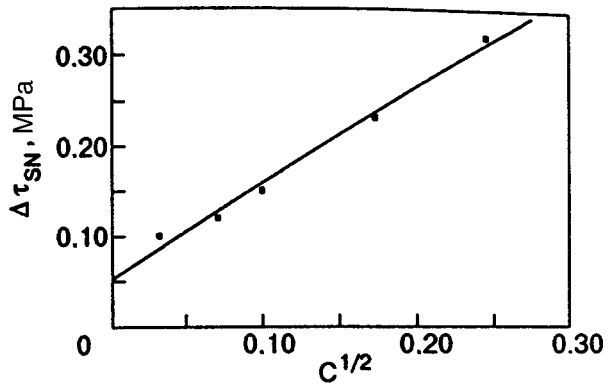

FIG. 8. Concentration dependence of the change in deforming stress $\Delta\tau_{NS}=\tau_{0N}-\tau_{0S}$ during the superconducting transition, $T=0.55$ K.

$\Delta\tau_{NS}(0,C)$ as well as the relative magnitude of the jump $\Delta\tau_{NS}(0,C)/\tau_c$, where τ_c is the critical stress of dislocation depinning from a barrier.

The analysis of experimental data carried in the previous sections convincingly proves that the kinetic of plastic flow in the region of existence of superconductivity is determined by the inertial mechanism of overcoming of impurity barriers by dislocations. Keeping this in mind, it is expedient to use the inertial mechanism of stress decrease effect developed by Granato[24] on the basis of the string model of a dislocation and modified by Kostorz[29] by taking into account the velocity of impingement of the dislocation on obstacles for interpreting the obtained results on the influence of the superconducting transition on the critical shear stress in Pb–Bi single crystals. This model predicts a monotonic enhancement of the effect with increasing impurity concentration according to the law $\Delta\tau_{NS}\sim C^{1/2}$ in the case when the length of dislocation segments changes in the interval $L\approx 10^{-5}-10^{-8}$ m. Such values of L are in accord with the estimates obtained by us. Furthermore, the inertial mechanism predicts the independence of the relative magnitude $\Delta\tau_{NS}/\tau_c$ of the effect of the barrier height.

The concentration dependence $\Delta\tau_{NS}(0,C)$ for Pb–Bi alloys is shown in Fig. 8, and the relative change in the stress $\Delta\tau_{NS}(0,C)/\tau_c$ is given in Table I (the values of $\Delta\tau_{NS}(0,C)$ were obtained by extrapolating the data for $T=0.55$ K). It can be seen that the concentration dependence of stress jump is correctly described by the empirical law

$$\Delta\tau_{NS}=\Delta\tau_{NS}^0+KC^{1/2}, \tag{17}$$

where $K=1.06$ MPa and $\Delta\tau_{NS}^0=0.05$ MPa corresponds to the effect in pure lead.[30] On the other hand, the relative change in stress in the course of the superconducting transition weakly depends on the impurity concentration $(\Delta\tau_{NS}/\tau_c\approx 0.31-0.24)$.

Thus, the experimental data are described satisfactorily by the inertial mechanism of the stress decrease effect in the alloy during the superconducting transition.

4. CONCLUSIONS

(1) The regularities of plastic flow in single crystals of Pb–Bi solid solutions with Bi concentration varying from 0.1 to 6.0 at. % are studied in a wide temperature range 0.5–295 K. The low-temperature anomaly of plasticity typical of solid solutions based on fcc and hcp metals is detected.

(2) A thermoactivation analysis of temperature dependences of plasticity parameters is carried out, and it is proved that plastic deformation in the temperature range 25–150 K is determined by thermoactivated motion of dislocations through impurity barriers. Empirical dependences of the parameters of dislocation–impurity interaction and internal stresses are obtained.

(3) It is shown that considerable deviation of temperature dependences of plasticity parameters from the regularities typical of a simple thermoinertial process below 25 K (low-temperature anomaly) is due to the mechanisms of thermoinertial and quantum–inertial motion of dislocations through impurity barriers.

(4) Empirical estimates for the electron and phonon components of the dynamic drag coefficient for dislocations are obtained from an analysis of the concentration dependence of the threshold temperature of the low-temperature anomaly.

(5) The effect of jump-wise variation of deforming stress upon a sample transition from the superconducting to the normal state induced by an external magnetic field is studied below the superconducting transition temperature. It is shown that the dependence of the jump in the deforming stress on the impurity concentration corresponds to the assumption concerning the fluctuation–inertial motion of dislocations through impurity barriers.

The authors are grateful to Yu. G. Kazarov for growing a batch of high-quality single crystals of Pb–Bi alloys studied by us and to V. V. Demirskii for his interest in this research and fruitful discussions of the results.

This research was carried out under the support of the Ukrainian Foundation of Fundamental Studies (Project No. 2.4/156 ''Bion-2'').

*E-mail: isaev@ilt.kharkov.ua

[1] U. F. Kocks, A. S. Argon, and M. F, Ashby, in *Progr. Mater. Sci.*, vol. 19, Pergamon Press, Oxford (1975).
[2] P. Haasen, in *Physical Metallurgy*, vol. 2 (ed. by R. W. Cahn and P. Haasen), North-Holland, Amsterdam (1983).
[3] I. A. Shepel', L. N. Zagoruiko, V. D. Natsik *et al.*, Fiz. Nizk. Temp. **17**, 390 (1991) [Sov. J. Low Temp. Phys. **17**, 202 (1991)].
[4] N. V. Isaev, V. D. Natsik, V. V. Pustovalov *et al.*, Fiz. Nizk. Temp. **18**, 911 (1992) [Sov. J. Low Temp. Phys. **18**, 641 (1992)].
[5] V. D. Natsik and H.-J. Kaufmann, Phys. Status Solidi A **65**, 571 (1981).
[6] V. I. Startsev, in *Dislocations in Solids*, vol. 6 (ed. by F. R. N. Nabarro), North-Holland, Amsterdam (1983).
[7] R. B. Schwarz, R. D. Isaak, and A. V. Granato, Phys. Rev. Lett. **38**, 554 (1977).
[8] Th. Wille, W. Gieseke, and Ch. Schwink, Acta Metall. **35**, 2679 (1987).
[9] V. D. Natsik, A. I. Osetskii, V. P. Soldatov, and V. I. Startsev, Phys. Status Solidi B **54**, 99 (1972).
[10] L. N. Zagoruiko, V. D. Natsik, and V. P. Soldatov, Fiz. Nizk. Temp. **12**, 1073 (1986) [Sov. J. Low Temp. Phys. **12**, 605 (1986)].
[11] N. V. Kovaleva, V. A. Moskalenko, and V. D. Natsik, Phil. Mag. **70**, 423 (1994).
[12] V. A. Moskalenko, N. V. Kovaleva, V. D. Natsik *et al.*, Fiz. Nizk. Temp. **22**, 1459 (1996) [Low Temp. Phys. **22**, 1108 (1996)].

[13] Yu. G. Kazarov, *Physics of Condensed State* [in Russian], vol. 11, Kharkov (1973).
[14] B. G. Verkin and V. V. Pustovalov, *Low-Temperature Studies of Plasticity and Strength* [in Russian], Energoizdat, Moscow (1982).
[15] V. I. Dotsenko, Phys. Status Solidi B **54**, 99 (1979).
[16] G. Kostorz and S. Michailovich, Proc. ICSMA-2, Asilomar (1970).
[17] I. Van der Planken and A. Deruyttere, J. Mater. Sci. **4**, 499 (1969).
[18] V. P. Soldatov, V. D. Natsik, and L. G. Ivanchenko, Fiz. Nizk. Temp. **22**, 1087 (1996) [Low Temp. Phys. **22**, 830 (1996)].
[19] J. Friedel, *Dislocations*, Pergamon, London (1964).
[20] V. I. Dotsenko, A. I. Landau, and V. V. Pustovalov, *Modern Problems of Low-Temperature Plasticity of Materials* [in Russian], Naukova Dumka, Kiev (1987).
[21] T. Suzuki and T. Ishi, *Physics of Strength and Plasticity* [Russian trans.], Metallurgiya, Moscow (1972).
[22] A. I. Osetskii, V. P. Soldatov, and V. I. Startsev, Fiz. Met. Metalloved. **38**, 604 (1974).
[23] V. D. Natsik, Fiz. Nizk. Temp. **5**, 400 (1979) [Sov. J. Low Temp. Phys. **5**, 191 (1979)].
[24] A. V. Granato, Phys. Rev. B **4**, 2196 (1971).
[25] V. R. Parameswaran and J. Weertman, Met. Trans. **2**, 1233 (1971).
[26] A. I. Landau, Phys. Status Solidi A **61**, 555 (1980); *ibid.* **65**, 119 (1981).
[27] V. I. Al'shits and V. L. Indenbom, Usp. Fiz. Nauk **115**, 3 (1975) [Sov. Phys. Usp. **15**, 1 (1975)].
[28] M. I. Kaganov, V. Ya. Kravchenko, and V. D. Natsik, Usp. Fiz. Nauk **111**, 655 (1973) [Sov. Phys. Usp. **16**, 878 (1973)].
[29] G. Kostortz, J. Low Temp. Phys. **10**, 167 (1973).
[30] V. V. Pustovalov, V. I. Startsev, and V. S. Fomenko, Phys. Status Solidi **37**, 319 (1970).

Translated by R. S. Wadhwa

BRIEF COMMUNICATIONS

Equation of state for liquid nitrogen in the high-density limit

V. Yu. Bardik and V. M. Sysoev

*Taras Shevchenko University, 252022 Kiev, Ukraine**

(Submitted September 5, 1997; revised January 19, 1998)
Fiz. Nizk. Temp. **24**, 797–799 (August 1998)

Equations of state are proposed for describing the isothermal compression of liquid argon. These equations are derived by the method of integral equations in the statistical theory of the condensed state of matter. The thermophysical data are analyzed for calculating the isotherms and parameters of molecular interaction potential. © *1998 American Institute of Physics.* [S1063-777X(98)01208-0]

In the method of integral equations in the statistical theory of the condensed state of matter used in our earlier publications,[1,2,3,4] we chose the generating functional

$$\Phi[g_1(\mathbf{r}/\Psi),\Psi(\mathbf{r})]=\sum \beta^i a_i[\Psi^i(q\mathbf{r})-\varphi(\mathbf{r})]g_1(\mathbf{r}/\Psi) \tag{1}$$

and, making q tend to infinity [$q=(V/V_0)^{1/3}$ is the scaling factor], which corresponds to a transition to high densities since in this case $V\to 0$ and $\rho\to\infty$, obtained the integral equation for the radial distribution function in the form

$$g_2(\mathbf{r})M_{\mathbf{r}}(0)\beta\varphi(\mathbf{r})+M_{\mathbf{r}}(0)[g_2(\mathbf{r})-1]+\rho\int g_2(\mathbf{r}-\mathbf{r}')\times M_{\mathbf{r}-\mathbf{r}'}(0)\beta\varphi(\mathbf{r}-\mathbf{r}')[g_2(\mathbf{r}')-1]d\mathbf{r}'=0 \tag{2}$$

with a direct correlation function satisfying the relation

$$M_{\mathbf{r}}(0)c(\mathbf{r})=-g_2(\mathbf{r})M_{\mathbf{r}}(0)\beta\varphi(\mathbf{r}),$$
$$M_{\mathbf{r}}(0)=\exp(-\mathbf{r}\cdot\nabla_{\mathbf{r}})-1=\sum (-1)^i(-\mathbf{r}\cdot\nabla_{\mathbf{r}})^i i!, \tag{3}$$

where $\varphi(\mathbf{r})$ is the intermolecular potential. Using the virial theorem, the compressibility theorem and the Euler's theorem on homogeneous functions, we obtain from Eqs. (3) the following equations of state

$$\rho(\partial P/\partial\rho)_T=2P-\rho kT \tag{4}$$

and

$$\frac{V_0-V}{V_0}=\frac{\ln[(P+B(T))/(P_0+B(T))]}{A_0^{-1}+\ln[(P+K)/(P_0+K)]}. \tag{5}$$

Equation (4) can be reduced to the familiar Tait's equation with parameters A and $B(T)$:

$$-(\partial P/\partial V)_T=(P+B(T))/AV_0. \tag{6}$$

Confining to the first term in the sum (3), we obtain $A=1/2$ and $B(T)=-\rho_0 kT/2$ for $i=1$ and $A=3/(m+2)$ and $B(T)=(A-1)\rho_0 kT$ for $i=2$. Here m is the exponent of the potential corresponding to the repulsive forces between molecules and defined in the form $\varphi(\mathbf{r})\sim\mathbf{r}^m$, or the uniformity of potential energy of molecular interaction. Retaining an arbitrary number i of terms in the series (3), we obtain the following relation[1]:

$$A^{-1}=12\sum\frac{(m+i-2)!}{(m-1)!i!}\sum\frac{(i+2)!}{i!}, \tag{7}$$

This leads to the following isothermal equation of state in the form (5) under the condition that the increase in the reciprocal value of the parameter A is characterized by the dependence[2]

$$A^{-1}=A_0^{-1}+\ln[(P+K)/(P_0+K)], \tag{8}$$

where A_0 is the parameter in the initial Tait's equation.

In Refs. 2 and 3, we verified the modified equation (5) for water under pressure up to 1 GPa. This equation reveals a good qualitative agreement between the experimental results and theoretical values of the specific volume of water and the isothermal derivative of volume with respect to pressure.

In order to analyze the experimental results on isothermal compression of argon, we used the data obtained in Ref. 5 for three isotherms $T=130$, 140 and 150 K. Table I shows the results for density obtained from experiments, Tait's equation, and the modified equation (5). The results obtained by using Eq. (5) were analyzed in two stages. At first, the parameters $A_0, B(T)$ and K were obtained at the reference points $P_0=10$ MPa, $P_1=20$ MPa, $P_2=40$ MPa and $P_3=100$ MPa. The values of parameters obtained in this way were then substituted into Eq. (5) for determining the density.

An analysis of the results presented in Table I shows that Eq. (5) correctly describes the experimental data on isothermal compression of liquid argon and gives fairly accurate results upon extrapolation. It should be observed that Tait's equation is applicable in the range of thermodynamic variables where the isothermal compressibility β_{T0} is low.[6,7] We processed the experimental data only in this region, where $\beta_{T0}P_0\ll 1$.

The processing of experimental results led to the values of the parameters A_0, $B(T)$ and K which are compiled in

TABLE I. Values of density ρ_{exp} (in units of 10^3 mole/m^3) calculated from experimental results, ρ_T calculated from Tait's equation (4), and ρ_m calculated from the modified equation (5).

P, MPa	130 K		140 K			150 K		
	ρ_{exp}	ρ_T	ρ_{exp}	ρ_T	ρ_m	ρ_{exp}	ρ_T	ρ_m
10	28.72	28.72	26.63	26.63	26.63	24.17	24.17	24.17
20	30.27	30.27	28.72	28.72	28.72	27.08	27.08	27.08
40	32.30	32.30	31.13	31.13	31.13	29.95	29.95	29.93
60	33.72	33.72	32.73	32.73	32.73	31.73	31.76	31.71
80	34.85	34.85	33.96	33.96	33.94	33.07	33.14	33.05
100	35.79	35.79	34.97	34.98	34.95	34.16	34.28	34.15
120	36.60	36.61	35.84	35.86	35.82	35.08	35.26	35.08
140	37.32	37.33	36.61	36.64	36.59	35.89	36.13	35.89
160	37.97	37.99	37.29	37.36	37.28	36.61	36.91	36.61
180	38.56	38.59	37.91	37.99	37.90	37.26	37.62	37.27
200	39.10	39.14	38.48	38.58	38.48	37.86	38.29	37.87
220	-	-	39.01	39.13	39.02	38.41	38.90	38.42
240	-	-	39.50	39.65	39.52	38.92	39.48	38.93
260	-	-	39.96	40.14	39.99	39.40	40.03	39.41
280	-	-	-	-	-	39.85	40.55	39.86
300	-	-	-	-	-	40.28	41.05	40.28
errors	$\delta_T=0.03\%$ $\Delta_T=0.1\%$		$\delta_T=0.15\%$ $\Delta_T=0.45\%$ $\delta_m=0.003\%$ $\Delta_m=0.07\%$			$\delta_T=0.90\%$ $\Delta_T=1.9\%$ $\delta_m=0.03\%$ $\Delta_m=0.07\%$		

Table II. The physical meaning of the parameter $B(T)$ lies in that it defines the internal pressure in the liquid and is a decreasing function of temperature. The parameter K characterizes the pressure at which the short-range structural variations begin to manifest themselves upon an increase in pressure. The parameter A_0 defines the structure of the short-range order and, as mentioned above, is related in a certain manner with the exponential index of the molecular interaction potential corresponding to the repulsive forces between molecules. For liquid argon, the value of the exponent m lies between 27.07 and 27.37. However, it does not match with value $m=12$ generally accepted for many model potentials. It should be recalled that the value $m=12$ does not have any theoretical basis and was chosen for the sake of convenience of computations. An analysis of the temperature dependence of the second and third virial coefficients for argon, krypton and xenon, as well as of the equations of state for these elements carried out by Dymond *et al.*[8] leads to the conclusion that the forces of repulsion between molecules in the investigated systems are characterized by a potential

$$\Phi(\mathbf{r})=\varepsilon[0.331(\mathbf{r}_{\min}/\mathbf{r})^{28}+2.072(\mathbf{r}_{\min}/\mathbf{r})^{18}],$$

where $\mathbf{r}_{\min}$ is the position of minimum of the intermolecular potential, and $m=28$. An analysis of the experimental data for a number of liquids and solids shows[9,10] that the value of m lies in the interval 24–33. Thus a consistent derivation of the equation of state carried out by using methods of statistical mechanics makes it possible to establish a relation between the parameters of molecular interaction potentials and thermodynamic properties of liquids.

Processing of the data obtained in a computer experiment carried out by us[11] for a model system of soft spheres in which the particle interaction is preset by the potential $\varphi=\varepsilon(\sigma/\mathbf{r})^{12}$ may serve as a serious argument in favor of the result presented in this work. A comparison of theoretical and experimental values of pressure indicates the correctness of the description of a system ''soft'' spheres with the help of equation of state (5). The error in determining the pressure in this case is of the order of 0.3%, which is in accord with the error of the computer experiment.

TABLE II. Values of parameters of Tait's equation (4), and of the modified equation (5).

Parameter	130 K	140 K	150 K
$A^{-1}(T)$	9.69	9.79	9.72
$B(T)$, MPa	5.56	−0.37	−4.57
$K(T)$, MPa	∞	3295	910

*E-mail: moldept@molphes.ups.kiev.ua

[1] V. M. Sysoev and A. V. Chalyĭ, Izv. Vuzov, ser. Fizika **12**, 43 (1981).
[2] M. S. Labinov, V. M. Sysoev, and A. V. Chalyĭ, Zh. Strukt. Khim. **24**, 88 (1983).
[3] M. S. Labinov, V. M. Sysoev, and A. V. Chalyĭ, Teplofiz. Vys. Temp. **20**, 1194 (1982).
[4] V. M. Sysoev, A. V. Chalyĭ, and M. S. Labinov, in *Proceedings XI AIRAPT Int. Conf. High Press. Science and Technology*, Naukova Dumka, Kiev (1989).
[5] W. B. Streett, Physica (Amsterdam) **B76**, 59 (1974).
[6] V. M. Sysoev, Teor. Mat. Fiz. **55**, 305 (1983).
[7] V. G. Boĭko, V. M. Sysoev, and A. V. Chalyĭ, Zh. Éksp. Teor. Fiz. **97**, 842 (1990) [Sov. Phys. JETP **70**, 472 (1990)].
[8] J. H. Dymond, M. Rigby, and E. B. Smith, J. Chem. Phys. **48**, 2801 (1965).
[9] P. R. Couhcman and C. I. Reynolds, Jr., Phys. Stat. Solidi **42**, K47 (1977).
[10] P. R. Couhcman and C. I. Reynolds, Jr., J. Appl. Phys. **47**, 5201 (1976).
[11] W. G. Hoover, M. Ross, and K. W. Johnson, J. Chem. Phys. **52**, 1198 (1970).

Translated by R. S. Wadhwa

EPR investigation of the fluctuating valence compound YbB_{12}

A. E. Altshuler

Institute of Biology, Russian Academy of Sciences, 420503 Kazan', Russia

T. S. Altshuler, B. S. Rameev, and E. P. Khaimovich

*Physicotechnical Institute, Russian Academy of Sciences, 420029 Kazan', Russia**

(Submitted November 28, 1997; revised March 4, 1998)
Fiz. Nizk. Temp. **24**, 800–802 (August 1998)

The compound YbB_{12} having a fluctuating valence is investigated by the EPR method. It is suggested that the valence fluctuation frequency of ytterbium ions $\nu > 10^{10}$ Hz. The electron excitation spectra reveal a gap of the order of 6–7 meV. © *1998 American Institute of Physics.* [S1063-777X(98)01308-5]

The strong electron–electron correlation in a number of compounds leads to anomalous phenomena like fluctuating valence and formation of heavy fermions. Unfortunately, in contrast to heavy fermions, the only compound in which fluctuating valence has been studied intensively so far is SmB_6. Investigations of a large number of such compounds are essential for revealing the general regularities for materials from this class. In this work, we describe the results of EPR studies of ytterbium dodecaboride YbB_{12}[1,2] which is also a fluctuating valence compound.

The compound YbB_{12} was synthesized in an induction furnace in vacuum at 1700 K by barometric reduction from the oxide Yb_2O_3. It was then melted in an arc furnace and dissolved in nitric acid to remove the YbB_6 impurity. The single-phase composition of the sample in the form of a black powder was verified by x-ray diffraction analysis. Measurements were made on two samples, viz., pure YbB_{12} and YbB_{12} doped with 1 at. % Gd^{3+}. Gadolinium has pure spin paramagnetism (with ground state $^8S_{7/2}$) and was used as a marker. Measurements were made at a frequency $\nu = 9.4$ GHz in the temperature interval 4.2–60 K.

Rare-earth dodecaborides RB_{12} have the same crystal lattice as NaCl with a metal atom at the Na position and a cubic octahedron formed by 12 boron atoms in the Cl positions.[3] The rare-earth ions in RB_{12} are usually trivalent and the dodecaborides have metal-type conductivity. The multiplet Yb^{3+} ($4f^{13}$, $^8F_{7/2}$) is split by a crystal field of cubic symmetry into a doublet Γ_6, a quartet Γ_8, and a doublet Γ_7. The ground state may contain Kramers doublets Γ_6 or Γ_7 and an EPR signal can be observed on them. However, we did not detect any EPR signal in pure YbB_{12}. This may be due to the following reason. Studies of electric conductivity, susceptibility, and photoemission[1,2] show that the valence of Yb in YbB_{12} is not integral, and amounts to 2.9, while its conductivity is of semiconductor type. Such a departure from the behavior of conventional dodecaborides is associated with the existence of a fluctuating valence of Yb ions in YbB_{12}, i.e., the valence fluctuates between the states Yb^{3+} and Yb^{2+}, the yttrium ion spending 90% of its time in the trivalent state and 10% of its time in the bivalent state. The EPR line corresponding to Yb^{3+} can be observed only if the frequency ν_{Yb} of valence fluctuation between Yb^{3+} and Yb^{2+} is lower than the frequency of the EPR spectrometer. Since the EPR spectrum was not detected, it means that the frequency ν_{Yb} is apparently higher than 10^{10} Hz. Probably, the fluctuation frequency in YbB_{12}, as in SmB_6, is of the order of 10^{12}–10^{14} Hz.[4]

In the entire temperature range, an intense EPR signal is observed from Gd^{3+} with a g-factor equal to 1.95 ± 0.02. The temperature dependence of the linewidth δH is shown in Fig. 1. The broadening of the EPR line observed below 10 K is due to magnetic ordering. Above 20 K, the linewidth increases rapidly from 200 to 1200 Oe at 50 K, and then attains saturation.

The temperature dependence of δH in this temperature interval can be described quite correctly by the exponential law

$$\delta H = A \exp(-\Delta/T),$$

where $A = 7220$, $\Delta = 75$ K.

Such a behavior of the dependence $\delta H(T)$ may be due to two reasons:

(1) It follows from the results obtained by Sugawara[5] and Moriya[6] that the linewidth δH varies exponentially as a result of exchange interaction of the impurity spin with excited states of the magnetic lattice. In our case, this is the exchange interaction of gadolinium spin with the f-electrons of the excited state of Yb^{3+} ions.
(2) The broadening $\delta H(T)$ may be due to the presence of electron excitations in a narrow gap arising, for example, due to hybridization of s-conduction electrons with the f-electrons from the valence band of Yb. The interaction of the spin of Gd^{3+} with the spins of electrons and holes causes a broadening of the EPR line. Since the number of $s-f$ excitations and hence the density of states at the edges of the gap increases exponentially, the dependence $\delta H(T)$ is exponential.

Sugawara[7] has presented the results of computation of the dependence of spin–spin relaxation rate T_2^{-1}

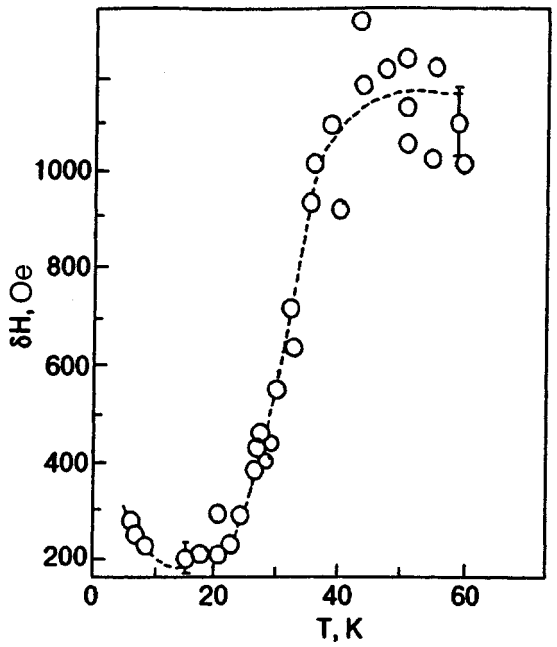

FIG. 1. Temperature dependence of the EPR linewidth for YbB_{12}.

($T_2^{-1} \propto \delta H$) of an impurity (with the S ground state) on $t = T/[E(\Gamma_8) - E(\Gamma_6)]$ for Yb^{3+} ions in a cubic symmetry field, where T is the temperature, $E(\Gamma_8)$ the energy of the excited quartet Γ_8, and $E(\Gamma_6)$ the energy of the ground state, viz., the doublet Γ_6 of Yb ions.

It follows from the results of computations that the relaxation rate T_2^{-1} increases just by 25% as a result of scattering of spins at f-electrons in the excited state of Γ_8 of Yb ions. Since the broadening δH in our case amounts to 500% upon a variation of temperature from 10 to 50 K, i.e., is much larger than 25%, the linewidth in YbB_{12} is due, in all probability to the presence of a gap in the spectrum of electron excitations as in SmB_6.

An indirect argument in favor of of this assumption is the relatively narrow EPR line of Gd^{3+} observed at low temperatures. Since there are no free holes and electrons in the system at $T = 0$ K, there can be no scattering of Gd electrons by them. In this case, if the EPR linewidth is determined by the interaction of Gd spins with the spins of electrons and holes in Yb, it will tend to zero. Indeed, extrapolating the curve $\delta H(T)$ to zero temperature and disregarding the ordering effects observed at $T \leqslant 15$ K, we find that $\delta H(0)$ is close to zero. If $\delta H(T)$ is determined by the scattering of Gd spins by the excited levels of Yb, a slight narrowing of the line (by about 25% according to Sugawara[7]) will be observed at $T = 0$ K, since spontaneous excitations of f-electrons of Yb are possible even at zero temperature.

The estimate obtained by us for the gap $\Delta = 75$ K $= 6.5$ meV is of the same order as for SmB_6 ($\Delta = 4.5-7$ meV).[4,8]

We propose to study in near future the question concerning the origin of the gap, i.e., find out if the gap is due to $s-f$-hybridization or due to exciton pairing of s-electrons with f-holes as in SmB_6.[8]

This work was supported financially by a grant from the Russian Foundation for Fundamental Research (project No. 97–02–1623).

*E-mail: tatiana@dionis.kfti.kcn.ru

[1] M. Kasaya, F. Iga, K. Negishi *et al.*, J. Magn. Magn. Mater. **31–34**, 437 (1983).
[2] F. Iga, Y. Takakuwa, T. Takahashi *et al.*, Solid State Commun. **50**, 903 (1984).
[3] F. Bertaut and P. Blum, CR Acad. Sci. **34**, 666 (1949).
[4] T. Kasuya, T. Tanaka, K. Takegahara *et al.*, J. Phys. (France) **40**, C5-308 (1979).
[5] K. Sugawara and C. Y. Huang, J. Phys. Soc. Jpn. **40**, 295 (1976).
[6] T. Moriya, Prog. Theor. Phys. **28**, 371 (1962).
[7] K. Sugawara, J. Phys. Soc. Jpn. **42**, 1154 (1977).
[8] T. S. Altshuler, G. G. Khaliullin, and D. I. Khomskiĭ, Zh. Éksp. teor. Fiz. **90**, 2104 (1986) [Sov. Phys. JETP **63**, 1234 (1986)].

Translated by R. S. Wadhwa

On the dielectric constant anomaly in the antiferromagnetic phase of $YMnO_3$

I. E. Chupis

B. Verkin Institute for Low Temperature Physics and Engineering, National Academy of Sciences of the Ukraine, 310164 Kharkov, Ukraine

(Submitted March 16, 1998)
Fiz. Nizk. Temp. **24**, 803–806 (August 1998)

It is proposed that the triangular antiferromagnetic β-structure precedes the triangular antiferromagnetic α-structure observed in $YMnO_3$ by neutron diffraction studies at 4.2 K. The experimental observation of the anomalous behavior of the dielectric constant below Néel temperature is attributed to the phase transition between β and α configurations. © *1998 American Institute of Physics.* [S1063-777X(98)01408-X]

The compound $YMnO_3$ belongs to the class of hexagonal rare-earth manganates $RMnO_3$ (R=Ho, Er, Tm, Yb, Lu, Y), which are ferroelectrics[1] and antiferromagnets.[2] The interaction between the electric and magnetic subsystems of $YMnO_3$ was indicated for the first time in a publication by Haang *et al.*[3] who observed an anomaly in the temperature dependence of the dielectric constant below the temperature of antiferromagnetic transition. The transition to the magnetically ordered state is accompanied by a break in the temperature dependence of the dielectric constant ε.[4] However, the temperature dependence of ε below Néel temperature observed in $YMnO_3$ is distinctly nonmonotonic, and appears in the form of an S-shaped curve (Fig. 1).

In this work, it is suggested that the nonmonotonicity of the $\varepsilon(T)$ dependence below Néel temperature is associated with the first order phase transition occurring between different antiferromagnetic configurations in the crystal.

The manganate $YMnO_3$ has a high ferroelectric (FE) transition temperature ($\Theta_e = 914$ K) and Néel temperature $T_N \approx 80$ K. Figure 1 clearly shows the change in the slope of the temperature dependence of ε at the Néel temperature: the dashed straight line is the extrapolation of ε from the paramagnetic phase to the low-temperature region, while segment 2 on the curve corresponds to the dielectric constant after variation as a result of magnetic ordering. The magnetoelectric (ME) interaction leads to the emergence of a kink on the $\varepsilon(T)$ curve at $T = T_N \approx 75$ K. It was shown earlier (see Ref. 4 and the literature cited therein) that this anomaly is of exchange type and is determined by ME exchange interaction. After the break at $T = T_N$, the $\varepsilon(T)$ dependence is expected to be monotonic (see, for example, the dependence $\varepsilon(T)$ in $BaMnF_4$).[5] However, the dielectric constant of $YMnO_3$ increases in a certain temperature interval after decreasing in the antiferromagnetic phase.

Apparently, the nonmonotonicity of the $\varepsilon(T)$ dependence is due to the magnetic properties of $YMnO_3$, since the S-shaped anomaly is also observed in the temperature dependence of the derivative $d\chi/dT$ of magnetic susceptibility,[3] and the magnetic field displaces the $\varepsilon(T)$ curve significantly in the magnetically ordered phase (see Fig. 1).

The presence of excitations in a crystal facilitates an increase in its dielectric susceptibility. In principle, the spin waves emerging at temperatures below T_N may make a contribution to ε owing to the dependence of the equilibrium magnetization of the magnetic sublattice on the electric field (this effect has the first order in ME interaction constant). Calculations, which we shall not present here, show that the observed shape of the $\varepsilon(T)$ curve cannot be due to the contribution from spin waves. The latter increase ε in the nearest neighborhood of $T \lesssim T_N$. If their contribution is significant, this would lead to an increase in the value of ε just below T_N. However, the decrease in the value of ε observed at $T \lesssim T_N$ indicates that the static ME effect dominates over the high-frequency effect. It is obvious even without any computations that the contribution of spin waves to ε decreases with temperature and cannot cause a sudden increase in the dielectric constant away from Néel temperature.

Consequently, the anomalous temperature dependence of ε is determined by the static magnetic properties of the system. There are six Mn^{3+} ions in $YMnO_3$, lying in planes perpendicular to the hexagonal axis. Neutron diffraction studies[6] at 4.2 K point in favor of the antiferromagnetic trigonal structure α (Fig. 2). Nedlin[7] studied theoretically the possible magnetic configurations in $YMnO_3$. In the exchange approximation, the thermodynamic potential per unit volume can be presented in the form

$$\begin{aligned}\Phi = &\frac{1}{2} A_1 \mathbf{s}^2 + A_2 \mathbf{l}^2 + A_3(\mathbf{g}_1^2 + \mathbf{g}_2^2) + A_4(\mathbf{r}_1^2 + \mathbf{r}_2^2) \\ &+ B_1(g_1^2 + g_2^2)^2 + B(r_1^2 + r_2^2)^2 \\ &+ D r_1^2 r_2^2 \sin^2 \varphi_r + D_1 g_1^2 g_2^2 \sin^2 \varphi_g \\ &+ \frac{1}{4} c s^2 (r_1^2 + r_2^2) + \frac{1}{4} c_1 s^2 (g_1^2 + g_2^2) + \dots . \end{aligned} \tag{1}$$

Here, $\mathbf{s} = \Sigma_{i=1}^{6} \mathbf{s}_i$ is the total spin, $\mathbf{l} = \Sigma_{i=1}^{6} (-1)^{i+1} \mathbf{s}_i$ is the antiferromagnetism vector, and $\mathbf{g}_1, \mathbf{g}_2, \mathbf{r}_1, \mathbf{r}_2$ are expressed in terms of the corresponding linear combinations of spin vectors $\mathbf{s}_i$.[7] The angle φ_r is the angle between the vectors $\mathbf{r}_1$ and $\mathbf{r}_2$, while φ_g is the angle between the vectors $\mathbf{g}_1$ and $\mathbf{g}_2$.

The coefficients A_i are positive in the paramagnetic phase. The potential (1) allows the following equilibrium antiferromagnetic structures:

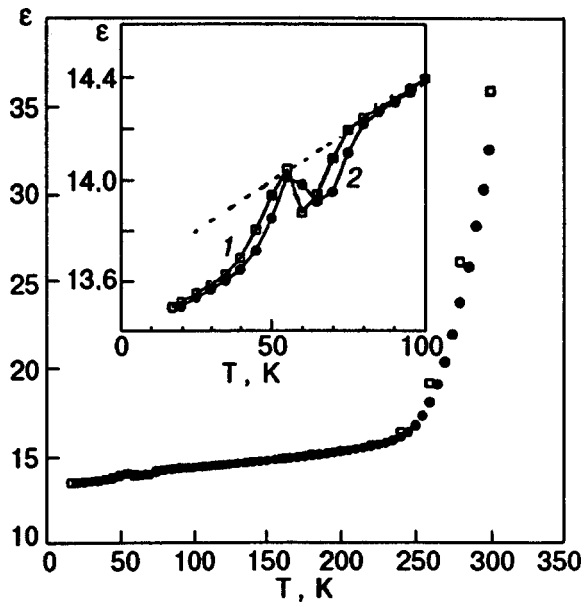

FIG. 1. Dielectric constant of $YMnO_3$ measured by Haang *et al.*[3] in zero magnetic field (□) and in a magnetic field $H=5$ T (●).

(1) $A_4<0$, $B>0$, $4B+D>0$, $\mathbf{s}=\mathbf{l}=\mathbf{g}_1=\mathbf{g}_2=0$, a) $D<0$, $\varphi_r=\pi/2$, $r_1=r_2$, $\mathbf{s}_{i+3}=\mathbf{s}_i$. Trigonal antiferromagnetic structure α (Fig. 2); b) $D>0$, $\varphi_r=0$, π, $r_{1(2)}=0$ or $r_{1(2)}=\pm\sqrt{3}r_{2(1)}$. Antiferromagnetic configuration with spins collinear with the hexagonal axis.

(2) $A_3<0$, $B_1>0$, $4B_1+D_1>0$, $D_1<0$, $\varphi_g=\pi/2$, $g_1=g_2$, $\mathbf{s}=\mathbf{l}=\mathbf{r}_1=\mathbf{r}_2=0$. Trigonal antiferromagnetic structure β in Fig. 2 with $\mathbf{s}_{i+3}=-\mathbf{s}_i$.

Neutron diffraction studies in monocrystalline samples of $YMnO_3$ at 4.2 K point in favor of the phase 1a, i.e., the trigonal structure α. In this phase, the magnetic susceptibility $\chi=\mu^2 v_c^{-2}(\partial^2\Phi/\partial s^2)^{-1}$ (μ is the Bohr magneton and v_c the unit cell volume) has the form

$$\chi=\mu^2 v_c^{-2}(A_1+cr_1^2)^{-1}, \quad r_1^2=-\frac{A_4}{4B+D}. \tag{2}$$

In the framework of the Landau theory, $A_4=a(T-\Theta)<0$, $a>0$. Since the phase transition temperature for $YMnO_3$ increases in a magnetic field (see Fig 1), the coefficient $c<0$.[8] The experimentally measured value of $\chi'=d\chi/dT$ is negative, and $\chi'(T)$ curve is S-shaped like the dependence $\varepsilon(T)$.[3]

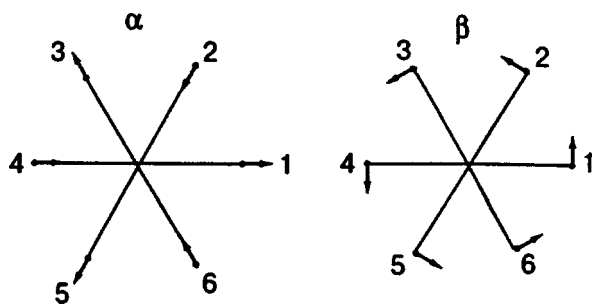

FIG. 2. Various types of trigonal antiferromagnetic configuration in $YMnO_3$. The even and odd Mn^{3+} ions lie in different planes at right angles to the hexagonal axis. Arrows indicate the directions of the spins.

It can be verified easily that the magnetic susceptibility (2) with the temperature-dependent coefficient A_4 leads to monotonicity of the function $\chi'(T)$. The next step in the analysis was the assumption that the coefficient D in the fourth-order invariants in (1) depends linearly on temperature and remains negative at all $T<T_N$: $D=-d+\beta T$($d>0$,$\beta>0$ or $\beta<0$). For $\beta>0$, such a dependence $D(T)$ does not violate the monotonicity of $\chi'(T)$, while for $\beta<0$ it may lead just to the emergence of an extremum. However, the experimental dependence shows that there must be two such extrema if we assume that the magnetic configuration α is preserved in the crystal in the interval $0\leqslant T\leqslant T_N$. The observed nonmonotonicity of $\chi'(T)$ is not obtained theoretically even if higher-order terms are taken into account in the expansion of potential (1).

Hence it is suggested that the anomalies in the dependences $\chi'(T)$ and $\varepsilon(T)$ are associated with the phase transition occurring in $YMnO_3$ between the above-mentioned magnetic configurations 1a, 1b, and 2. An analysis shows that transitions between these configurations are first-order phase transitions. A sharp variation in the dielectric constant in zero magnetic field (Fig. 1) and an analogous variation in the slope of the dielectric losses[3] point towards a first-order phase transition.

A transition between states 1a and 1b is possible upon a reversal of the sign of the constant D in (1). In the vicinity of T_N, the energies of these states are given by

$$\Phi_{1a}=-\frac{A_4^2}{4B+D}, \quad \Phi_{1\mathscr{P}}=-\frac{A_4^2}{4B}, \tag{3}$$

since $D<0$, $\Phi_{1a}<\Phi_{1b}$. This means that it is not advantageous for the system to go over from paramagnetic state to the state 1b, i.e., the phase 1b cannot precede the low-temperature phase 1a.

The configuration 1a can precede the state 2 if the sign of the coefficient A_3 in (1) is reversed at the Néel temperature, $A_3=b(T-T_N)$, $b>0$. State 2, i.e., the β configuration, is stable for all $T<T_N$. However, A_4 becomes negative at $T<\Theta<T_N$, and this leads to the emergence of the equilibrium state 1a (configuration α) whose energy is lower than the energy of the β-configuration below a certain temperature $T_n\leqslant\Theta$. Since β configuration does not lose stability, the left boundary of the temperature hysteresis may be considerably extended, while the right boundary is equal to the temperature Θ at which the configuration α becomes unstable.

According to the above assumption about the configurational magnetic transition, curve *1* in Fig. 1 corresponds to the α-configuration while curve *2* corresponds to the β-configuration.

The change in ε due to antiferromagnetic ordering is associated with the exchange ME interaction[4] with an energy

$$\Phi_{me}=\frac{1}{2}\gamma_1 P^2(\mathbf{r}_1^2+\mathbf{r}_2^2)+\frac{1}{2}\gamma_2 P^2(\mathbf{g}_1^2+\mathbf{g}_2^2), \tag{4}$$

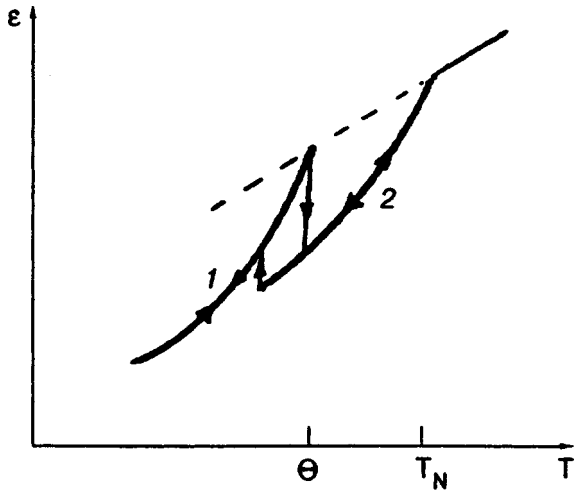

FIG. 3. Temperature hysteresis of the dielectric constant (theoretical) during heating and cooling of the crystal.

where P is the electric polarization. The dielectric susceptibility χ_e in the phenomenological theory is given by $\chi_e^{-1} = \partial^2\Phi/\partial P^2$, where $\Phi = \Phi_e(P) + \Phi_{me}$, $\Phi_e(P)$ is the thermodynamic potential of the ferroelectric subsystem in the form of an expansion in powers of P^2. Taking into account the smallness of the ME energy (4), we can present the dielectric constant $\varepsilon_{1,2}$ in the antiferromagnetic phases 1 and 2 in the form

$$\varepsilon_i(T) = \varepsilon_0 + (\varepsilon_0 - 1)^2 \Gamma_i (T_i - T), \quad i = 1,2. \tag{5}$$

$$T_1 = \Theta, \quad T_2 = T_N,$$

$$\Gamma_1 = \frac{\gamma_1 a}{2\pi(4B + D)}, \quad \Gamma_2 = \frac{\gamma_2 b}{2\pi(4B_1 + D_1)}.$$

Here, $\varepsilon_0 = \varepsilon_0(T)$ is the dielectric constant in the paramagnetic phase (dashed line in Fig. 1).

The dielectric constant in a first-order phase transition must have a temperature hysteresis shown qualitatively in Fig. 3. The dependence $\chi'(T)$ will also have a similar form. The right boundary of the hysteresis corresponds to $T = \Theta$. In this case, it follows from formula (5) that $\varepsilon = \varepsilon_0$, i.e., the value of ε lies on the straight line $\varepsilon_0(T)$ extrapolated to the temperatures $T < T_N$. The left boundary of the hysteresis may be the temperature T_n at which energies of the phases become equal, or a lower temperature since phase 2 remains stable.

The experimental curve $\varepsilon(T)$ in zero magnetic field (light points in Fig. 1) corresponds to the dependence $\varepsilon(T)$ in Fig. 3 obtained during heating. The value of the temperature Θ corresponding to $\varepsilon = \varepsilon_0$ is equal to 55 K. The dependence $\varepsilon_0(T)$ is linear: $\varepsilon_0(T) = \lambda + \nu T$, where $\lambda = 13.6$ and $\nu = 7.7 \times 10^{-3}$ deg^{-1} (Fig. 1). The Néel temperature $T_N \approx 75$ K. Using the experimental data and formula (5), we obtain the following estimates for the ME interaction constants: $\Gamma_1 \approx -2 \times 10^{-4}$ deg^{-1} and $\Gamma_2 \approx -9 \times 10^{-5}$ deg^{-1}.

Hence it is assumed that the nonmonotonic temperature dependence of the dielectric constant of $YMnO_3$ in the antiferromagnetic state is a consequence of the first-order phase transition between magnetic configurations β and α.

A transition from β- to α-configuration upon a decrease in temperature was observed by the neutron diffraction measurements in the hexagonal $HoMnO_3$.[9] In $YMnO_3$, the neutron diffraction measurements were made only at 4.2 K. The authenticity of the above hypothesis could be verified by carrying out such measurements in the temperature interval 55–80 K, where the existence of magnetic β-configuration is assumed.

Note that since the magnetic field blurs the temperature phase transition, the anomalies of magnetic characteristics which can be determined by applying a magnetic field are less pronounced than the anomaly of the dielectric constant measured in zero magnetic field. In this case, the ME measurements may be preferable to the magnetic measurements for studying the magnetic properties.

[1] F. Bertaut, F. Forrat, and P. Farg, C. R. Acad. Sci. **256**, 1958 (1963).
[2] V. A. Bokov, G. A. Smolenskii, S. A. Kizhaev, and I. E. Myl'nikova, Fiz. Tverd. Tela (Leningrad) **5**, 3607 (1963) [Sov. Phys. Solid State **5**, 2646 (1963)].
[3] Z. J. Haang, Y. Cao, Y. Y. Sun *et al.*, Phys. Rev. B **56**, 2623 (1997).
[4] G. A. Smolenskii and I. E. Chupis, Usp. Fiz. Nauk **137**, 415 (1982) [Sov. Phys. Usp. **25**, 475 (1982)].
[5] G. A. Samara and P. M. Richards, Phys. Rev. B **14**, 5073 (1976).
[6] F. Bertaut, G. Buisson, A. Delapabne *et al.*, in *Theses of Intern. Conf. on Magnetism*, Nottingham (1964).
[7] G. M. Nedlin, Fiz. Tverd. Tela (Leningrad) **6**, 2708 (1964) [Sov. Phys. Solid State **6**, 2156 (1964)].
[8] A. S. Borovik–Romanov, *Antiferromagnetism and Ferrites* [in Russian], Izd. Akad. Nauk SSSR, Moscow (1962).
[9] W. C. Koehler, H. L. Yakel, E. Q. Wollan, and J. W. Cable, Phys. Lett. **9**, 93 (1964).

Translated by R. S. Wadhwa

LETTERS TO THE EDITOR

Acoustically stimulated phase transition and low temperature optical spectra in PbI_2 crystal

M. M. Bilyi, I. S. Gorban, I. M. Dmitruk, I. M. Salivonov, and I. V. Ostrovskii

Physical Faculty, Kiev Taras Shevchenko University, 6 Akademic Glushkov Prs., 252127, Kiev, Ukraine
(Submitted April 9, 1998)
Fiz. Nizk. Temp. **24**, 807–808 (August 1998)

The influence of an intensive ultrasonic wave on the crystal structure of PbI_2 was investigated. Acoustically stimulated phase transition have been observed for the first time. © *1998 American Institute of Physics.* [S1063-777X(98)01508-4]

PbI_2 is a layered crystal and it consists of strongly (ionic forces) bounded layers. Layers interact with each other by the weak Van-der-Vaals forces. Many polytypes of PbI_2 exist because of different possible orders of a layers package. As a result of weakness of interlayer forces, the phase polytype transitions are possible under the pressure or temperature change. Such a transition $2H-PbI_2(D_{3d}^3)\rightarrow 4H-PbI_2(C_{6v}^4)$ (Ref. 1) can be observed under heating up to 130 °C. The reverse transition takes place because of a metastable character of the $4H$ polytype phase after 1–2 months. Under the hydrostatic pressure other types of phase transitions—polymorphous transitions—were observed. In such a type of the transition not only the layers orientation but the structure of layers are being changed.[2]

The aim of this work is to study an influence of an ultrasonic wave on the PbI_2 structure. We studied the transformations of the simplest and the most stable $2H$ polytype single crystals after the exposure to the acoustical wave of the 2.25 MHz frequency and the intensity about 1 W/cm^2. The PZT-type piezoceramic transducer was used to excite an ultrasonic wave in the sample. The maximum amplitude of rf-voltage applied to transducer V_{pp} was 40 V. The direction of the ultrasonic wave propagation was perpendicular to the crystal layers. A nondestructive study of crystal structure was performed by means of optical methods: reflectance and photoluminescence (PL), the low temperature spectroscopy and the Raman spectroscopy. We also measured acoustical noises (an acoustic emission, AE) from our sample, the frequency range of measurements was 0.02 to 0.5 MHz.

The optical reflection spectra at the low temperature ($T=1.4$ K) measured before and after the acoustical irradiation are presented in Fig. 1. One can see the 2 nm shift of a polariton reflection curve after the acoustical irradiation. This fact reflects the alteration of band width caused by the phase transformation: $2H-PbI_2\rightarrow 4H-PbI_2$. The same shift was observed in photoluminescence spectra (Fig. 2). The initial spectrum of PbI_2-2H (curve *1*) has the emission bands of free excitons (FE) 496.5 nm, excitons localized on impurities or defects (LE) 497.4 nm, and the lower energy so called K-series. After the ultrasonic action a PL spectrum corresponds to the $4H-PbI_2$ PL spectrum except the weak band at 497.4 nm which is due to the residue of the $2H$ polytype. The K-series disappearing proves the existence of a phase transition, because this series is absent in the PL

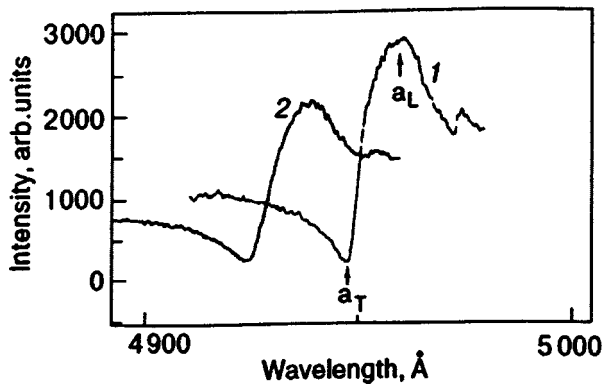

FIG. 1. Reflection spectra of PbI_2 single crystals before (*1*) and after (*2*) ultrasonic irradiation; a_L, a_T—upper and lower polaritonic branches, correspondingly; $T=1.4$ K.

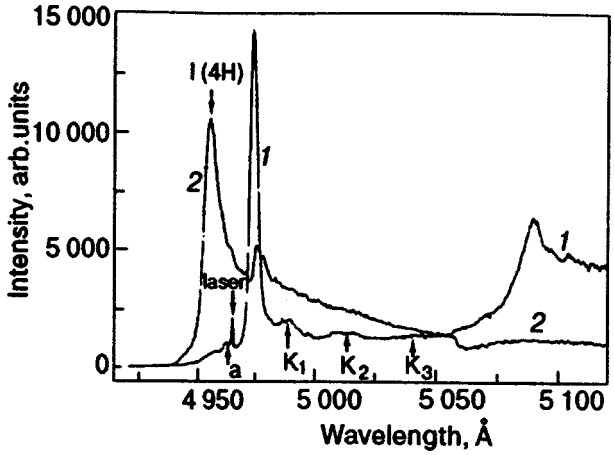

FIG. 2. Photoluminescence spectra of PbI_2 single crystals before (*1*) and after (*2*) ultrasonic irradiation; a—free excition, I—localized excition, K_1,K_2,K_3—K-series. $T=1.4$ K.

spectrum of the $4H$ polytype. This conclusion is confirmed with Raman spectra measurements.

Type of the AE signal, its kinetics reflects the changes in a defect structure inside the sample initiated by the ultrasonic wave. The AE appeared when the ultrasound reached a certain threshold amplitude (rf-voltage $V_{pp}=24$ V). Under the ultrasound irradiation the intensity of AE signals increased with V_{pp} increasing up to 40 V. Then, under $V_{pp}=40$ V$=$const, an evolution of the AE intensity in time achieved the maximum value and then decreased to zero. It lasted approximately 10 min. After switching off the acoustic irradiation and following next increasing of V_{pp}, the AE reappeared at $V_{pp}>24$ V, lasted 10 min and then disappeared under the constant V_{pp}. Such a behavior of the AE signal is explained by the changes of a dislocation structure inside the sample.[3]

An interesting result was obtained when measuring the low temperature ($T=1.4$ K) photoluminescence spectra from a natural crystal surface. In these spectra the localized exciton line disappeared after the ultrasonic irradiation. This fact can be explained by the considerable increase of the near-surface nonradiative recombination rate caused by a migration of defects to the surface of the sample.

In our experiments we have observed for the first time an acoustically stimulated phase transition. It is shown that a dislocation structure is changing under the ultrasonic irradiation. The high stability of the obtained $4H$ polytype is of special interest. These fact and acoustic emission anomalies are under discussion.

[1] R. S. Mitchell, Z. Kristallogr. **111**, 372 (1959).
[2] N. M. Belyi, A. V. Bobyr, E. A. Vinogradov, I. S. Gorban', V. A. Gubanov, and G. N. Zhyzhyn, Fiz. Tverd. Tela **24**, 887 (1982) [Sov. Phys. Solid State **24**, 502 (1982)].
[3] V. S. Boiko, R. I. Garber, V. F. Kivshyk, and L. F. Krivenko, Fiz. Tverd. Tela **17**, 1541 (1975) [Sov. Phys. Solid State **17**, 1010 (1975)].

This article was published in English in the original Russian journal.